

**Structural Evolution of a Bifunctional Mu-Opioid Receptor (MOR)/Delta-Opioid Receptor
(DOR) Peptidomimetic as Nonaddictive Opioid Analgesics**

by

Sean P. Henry

A dissertation submitted in partial fulfillment
of the requirements for the degree of
Doctor of Philosophy
(Medicinal Chemistry)
in the University of Michigan
2019

Doctoral Committee:

Professor Henry I. Mosberg, Chair
Professor Scott D. Larsen
Associate Professor Peter J. H. Scott
Professor John. R. Traynor

Sean P. Henry

seanph@med.umich.edu

ORCID iD: 0000-0002-4405-062X

© Sean P. Henry 2019

Acknowledgements

I would first and foremost like to thank the Lord my God. Without His grace, I would not have been able to enter this PhD program, nor would I have been able to complete the research presented herein. Without His guidance, I would not have been able to find my calling: the synthesis and development of novel pharmaceuticals. For that, I am eternally grateful.

To my family back home, Timothy Henry, Brenda Skinner, Kevin Henry, and Joan Henry, thank you all for supporting me and blessing me with all you know. I love you all and hope to give to others what you have given to me. Timothy, you have been a source of inspiration, for both your love of science and for your enduring patience. May you rest in peace.

Dr. Henry Mosberg, your guidance and wisdom throughout my time here has thoroughly enriched my understanding of medicine and drug design. Without your efforts, I would not have been able to complete this program and the quality of our work would have suffered. For that, I thank you. I also would like to thank the members of my committee: Dr. Scott Larsen, Dr. Peter Scott, and Dr. John Traynor. Your insights have broadened my horizons and have contributed greatly to my development as a scientist.

I would like to thank Dr. Nicholas Griggs, Thomas Fernandez, and Dr. Jess Anand for acquiring the *in vitro* data presented herein. Without these data, this project would only be an exercise in organic synthesis and the contributions to our understanding of the opioid receptors would be lost. I would also like to thank Bryan Sears, whose studious efforts in acquiring our *in vivo* data have proven invaluable for the development of these ligands. Finally, I would like Kate Kojiro, whose knowledge in the laboratory have streamlined my work by no small means.

To Dr. Larisa Yeomans and your husband Matthew Cruz, your kindness and grace have always been warm and welcoming. You have always been there when I needed you, and for that, I count among my dearest of friends. To my coworkers Dr. Tanpreet Kaur, Dr. Deanna Montgomery, Dr. Tony Nastase, and Jay Kim, your levity and companionship have lightened many a rainy day. The completion of this dissertation would have been much less wholesome without you all. Finally, I would like to thank my friends from both GCF and 2:42. Your friendship has contributed to my growth in innumerable ways and I will never forget the good times that we have had together.

TABLE OF CONTENTS

Acknowledgments	ii
List of Figures	vi
List of Schemes	viii
List of Tables	ix
List of Abbreviations	xi
Abstract	xv
Chapter 1: On Opioids	1
1.1 The Opioid Epidemic	1
1.2 The Opioid Receptors and their Effects	2
1.3 Bifunctional MOR/DOR Ligands	4
1.4 From the Opioid Peptides to AAH8	6
1.5 Project Overview	10
Chapter 2: Breaking the THQ Core	14
2.1 Introduction	14
2.2 Results	15
2.3 Discussion and Conclusions	24
2.4 Experimental	29
Chapter 3: Further Derivatization of the Aromatic Core	63
3.1 Introduction	63
3.2 Results	64
3.3 Discussion and Conclusion	73
3.4 Experimental	78

Chapter 4: Amine Pendants as MOR Pharmacophores with Improved Stability	100
4.1 Introduction	100
4.2 Results	101
4.3 Discussion and Conclusion	110
4.4 Experimental	114
Chapter 5: Discovery of Aromatic-Amine Pharmacophore	133
5.1 Introduction	133
5.2 Results	135
5.3 Discussion and Conclusions	146
5.4 Experimental	154
Chapter 6: Aromatic-Amine Pharmacophore Enables Removal of Aromatic Core	183
6.1 Introduction	183
6.2 Results	193
6.3 Discussion and Conclusions	183
6.4 Experimental	198
Chapter 7: Aliphatic Heterocycles as Novel Core Elements	216
7.1 Introduction	216
7.2 Results	217
7.3 Discussion and Conclusions	223
7.4 Experimental	226
Chapter 8: Conclusions and Future Directions	246
8.1 Conclusions	246
8.2 Future Directions	251
Appendix	258
References	259

List of Figures

Figure 1: Notable small molecules that exhibit a MOR-agonist/DOR-antagonist profile.	5
Figure 2: General SAR of the opioid peptides.	7
Figure 3: Structural evolution of the endogenous peptide Met-enkephalin into the lead peptidomimetic KSKPP1E .	9
Figure 4: Diversification strategies employed to explore the SAR of KSKPP1E .	10
Figure 5: Normalized metabolic half-life of peptidomimetics that contain a THQ core or similar bicyclic core structure.	11
Figure 6: Known metabolites of KSKPP1E from MLM.	12
Figure 7: Pharmacophore and linker elements of KSKPP1E and our initial monocyclic core series.	15
Figure 8: Molecular modeling of analogue 70 at MOR.	24
Figure 9: Further derivatization of compounds 60 and 70 .	64
Figure 10: Proposed CYP450 reaction mechanism on analogues 70 , 106 , 107 , and 114 .	77
Figure 11: Design path leading to stable peptidomimetics with basic amine pendants.	101
Figure 12: Antinociceptive activity of analogues 70 , 127-128 , and 131-134 using the acetic acid stretch assay.	109
Figure 13: Stability ratio of analogues 127-128 and 131-136 against their cLogP.	112
Figure 14: Design of amine pendant analogues with different aromatic core modifications.	135
Figure 15: Molecular docking of superagonist 168 at the three opioid receptors.	145
Figure 16: Antinociceptive activity of 132 and analogues 168 , 172 , 176 , and 180 using the AASA.	146
Figure 17: Literature structures that are close to our discovered aromatic-amine pharmacophore outside of our previously reported peptidomimetic series.	153
Figure 18: Design of analogues possessing greater simplification of core elements.	184
Figure 19: Molecular docking of analogue 193 at the three opioid receptors.	192

Figure 20: Antinociceptive activity of the 168 and analogues 193-194 , and 197-200 using the AASA.	193
Figure 21: Conversion of aromatic core peptidomimetic to cyclic aliphatic core peptidomimetics.	217
Figure 22: Summary of results from Chapters 2 and 3.	247
Figure 23: Summary of results from Chapters 4 and 5.	248
Figure 24: Summary of results from Chapter 6.	250
Figure 25: Summary of Results from Chapter 7.	251
Figure 26: General design scope upon which further analogues may be developed.	252
Figure 27: Proposed analogues to be synthesized that modify the aromatic-amine pharmacophore.	253
Figure 28: Proposed peptide derivatives of analogues 199 and 200 .	253
Figure 29: Proposed analogues that modify the aromatic core.	254
Figure 30: Rigid cyclic core derivatives akin to analogues 196-197 .	255
Figure 26: Proposed derivatives of the cyclic aliphatic analogue 229 .	256

List of Schemes

Scheme 1: Synthesis of AAH8 .	13
Scheme 2: Synthesis of Substituted Monocyclic Core Analogues 59-74 .	16
Scheme 3: Synthesis of Analogues 101-104 .	65
Scheme 4: Synthesis of Analogue 105 .	66
Scheme 5: Synthesis of Analogues 106-107 .	66
Scheme 6: Synthesis of Analogue 114 .	67
Scheme 7: Synthesis of Amine or Amide Pendant Analogues Containing an Ethyl Ether.	102
Scheme 8: Synthesis of aromatic core analogues containing amine pendants to produce SAR matrices.	136
Scheme 9: Synthesis of Analogues 193-197 .	185
Scheme 10: Synthesis of Peptide Core Analogues 198-200 .	186
Scheme 11: Synthesis of Analogues 224-231 .	219

List of Tables

Table 1: The opioid receptors, their location, and their phenotypic effects on activation.	2
Table 2: Binding affinity of the benzylic core compounds at MOR, DOR, and KOR.	19
Table 3: Potency and efficacy of benzylic core compounds at MOR, DOR, and KOR.	20
Table 4: Metabolic stability of benzylic core compounds in MLM.	22
Table 5: Binding affinity of 2 nd generation benzylic derivatives at MOR, DOR, and KOR.	68
Table 6: Potency and efficacy of 2 nd generation benzylic derivatives at MOR, DOR, and KOR.	69
Table 7: Binding affinity of 2 nd generation aromatic derivatives at MOR, DOR, and KOR.	70
Table 8: Potency and efficacy of 2 nd generation aromatic derivatives at MOR, DOR, and KOR.	71
Table 9: Metabolic stability of 2 nd generation benzylic derivatives in MLM.	72
Table 10: Metabolic stability of 2 nd generation aromatic derivatives in MLM.	73
Table 11: Binding affinity of amine or amide pendant analogues at MOR, DOR, and KOR.	104
Table 12: Efficacy and potency of amine or amide pendant analogues at MOR, DOR, and KOR.	106
Table 13: Metabolic stability of amine or amide pendant analogues in MLM.	107
Table 14: Binding affinity matrix (K _i (nM)) of amine analogues of benzylic core structures from Chapter 2 at MOR and DOR.	138
Table 15: Binding affinity (K _i (nM)) matrices of amine analogues of benzylic core structures from Chapter 2 at KOR and their selectivity.	140
Table 16: Potency matrices of amine analogues of previously reported benzylic core structures from Chapter 2 at MOR, DOR, and KOR.	141
Table 17: Efficacy matrices of amine analogues of previously reported benzylic core structures from Chapter 2 at MOR, DOR, and KOR.	143
Table 18: Metabolic stability matrix of amine analogues of previously reported benzylic core structures from Chapter 2.	144
Table 19: Binding affinity of simple core compounds at MOR, DOR, and KOR.	188
Table 20: Efficacy and potency of simple core compounds at MOR, DOR, and KOR.	189

Table 21: Metabolic stability of simple core compounds in MLM.	190
Table 22: Binding affinity of cyclic aliphatic core compounds at human MOR, DOR, and KOR.	220
Table 23: Efficacy and potency of cyclic aliphatic core compounds at human MOR, DOR, and KOR.	222
Table 24: Metabolic stability of cyclic aliphatic core compounds in MLM.	223

List of Abbreviations

AASA	acetic acid stretch assay
Aba	4-amino-1,2,4,5-tetrahydro-2-benzazepin-3-one
Ac	acetyl
Ac₂O	acetic anhydride
Ala	alanine
Alk-Br	alkyl bromide
BBB	blood-brain barrier
BCA	bicinchoninic acid
BH₃*Me₂S	borane-dimethyl sulfide complex
Bn	benzyl
BnBPin	benzylboronic acid pinacol ester
Boc	tert-butoxycarbonyl
Boc₂O	di-tert-butyl decarbonate
CHO	Chinese hamster ovary
6-Cl-HOBt	6-chloro-1-hydroxybenzotriazole
cLogP	calculated logarithm of the partition coefficient
conc	concentrated
CPM	cyclopropyl methyl
CYP	cytochrome P450
CYP2A6	cytochrome P450 2A6
CYP3A4	cytochrome P450 3A4
DAMGO	[D-Ala ² -N-Me-Phe ⁴ -Gly-ol]-enkephalin
DCE	1,2-dichloroethane
DCM	dichloromethane
DI	deionized

DiBocDMT	N-Boc-O-Boc-2',6'-dimethyl-L-tyrosine
DIEA	N,N-diisopropylethylamine
DIPP[Ψ]-NH₂	H-Dmt-TicΨ[CH ₂ NH]Phe-Phe-NH ₂
DMEM	Dulbecco's modified Eagle medium
DMF	dimethylformamide
DMSO	dimethylsulfoxide
DMT	2',6'-dimethyl-L-tyrosine
DNS	does not stimulate
DOR	δ-opioid receptor
DPDPE	[D-Pen ² -D-Pen ⁵]enkephalin
EC₅₀	half maximal effective concentration
EDTA	ethylenediaminetetraacetic acid
ESI-MS	electrospray ionization mass spectroscopy
Et	ethyl
EtBr	ethyl bromide
EtOAc	ethyl acetate
FDA	Food and Drug Administration
GDP	guanosine diphosphate
Gly	glycine
GPCR's	G-protein Coupled Receptors
GTPγS	guanosine 5'-O-[γ- thio]triphosphate
HEPES	4-(2-hydroxyethyl)-1-piperazineethanesulfonic acid
hERG	human ether-à-go-go-related gene
HPLC	high-performance liquid chromatography
ip	intraperitoneal
K_i	binding affinity
KOR	κ-opioid receptor
LC	liquid chromatography
Me	methyl
MeCN	acetonitrile

MLM	mouse liver microsome
MOR	μ -opioid receptor
MS	mass spectroscopy
NADPH	nicotinamide adenine dinucleotide phosphate
NaOtBu	sodium tert-butoxide
NBS	N-bromosuccinimide
ND	no data
NLX	naloxone
NMM	N-methyl morpholine
NMR	nuclear magnetic resonance
nPr	n-propyl
NSAID's	Non-Steroidal Anti-Inflammatory Drugs
Pd(dppf)Cl₂	[1,1'-bis(diphenylphosphino)ferrocene]palladium(II) dichloride
Pen	penicillamine
PDB	protein data bank
Phe	phenylalanine
PK	pharmacokinetic
PyBOP	benzotriazol-1-yl-oxytripyrrolidinophosphonium hexafluorophosphate
SAR	structure-activity relationship
sc	subcutaneous
SE	standard error
SEM	standard error of the mean
T_{1/2}	half-life
Tandem MS-MS	tandem mass spectrometry
TEA	triethylamine
TFA	trifluoroacetic acid
TFAA	trifluoroacetic anhydride
TfOH	triflic acid
THF	tetrahydrofuran
THIQ	1,2,3,4-tetrahydroisoquinoline

THQ	1,2,3,4-tetrahydroquinoline
Tic	1,2,3,4-tetrahydroisoquinoline-3-carboxylate
Ti(OEt)₄	titanium (IV) ethoxide
TIPP[Ψ]	H-Tyr-TicΨ[CH ₂ NH]Phe-Phe-OH
TOF	time-of-flight
tPSA	total polar surface area
Tris	tris(hydroxymethyl)aminomethane
Tyr	tyrosine
UV	ultraviolet
WHO	World Health Organization
WWTW	warm water tail withdrawal.

Abstract

Opioids have been used since antiquity for their ability to treat chronic and severe pain. However, their potent analgesic activity comes with severe side effects, including dependence, abuse, and even death by respiratory depression. Since these opioids are unmatched in their ability to treat pain, the development of alternatives without these negative side effects is sorely needed. While numerous strategies have been implemented, none yet have been successful. One promising new strategy involves targeting multiple different opioid receptors at the same time. More specifically, agonism at the μ -opioid receptor (MOR) with simultaneous activity at the δ -opioid receptor (DOR) can attenuate these negative side effects without compromising their analgesic effects.

Previously, our lab has synthesized a peptidomimetic series that expresses a MOR-agonist/DOR-antagonist profile. Members of this series were found to express antinociception (a proxy measure for analgesia) *in vivo* without producing dependence, drug-seeking behavior, or tolerance to the antinociceptive effects. While these effects show great promise, they are only active upon intraperitoneal injection. Since chronic pain requires the administration of drug over a long period of time, enabling oral bioavailability is an important goal to transform these peptidomimetics into nonaddictive analgesics. Unfortunately, these ligands express very poor metabolic stability in mouse liver microsomes (MLM), and this instability is a product of the tetrahydroquinoline core structure of the peptidomimetic. This structure requires numerous synthetic steps to create, and its instability is manifest in several key intermediates. As such, this

dissertation describes a series of structure-activity relationship (SAR) campaigns that sought to remove this unstable core while preserving our desired bifunctional opioid activity.

Initially, we sought to convert the bicyclic tetrahydroquinoline core of our peptidomimetic series to a monocyclic aromatic core. This immediately resulted in improvements in metabolic stability, and no unstable intermediates were observed. However, the MOR-agonist properties of these ligands, necessary for inducing their analgesic properties, was lost in most analogues in this series, and while a few were better than morphine *in vitro*, they were not as potent or efficacious as our original peptidomimetics.

Using the results of this SAR campaign as a springboard, we next sought to further improve their MOR-agonist properties and metabolic stability. To this end, a series of amine pendants were incorporated onto our monocyclic core analogues. These pendants managed to further improve the metabolic stability of these ligands. It was also discovered that these amines can induce high MOR-efficacy in our peptidomimetics, and when combined with an aromatic ring on the pendant, can induce high MOR-potency. This “aromatic-amine” pharmacophore was found to produce highly potent and efficacious MOR-agonists, independent of the functionalization of the monocyclic aromatic core. In fact, MOR-superagonists with efficacy of up to 147% compared to the standard MOR-agonist DAMGO were discovered using this pharmacophore, and the pharmacophore even enabled elimination of the aromatic core entirely. All this came with consistent DOR-antagonism or weak partial DOR-agonism, in line with the opioid profile we sought to maintain.

Herein, the SAR campaigns that led to the improvement in metabolic stability of these ligands are discussed, as well as the discovery and scope of this aromatic-amine pharmacophore. These campaigns significantly simplified the synthesis of the ligands, yielding no unstable intermediates and enabling a greater degree of structure diversification for future opioid ligands.

Chapter 1: On Opioids

1.1 The Opioid Epidemic

Incidences of the abuse of opioids and subsequent overdose have been on the rise in the United States. This opioid epidemic traces its inception to the late 1990's, and was in no small part fueled by an aggressive marketing campaign by Purdue pharmaceuticals which touted the safety of its newly released drug OxyContin.¹ An extended release formulation of oxycodone, this drug was advertised to have reduced addiction liabilities. This caused sales of OxyContin to increase from \$48 million in 1996 to \$1.1 billion in 2000¹ and OxyContin became the most prescribed opioid for the treatment of moderate-to-severe pain.² In reality, OxyContin was addictive, and it soon became the most abused prescription opioid by 2004.³

The prescription rate of other opioids also increased during this time. Medical use by mass of fentanyl, hydromorphone, and morphine increased by 227%, 96%, and 73%, and yielded increased mentions of abuse of 642%, 342%, and 113% respectively from 1997 to 2002.⁴ The abuse of these opioids has only increased since 2002, with opioid overdose deaths increasing from 8,048 in 1999 to 47,600 in 2017.⁵ More specifically, the number of overdoses related to prescription opioids has increased from 1.2-1.4 per 100,000 in 1999 to 5.2-10.2 per 100,000 in 2016.⁶ These values each year are difficult to determine exactly, largely due to the uncertainty of the source of many opioids (such as fentanyl), which are both illicitly and legally available.⁶ Ultimately, these overdose deaths are related to the reported 9.9 million of Americans who have misused prescription opioids, 1.7 million of which possessed substance use disorders in 2018.⁷

While the wide distribution of these opioids has led to their misuse and overdose, it must not be forgotten that these opioids are prescribed for a purpose. A 2016 survey estimated that approximately 50 million Americans suffer from chronic pain,⁸ defined by the National Pain Strategy as: “pain that occurs on at least half the days for six months or more.”⁹ In the treatment of pain, the World Health Organization (WHO) developed what is called an analgesic ladder, a general set of guidelines that describes the analgesic to be prescribed in response to different levels and durations of pain. In short, mild to moderate and acute pain should be treated with NSAID’s, whereas moderate to severe and chronic pain should be treated with opioids.¹⁰ Modest updates to this model have been proposed, including neurosurgical procedures,¹¹ but the ladder has changed little since its inception. Nevertheless, opioids remain the drug of choice for severe and chronic pain, despite their negative side-effects. As such, the development of novel analgesics that have the analgesic power of opioids without their negative side-effects is sorely needed.

1.2 The Opioid Receptors and their Effects

The opioid analgesics primarily act on a set of G-protein coupled receptors (GPCR’s) found in various locations throughout the brain. There are three opioid receptors that are relevant to this work: the μ -opioid receptor (MOR), the δ -opioid receptor (DOR), and the κ -opioid receptor (KOR). These receptors are all associated with different phenotypic effects, which are summarized in **Table 1**.^{12,13}

<i>Opioid Receptor</i>	<i>Effects on Activation</i>	<i>Location in Brain</i>
μ (MOR)	Analgesia, physical dependence, respiratory depression, euphoria, abuse potential, constipation, miosis	Cortex, periaqueductal grey, thalamus, ventral tegmental area
δ (DOR)	Convulsions, analgesia, physical dependence	Amygdala, cortex
κ (KOR)	Dysphoria, analgesia, miosis, sedation	Hypothalamus, periaqueductal grey

Table 1: The opioid receptors, their location, and phenotypic effects on activation.

More specifically, the opioid analgesics operate by acting as MOR-agonists. This produces the most potent analgesia, but also yields their addictive effects and death through respiratory depression. These effects are mainly driven through the location with which these receptors are activated. Briefly, μ -opioid receptors located in the periaqueductal grey are largely responsible for regulating pain,¹⁴ whereas μ -opioid receptors located in the ventral tegmental area are responsible for the opioid's abuse symptoms.¹⁵

Unfortunately, all these side-effects are the result of on-target effects. As the analgesic effects of the opioid drugs are unmatched for relieving pain, current pharmacological research is focused on ways to stimulate the opioid receptors such that their analgesic properties may be manifest without the negative effects. These include biased agonists that operate solely at MOR and activate the G-protein signaling cascade without inducing β -arrestin recruitment.¹⁶⁻¹⁸ The G-protein signaling cascade is responsible for proper signaling of the receptor, while the β -arrestin pathway is involved in blocking the interaction between the GPCR and the G protein, producing receptor desensitization.¹⁹ Thus, activation of the G-protein signaling cascade produces the desired analgesia, whereas failure to activate the β -arrestin pathway was believed to reduce adverse side-effects.¹⁹ However, the biased MOR-agonist PZM21 was found to produce tolerance to antinociception and induce respiratory depression in a recent report.²⁰ Furthermore, the biased MOR-agonist oliceridine was also found to produce constipation and abuse liabilities in rodents.^{21,22} Mouse knock-in studies have also found that opioid receptors with a reduced ability to recruit β -arrestin possess enhanced analgesia on activation, but also enhanced or unaltered constipation, respiratory depression, and withdrawal symptoms.²³ These data, coupled with the fact that oliceridine failed to achieve FDA approval due to its safety profile, suggests that alternative avenues of opioid development may be needed to reduce side-effects.

A growing body of preclinical evidence has emerged suggesting that stimulation of the μ -opioid receptor (MOR) in conjunction with antagonism at the δ -opioid receptor (DOR) can produce the desired analgesic effects without producing analgesic tolerance or dependence. For instance, rats given morphine and co-treated with the DOR-antagonists TIPP[Ψ]²⁴ or naltrindole²⁵⁻²⁶ displayed antinociception with significantly diminished chronic antinociceptive tolerance and dependence as measured by reduced withdrawal symptoms. These trends are supported by experiments whereby DOR knockout mice²⁷ did not develop chronic tolerance to the analgesic effects of morphine. Furthermore, mice treated with antisense DOR oligodeoxynucleotide did not develop acute dependence or chronic tolerance to the analgesic effects of morphine.²⁸

Curiously, DOR-agonism instead of antagonism has also been shown to reduce the side-effect profile of MOR-agonists. Coadministration of DOR-agonists with MOR-agonists has been shown to attenuate dependence²⁹ and respiratory depression³⁰ without affecting antinociception. These beneficial effects work both ways, as MOR-agonists can attenuate the convulsive effects associated with activation of DOR.³¹ To this end, many MOR-agonist/DOR-agonist ligands have been synthesized and were shown to have reduced abuse profiles, including reduced dependence,³² and tolerance.³³⁻³⁵

In short, bifunctional opioid ligands may allow for the development of opioid analgesics with reduced side-effects. While the mechanisms underlying these data are not yet well understood, these data show potential and warrant further investigation.

1.3 Bifunctional MOR/DOR ligands

To this end, a substantial number of bifunctional MOR/DOR ligands have been developed,^{36,37} and some small molecule bifunctional MOR-agonist/DOR-antagonists have been reported that show reduced side-effect profiles (**Figure 1**). Some of these are based on the classical

morphinan scaffold (**Figure 1A**), and show attenuated chronic tolerance and dependence.³⁸⁻⁴⁰ Mitragynine pseudoindoxyl (**Figure 1B**), derived from the kratom alkaloid mitragynine, was found to possess reduced withdrawal, reduced respiratory depression, and does not produce conditioned-place preference.⁴¹ Others still are derived from opioid peptides (**Figure 1C-D**). DIPP[Ψ]-NH₂ (**Figure 1C**), an endomorphin derivative, produces antinociception in murine models without acute tolerance and chronic physical dependence.⁴² AAH8 (**Figure 1D**) has also been shown to produce antinociception in murine models without developing tolerance to antinociceptive effects, physical dependence, and does not evoke conditioned-place preference, suggesting it does not have reward properties.⁴³

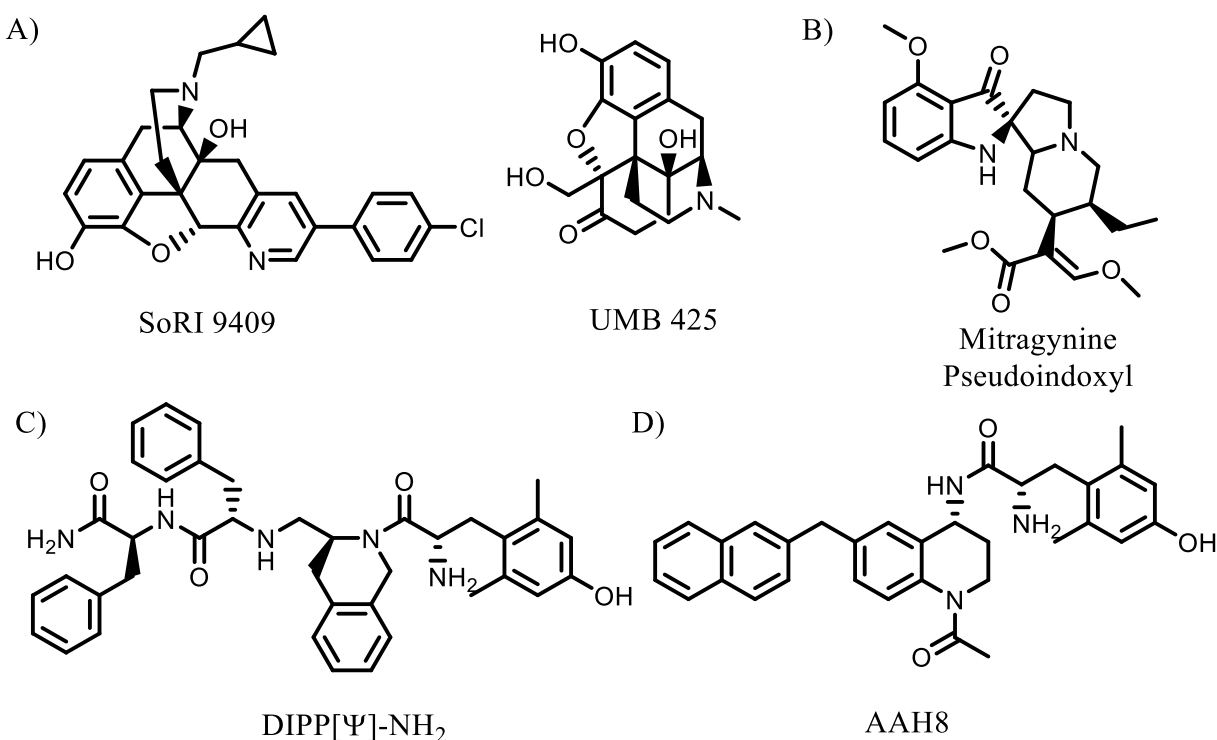


Figure 1: Notable small molecules that exhibit a MOR-agonist/DOR-antagonist profile. Some of these compounds utilize the morphinan scaffold shared by many opioids (A), or are derivative of kratom alkaloids (B), while others are derived from endomorphins (C), or cyclic opioid peptides (D).

The research presented here will focus more on this last analogue **AAH8**. **AAH8** is a peptidomimetic that is derived from the cyclic opioid peptide **JOM13**. **AAH8** possesses a tetrahydroquinoline (THQ) core and it along with many other THQ core containing analogues were developed in our lab. Since these analogues mimic the endogenous peptides, an understanding of the opioid peptides and their SAR will be useful.

1.4 From the Opioid Peptides to **AAH8**

The opioid receptors are acted on by a host of different endogenous ligands. These endogenous opioids were found to be peptides, the first of which discovered were the enkephalins,⁴⁴ followed soon by endorphins⁴⁵ and dynorphins.⁴⁶ Eventually, this list of naturally occurring opioid peptides would expand to include the endomorphins,⁴⁷ dermorphins,⁴⁸ and deltorphins,⁴⁹ the latter two of which are derived from the skin of frogs. These discoveries prompted great interest in the structure-activity relationship (SAR) of these peptides at each of the opioid receptors. Over time, important SAR trends became apparent (**Figure 2**).⁵⁰ In general, it was found that two key pharmacophore features were responsible for activation of the opioid receptors (**Figure 2**, blue). These included an N-terminal tyrosine residue and a phenylalanine residue. These two pharmacophores need to be separated by one or two amino acids (**Figure 2**, purple), and all together compose what is termed the message sequence, which is responsible for opioid receptor activation. Amino acids found after the phenylalanine residue vary widely in terms of their composition and number, comprising what is called the address sequence (**Figure 2**, red) which is responsible for selectivity between the opioid receptors.

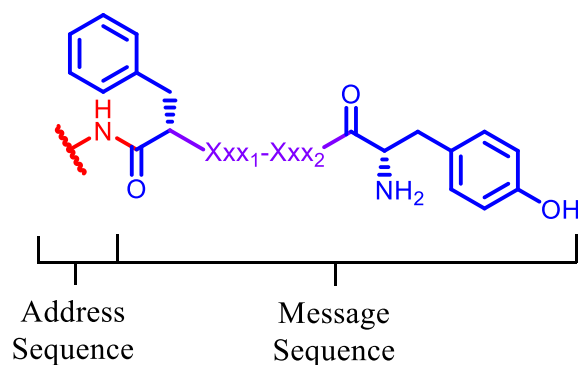


Figure 2: General SAR of the opioid peptides. The key pharmacophore elements include an N-terminal tyrosine and a phenylalanine residue (Blue). These are separated by one or two amino acids (purple) and together compose the message sequence that activates the opioid receptor. Selectivity between each opioid receptor is dictated by the C-terminal address sequence (Red), which can vary widely in composition and length. Conventionally, peptides are presented with the N-terminus on the left and the C-terminus on the right but will be represented in the reverse for the sake of consistency with other structures in this work.

The broad SAR campaign that discovered these trends produced many notable peptides. For example, the peptides [D-Ala², N-MePhe⁴, Gly-ol]-enkephalin (DAMGO)⁵¹ and [D-Pen², D-Pen⁵]enkephalin (DPDPE)⁵² are now used as standard agonists for the study of MOR and DOR, respectively. Eventually, it was found that replacement of the N-terminal tyrosine residue with an N-terminal 2',6'-dimethyltyrosine residue (DMT) can greatly alter and amplify the effects of an opioid peptide.⁵³ This DMT pharmacophore is commonly attached to a 1,2,3,4-tetrahydroisoquinoline-3-carboxylic acid (Tic) residue, which is found in a host of synthetic opioid peptides. Of note are H-Tyr-TicΨ[CH₂NH]Phe-Phe-OH (TIPP[Ψ]) and H-Dmt-TicΨ[CH₂NH]Phe-Phe-NH₂ (DIPP-NH₂[Ψ]), opioid peptides that were used to demonstrate that MOR-agonist activity used in conjunction with DOR-antagonist activity can produce the antinociceptive effects of opioids without the abuse liabilities that are commonly associated with them.^{24,42}

One series of interest was that of cyclic peptides derived from Met-enkephalin. It was observed that Met-enkephalin was a largely flexible peptide, and early research was focused on

inducing conformational restrictions within the peptide to determine which orientation the peptide adopts on binding to DOR. One such analogue involved cyclization of the linear peptide via a disulfide bond, followed by steric rigidification through the introduction of two gem dimethyl groups, yielding DPDPE.⁵² As stated above, DPDPE is used as a standard DOR-agonist due to its high potency and selectivity for DOR. In a later analogue, the gem dimethyl group on the 2-position amino acid was removed, and the 3-position glycine residue was eliminated, yielding a smaller peptide.⁵⁴ This peptide is Tyr-c[D-Cys-Phe-D-Pen]-OH (**JOM-13**), which had similar levels of selectivity and potency as DPDPE, albeit in a smaller structure. The structural evolution of these peptides is shown in **Figure 3A**.

After the initial characterization of **JOM-13**, a series of computational studies were performed using this peptide and similar analogues.⁵⁵⁻⁵⁹ These were aimed at further probing the conformations of the tyrosine and phenylalanine pharmacophores necessary to facilitate DOR activation. These studies were then used to computationally design a peptidomimetic that possessed a tetrahydroquinoline core structure instead of the cyclic peptide (**Figure 3B**).⁶⁰ This peptidomimetic, hereafter termed **KSKPP1E**, uses a benzyl group to mimic the phenylalanine of **JOM-13**, and uses DMT instead of tyrosine to improve potency. Curiously, this peptidomimetic was found to be a potent MOR-agonist/DOR-antagonist, a profile very different from the selective DOR-agonist upon which it was based. Nevertheless, this conversion had the effect of further reducing the mass of the opioid.

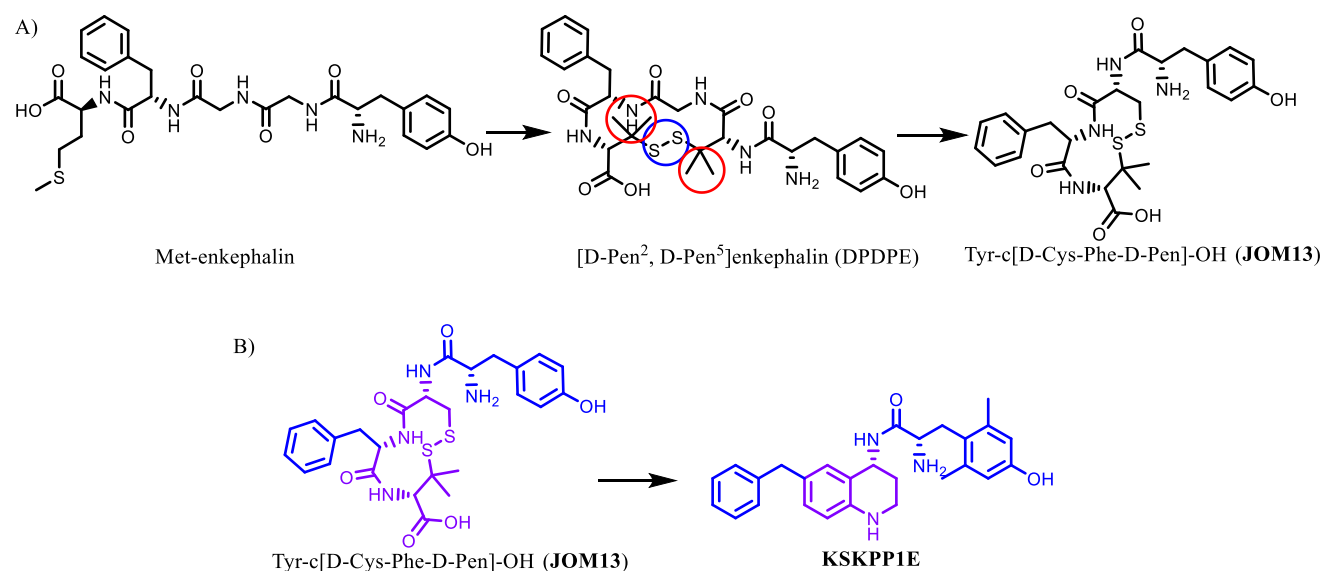


Figure 3: Structural evolution of the endogenous peptide Met-enkephalin into the lead peptidomimetic **KSKPP1E**. A) Initially, a series of SAR studies yielded the cyclic peptide **JOM-13**. Blue circles represent peptide cyclization through a disulfide bond, while red circles indicate the incorporation of gem dimethyl groups to confer additional rigidity. B) **JOM-13** was then used in a series of computational studies that ultimately yielded **KSKPP1E**. The key pharmacophore elements are in blue, whereas the structures holding these elements together are in violet.

Derivatization of **KSKPP1E** was inevitable, especially considering the growing interest in bifunctional opioid ligands and the fact that **KSKPP1E** was found to express antinociceptive effects *in vivo*.⁶¹ Derivatization here followed one of three strategies (**Figure 4A**). The bulk of these analogues were on the benzyl pharmacophore, and in general found that bicyclic pendants here were more potent at MOR and had improved balance in binding affinity between MOR and DOR.^{62–64} Substitutions to the THQ core were found to also enhance binding affinity balance between MOR and DOR without drastic changes in the profile.^{65,66} Here, the N-acetyl modification became standard for this series. These two modifications were also combined into a series of SAR matrices in a recent report.⁶⁷ Finally, a few analogues were synthesized that altered the DMT pharmacophore. These proved to do more harm than good, and therefore further diversification here was not explored.⁶⁸ Two compounds of note came out of these studies (**Figure 4B**). **AAH8**

was found to have the beneficial effects *in vivo* described above, whereas the analogue **AMB47** also expressed *in vivo* antinociception without tolerance, though still produced dependence and constipation.⁴³ The tetrahydroisoquinoline pendant of **AMB47** will become important later in this work.

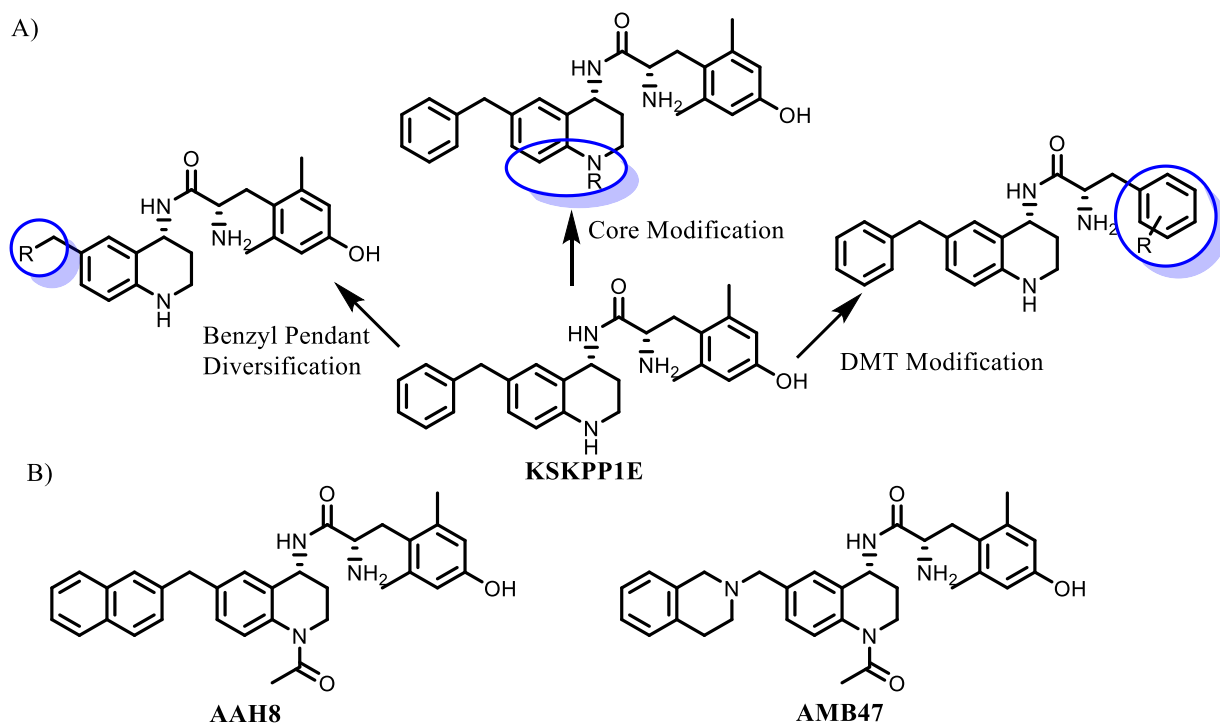


Figure 4: A) Diversification strategies employed to explore the SAR of **KSKPP1E**. Areas explored are in blue rings and include exploration of the benzyl pendant, the THQ core, and the DMT pharmacophore. B) Notable analogues that were produced from this SAR campaign. Shown are **AAH8** and **AMB47**.

1.5 Project Overview

The development of these peptidomimetics thus far has produced some promising compounds. **AAH8** was shown to possess antinociception *in vivo* with reduced side-effects, albeit through intraperitoneal (ip.) administration. However, any drug must possess good pharmacokinetic properties and must be able to be synthesized on a large scale. Patient quality of life must also be a factor, particularly if drugs are taken over a long period of time (such as when

treating chronic pain). As such, enabling oral bioavailability is an important milestone that must be met to convert these peptidomimetics into viable nonaddictive opioid analgesics. In this spirit, we opted to test these compounds in mouse liver microsomes (MLM) as a proxy for their behavior during first-pass metabolism. Unfortunately, these ligands show poor metabolic stability in MLM ($T_{1/2} \sim 5$ min) (**Figure 5**). A tandem MS-MS analysis of **KSKPP1E** identified a total of ten metabolites, six of which involved aromatization of the THQ core (**Figure 6**).

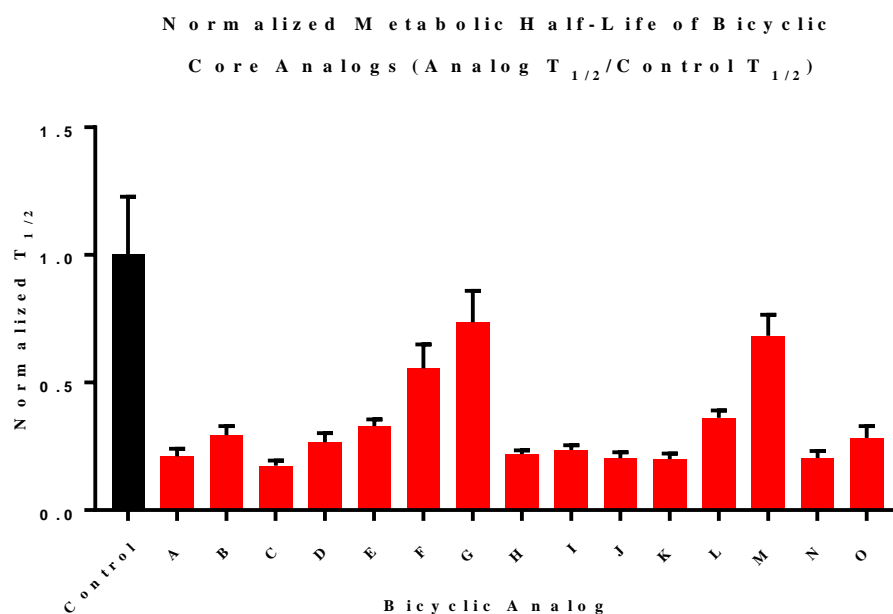


Figure 5: Normalized metabolic half-life of peptidomimetics that contain a THQ core or similar bicyclic core structure. These analogues were normalized to the positive control verapamil (black). None of these bicyclic analogues had a half-life greater than the positive control. The structures of these analogues can be found in the **Appendix**.

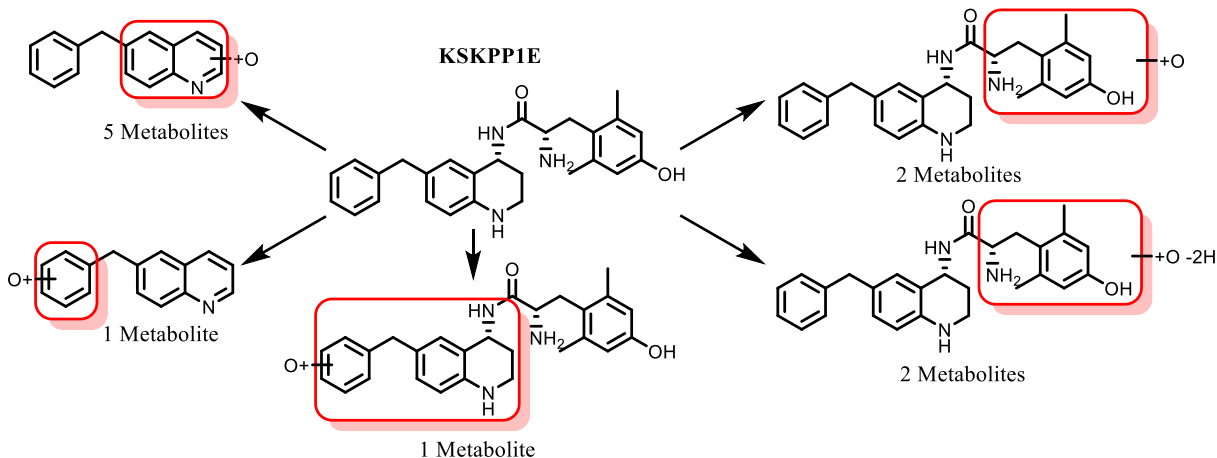
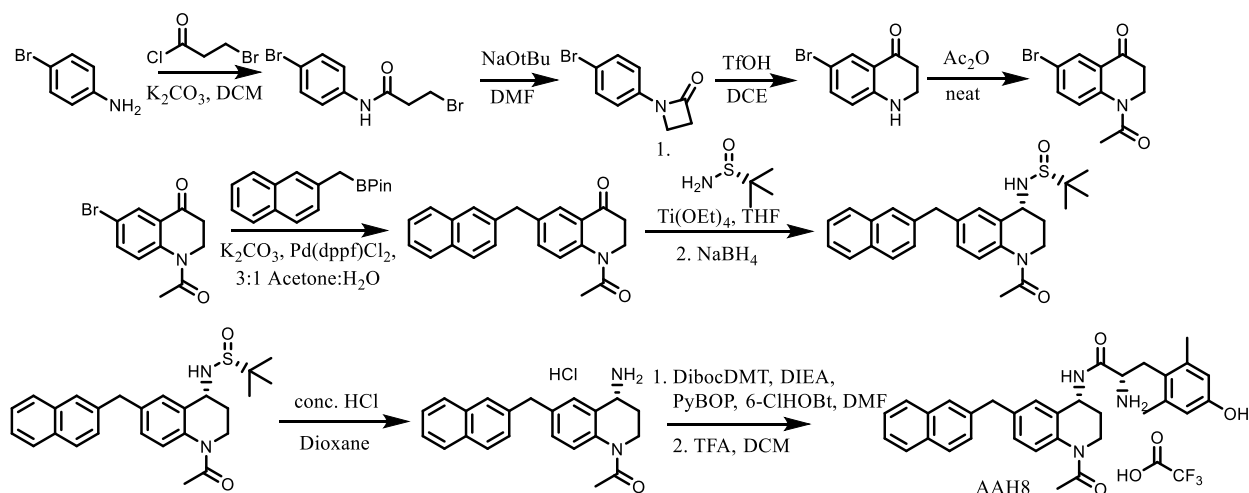


Figure 6: Known metabolites of **KSKPP1E** from MLM. O+ indicates insertion of an oxygen atom into the structure, H- indicates loss of a hydrogen atom. Six metabolites involve aromatization of the THQ core with subsequent bifurcation of the peptidomimetic. Four metabolites involve oxidation of the DMT pharmacophore.

In addition to the metabolic stability issues described above, the synthesis of these analogues requires multiple steps (**Scheme 1**). A total of nine steps are involved in the synthesis of **AAH8**, with a few extra needed to enable further diversification of the benzyl pendant if desired. Notably, the HCl salt of the primary chiral amine formed before coupling to DMT is unstable at room temperature and can aromatize spontaneously if not used quickly. This instability is reflected in the MLM studies described above. This long synthesis, of which most steps involve manipulations of the THQ core, combined with unstable intermediates, produces a synthetic barrier to these peptidomimetics if they are to be made at scale. As such, there is utility in designing our subsequent analogues such that this instability is removed, and the number of synthetic steps is reduced.



Scheme 1: Synthesis of **AAH8**. The synthesis of this analogue requires nine steps and possesses unstable intermediates.

We therefore sought to improve the poor metabolic stability of these ligands, while maintaining the desired bifunctional opioid profile and simplify their synthesis. With this goal in mind, we sought to identify regions that would be most amenable to modifications aimed at improving metabolic stability. Tetrahydroquinolines have been shown to aromatize upon action by CYP2A6 enzymes,⁶⁹ commonly found in mouse liver microsomes, which is supported by our analyses of **KSKPP1E**. Since the THQ core is not one of the two key pharmacophore elements in our series, and since most of the steps of our synthesis involve this structure, we opted to focus our synthetic efforts on simplifying this core.

Chapter 2: Breaking the THQ Core

2.1 Introduction

Given the role of the THQ core to connect the 2'6'-dimethyltyrosine (DMT) and benzyl pharmacophores together, an SAR campaign aimed at transforming this core into a more stable form was pursued. Initially, we sought to remove the aliphatic ring of the THQ system, producing more conformationally flexible ligands while removing the metabolically labile cycle (**Figure 7**). We were encouraged by other opioids that relied on similar strategies to connect these two pharmacophore elements together, such as a urea,¹⁶ piperidine or piperazine,⁷⁰ pyrazinone,⁷¹⁻⁷⁴ alkyl diamine,^{75,76} or long alkyl chains.⁷⁷ In this chapter, the initial SAR campaign that eliminates the bicyclic system of the THQ core to both produce our desired MOR-agonist/DOR-antagonist profile and to improve metabolic stability is discussed. This SAR campaign focused on introducing substituents that comprised the aliphatic ring without cyclization of the structure.

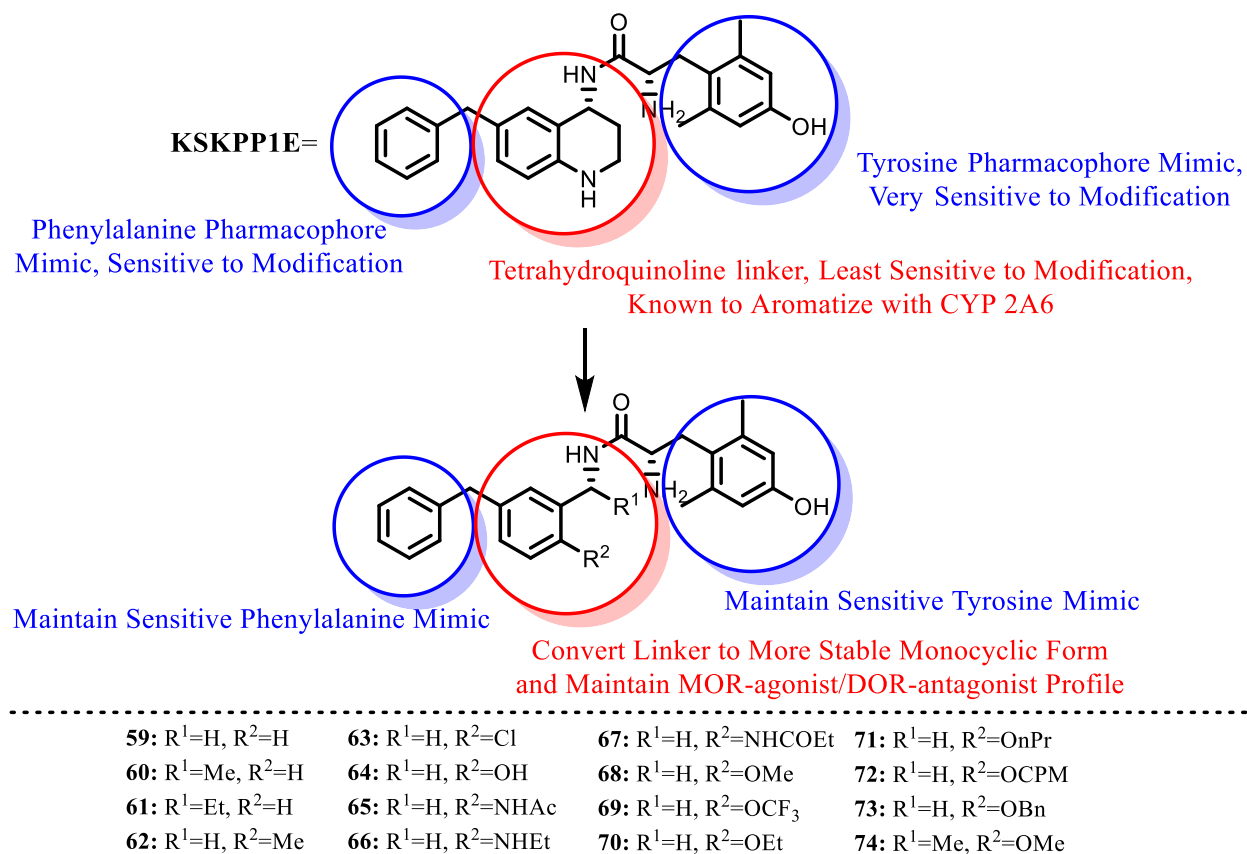


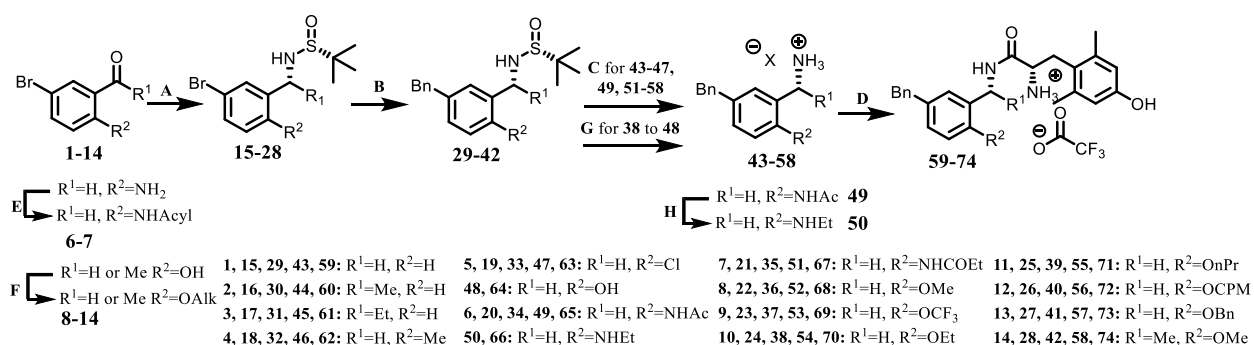
Figure 7: Pharmacophore and linker elements of **KSKPP1E** and our initial monocyclic core series.^{60,61} The pharmacophore elements include 2',6'-dimethyltyrosine and benzyl pendants that are sensitive to modification, and the linker consists of a tetrahydroquinoline core. Here we sought to convert this core to a monocyclic core and pursue derivatives that maintain our desired MOR/DOR profile. Included are new compounds synthesized in this chapter.

2.2 Results

General Chemistry: All the described monocyclic compounds were synthesized according to **Scheme 2**. Before engaging in the main route of synthesis, the ethers and the anilines were diversified. To synthesize functionalized anilines, 2-amino-5-bromobenzaldehyde was subjected to acylation using the appropriate neat anhydride at 100 °C, producing the acetyl and propionyl anilines **6** and **7** respectively. To produce aromatic ethers, 5-bromo-2-hydroxybenzaldehyde was functionalized using an alkyl bromide or iodide, producing the methyl, ethyl, n-propyl, cyclopropyl methyl, and benzyl ethers **8, 10-13**. The exceptions here are trifluoromethoxy ether **9**,

which was purchased, and **14**, which used 1-(5-bromo-2-hydroxyphenyl)ethan-1-one as starting material instead of 5-bromo-2-hydroxybenzaldehyde. The functionalized aromatic bromo ketone or aldehydes **1-14** were then reduced through imine formation with an Ellman's chiral sulfonamide and subsequent reduction with sodium borohydride, producing compounds **15-28**. The Ellman's chiral sulfonamide both enables enantioselective amine formation (if applicable) as used previously,⁶⁴ and protects the amine during subsequent Suzuki coupling to generate compounds **29-42**. This was followed by Ellman deprotection using concentrated HCl and dioxane to produce **43-47, 49, 51-58**. The exception here being the synthesis of the 6-phenol (**48**) which utilized BBr₃ to both remove the Ellman's chiral sulfonamide and cleave the 6-position ether **38**. The ethyl aniline analogue **50** was synthesized by reduction of the acetyl aniline **49** with borane-dimethylsulfide complex (BH₃*Me₂S). Finally, Boc-protected DMT was coupled to the free primary amine of structures **43-58** using PyBOP, followed by removal of the Boc groups using trifluoroacetic acid to yield the final peptidomimetics **59-74**. It should be noted that this synthetic scheme can yield peptidomimetics in six to seven steps as opposed to nine for the bicyclic analogues.

Scheme 2: Synthesis of Substituted Monocyclic Core Analogues 59-74.



A) 1. (R)-(+)-2-methyl-propane-2-sulfinamide, Ti(OEt)₄, THF, 75 °C 2. NaBH₄. B) BnBPIn, K₂CO₃, Pd(dppf)Cl₂, 3:1 Acetone:Water, 80-100 °C. C) HCl conc., Dioxane. D) 1. DiBocDMT, DIEA, PyBOP, 6-Cl-HOBt, DMF. 2. TFA, DCM. E) Neat acyl anhydride, 100 °C. F) MeI or Alk-Br, K₂CO₃, DMF. G) BBr₃, DCM. H) BH₃*Me₂S, THF, 75 °C.

SAR: Our studies began by first probing the structural components of the aliphatic ring of the THQ core. These studies focused on binding affinity, efficacy, and potency at MOR and DOR, though the κ -opioid receptor (KOR) was also examined to determine compound selectivity. The binding affinity data can be found in **Table 2**, whereas the efficacy and potency data can be found in **Table 3** (see footnotes of each table for how these values were measured). Initially, all substituents and functional groups comprising this aliphatic ring were removed, yielding **59**. This conversion had little effect on binding affinity compared to the original lead **KSKPP1E** but had a significant effect on relative efficacy. Indeed, **59** did not stimulate any of the three classical opioid receptors.

We then began to restore different portions of the original aliphatic ring to elucidate the importance of each component. The incorporation of short linear alkyl chains (**60-61**) on the benzylic position (R^1) connecting the aromatic core to the DMT pharmacophore partially restored MOR agonism (41 % stimulation for compound **60**). In this case, the methyl group (**60**) was superior to an ethyl group (**61**), however MOR efficacy was less than that of morphine (57 % stimulation), which serves here as a benchmark for MOR activity. It should be noted that morphine's intrinsic activity of 57 % should not be interpreted as poor MOR efficacy, only that the standard agonist DAMGO in this assay has exceptional efficacy. DOR affinity was found to decrease when these alkyl chains are incorporated, though these compounds still did not stimulate DOR. KOR binding improved with increasing chain size, and weak KOR agonism was observed with both alkyl groups.

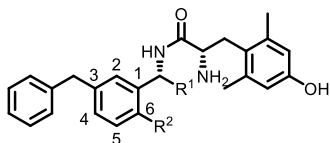
In parallel with the analogues described above, an assortment of compounds was made with functional groups at the 6-position, matching that of the THQ nitrogen. Initially, a few simple substituents were incorporated at this position. These included methyl, chloro, and hydroxy groups (**62-64**). Each of these managed to restore MOR agonism to between 17 % and 39 %, but still fell

short of our goal. None of these ligands produced agonism at DOR, though the hydroxyl group (**64**) significantly reduced the binding at DOR compared to **59**.

A small number of nitrogen containing substituents were also incorporated at the 6-position, resulting in ethyl, acetyl, and propionyl anilines (**65-67**). These were made to mimic the substituents of the original THQ core without ring cyclization, or to mimic some N-acyl compounds that had utility in our previously reported THQ series.⁶⁵ These ligands were all weak partial MOR agonists and had reduced binding affinity at DOR compared to **59**. The ethyl aniline also displayed reduced affinity at MOR.

Several ethers were examined due to their synthetic accessibility, their ability to be rapidly diversified, and to probe the effect of hydrogen bond acceptors at the 6-position. The alkyl ethers included methyl, trifluoromethyl, ethyl, n-propyl, cyclopropyl methyl (CPM), and benzyl (**68-73**). Here, an activity maximum was observed between the ethyl ether (**70**), and the n-propyl ether (**71**). Both ethers proved to be more potent than morphine and displayed similar levels of efficacy to morphine at MOR. This, in combination with the high DOR affinity and the lack of DOR efficacy of these two compounds, demonstrates that these monocyclic core compounds can retain our desired *in vitro* profile.

A final compound was synthesized to determine if a combination of R¹ and R² substituents could yield additive effects. To this end, **74** was synthesized, in which R¹=-Me and R²=-OMe. These substituents were selected as they have the same number of large atoms as the original THQ core, while also utilizing the more desirable ethers. When compared to **60**, this compound appears to have reduced binding affinity, efficacy, and potency at MOR. DOR binding, however, shows a modest improvement over **60**, and **74** retains an antagonist profile at DOR.



Binding Affinity, K_i (nM)

Selectivity

Name	-R ¹	-R ²	MOR	DOR	KOR	MOR:DOR:KOR
KSKPPIE	-CH ₂ CH ₂ NH-		0.22±0.02 ^a	9.4±0.8 ^a	68±2 ^a	1:43:309
Morphine	-	-	6.3±2.5 ^b	171±19 ^b	61±17 ^b	1:27:9.7
59	H	H	1.0±0.2	14.7±0.6	410±47	1:15:410
60	Me	H	1.1±0.3	46±10	201±36	1:42:180
61	Et	H	3.2±0.6	61±10	49.5±1.7	1:19:15
62	H	Me	5.2±0.9	33.9±4.9	360±60	1:6.5:69
63	H	Cl	5.6±0.8	38.1±3.9	528±49	1:6.8:94
64	H	OH	9.5±0.5	175±26	307±34	1:18:32
65	H	NHAc	7.9±1.1	387±31	1550±130	1:49:200
66	H	NHEt	23.5±6.5	63.8±5.2	408±54	1:2.7:17
67	H	NHCOEt	4.2±1.1	108±27	1090±290	1:26:260
68	H	OMe	3.6±0.1	21.5±4.5	610±100	1:6.0:170
69	H	OCF ₃	1.4±0.5	7.3±0.5	370±83	1:5.2:260
70	H	OEt	2.8±0.5	23.8±3.3	1180±120	1:8.5:420
71	H	OnPr	0.91±0.06	5.3±1.0	390±150	1:5.8:430
72	H	OCPM	2.7±0.6	13.9±1.8	319±51	1:5.1:120
73	H	OBn	8.0±1.5	70.4±5.4	575±80	1:8.8:71
74	Me	OMe	8.0±0.8	6.8±1.1	330±150	1:0.85:41

Table 2: Binding affinity of the benzylic core compounds at MOR, DOR, and KOR. Binding affinities (K_i) were obtained by competitive displacement of radiolabeled [³H] diprenorphine in membrane preparations. Included are morphine and the original lead peptidomimetic (**KSKPPIE**) for comparison. All data were from three separate experiments, performed in duplicate. These data are reported as the average ± standard error of the mean. Selectivity was calculated by dividing the K_i of each receptor by the K_i at MOR for a given compound. DNS=Does Not Stimulate. ^aFrom Reference⁶⁰. ^bFrom Reference⁷⁸.

<i>Name</i>	<i>Potency, EC₅₀ (nM)</i>					<i>Efficacy, (% Stimulation)</i>		
	-R¹	-R²	MOR	DOR	KOR	MOR	DOR	KOR
<i>KSKPPIE</i>	-CH ₂ CH ₂ NH-		1.6±0.3 ^a	110±6 ^a	540±72 ^a	81±2 ^a	16±2 ^a	22±2 ^a
<i>Morphine</i>	-	-	194±21 ^b	>593 ^c	DNS	57±5 ^b	>30 ^c	DNS
59	H	H	DNS	DNS	DNS	DNS	DNS	DNS
60	Me	H	44.4±7.5	DNS	>1700	41±12	DNS	>40
61	Et	H	158±17	DNS	2200±500	15.0±2.6	DNS	26.6±3.0
62	H	Me	111±29	DNS	DNS	21.9±5.3	DNS	DNS
63	H	Cl	250±24	DNS	DNS	39.2±1.0	DNS	DNS
64	H	OH	552±90	DNS	DNS	17.0±1.1	DNS	DNS
65	H	NHAc	117±13	DNS	DNS	32.5±2.6	DNS	DNS
66	H	NHEt	156±20	DNS	>2440	25.9±5.8	DNS	>40
67	H	NHCOEt	84±26	DNS	>4000	28.7±7.1	DNS	>35
68	H	OMe	264±21	DNS	DNS	37.2±1.7	DNS	DNS
69	H	OCF ₃	342±80	DNS	DNS	45.0±6.1	DNS	DNS
70	H	OEt	77±10	DNS	DNS	65.9±5.2	DNS	DNS
71	H	OnPr	68±10	DNS	DNS	54.9±4.0	DNS	DNS
72	H	OCPM	71±13	DNS	DNS	37.5±1.3	DNS	DNS
73	H	OBn	107±19	DNS	DNS	34.7±3.8	DNS	DNS
74	Me	OMe	296±69	DNS	DNS	20.2±1.4	DNS	DNS

Table 3: Potency and efficacy of benzylic core compounds at MOR, DOR, and KOR. These data were obtained using agonist induced stimulation of [³⁵S] GTPγS binding. Potency is represented as EC₅₀ (nM) and efficacy as percent maximal stimulation relative to standard agonist DAMGO (MOR), DPDPE (DOR), or U69,593 (KOR) at 10 μM. Included are morphine and the original lead peptidomimetic (**KSKPPIE**) for comparison. All data were from three separate experiments, performed in duplicate. These data are reported as the average ± standard error of

the mean. DNS=Does Not Stimulate. ^aFrom Reference⁶¹. ^bFrom Reference⁷⁹. ^cTested against human DOR.

With regards to KOR, most of the ligands express a reduced binding affinity at this receptor compared to **KSKPP1E**, with the exception of **61**. Similarly, only **61**, **66**, and **67** were shown to have weak KOR efficacy; the rest have no efficacy at this receptor. Since we were interested in balancing the binding affinity between MOR and DOR, and since we were screening KOR for selectivity, we calculated binding ratios between MOR, DOR, and KOR normalized to MOR. Most of these ligands synthesized here show an improved balance between MOR and DOR than that of the lead compound **KSKPP1E**, the exception being **65**. The greatest balance can be found with various functional groups at the R²-position, namely the methyl (**62**), chloro (**63**), ethyl aniline (**66**), and all the ethers (**68-74**). When comparing MOR and KOR for selectivity, only the unfunctionalized compound **59**, and the ethyl (**70**) and n-propyl (**71**) ethers exhibited greater selectivity than **KSKPP1E**.

Antagonist Potency of Representative Analogues: Finally, while analogues displaying reasonably high DOR affinity (~20 nM or less) and no DOR efficacy are presumptive DOR antagonists, this was tested explicitly for **70**, **71**, and **72**. DOR antagonism was confirmed for all three analogues, which induced rightward shifts in the EC₅₀ of the standard DOR agonist DPDPE that equated to K_e values of 20.2 nM, 7.4 nM, and 20.5 nM, respectively (calculated as described in Methods). These values are very similar to the K_i's of these ligands shown in **Table 2**. The only exception here is analogue **72**, which has a K_i approximately half of the K_e at a value of 13.9 nM.

Metabolic Stability: In tandem with the opioid SAR acquired above, the metabolic stability of these monocyclic core compounds was characterized in mouse liver microsomes (MLM) (**Table 4**) using verapamil as the positive control. Because of the variability between the measures of metabolic half-life for verapamil (from 13.8 to 22.6 min) in the different assay preparations, the

ratio of $T_{1/2}$ for the compound and verapamil was calculated as a stability ratio. This was to ensure consistent comparisons between different analogues.

<i>Name</i>	<i>R¹</i>	<i>R²</i>	<i>T_{1/2} (min)</i>	<i>Verapamil T_{1/2} (min)</i>	<i>Stability Ratio</i>	<i>cLogP</i>
KSKPPIE	CH ₂ CH ₂ NH		3.1±0.1	14.7±2.0	0.21±0.03	3.74
59	H	H	13.0±2.6	14.6±1.0	0.89±0.19	4.30
60	Me	H	8.5±0.8	22.6±1.4	0.38±0.04	4.61
61	Et	H	4.1±0.2	13.8±1.6	0.29±0.04	5.14
62	H	Me	12.2±0.0	22.6±1.4	0.54±0.03	4.75
63	H	Cl	16.3±2.5	22.6±1.4	0.72±0.12	5.01
64	H	OH	15.4±1.3	14.4±1.0	1.1±0.1	3.58
65	H	NHAc	10.2±0.4	14.4±1.0	0.71±0.06	2.45
66	H	NHEt	12.1±1.5	22.6±1.4	0.54±0.07	4.33
68	H	OMe	19.7±2.0	13.8±1.6	1.4±0.2	4.22
69	H	OCF ₃	5.7±0.0	14.6±1.0	0.39±0.03	5.33
70	H	OEt	23.7±5.9	14.6±1.0	1.6±0.4	4.75
71	H	OnPr	33.1±2.8	19.6±2.3	1.7±0.2	5.28
72	H	OCPM	56±10	22.6±1.4	2.5±0.5	5.19
73	H	OBn	15.6±0.1	22.6±1.4	0.69±0.04	5.99
74	Me	OMe	4.3±0.0	14.6±1.0	0.30±0.02	4.53

Table 4: Metabolic stability of benzylic core compounds in MLM. Included are the compound half-life ($T_{1/2}$), the half-life of the positive control verapamil, and the stability ratio between the compound and the positive control. The stability ratio was calculated by dividing the half-life of the analogue of interest by the half-life of the positive control in that assay. Individual compounds were tested once, with errors representing the SE in the decay curve regressed onto the data collected in 15-minute intervals. Finally, the cLogP of these analogues are included and were calculated using PerkinElmer's ChemDraw® Professional Software.

To evaluate the improvement in stability of these compounds, the original lead compound **KSKPP1E** is included in **Table 4**. This compound displays the poorest metabolic stability, with a ratio of 0.21 compared to verapamil and is characteristic of the other THQ containing analogues in our previously reported series. Stripping away the substituents that make up the aliphatic portion of the tetrahydroquinoline ring (**59**) improves the ratio 4-fold to 0.89. However, introducing alkyl chains off this benzylic position (R^1 , **60-61**) reduces the stability of these compounds back to that of **KSKPP1E**.

Next, we examined our analogues at the 6-position (R^2). The small substituents at this position (**62-64**) did not improve the stability of these compounds, even though some of these modifications are polar (which would reduce $cLogP^{80}$) or are electron withdrawing groups (which would inhibit free radical formation during the CYP catalytic cycle). This also extends to the acetyl and ethyl anilines (**65-66**), in which no improvements were observed.

The ethers (**68-73**), generally produced significant improvements in metabolic stability. This is particularly true for cyclopropyl methyl ether (**72**), which was x2.5 more stable than verapamil, reflecting a half-life of 56 minutes. This was not true of all the ethers however, as the trifluoromethyl ether (**69**) showed lower stability levels than **59**. Finally, the hybrid analogue **74** had low stability, similar to compound **60**.

Molecular Modeling: To complement the *in vitro* data acquired thus far, molecular modeling studies were performed to dock compound **70** to MOR (**Figure 8**) with the goal of explaining the acquired MOR-agonism in this ligand. Instead of the ethyl ether orienting itself to mimic the structure of the original THQ core, it instead appears to wedge itself between His54 and Tyr148 in the active state of MOR. Here the ethyl group of the ether appears to interact with the imidazole ring of His 54 and the hydroxyl of Tyr148.

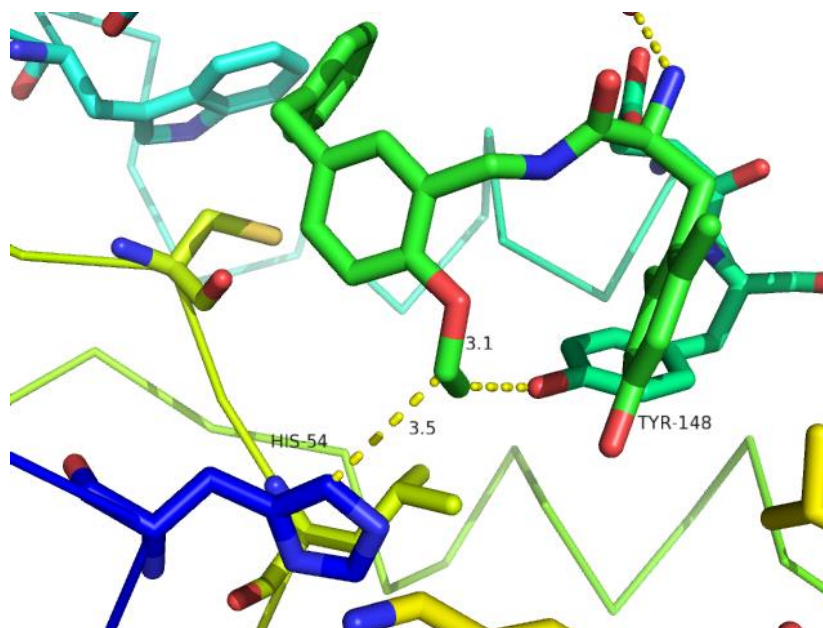


Figure 8: Molecular modeling of analogue **70** at MOR. His54, Tyr148 are labelled and their distance from the ethyl group is shown.

2.3 Discussion and Conclusions

SAR: Using **KSKPP1E** as a baseline, it appears that moving to **59** causes a loss in MOR-agonism and affinity. This can in part be explained by increased conformational flexibility that occurs upon elimination of the aliphatic portion of the tetrahydroquinoline ring. This activity can be restored through the introduction of small alkyl chains at the benzylic position (**60-61**), likely due to steric interactions with the receptor that **KSKPP1E** would also possess.

Introducing the methyl, chloro, or hydroxy group to the 6-position of the benzylic core (**62-64**) produced partial MOR-agonism compared to **59**. The hydroxyl group (**64**) was the least potent and efficacious of the three, suggesting that either an electron donating group on the benzylic core or a hydrogen bond donor at the 6-position interferes with the ability of substituents at this position to activate MOR. This trend is also seen with binding affinity at DOR, as the hydroxy substituent possesses the lowest affinity. The chloro substituent (**63**) is similar to the methyl (**62**) substituent

in its activity at the three receptors, and differed only from **62** in that it had twice the efficacy at MOR. This reinforces the electronics argument, as the chloro group is more electron withdrawing than the methyl group due to induction.

The 6-position ethers produced some of the most promising ligands in this series. These ligands generally had high MOR and DOR affinity, except for the benzyl ether at DOR (**73**). However, the potency and efficacy of these compounds at MOR vary greatly. The optimum here appears to be with the ethyl (**70**) and n-propyl (**71**) ethers, which proved comparable to morphine in efficacy and potency. This is particularly interesting when these data are compared to the 6-anilines (**65-67**) and the 6-hydroxyl (**64**), as they suggest that the hydrogen bond donor present in these latter compounds is detrimental for MOR efficacy, rather than the presence of electron donating groups. The orientation of the hydrogen bond donor may be important, as the lead compound **KSKPP1E** displays high MOR efficacy. From the data illustrated in compounds **65-67**, it appears that orientating the hydrogen bond donor toward the DMT pendant is detrimental to MOR agonism. Since these ethers also antagonize DPDPE, these data suggest that the small chain ethers are best for producing our desired MOR-agonist/DOR-antagonist profile.

It should be noted that the ethers **70** and **71** do not possess the level of potency or efficacy at MOR as the original lead compound **KSKPP1E**. Since we are ultimately interested in determining if MOR-agonist/DOR-antagonist ligands are suitable for use as opioid analgesics without abuse liabilities, the stability improvements of **70** and **71** represents a necessary developmental step toward this end. This is particularly true considering the instability of the THQ core compounds such as **KSKPP1E**. However, **70** and **71** have improved potency and similar efficacy at MOR compared to morphine, which is the classic opioid analgesic. As such, sacrificing

some potency and efficacy at MOR to improve some pharmacokinetic parameters is worthwhile, especially if they still perform better than morphine *in vitro*.

The hybrid compound **74** is also notable due to its poor MOR efficacy and potency. While the potency of this compound was akin to the simple 6-OMe precursor (**68**), the efficacy here was less than either precursor analogue **60** and **68**. This suggests that steric effects within the ligand may be detrimental to activation of MOR, a problem that vanishes when these two groups are tied together in the bicyclic ring of the original THQ core.

With regards to selectivity, two notable trends can be observed. Selectivity for MOR over KOR can be reduced compared to our original lead **KSKPP1E** through two different means. Extending alkyl chains off the benzylic position (R^1 , **60-61**) do this largely through improving KOR binding and max out with the ethyl group (**61**) in this series, whereas some substituents containing a hydrogen bond donor off the 6-position (R^2), namely the hydroxyl (**64**) and ethyl aniline (**66**) do this through reduced MOR binding. Conversely, the ethyl and n-propyl ethers (**70**, **71**) show the best selectivity over KOR, largely due to reduced KOR binding compared to **KSKPP1E**. While almost all of our compounds show improved MOR/DOR affinity balance, possibly due to elimination of the bicyclic ring system, all of our ethers (**68-74**) are among those that have the best balance. Overall, the ethers **70** and **71** show the best selectivity over KOR, and are among the best compounds that balance MOR and DOR.

Metabolic Stability: Stripping away all the components of the THQ core (**59**) produced a 4-fold improvement in metabolic stability over **KSKPP1E**. When incorporating alkyl chains onto the benzylic position (**60-61**, and **74**), this improvement is lost, suggesting that this benzylic position in both this series and in the original THQ series is a metabolic hot spot. This is consistent with the mechanism of CYP metabolism, namely that the benzylic methylene present in compounds **60-**

61, and **74** can greater stabilize the radical formed upon interaction with the enzyme than can the methylene alone. Simple chloro (**63**) and hydroxyl (**64**) functional groups at the 6-position were no different than the unfunctionalized system (**59**). The ethers (**68-73**), apart from the trifluoro (**69**) and benzyl (**73**) ethers, displayed the greatest levels of stability, reaching stability ratios of 2.5 and half-lives near an hour, as determined for **72**.

Interestingly, these ethers were more stable than the functionalized anilines, despite their greater cLogP, which is commonly associated with reduced stability.⁸⁰ Nitrogen is a better electron donating substituent than oxygen. As such, these nitrogens may further stabilize metabolism at the adjacent benzylic positions on the aromatic ring than would the oxygens of the ethers. Notably, the most stable ether contained a cyclopropyl moiety. This can likely be attributed to a combination of steric effects, and ring strain, as the cyclopropyl group can both block metabolism at adjacent positions (which is also possible with most of the other ethers) and the ring strain destabilizes free radical formation on the cyclopropyl group itself.

Fortunately, the SAR regarding the restoration of our MOR-agonist/DOR-antagonist profile overlapped with the SAR aimed at improving metabolic stability. This suggests that these 6-position ethers are a promising new direction for the development of these peptidomimetics. As such, our future derivatization of these analogues will follow the lead provided by these promising ethers.

Molecular Modeling: The ethyl ether of analogue **70** wedges itself between His54 and Tyr148. This may force the ligand to adopt a conformation within the receptor that enables activation of MOR. However, it is the alkyl chain that is interacting with these two residues in the receptor, not the ether itself. This may explain the reduced potency of this analogue compared to **KSKPP1E**, as the lipophilic alkyl chain does not produce an ideal interaction with the polar imidazole of His

54 and the polar hydroxyl of Tyr148. As such, replacement of the ethyl group with substituents that are more polar may be of value. Regardless, the potency of this ligand is still better than morphine, and it may be better to keep pursuing stability instead of exploring this position.

It should be noted that the oxygen of the ether does not appear to interact with MOR, yet when replaced with a nitrogen as in analogue **66**, a 40 % loss in efficacy is observed. While docked structures of **66** to MOR are not available, presumably the ethyl group in **66** would orient itself in the same manner as the ethyl group of **70**. This would leave the hydrogen bond donor of the aniline pointing toward the aromatic ring of the DMT residue instead of a hydrogen bond acceptor in the ether. This could produce an intramolecular polar- π interaction within **66** that prevents the ligand from assuming a conformation that can activate MOR.

Conclusion: The results presented here show that the metabolically labile THQ core can be changed to a monocyclic core to improve metabolic stability. Initial modification of the simplified benzyl core yielded analogues (**70** and **71**) which display similar potency and efficacy as morphine at MOR, are antagonists at DOR, possess a more balanced affinity between MOR and DOR, are more selective over KOR, and show improved metabolic stability in mouse liver microsome assays compared to our original THQ core ligands. These monocyclic compounds represent an attractive new direction through which more stable MOR-agonist/DOR-antagonist ligands may be developed. The work in this chapter was recently published in the Journal of Medicinal Chemistry.⁸¹

2.4 Experimental

Chemistry

General Methods: All reagents and solvents were obtained commercially and were used without further purification. Intermediates were purified by flash chromatography using a Biotage Isolera One instrument. Most purification methods utilized a hexanes/ethyl acetate solvent system in a Biotage SNAP KP-Sil column, with a linear gradient between 0 and 100% ethyl acetate. Reverse phase column chromatography using a linear gradient of 0 % to 100 % solvent B (0.1 % TFA in acetonitrile) in solvent A (0.1 % TFA in water) using a Biotage SNAP Ultra C18 column was utilized for some intermediate amine salts. Purification of final compounds was performed using a Waters semipreparative HPLC with a Vydac protein and peptide C18 reverse phase column, using a linear gradient of 0 % to 100 % solvent B in solvent A at a rate 1 % per minute, monitoring UV absorbance at 230 nm. The purity of final compounds was assessed using a Waters Alliance 2690 analytical HPLC instrument with a Vydac protein and peptide C18 reverse phase column. A linear gradient (gradient A) of 0 % to 70 % solvent B in solvent A in 70 min, measuring UV absorbance at 230 nm was used to determine purity. All final compounds used for testing were ≥ 95 % pure, as determined by analytical HPLC. ^1H NMR and ^{13}C NMR data were obtained on a 500 or 400 MHz Varian spectrometer using CDCl_3 or CD_3OD solvents. The identities of final compounds were verified by mass spectrometry using an Agilent 6130 LC-MS mass spectrometer in the positive ion mode, or an Agilent 6230 TOF HPLC-MS in the positive ion mode. Suzuki couplings using microwave irradiation were performed on a Discover S-class (CEM) microwave in a closed vessel with maximum power input of 300 W and temperature set to 100 °C for 30 min under the standard method using their Synergy software.

General Procedure for Ellman Reductions (Procedure A): A flamed-dried round bottom flask containing 1 equivalent of aldehyde or ketone and 3 equivalents of (R)-(+)-2-methylpropane-2-sulfinamide was attached to a reflux condenser and flushed with argon. 4 mL of THF was added and cooled to 0 °C. 6 or 7.5 equivalents of titanium (IV) ethoxide was added, followed by an additional 4 mL of THF. The solution was stirred and heated to 75 °C overnight with TLC monitoring until all ketone or aldehyde was consumed. A separate flame-dried flask containing 6 equivalents of sodium borohydride was flushed with argon. 4 mL of THF was added, at which point the solution was cooled to -78 °C. The solution containing Ellman adduct was cooled to room temperature and slowly transferred to the sodium borohydride solution via syringe. This final solution was then allowed to warm to room temperature and stirred for 2 hours, at which point the reaction mixture was quenched with methanol to consume the sodium borohydride, followed by DI water to precipitate the titanium. The solution was vacuum filtered, and the precipitate was washed with ethyl acetate. The filtrate was then concentrated in vacuo and purified via column chromatography (0-100 % EtOAc in Hexanes).

General Procedure for Suzuki Couplings Using Microwave Irradiation (Procedure Ba): To a microwave vessel containing the protected amine was added 2 equivalents of benzylboronic acid pinacol ester, 3 equivalents of potassium carbonate, and 0.1 equivalents of 1,1'-Bis(diphenylphosphino)ferrocene] dichloropalladium. The vessel was purged with argon and 2.5 mL of degassed 3:1 acetone:water was added. The vessel was then subject to microwave irradiation to a temperature of 100 °C for 30 min. The solution was cooled, partitioned between brine and ethyl acetate, and extracted with ethyl acetate. The organic layer was then dried with magnesium sulfate, filtered, and concentrated in vacuo. Column chromatography was then performed (0-100 % ethyl acetate in hexanes), yielding the desired Suzuki coupled derivatives.

General Procedure for Suzuki Couplings without Microwave Irradiation (Procedure Bb):

To a round bottom flask containing protected amine, 2 equivalents of potassium carbonate, and 0.1 equivalents of 1,1'-Bis(diphenylphosphino)ferrocene] dichloropalladium was added 2.5 equivalents of benzylboronic acid pinacol ester. The flask was equipped with a reflux condenser, purged with argon, and 5 mL of degassed 3:1 acetone:water was added. The vessel was then heated to a temperature of 80 °C overnight. The solution was cooled, partitioned between brine and ethyl acetate, and extracted with ethyl acetate. The organic layer was then dried with magnesium sulfate, filtered, and concentrated in vacuo. Column chromatography was then performed (0-100 % ethyl acetate in hexanes), yielding the desired Suzuki coupled derivatives.

General Procedure for Removal of Ellman's chiral sulfonamide (Procedure C): To a flask containing Ellman protected amine was added 2 mL of Dioxane and 0.2 mL concentrated HCl. The solution was stirred at room temperature for 1 minute and concentrated in vacuo. The ensuing salt was then purified via one of two methods. If the product is insoluble in diethyl ether, it was triturated with diethyl ether, and the precipitate was concentrated in vacuo to dryness, yielding the product as an HCl salt. If the product was soluble in diethyl ether, it was purified using a reverse phase chromatography (0-100% B in A), yielding the product as a TFA salt.

General Procedure for the Coupling of 2',6'-Dimethyltyrosine to Functionalized Amine Salt (Procedure D): To a dried flask containing the amine salt under argon was added 3 mL of DMF and 10 equivalents of Hunig's base. 1 equivalent of PyBOP and 1 equivalent of 6-Cl-HOBt was added, followed by 1 equivalent of N-Boc-O-Boc-2',6'-dimethyl-L-tyrosine in 1.5 mL DMF. The solution was stirred overnight at room temperature and concentrated in vacuo. 2 mL of TFA and 2 mL of DCM were then added, and the solution was stirred for an additional hour. The

reaction mixture was concentrated in vacuo and purified via semipreparative reverse phase HPLC (0.1% TFA in water: 0.1% TFA in acetonitrile). The product was concentrated in vacuo and lyophilized overnight to yield the final peptidomimetic.

General procedure for the acylation of 2-amino-5-bromobenzaldehyde (Procedure E): To a dried flask containing 2-amino-5-bromobenzaldehyde under argon was added neat acyl anhydride. The reaction was stirred overnight at 100 °C and concentrated in vacuo. The product was then partitioned between sat. NaHCO₃ and DCM. The compound was extracted with DCM, filtered, and concentrated in vacuo yielding the desired acylated compound.

General Procedure for the Synthesis of 6-position Ethers (Procedure F): To a flame dried flask containing phenolic aldehyde or ketone was added 3 equivalents of potassium carbonate. The flask was purged with argon and 4 mL of DMF was added. 3 equivalents of an alkyl iodide or bromide was then added, and the solution was stirred at room temperature overnight. The solution was then concentrated in vacuo, partitioned between ethyl acetate and saturated sodium bicarbonate, and extracted with ethyl acetate. The organic layers were combined, dried with magnesium sulfate, filtered, and concentrated in vacuo, yielding the desired ether.

General procedure for the Cleavage of Phenolic Ethers (Procedure G): To a flame dried flask containing 1 equivalent of phenolic ether under argon was added 5 mL DCM and 3.0 equivalents of 1M BBr₃ in DCM was added dropwise. The solution was stirred at room temperature for 4 hours and quenched with methanol. The solution was concentrated in vacuo, suspended in diethyl ether, and filtered. The precipitate was then dissolved in methanol and filtered. The product in methanol was then concentrated in vacuo, yielding the desired phenol.

General procedure for the Reduction of Acyl Anilines (Procedure H): To a dried flask containing the desired acyl aniline under argon was added 2M BH₃*Me₂S in THF and additional THF. The solution was heated to 75 °C for 3 hours, at which point the solution was quenched with methanol and stirred an additional 15 minutes at 75 °C. The solution was cooled, concentrated in vacuo, yielding the reduced alkyl aniline.

N-(4-bromo-2-formylphenyl)acetamide (6): See Procedure E: 74 mg (0.37 mmol) of **2-amino-5-bromobenzaldehyde**, and 3 mL of acetic anhydride. The compound was purified after aqueous workup via column chromatography (0-10% ethyl acetate in hexanes) to produce compound **6** (59 mg, 65.9 % yield) which was isolated as an orange solid. ¹H NMR (500 MHz, Chloroform-*d*) δ 11.00 (br s, 1H), 9.84 (s, 1H), 8.65 (d, *J* = 8.9 Hz, 1H), 7.76 (d, *J* = 2.4 Hz, 1H), 7.67 (dd, *J* = 9.0, 2.4 Hz, 1H), 2.24 (s, 3H). ¹³C NMR (126 MHz, Chloroform-*d*) δ 194.22, 169.53, 139.84, 138.80, 137.98, 122.78, 121.70, 114.91, 25.38.

N-(4-bromo-2-formylphenyl)propionamide (7): See Procedure E: 98 mg (0.49 mmol) of **2-amino-5-bromobenzaldehyde**, and 3 mL of propionic anhydride. Compound **7** (113 mg, 90.1 % yield) was isolated as an orange solid. ¹H NMR (500 MHz, Chloroform-*d*) δ 11.00 (s, 1H), 9.81 (s, 1H), 8.65 (d, *J* = 9.0 Hz, 1H), 7.72 (d, *J* = 2.5 Hz, 1H), 7.64 (dd, *J* = 9.0, 2.4 Hz, 1H), 2.46 (q, *J* = 7.6 Hz, 2H), 1.24 (t, *J* = 7.6 Hz, 3H). ¹³C NMR (126 MHz, Chloroform-*d*) δ 194.21, 173.28, 139.94, 138.75, 137.95, 122.83, 121.70, 114.71, 31.48, 9.33.

5-bromo-2-methoxybenzaldehyde (8): See Procedure F: 157 mg (0.78 mmol) of **5-bromosalicylaldehyde**, 320 mg (2.3 mmol, 3.0 eq.) of K₂CO₃, 150 μL (342 mg, 2.4 mmol, 3.1 eq) of MeI, 3 mL of DMF. Compound **8** (170 mg, Quantitative Yield) was isolated as a yellow solid. ¹H-NMR (400MHz, CDCl₃) δ 10.34 (s, 1H), 7.86 (d, *J*=2.3 Hz, 1H), 7.58 (dd, *J*=8.9, 2.3 Hz,

1H), 6.86 (d, $J=8.9$ Hz, 1H) 3.89 (s, 3H); ^{13}C -NMR (101 MHz, CDCl_3) δ 183.3, 169.7, 138.3, 130.9, 126.0, 113.7, 113.4, 56.0.

5-bromo-2-ethoxybenzaldehyde (10): See Procedure F: 451 mg (1.5 mmol) of **5-bromosalicylaldehyde**, 608 mg (4.4 mmol, 3.0 eq.) of K_2CO_3 , 330 μL (482 mg, 4.4 mmol, 3.0 eq.) of EtBr, 4 mL of DMF. Compound **10** (495 mg, 96.3 % yield) was isolated as a white solid. ^1H NMR (400 MHz, Chloroform- d) δ 10.36 (s, 1H), 7.85 (d, $J = 2.6$ Hz, 1H), 7.55 (dd, $J = 8.8, 2.6$ Hz, 1H), 6.83 (d, $J = 8.9$ Hz, 1H), 4.10 (q, $J = 7.0$ Hz, 2H), 1.44 (t, $J = 7.0$ Hz, 3H). ^{13}C NMR (101 MHz, Chloroform- d) δ 188.4, 160.2, 138.2, 130.7, 126.0, 114.5, 113.2, 64.6, 14.5.

5-bromo-2-propoxybenzaldehyde (11): See Procedure F: 123 mg (0.61 mmol) of **5-bromosalicylaldehyde**, 251 mg (1.8 mmol, 3.0 eq.) of K_2CO_3 , 160 μL (217 mg, 1.8 mmol, 2.9 eq.) of $n\text{PrBr}$, 4 mL of DMF. Compound **11** (155 mg, Quantitative Yield) was isolated as a white waxy solid. ^1H NMR (400 MHz, Chloroform- d) δ 10.41 (s, 1H), 7.89 (d, $J = 2.6$ Hz, 1H), 7.58 (dd, $J = 8.9, 2.6$ Hz, 1H), 6.86 (d, $J = 8.9$ Hz, 1H), 4.01 (t, $J = 6.4$ Hz, 2H), 1.86 (h, $J = 7.3$ Hz, 2H), 1.06 (t, $J = 7.4$ Hz, 3H). ^{13}C NMR (101 MHz, Chloroform- d) δ 188.4, 160.4, 138.2, 130.7, 126.1, 114.5, 113.2, 70.4, 22.4, 10.5.

5-bromo-2-(cyclopropylmethoxy)benzaldehyde (12): See Procedure F: 99 mg (0.49 mmol) of **5-bromosalicylaldehyde**, 204 mg (1.5 mmol, 3.0 eq.) of K_2CO_3 , 140 μL (195 mg, 1.4 mmol, 2.9 eq.) of (bromomethyl)cyclopropane, 3 mL of DMF. Compound **12** (128 mg, Quantitative Yield) was isolated as a white solid. ^1H NMR (500 MHz, Chloroform- d) δ 10.42 (s, 1H), 7.87 (s, 1H), 7.55 (d, $J = 8.9$ Hz, 1H), 6.82 (d, $J = 8.7$ Hz, 1H), 3.89 (d, $J = 6.6$ Hz, 2H), 1.27 (m, 1H), 0.65 (m, 2H), 0.36 (m, 2H). ^{13}C NMR (126 MHz, Chloroform- d) δ 188.5, 160.3, 138.2, 130.7, 126.3, 114.9, 113.3, 73.7, 10.0, 3.2.

2-(benzyloxy)-5-bromobenzaldehyde (13): See Procedure F: 401 mg (2.0 mmol) of **5-bromosalicylaldehyde**, 828 mg (6.0 mmol, 3.0 eq.) of K₂CO₃, 710 μ L (1021 mg, 6.0 mmol, 3.0 eq.) of BnBr, 5 mL of DMF. Compound **13** (569 mg, 97.9 % yield) was isolated as a white solid. ¹H NMR (500 MHz, Chloroform-*d*) δ 10.46 (s, 1H), 7.94 (d, *J* = 2.6 Hz, 1H), 7.60 (dd, *J* = 8.9, 2.6 Hz, 1H), 7.45 – 7.33 (m, 5H), 6.95 (d, *J* = 8.9 Hz, 1H), 5.18 (s, 2H). ¹³C NMR (126 MHz, Chloroform-*d*) δ 188.2, 159.9, 138.2, 135.5, 131.0, 128.8, 128.5, 127.3, 126.5, 115.2, 113.8, 70.9.

1-(5-bromo-2-methoxyphenyl)ethan-1-one (14): See Procedure F: 198 mg (0.92 mmol) of **1-(5-bromo-2-hydroxyphenyl)ethan-1-one**, 380 mg (2.8 mmol, 3.0 eq.) of K₂CO₃, 0.170 mL (388 mg, 2.7 mmol, 3.0 eq.) of MeI, 3 mL of DMF. Compound **14** (205 mg, 97.2 % yield) was isolated as a white solid. ¹H NMR (500 MHz, Chloroform-*d*) δ 7.77 (d, *J* = 2.7 Hz, 1H), 7.48 (dd, *J* = 8.8, 2.6 Hz, 1H), 6.81 (d, *J* = 8.9 Hz, 1H), 3.86 (s, 3H), 2.55 (s, 3H). ¹³C NMR (126 MHz, Chloroform-*d*) δ 198.1, 157.9, 136.0, 132.8, 129.5, 113.6, 113.0, 55.8, 31.7.

(R)-N-(3-bromobenzyl)-2-methylpropane-2-sulfinamide (15): See Procedure A: Step 1: 90 mg (0.49 mmol) of **3-bromobenzaldehyde (1)**, 179 mg (1.5 mmol, 3.0 eq.) of (R)-(+)-2-methyl-propane-2-sulfinamide, 600 μ L (653 mg, 2.9 mmol, 5.9 eq.) of Ti(OEt)₄, and 4+4 mL THF. Step 2: 115 mg (3.0 mmol, 6.3 eq.) of sodium borohydride in 4 mL THF. Compound **15** (111 mg, 78.6 % yield) was isolated as a white solid. ¹H NMR (500 MHz, Chloroform-*d*) δ 7.47 (s, 1H), 7.40 (d, *J* = 8.0 Hz, 1H), 7.26 (d, *J* = 7.1 Hz, 1H), 7.19 (t, *J* = 7.7 Hz, 1H), 4.30 (dd, *J* = 14.2, 5.1 Hz, 1H), 4.22 (dd, *J* = 14.2, 7.5 Hz, 1H), 3.56 (t, *J* = 6.3 Hz, 1H), 1.23 (s, 9H). ¹³C NMR (126 MHz, Chloroform-*d*) δ 140.8, 131.1, 130.7, 130.2, 126.6, 122.6, 56.0, 48.7, 22.7.

(R)-N-((R)-1-(3-bromophenyl)ethyl)-2-methylpropane-2-sulfinamide (16): See Procedure A: Step 1: 155 mg (0.78 mmol) of **3'-bromoacetophenone (2)**, 261 mg (2.2 mmol, 2.8 eq.) of (R)-(+)-2-methyl-propane-2-sulfinamide, 1.00 mL (1.09 g, 4.8 mmol, 6.1 eq.) of Ti(OEt)₄,

and 4+4 mL THF. Step 2: 179 mg (4.7 mmol, 6.1 eq.) of sodium borohydride in 4 mL THF. Compound **16** (125 mg, 62.5 % yield) was isolated as a white solid. ¹H NMR (400 MHz, Chloroform-*d*) δ 7.46 (t, *J* = 1.8 Hz, 1H), 7.39 (ddd, *J* = 7.8, 2.0, 1.2 Hz, 1H), 7.26 (dt, *J* = 7.8, 1.4 Hz, 1H), 7.19 (t, *J* = 7.7 Hz, 1H), 4.48 (qd, *J* = 6.6, 3.1 Hz, 1H), 3.41 (d, *J* = 3.2 Hz, 1H), 1.48 (d, *J* = 6.6 Hz, 3H), 1.21 (s, 9H). ¹³C NMR (101 MHz, Chloroform-*d*) δ 146.3, 130.9, 130.4, 129.6, 125.4, 122.7, 55.6, 53.6, 22.8, 22.6.

(R)-N-((R)-1-(3-bromophenyl)propyl)-2-methylpropane-2-sulfinamide (17): See Procedure A: Step 1: 106 mg (0.50 mmol) of **1-(3-bromophenyl)propan-1-one (3)**, 185 mg (1.5 mmol, 3.1 eq.) of (R)-(+)-2-methyl-propane-2-sulfinamide, 800 μL (870 mg, 3.8 mmol, 7.7 eq.) of Ti(OEt)₄, and 4+4 mL THF. Step 2: 111 mg (2.9 mmol, 5.9 eq.) of sodium borohydride in 4 mL THF. Compound **17** (125 mg, 78.9 % yield) was isolated as a white solid. ¹H NMR (500 MHz, Chloroform-*d*) δ 7.43 (t, *J* = 1.8 Hz, 1H), 7.39 (dt, *J* = 7.6, 1.7 Hz, 1H), 7.25 – 7.16 (m, 2H), 4.21 (ddd, *J* = 8.9, 5.4, 4.1 Hz, 1H), 3.40 (d, *J* = 4.0 Hz, 1H), 2.01 (dtd, *J* = 14.7, 7.4, 5.5 Hz, 1H), 1.77 – 1.65 (m, 1H), 1.21 (s, 9H), 0.79 (t, *J* = 7.4 Hz, 3H). ¹³C NMR (126 MHz, Chloroform-*d*) δ 144.7, 130.9, 130.20, 130.15, 126.1, 122.7, 60.1, 55.8, 29.4, 22.6, 10.0.

(R)-N-(5-bromo-2-methylbenzyl)-2-methylpropane-2-sulfinamide (18): See Procedure A: Step 1: 77 mg (0.39 mmol) of **5-bromo-2-methylbenzaldehyde (4)**, 143 mg (1.2 mmol, 3.1 eq.) of (R)-(+)-2-methyl-propane-2-sulfinamide, 490 μL (533 mg, 2.3 mmol, 6.0 eq.) of Ti(OEt)₄, and 4+4 mL THF. Step 2: 89 mg (2.4 mmol, 6.1 eq.) of sodium borohydride in 4 mL THF. Compound **18** (108 mg, 91.8 % yield) was isolated as a colorless oil that solidified on standing. ¹H NMR (500 MHz, Chloroform-*d*) δ 7.43 (s, 1H), 7.30 (d, *J* = 8.0 Hz, 1H), 7.02 (d, *J* = 8.0 Hz, 1H), 4.27 (dd, *J* = 13.9, 3.7 Hz, 1H), 4.16 (dd, *J* = 13.7, 8.4 Hz, 1H), 3.43 (dt, *J* = 8.4, 3.7 Hz, 1H),

2.26 (s, 3H), 1.22 (s, 9H). ¹³C NMR (126 MHz, Chloroform-*d*) δ 138.4, 135.5, 132.1, 131.4, 130.7, 119.5, 56.0, 46.7, 22.7, 18.6.

(R)-N-(5-bromo-2-chlorobenzyl)-2-methylpropane-2-sulfinamide (19): See Procedure A: Step 1: 104 mg (0.47 mmol) of 5-bromo-2-chlorobenzaldehyde (**5**), 162 mg (1.3 mmol, 2.8 eq.) of (R)-(+)-2-methylpropane-2-sulfinamide, 600 μL (653 mg, 2.9 mmol, 6.0 eq.) of Ti(OEt)₄, and 4+4 mL THF. Step 2: 107 mg (2.8 mmol, 6.0 eq.) of sodium borohydride in 4 mL THF. Compound **19** (134 mg, 87.1 % yield) was isolated as a white solid. ¹H NMR (400 MHz, Chloroform-*d*) δ 7.54 (d, *J* = 2.3 Hz, 1H), 7.33 (dd, *J* = 8.5, 2.4 Hz, 1H), 7.21 (d, *J* = 8.5 Hz, 1H), 4.40 (dd, *J* = 15.0, 5.8 Hz, 1H), 4.28 (dd, *J* = 15.0, 7.5 Hz, 1H), 3.68 (t, *J* = 6.7 Hz, 1H), 1.22 (s, 9H). ¹³C NMR (126 MHz, Chloroform-*d*) δ 138.3, 132.7, 132.6, 131.9, 131.0, 120.6, 56.2, 46.9, 22.6.

(R)-N-(4-bromo-2-(((tert-butylsulfinyl)amino)methyl)phenyl)acetamide (20): See Procedure A: Step 1: 93 (0.38 mmol) of **6**, 144 mg (1.2 mmol, 3.1 eq.) of (R)-(+)-2-methylpropane-2-sulfinamide, 600 μL (653 mg, 2.9 mmol, 7.5 eq.) of Ti(OEt)₄, and 4+4 mL THF. Step 2: 87 mg (2.3 mmol, 6.0 eq.) of sodium borohydride in 3 mL THF. This compound was purified using 0-10 % methanol in DCM as the mobile phase during column chromatography. Compound **20** (130 mg, 97.5 % yield) was isolated as a colorless oil. ¹H NMR (400 MHz, Chloroform-*d*) δ 8.89 (s, 1H), 7.80 (d, *J* = 8.7 Hz, 1H), 7.41 (dd, *J* = 8.7, 2.4 Hz, 1H), 7.37 (d, *J* = 2.4 Hz, 1H), 4.22 (dd, *J* = 13.5, 5.8 Hz, 1H), 4.11 (dd, *J* = 13.5, 4.5 Hz, 1H), 3.72 (t, *J* = 5.1 Hz, 1H), 2.19 (s, 3H), 1.23 (s, 9H). ¹³C NMR (101 MHz, Chloroform-*d*) δ 169.53, 135.72, 133.03, 132.03, 130.51, 126.03, 117.34, 56.50, 44.54, 24.08, 22.85.

(R)-N-(4-bromo-2-(((tert-butylsulfinyl)amino)methyl)phenyl)propionamide (21): See Procedure A: Step 1: 84 (0.33 mmol) of **7**, 123 mg (1.0 mmol, 3.1 eq.) of (R)-(+)-2-methyl-

propane-2-sulfinamide, 410 μL (446 mg, 2.0 mmol, 6.0 eq.) of $\text{Ti}(\text{OEt})_4$, and 4+4 mL THF. Step 2: 76 mg (2.0 mmol, 6.1 eq.) of sodium borohydride in 4 mL THF. Compound **21** (78 mg, 65.8 % yield) was isolated as a colorless oil. ^1H NMR (500 MHz, Chloroform-*d*) δ 8.70 (s, 1H), 7.83 (d, $J = 8.7$ Hz, 1H), 7.41 (dd, $J = 8.7, 2.2$ Hz, 1H), 7.36 (d, $J = 2.4$ Hz, 1H), 4.20 (dd, $J = 13.4, 5.9$ Hz, 1H), 4.08 (dd, $J = 13.1, 4.5$ Hz, 1H), 3.67 (t, $J = 5.1$ Hz, 1H), 2.44 (q, $J = 7.6$ Hz, 2H), 1.22 (m, 12H). ^{13}C NMR (126 MHz, Chloroform-*d*) δ 173.14, 135.81, 133.02, 132.07, 130.19, 125.87, 117.15, 56.47, 44.52, 30.22, 22.82, 9.69.

(R)-N-(5-bromo-2-methoxybenzyl)-2-methylpropane-2-sulfinamide (22): See Procedure A: Step 1: 142 mg (0.66 mmol) of **8**, 240 mg (2.0 mmol, 3.0 eq.) of (R)-(+)-2-methylpropane-2-sulfinamide, 1.00 mL (1.09 g, 4.8 mmol, 7.2 eq.) of $\text{Ti}(\text{OEt})_4$, and 4+4 mL THF. Step 2: 152 mg (4.0 mmol, 6.1 eq.) of sodium borohydride in 4 mL THF. Compound **22** (159 mg, 75.2 % yield) was isolated as a colorless oil. ^1H NMR (400 MHz, Chloroform-*d*) δ 7.36 (d, $J = 2.5$ Hz, 1H), 7.33 (dd, $J = 8.6, 2.5$ Hz, 1H), 6.72 (d, $J = 8.6$ Hz, 1H), 4.34 (dd, $J = 14.4, 5.6$ Hz, 1H), 4.11 (dd, $J = 14.5, 7.6$ Hz, 1H), 3.80 (s, 3H), 3.66 (t, $J = 6.9$ Hz, 1H), 1.19 (s, 9H). ^{13}C NMR (101 MHz, Chloroform-*d*) δ 156.4, 131.9, 131.4, 129.3, 112.6, 112.0, 55.9, 44.8, 22.6.

(R)-N-(5-bromo-2-(trifluoromethoxy)benzyl)-2-methylpropane-2-sulfinamide (23): See Procedure A: Step 1: 70 μL (119 mg, 0.44 mmol) of **5-bromo-2-(trifluoromethoxy)benzaldehyde (9)**, 163 mg (1.3 mmol, 3.0 eq.) of (R)-(+)-2-methylpropane-2-sulfinamide, 700 μL (762 mg, 3.3 mmol, 7.5 eq.) of $\text{Ti}(\text{OEt})_4$, and 4+4 mL THF. Step 2: 103 mg (2.7 mmol, 6.1 eq.) of sodium borohydride in 4 mL THF. Compound **23** (128 mg, 77.1 % yield) was isolated as a white solid. ^1H NMR (500 MHz, Chloroform-*d*) δ 7.61 (d, $J = 2.4$ Hz, 1H), 7.43 (dd, $J = 8.7, 2.5$ Hz, 1H), 7.11 (dd, $J = 8.7, 1.6$ Hz, 1H), 4.38 (dd, $J = 15.1, 5.8$ Hz, 1H), 4.27 (dd, $J = 15.1, 7.4$ Hz, 1H), 3.61 (t, $J = 6.6$ Hz, 1H), 1.22 (s, 9H). ^{13}C NMR (126 MHz, Chloroform-*d*)

δ 146.2 (q, $J = 1.7$ Hz), 133.5, 133.0, 132.0, 122.2 (q, $J = 1.7$ Hz), 121.4, 120.2, 119.3, 56.2, 43.7, 22.6.

(R)-N-(5-bromo-2-ethoxybenzyl)-2-methylpropane-2-sulfinamide (24): See Procedure A: Step 1: 73 mg (0.32 mmol) of **10**, 116 mg (0.96 mmol, 3.0 eq.) of (R)-(+)-2-methylpropane-2-sulfinamide, 500 μ L (544 mg, 2.4 mmol, 7.5 eq.) of Ti(OEt)₄, and 4+4 mL THF. Step 2: 74 mg (2.0 mmol, 6.1 eq.) of sodium borohydride in 3 mL THF. Compound **24** (97 mg, 91.1 % yield) was isolated as a white solid. ¹H NMR (500 MHz, Chloroform-*d*) δ 7.36 (d, $J = 2.5$ Hz, 1H), 7.30 (dd, $J = 8.7, 2.5$ Hz, 1H), 6.70 (d, $J = 8.7$ Hz, 1H), 4.35 (dd, $J = 14.3, 5.6$ Hz, 1H), 4.12 (dd, $J = 14.4, 7.9$ Hz, 1H), 4.00 (q, $J = 7.0$ Hz, 2H), 3.72 (t, $J = 6.8$ Hz, 1H), 1.40 (t, $J = 7.0$ Hz, 3H), 1.20 (s, 9H). ¹³C NMR (126 MHz, Chloroform-*d*) δ 155.8, 131.8, 131.3, 129.4, 112.8, 112.5, 63.9, 55.9, 45.0, 22.6, 14.8.

(R)-N-(5-bromo-2-propoxybenzyl)-2-methylpropane-2-sulfinamide (25): See Procedure A: Step 1: 133 mg (0.55 mmol) of **11**, 98 mg (0.81 mmol, 1.5 eq.) of (R)-(+)-2-methylpropane-2-sulfinamide, 420 μ L (457 mg, 2.0 mmol, 3.7 eq.) of Ti(OEt)₄, and 3+3 mL THF. Step 2: 121 mg (3.2 mmol, 5.9 eq.) of sodium borohydride in 3 mL THF. Compound **25** (169 mg, 88.7 % yield) was isolated as a white solid. ¹H NMR (500 MHz, Chloroform-*d*) δ 7.35 (d, $J = 2.5$ Hz, 1H), 7.28 (dd, $J = 8.7, 2.5$ Hz, 1H), 6.68 (d, $J = 8.7$ Hz, 1H), 4.33 (dd, $J = 14.4, 5.6$ Hz, 1H), 4.11 (dd, $J = 14.4, 7.8$ Hz, 1H), 3.88 (t, $J = 6.5$ Hz, 2H), 3.72 (dd, $J = 7.8, 5.6$ Hz, 1H), 1.78 (h, $J = 7.4$ Hz, 2H), 1.18 (s, 9H), 1.01 (t, $J = 7.4$ Hz, 3H). ¹³C NMR (126 MHz, Chloroform-*d*) δ 155.8, 131.8, 131.3, 129.4, 112.8, 112.4, 69.8, 55.9, 44.9, 22.6, 22.5, 10.6.

(R)-N-(5-bromo-2-(cyclopropylmethoxy)benzyl)-2-methylpropane-2-sulfinamide (26): See Procedure A: Step 1: 135 mg (0.53 mmol) of **12**, 197 mg (1.6 mmol, 3.1 eq.) of (R)-(+)-2-methylpropane-2-sulfinamide, 840 μ L (914 mg, 4.0 mmol, 7.6 eq.) of Ti(OEt)₄, and 4+4 mL

THF. Step 2: 115 mg (3.0 mmol, 5.8 eq.) of sodium borohydride in 3 mL THF. Compound **26** (165 mg, 86.5 % yield) was isolated as a colorless oil that solidifies to a white solid on standing. ¹H NMR (500 MHz, Chloroform-*d*) δ 7.36 (d, *J* = 2.5 Hz, 1H), 7.30 (dd, *J* = 8.7, 2.5 Hz, 1H), 6.67 (d, *J* = 8.7 Hz, 1H), 4.39 (dd, *J* = 14.4, 5.7 Hz, 1H), 4.14 (dd, *J* = 14.4, 7.9 Hz, 1H), 3.88 – 3.75 (m, 3H), 1.21 (s, 9H), 0.62 (dt, *J* = 8.9, 3.2 Hz, 2H), 0.32 (dd, *J* = 4.7, 2.1 Hz, 2H). ¹³C NMR (126 MHz, Chloroform-*d*) δ 155.9, 131.8, 131.3, 129.6, 113.0, 112.5, 73.1, 55.9, 45.3, 22.6, 10.2, 3.24, 3.18.

(R)-N-(2-(benzyloxy)-5-bromobenzyl)-2-methylpropane-2-sulfinamide (27): See Procedure A: Step 1: 440 mg (1.5 mmol) of **13**, 558 mg (4.6 mmol, 3.1 eq.) of (R)-(+)-2-methylpropane-2-sulfinamide, 2.4 mL (2.6 g, 11.4 mmol, 7.6 eq.) of Ti(OEt)₄, and 5+5 mL THF. Step 2: 341 mg (9.0 mmol, 6.0 eq.) of sodium borohydride in 4 mL THF. Compound **27** (582 mg, 97.2 % yield) was isolated as a white solid. ¹H NMR (400 MHz, Chloroform-*d*) δ 7.29 (d, *J* = 2.5 Hz, 1H), 7.27 – 7.18 (m, 4H), 7.18 – 7.11 (m, 2H), 6.62 (d, *J* = 8.7 Hz, 1H), 4.98 (s, 2H), 4.32 (dd, *J* = 14.6, 5.7 Hz, 1H), 4.18 (dd, *J* = 14.6, 7.2 Hz, 1H), 4.12 (dd, *J* = 7.2, 5.8 Hz, 1H), 1.14 (s, 9H). ¹³C NMR (101 MHz, Chloroform-*d*) δ 155.3, 136.2, 131.7, 131.0, 129.9, 128.5, 128.1, 128.0, 127.2, 126.7, 113.3, 112.8, 70.0, 55.7, 44.5, 22.5.

(R)-N-((R)-1-(5-bromo-2-methoxyphenyl)ethyl)-2-methylpropane-2-sulfinamide (28): See Procedure A: Step 1: 129 mg (0.59 mmol) of **14**, 193 mg (1.6 mmol, 2.7 eq.) of (R)-(+)-2-methylpropane-2-sulfinamide, 720 μL (783 mg, 3.4 mmol, 5.8 eq.) of Ti(OEt)₄, 4+4 mL THF, Step 2: 137 mg (3.6 mmol, 6.1 eq.) of sodium borohydride in 4 mL THF. Compound **28** (173 mg, 91.9 % yield) was isolated as a colorless oil. ¹H NMR (500 MHz, Chloroform-*d*) δ 7.33 (d, *J* = 2.5 Hz, 1H), 7.26 (dd, *J* = 8.7, 2.5 Hz, 1H), 6.69 (d, *J* = 8.7 Hz, 1H), 4.69 (p, *J* = 6.5 Hz, 1H), 3.77 (s,

3H), 3.75 (d, $J = 5.8$ Hz, 1H), 1.40 (d, $J = 6.7$ Hz, 3H), 1.16 (s, 9H). ^{13}C NMR (126 MHz, Chloroform- d) δ 155.6, 134.5, 131.1, 129.7, 113.0, 112.6, 55.6, 49.6, 23.6, 22.6, 21.0.

(R)-N-(3-benzylbenzyl)-2-methylpropane-2-sulfinamide (29): See Procedure Bb: 55 mg (0.19 mmol) of **15**, 120 μL (118 mg, 0.54 mmol, 2.8 eq.) of benzyl boronic acid pinacol ester, 54 mg (0.39 mmol, 2.1 eq.) of potassium carbonate, 17 mg (0.023 mmol, 0.12 eq.) of 1,1'-bis(diphenylphosphino)ferrocene]dichloropalladium, 4 mL of 3:1 acetone:water. Compound **29** (38 mg, 66.5% yield) was isolated as a colorless oil that solidified to a white solid on standing. ^1H NMR (400 MHz, Chloroform- d) δ 7.32 – 7.24 (m, 3H), 7.23 – 7.10 (m, 6H), 4.31 (dd, $J = 13.8$, 4.6 Hz, 1H), 4.21 (dd, $J = 13.8$, 7.8 Hz, 1H), 3.98 (s, 2H), 3.45 (dd, $J = 7.6$, 4.6 Hz, 1H), 1.22 (s, 9H). ^{13}C NMR (101 MHz, Chloroform- d) δ 141.6, 140.8, 138.7, 128.9, 128.7, 128.6, 128.5, 128.3, 126.2, 125.8, 55.9, 49.3, 41.8, 22.7.

(R)-N-((R)-1-(3-benzylphenyl)ethyl)-2-methylpropane-2-sulfinamide (30): See Procedure Bb: 98 mg (0.32 mmol) of **16**, 180 μL (176 mg, 0.81 mmol, 2.5 eq.) of benzyl boronic acid pinacol ester, 86 mg (0.62 mmol, 1.9 eq.) of potassium carbonate, 21 mg (0.029 mmol, 0.089 eq.) of 1,1'-bis(diphenylphosphino)ferrocene]dichloropalladium, 5 mL of 3:1 acetone:water. Compound **30** (58 mg, 57.1 % yield) was isolated as a colorless oil. ^1H NMR (500 MHz, Chloroform- d) δ 7.33 – 7.23 (m, 3H), 7.24 – 7.14 (m, 5H), 7.11 (dt, $J = 7.7$, 1.4 Hz, 1H), 4.51 (qd, $J = 6.5$, 2.6 Hz, 1H), 3.99 (s, 2H), 3.39 (d, $J = 2.6$ Hz, 1H), 1.49 (d, $J = 6.5$ Hz, 3H), 1.22 (s, 9H). ^{13}C NMR (126 MHz, Chloroform- d) δ 144.3, 141.7, 140.8, 128.91, 128.87, 128.5, 128.3, 127.2, 126.1, 124.2, 55.4, 53.8, 41.9, 22.8, 22.6.

(R)-N-((R)-1-(3-benzylphenyl)propyl)-2-methylpropane-2-sulfinamide (31): See Procedure Ba: 83 mg (0.28 mmol) of **17**, 130 μL (127 mg, 0.58 mmol, 2.1 eq.) of benzyl boronic acid pinacol ester, 116 mg (0.84 mmol, 3.0 eq.) of potassium carbonate, 20 mg (0.027 mmol, 0.098

eq.) of 1,1'-bis(diphenylphosphino)ferrocene]dichloropalladium, 2.5 mL of 3:1 acetone:water. Compound **31** (81 mg, 94.3 % yield) was isolated as a colorless oil. ¹H NMR (500 MHz, Chloroform-*d*) δ 7.30 – 7.23 (m, 3H), 7.21 – 7.07 (m, 6H), 4.23 (dt, *J* = 8.5, 4.6 Hz, 1H), 3.98 (s, 2H), 2.02 (dp, *J* = 13.2, 7.4 Hz, 1H), 1.73 (dq, *J* = 21.7, 7.3 Hz, 1H), 1.20 (s, 9H), 0.77 (t, *J* = 7.5 Hz, 3H). ¹³C NMR (126 MHz, Chloroform-*d*) δ 142.4, 141.4, 140.9, 128.9, 128.7, 128.5, 128.4, 127.9, 126.1, 124.9, 60.2, 55.7, 41.8, 29.3, 22.6, 10.0.

(R)-N-(5-benzyl-2-methylbenzyl)-2-methylpropane-2-sulfinamide (32): See Procedure Bb: 89 mg (0.29 mmol) of **18**, 200 μL (196 mg, 0.90 mmol, 3.1 eq.) of benzyl boronic acid pinacol ester, 82 mg (0.59 mmol, 2.0 eq.) of potassium carbonate, 22 mg (0.030 mmol, 0.10 eq.) of 1,1'-bis(diphenylphosphino)ferrocene]dichloropalladium, 4 mL of 3:1 acetone:water. Compound **32** (65 mg, 70.4 % yield) was isolated as a tan solid. ¹H NMR (500 MHz, Chloroform-*d*) δ 7.30 – 7.26 (m, 2H), 7.19 (t, *J* = 8.7 Hz, 3H), 7.12 – 7.07 (m, 2H), 7.05 (dd, *J* = 7.8, 1.9 Hz, 1H), 4.30 (dd, *J* = 13.3, 3.9 Hz, 1H), 4.18 (dd, *J* = 13.3, 8.8 Hz, 1H), 3.94 (s, 2H), 3.27 (dd, *J* = 9.1, 3.9 Hz, 1H), 2.31 (s, 3H), 1.20 (s, 9H). ¹³C NMR (126 MHz, Chloroform-*d*) δ 141.0, 139.0, 136.2, 134.4, 130.6, 129.4, 128.9, 128.5, 128.3, 126.1, 55.9, 47.4, 41.5, 22.7, 18.6.

(R)-N-(5-benzyl-2-chlorobenzyl)-2-methylpropane-2-sulfinamide (33): See Procedure Bb: 59 mg (0.18 mmol) of **19**, 100 μL (98 mg, 0.45 mmol, 2.5 eq.) of benzyl boronic acid pinacol ester, 47 mg (0.34 mmol, 1.9 eq.) of potassium carbonate, 13 mg (0.018 mmol, 0.098 eq.) of 1,1'-bis(diphenylphosphino)ferrocene]dichloropalladium, 4 mL of 3:1 acetone:water. Compound **33** (45 mg, 73.7 % yield) was isolated as a colorless oil that solidifies to a white solid on standing. ¹H NMR (500 MHz, Chloroform-*d*) δ 7.30 – 7.24 (m, 3H), 7.21-7.18 (m, 2H), 7.15 (d, *J* = 7.5 Hz, 2H), 7.05 (d, *J* = 8.1 Hz, 1H), 4.40 (dd, *J* = 14.4, 5.1 Hz, 1H), 4.27 (dd, *J* = 14.3, 7.8 Hz, 1H), 3.93

(s, 2H), 3.60 (t, $J = 6.8$ Hz, 1H), 1.18 (d, $J = 1.4$ Hz, 9H). ^{13}C NMR (126 MHz, Chloroform- d) δ 140.3, 136.0, 131.4, 130.5, 129.6, 129.5, 128.9, 128.6, 126.3, 56.1, 47.3, 41.2, 22.6.

(R)-N-(4-benzyl-2-(((tert-butylsulfinyl)amino)methyl)phenyl)acetamide (34): See Procedure Ba: 125 mg (0.36 mmol) of **20**, 140 μL (137 mg, 0.63 mmol, 1.8 eq.) of benzyl boronic acid pinacol ester, 136 mg (0.98 mmol, 2.7 eq.) of potassium carbonate, 29 mg (0.040 mmol, 0.11 eq.) of 1,1'-bis(diphenylphosphino)ferrocene]dichloropalladium, 3.2 mL of 3:1 acetone:water. Compound **34** (94 mg, 72.8 % yield) was isolated as a yellow oil ^1H NMR (500 MHz, Chloroform- d) δ 8.72 (s, 1H), 7.79 (d, $J = 8.3$ Hz, 1H), 7.29 – 7.22 (m, 2H), 7.20 – 7.12 (m, 4H), 7.04 (d, $J = 2.1$ Hz, 1H), 4.20 (dd, $J = 13.2, 6.0$ Hz, 1H), 4.12 (dd, $J = 13.3, 4.4$ Hz, 1H), 3.90 (s, 2H), 3.65 (t, $J = 5.3$ Hz, 1H), 2.18 (s, 3H), 1.21 (s, 9H). ^{13}C NMR (126 MHz, Chloroform- d) δ 169.48, 140.67, 137.91, 134.64, 130.73, 129.71, 128.89, 128.74, 128.51, 126.19, 124.72, 56.34, 45.48, 41.28, 24.05, 22.84.

(R)-N-(4-benzyl-2-(((tert-butylsulfinyl)amino)methyl)phenyl)propionamide (35): See Procedure Bb: 76 mg (0.21 mmol) of **21**, 120 μL (118 mg, 0.54 mmol, 2.6 eq.) of benzyl boronic acid pinacol ester, 59 mg (0.43 mmol, 2.0 eq.) of potassium carbonate, 15 mg (0.020 mmol, 0.098 eq.) of 1,1'-bis(diphenylphosphino)ferrocene]dichloropalladium, 5 mL of 3:1 acetone:water. Compound **35** (68 mg, 86.8 % yield) was isolated as a yellow oil. ^1H NMR (500 MHz, Chloroform- d) δ 8.56 (s, 1H), 7.84 (d, $J = 8.3$ Hz, 1H), 7.27 (t, $J = 7.3$ Hz, 2H), 7.23 – 7.11 (m, 4H), 7.05 (s, 1H), 4.19 (dd, $J = 13.1, 6.2$ Hz, 1H), 4.11 (dd, $J = 13.1, 4.3$ Hz, 1H), 3.92 (s, 2H), 3.55 (t, $J = 5.2$ Hz, 1H), 2.44 (q, $J = 7.6$ Hz, 2H), 1.25 – 1.21 (m, 12H). ^{13}C NMR (126 MHz, Chloroform- d) δ 173.06, 140.73, 137.67, 134.78, 130.73, 129.71, 128.88, 128.50, 128.46, 126.18, 124.49, 56.27, 45.47, 41.28, 30.28, 22.83, 9.87.

(R)-N-(5-benzyl-2-methoxybenzyl)-2-methylpropane-2-sulfinamide (36): See Procedure Bb: 149 mg (0.47 mmol) of **22**, 200 μ L (196 mg, 0.90 mmol, 1.9 eq.) of benzyl boronic acid pinacol ester, 193 mg (1.4 mmol, 3.0 eq.) of potassium carbonate, 33 mg (0.045 mmol, 0.096 eq.) of 1,1'-bis(diphenylphosphino)ferrocene]dichloropalladium, 3 mL of 3:1 acetone:water. Compound **36** (98 mg, 63.5 % yield) was isolated. ^1H NMR (400 MHz, Chloroform-*d*) δ 7.26 (ddd, $J = 7.6, 6.3, 1.3$ Hz, 2H), 7.20 – 7.13 (m, 3H), 7.09 – 7.04 (m, 2H), 6.77 (d, $J = 9.0$ Hz, 1H), 4.36 (dd, $J = 13.8, 5.1$ Hz, 1H), 4.10 (dd, $J = 13.8, 8.0$ Hz, 1H), 3.90 (s, 2H), 3.79 (s, 3H), 3.76 (dd, $J = 8.0, 5.3$ Hz, 1H), 1.17 (s, 9H). ^{13}C NMR (101 MHz, Chloroform-*d*) δ 155.8, 141.3, 133.2, 129.9, 129.0, 128.8, 128.4, 126.9, 126.0, 110.4, 55.9, 55.4, 45.5, 41.0, 22.6.

(R)-N-(5-benzyl-2-(trifluoromethoxy)benzyl)-2-methylpropane-2-sulfinamide (37): See Procedure Bb: 141 mg (0.38 mmol) of **23**, 110 μ L (108 mg, 0.49 mmol, 1.3 eq.) of benzyl boronic acid pinacol ester, 94 mg (0.68 mmol, 1.8 eq.) of potassium carbonate, 28 mg (0.038 mmol, 0.10 eq.) of 1,1'-bis(diphenylphosphino)ferrocene]dichloropalladium, 5 mL of 3:1 acetone:water. Compound **37** (105 mg, 72.3 % yield) was isolated as a tan solid. ^1H NMR (500 MHz, Chloroform-*d*) δ 7.33 – 7.27 (m, 2H), 7.26 (s, 1H), 7.25 – 7.11 (m, 5H), 4.39 (dd, $J = 14.5, 5.4$ Hz, 1H), 4.26 (dd, $J = 14.5, 7.7$ Hz, 1H), 3.97 (s, 2H), 3.53 (dd, $J = 7.7, 5.4$ Hz, 1H), 1.19 (s, 9H). ^{13}C NMR (126 MHz, Chloroform-*d*) δ 145.6 (q, $J = 1.5$ Hz), 140.2, 140.1, 131.1, 130.5, 129.3, 128.9, 128.6, 126.4, 121.6, 120.6 (q, $J = 1.4$ Hz), 119.5, 56.03, 44.1, 41.2, 22.5.

(R)-N-(5-benzyl-2-ethoxybenzyl)-2-methylpropane-2-sulfinamide (38): See Procedure Ba: 119 mg (0.36 mmol) of **24**, 160 μ L (157 mg, 0.72 mmol, 2.0 eq.) of benzyl boronic acid pinacol ester, 151 mg (1.1 mmol, 3.1 eq.) of potassium carbonate, 29 mg (0.040 mmol, 0.11 eq.) of 1,1'-bis(diphenylphosphino)ferrocene] dichloropalladium, 2.5 mL of 3:1 acetone:water. Compound **38** (87 mg, 70.7 % yield) was isolated as a colorless oil. ^1H NMR (500 MHz, Chloroform-*d*) δ 7.29 –

7.24 (m, 2H), 7.20 – 7.15 (m, 3H), 7.07 (d, $J = 2.3$ Hz, 1H), 7.05 (dd, $J = 8.2, 2.3$ Hz, 1H), 6.76 (d, $J = 8.3$ Hz, 1H), 4.39 (dd, $J = 13.8, 5.1$ Hz, 1H), 4.11 (dd, $J = 13.8, 8.1$ Hz, 1H), 4.02 (qd, $J = 7.0, 1.1$ Hz, 2H), 3.91 (s, 2H), 3.76 (dd, $J = 8.3, 5.2$ Hz, 1H), 1.40 (t, $J = 7.0$ Hz, 3H), 1.18 (s, 9H). ^{13}C NMR (126 MHz, Chloroform-*d*) δ 155.2, 141.4, 133.0, 129.9, 129.0, 128.8, 128.4, 127.1, 126.0, 111.2, 63.6, 55.8, 45.6, 41.0, 22.6, 15.0.

(R)-N-(5-benzyl-2-propoxybenzyl)-2-methylpropane-2-sulfinamide (39): See Procedure Ba: 122 mg (0.35 mmol) of **25**, 130 μL (127 mg, 0.58 mmol, 1.7 eq.) of benzyl boronic acid pinacol ester, 135 mg (0.98 mmol, 2.8 eq.) of potassium carbonate, 25 mg (0.034 mmol, 0.098 eq.) of 1,1'-bis(diphenylphosphino)ferrocene]dichloropalladium, 2.5 mL of 3:1 acetone:water. Compound **39** (92 mg, 73.1 % yield) was isolated as a yellow oil. ^1H NMR (500 MHz, Chloroform-*d*) δ 7.26 (dd, $J = 8.1, 6.9$ Hz, 2H), 7.20 – 7.14 (m, 3H), 7.08 (d, $J = 2.3$ Hz, 1H), 7.05 (dd, $J = 8.3, 2.3$ Hz, 1H), 6.76 (d, $J = 8.3$ Hz, 1H), 4.39 (dd, $J = 13.8, 5.2$ Hz, 1H), 4.12 (dd, $J = 13.8, 8.2$ Hz, 1H), 3.91 (t, $J = 6.5$ Hz, 2H), 3.90 (s, 2H) 3.76 (dd, $J = 8.2, 5.2$ Hz, 1H), 1.80 (h, $J = 7.2$ Hz, 2H), 1.17 (s, 9H), 1.04 (t, $J = 7.4$ Hz, 3H). ^{13}C NMR (126 MHz, Chloroform-*d*) δ 155.3, 141.4, 133.0, 129.9, 129.0, 128.8, 128.4, 127.1, 126.0, 111.2, 69.6, 55.8, 45.6, 41.0, 22.7, 22.6, 10.7.

(R)-N-(5-benzyl-2-(cyclopropylmethoxy)benzyl)-2-methylpropane-2-sulfinamide (40): See Procedure Ba: 48 mg (0.13 mmol) of **26**, 60 μL (59 mg, 0.27 mmol, 2.0 eq.) of benzyl boronic acid pinacol ester, 56 mg (0.41 mmol, 3.1 eq.) of potassium carbonate, 10 mg (0.014 mmol, 0.10 eq.) of 1,1'-bis(diphenylphosphino)ferrocene]dichloropalladium, 3.25 mL of 3:1 acetone:water. Compound **40** (41 mg, 82.8 % yield) was isolated as a colorless oil. ^1H NMR (500 MHz, Chloroform-*d*) δ 7.30 – 7.25 (m, 2H), 7.22 – 7.15 (m, 3H), 7.08 (d, $J = 2.3$ Hz, 1H), 7.04 (dd, $J = 8.3, 2.3$ Hz, 1H), 6.74 (d, $J = 8.3$ Hz, 1H), 4.43 (dd, $J = 13.8, 5.1$ Hz, 1H), 4.13 (dd, $J = 13.8, 8.1$ Hz, 1H), 3.91 (s, 2H), 3.86 (dd, $J = 8.0, 5.3$ Hz, 1H), 3.80 (qd, $J = 9.9, 6.9$ Hz, 2H), 1.28

– 1.22 (m, 1H), 1.20 (s, 9H), 0.68 – 0.58 (m, 2H), 0.33 (tdd, $J = 4.8, 3.3, 2.2$ Hz, 2H). ^{13}C NMR (126 MHz, Chloroform-*d*) δ 155.3, 141.4, 133.1, 129.9, 128.9, 128.8, 128.4, 127.3, 126.0, 111.4, 72.8, 55.7, 45.9, 41.0, 22.6, 10.4, 3.2, 3.1.

(R)-N-(5-benzyl-2-(benzyloxy)benzyl)-2-methylpropane-2-sulfinamide (41): See Procedure Ba: 500 mg (1.3 mmol) of **27**, 590 μL (578 mg, 2.7 mmol, 2.0 eq.) of benzyl boronic acid pinacol ester, 564 mg (4.1 mmol, 3.1 eq.) of potassium carbonate, 98 mg (0.13 mmol, 0.10 eq.) of 1,1'-bis(diphenylphosphino)ferrocene]dichloropalladium, 2.5 mL of 3:1 acetone:water. Compound **41** (363 mg, 70.6 % yield) was isolated as a white solid. ^1H NMR (500 MHz, Chloroform-*d*) δ 7.43 – 7.35 (m, 4H), 7.34 – 7.25 (m, 3H), 7.21 – 7.15 (m, 3H), 7.12 (d, $J = 2.2$ Hz, 1H), 7.06 (dd, $J = 8.3, 2.2$ Hz, 1H), 6.85 (d, $J = 8.3$ Hz, 1H), 5.06 (s, 2H), 4.41 (dd, $J = 14.0, 5.4$ Hz, 1H), 4.20 (dd, $J = 14.0, 7.8$ Hz, 1H), 3.92 (s, 2H), 3.81 (dd, $J = 7.8, 5.4$ Hz, 1H), 1.13 (s, 9H). ^{13}C NMR (126 MHz, Chloroform-*d*) δ 154.9, 141.3, 136.9, 133.6, 130.0, 129.0, 128.9, 128.6, 128.5, 128.0, 127.32, 127.29, 126.1, 111.7, 70.1, 55.9, 45.6, 41.1, 22.6.

(R)-N-((R)-1-(5-benzyl-2-methoxyphenyl)ethyl)-2-methylpropane-2-sulfinamide (42): See Procedure Bb: 134 mg (0.40 mmol) of **28**, 240 μL (235 mg, 1.1 mmol, 2.7 eq.) of benzyl boronic acid pinacol ester, 101 mg (0.73 mmol, 1.8 eq.) of potassium carbonate, 28 mg (0.038 mmol, 0.096 eq.) of 1,1'-bis(diphenylphosphino)ferrocene]dichloropalladium, 4 mL of 3:1 acetone:water. Compound **42** (75 mg, 54.2 % yield) was isolated as a colorless oil. ^1H NMR (500 MHz, Chloroform-*d*) δ 7.30 – 7.23 (m, 2H), 7.21 – 7.13 (m, 3H), 7.09 (d, $J = 2.2$ Hz, 1H), 7.02 (dd, $J = 8.4, 2.2$ Hz, 1H), 6.78 (d, $J = 8.4$ Hz, 1H), 4.75 (p, $J = 6.5$ Hz, 1H), 3.92 (s, 2H), 3.80 (s, 3H), 3.77 (d, $J = 5.0$ Hz, 1H), 1.44 (d, $J = 6.7$ Hz, 3H), 1.17 (s, 9H). ^{13}C NMR (126 MHz, Chloroform-*d*) δ 154.9, 141.4, 133.3, 132.2, 128.9, 128.6, 128.4, 127.4, 126.0, 110.9, 55.40, 55.37, 49.9, 41.1, 22.6, 21.9.

(3-benzylphenyl)methanaminium chloride (43): See Procedure C: 123 mg (0.41 mmol) of **29**, 0.4 mL HCl conc., 2 mL dioxane. Compound **43** (85 mg, 89.1 % yield) was isolated as a white solid. ^1H NMR (500 MHz, Methanol- d_4) δ 7.38 – 7.32 (m, 2H), 7.32 – 7.23 (m, 4H), 7.23 – 7.19 (m, 2H), 7.19 – 7.12 (m, 1H), 4.07 (s, 2H), 4.00 (s, 2H). ^{13}C NMR (126 MHz, Methanol- d_4) δ 142.6, 140.8, 133.2, 129.4, 129.1, 128.9, 128.5, 128.1, 126.3, 125.8, 42.9, 41.2.

(R)-1-(3-benzylphenyl)ethan-1-aminium chloride (44): See Procedure C: 43 mg (0.14 mmol) of **30**, 0.2 mL HCl conc., 2 mL dioxane. Compound **44** (35 mg, Quantitative Yield) was isolated as a white solid. ^1H NMR (500 MHz, Methanol- d_4) δ 7.39 – 7.33 (m, 2H), 7.31 (dt, J = 7.7, 1.6 Hz, 1H), 7.29 – 7.23 (m, 3H), 7.23 – 7.19 (m, 2H), 7.19 – 7.14 (m, 1H), 4.41 (q, J = 6.9 Hz, 1H), 4.01 (s, 2H), 1.61 (d, J = 6.8 Hz, 3H). ^{13}C NMR (126 MHz, Methanol- d_4) δ 142.6, 140.8, 138.4, 129.3, 129.0, 128.5, 128.1, 126.8, 125.8, 123.9, 51.0, 41.3, 19.4.

(R)-1-(3-benzylphenyl)propan-1-aminium chloride (45): See Procedure C: 81 mg (0.25 mmol) of **31**, 0.4 mL HCl conc., 2 mL dioxane. Compound **45** (26 mg, 40.4 % yield) was isolated as a white solid. ^1H NMR (400 MHz, Methanol- d_4) δ 7.38 (dd, J = 8.2, 6.9 Hz, 1H), 7.31 (t, J = 1.7 Hz, 1H), 7.29 – 7.23 (m, 4H), 7.23 – 7.14 (m, 3H), 4.11 (dd, J = 9.3, 5.9 Hz, 1H), 4.01 (s, 2H), 2.09 – 1.85 (m, 2H), 0.86 (t, J = 7.4 Hz, 3H). ^{13}C NMR (101 MHz, Methanol- d_4) δ 142.7, 140.8, 136.9, 129.4, 129.0, 128.5, 128.1, 127.5, 125.8, 124.5, 56.9, 41.3, 27.3, 9.1.

(5-benzyl-2-methylphenyl)methanaminium chloride (46): See Procedure C: 65 mg (0.21 mmol) of **32**, 0.3 mL HCl conc., 3 mL dioxane. Compound **46** (42 mg, 82.3 % yield) was isolated as a white solid. ^1H NMR (500 MHz, Methanol- d_4) δ 7.29 (d, J = 1.7 Hz, 1H), 7.26 – 7.22 (m, 2H), 7.21 – 7.10 (m, 5H), 4.11 (s, 2H), 3.94 (s, 2H), 2.36 (s, 3H). ^{13}C NMR (126 MHz, Methanol- d_4) δ 141.0, 139.9, 134.3, 131.3, 130.7, 129.5, 129.4, 128.5, 128.1, 125.7, 40.9, 40.2, 17.2.

(5-benzyl-2-chlorophenyl)methanaminium chloride (47): See Procedure C: 45 mg (0.30 mmol) of **33**, 0.2 mL HCl conc., 2 mL dioxane. Compound **47** (33 mg, 91.8 % yield) was isolated as a white solid. ¹H NMR (500 MHz, Methanol-*d*₄) δ 7.45 – 7.40 (m, 2H), 7.30 – 7.25 (m, 3H), 7.24 – 7.16 (m, 3H), 4.22 (s, 2H), 4.00 (s, 2H). ¹³C NMR (126 MHz, Methanol-*d*₄) δ 141.7, 140.3, 131.4, 131.1, 130.6, 129.6, 128.5, 128.3, 126.0, 40.6, 40.3.

(5-benzyl-2-hydroxyphenyl)methanaminium bromide (48): See Procedure G: 103 mg (0.298 mmol) of **38**, 900 μL 1M BBr₃ in DCM (0.90 mmol, 3.02 eq.), 5 mL DCM. Compound **48** (64 mg, 73.0 % yield) was isolated as a yellow solid as the bromide salt. ¹H NMR (400 MHz, Methanol-*d*₄) δ 7.27 – 7.21 (m, 2H), 7.20 – 7.11 (m, 4H), 7.09 (dd, *J* = 8.2, 2.3 Hz, 1H), 6.83 (d, *J* = 8.2 Hz, 1H), 4.04 (s, 2H), 3.88 (s, 2H). ¹³C NMR (101 MHz, Methanol-*d*₄) δ 154.1, 141.5, 132.8, 130.8, 130.6, 128.4, 128.0, 125.6, 119.1, 114.8, 40.4, 39.4.

(2-acetamido-5-benzylphenyl)methanaminium chloride (49): See Procedure C: 94 mg (0.26 mmol) of **34**, 0.4 mL HCl conc., 2 mL dioxane. Compound **49** (69 mg, 90.6 % yield) was isolated as a white solid. ¹H NMR (500 MHz, Methanol-*d*₄) δ 7.43 (s, 1H), 7.30 – 7.24 (m, 3H), 7.24 – 7.20 (m, 2H), 7.20 – 7.15 (m, 2H), 4.00 (s, 2H), 3.99 (s, 2H), 2.20 (s, 3H). ¹³C NMR (126 MHz, Methanol-*d*₄) δ 173.9, 142.6, 142.1, 135.3, 132.2, 131.7, 130.2, 130.0, 129.7, 127.9, 127.4, 42.2, 40.9, 23.2.

(5-benzyl-2-(ethylamino)phenyl)methanaminium chloride (50): See Procedure H: 21 mg (0.072 mmol) of **49**, 260 μL (0.52 mmol, 7.2 eq.) of 2M BH₃*Me₂S in THF, and 4 mL of THF. Compound **50** continued to the next step without further purification.

(5-benzyl-2-propionamidophenyl)methanaminium chloride (51): See Procedure C: 68 mg (0.18 mmol) of **35**, 0.2 mL HCl conc., 2 mL dioxane. Compound **51** (50 mg, 89.9 % yield) was isolated as a yellow oil. ¹H NMR (500 MHz, Methanol-*d*₄) δ 7.38 (s, 1H), 7.31 – 7.12 (m, 7H),

3.99 (s, 2H), 3.94 (s, 2H), 2.46 (q, $J = 7.0$ Hz, 2H), 1.22 (t, $J = 6.6$ Hz, 3H). ^{13}C NMR (126 MHz, Methanol- d_4) δ 176.1, 141.0, 140.5, 133.9, 130.8, 130.4, 128.7, 128.6, 128.2, 126.4, 126.0, 40.9, 40.0, 29.1, 9.0.

(5-benzyl-2-methoxyphenyl)methanaminium chloride (52): See Procedure C: 98 mg (0.30 mmol) of **36**, 0.3 mL HCl conc., 1 mL dioxane. Compound **52** (44 mg, 56.4 % yield) was isolated as a white solid. ^1H NMR (500 MHz, Methanol- d_4) δ 7.27-7.23 (m, 3H), 7.21 – 7.12 (m, 4H), 6.99 (d, $J = 8.3$ Hz, 1H), 4.05 (s, 2H), 3.92 (s, 2H), 3.89 (s, 3H). ^{13}C NMR (126 MHz, Methanol- d_4) δ 156.2, 141.3, 133.9, 131.0, 130.9, 128.4, 128.1, 125.7, 120.7, 110.5, 54.8, 40.4, 39.2.

(5-benzyl-2-(trifluoromethoxy)phenyl)methanaminium chloride (53): See Procedure C: 105 mg (0.27 mmol) of **37**, 0.2 mL HCl conc., 2 mL dioxane. Compound **53** (76 mg, 87.8 % yield) was isolated as a yellow-white solid. ^1H NMR (400 MHz, Methanol- d_4) δ 7.50 (d, $J = 2.0$ Hz, 1H), 7.39 (dd, $J = 8.5, 1.9$ Hz, 1H), 7.33 (dq, $J = 8.5, 1.8$ Hz, 1H), 7.31 – 7.14 (m, 5H), 4.18 (s, 2H), 4.04 (s, 2H). ^{13}C NMR (101 MHz, Methanol- d_4) δ 145.6, 141.6, 140.2, 131.1, 130.9, 128.6, 128.3, 126.1, 125.4, 121.8, 120.5, 119.2, 40.5, 37.2.

(5-benzyl-2-ethoxyphenyl)methanaminium chloride (54): See Procedure C: 70 mg (0.20 mmol) of **38**, 0.4 mL HCl conc., 2 mL dioxane. Compound **54** (37 mg, 65.7 % yield) was isolated as a white solid. ^1H NMR (500 MHz, Methanol- d_4) δ 7.24 (d, $J = 7.0$ Hz, 3H), 7.21 – 7.12 (m, 4H), 6.98 (d, $J = 8.3$ Hz, 1H), 4.13 (q, $J = 6.6$ Hz, 2H), 4.06 (s, 2H), 3.92 (s, 2H), 1.44 (t, $J = 6.8$ Hz, 3H). ^{13}C NMR (126 MHz, Methanol- d_4) δ 155.4, 141.3, 133.8, 130.9, 130.7, 128.4, 128.1, 125.7, 120.8, 111.4, 63.7, 40.4, 39.0, 13.6.

(5-benzyl-2-propoxyphenyl)methanaminium chloride (55): See Procedure C: 37 mg (0.10 mmol) of **39**, 0.4 mL HCl conc., 2 mL dioxane. Compound **55** (27 mg, 71.0 % yield) was

purified via reverse phase chromatography and isolated as a colorless oil. ^1H NMR (500 MHz, Methanol- d_4) δ 7.27 – 7.22 (m, 3H), 7.20 – 7.13 (m, 4H), 6.98 (d, $J = 8.4$ Hz, 1H), 4.06 (s, 2H), 4.03 (t, $J = 6.6$ Hz, 2H), 3.92 (s, 2H), 1.86 (h, $J = 7.2$ Hz, 2H), 1.06 (t, $J = 7.4$ Hz, 3H). ^{13}C NMR (126 MHz, Methanol- d_4) δ 155.4, 141.3, 133.8, 130.9, 130.6, 128.4, 128.1, 125.7, 120.8, 111.4, 69.6, 40.4, 38.8, 22.0, 9.4.

(5-benzyl-2-(cyclopropylmethoxy)phenyl)methanaminium chloride (56): See Procedure D: 43 mg (0.12 mmol) of **40**, 0.2 mL HCl conc., 2 mL dioxane. Compound **56** (20 mg, 56.9 % yield) was isolated as a white solid. ^1H NMR (500 MHz, Methanol- d_4) δ 7.27 – 7.21 (m, 3H), 7.21 – 7.13 (m, 4H), 6.97 (d, $J = 8.4$ Hz, 1H), 4.09 (s, 2H), 3.94 – 3.90 (m, 4H), 1.36 – 1.27 (m, 1H), 0.66 – 0.60 (m, 2H), 0.38 (dt, $J = 6.1, 4.5$ Hz, 2H). ^{13}C NMR (126 MHz, Methanol- d_4) δ 155.5, 141.3, 133.9, 130.9, 130.6, 128.4, 128.1, 125.7, 120.9, 111.8, 73.0, 40.4, 38.9, 9.7, 2.2.

(5-benzyl-2-(benzyloxy)phenyl)methanaminium chloride (57): See Procedure D: 57 mg (0.14 mmol) of **41**, 0.3 mL HCl conc., 2 mL dioxane. Compound **57** (31 mg, 65.3 % yield) was isolated as a white solid. ^1H NMR (500 MHz, Methanol- d_4) δ 7.50 – 7.45 (m, 2H), 7.41 – 7.36 (m, 2H), 7.35 – 7.30 (m, 1H), 7.28 – 7.21 (m, 4H), 7.21 – 7.14 (m, 3H), 7.07 – 7.01 (m, 1H), 5.19 (s, 2H), 4.10 (s, 2H), 3.92 (s, 2H). ^{13}C NMR (126 MHz, Methanol- d_4) δ 155.1, 141.2, 136.8, 134.3, 130.9, 130.7, 128.4, 128.3, 128.1, 127.7, 127.3, 125.7, 121.1, 112.2, 70.0, 40.4, 38.8.

(R)-1-(5-benzyl-2-methoxyphenyl)ethan-1-aminium chloride (58): See Procedure D: 29 mg (0.084 mmol) of **42**, 0.4 mL HCl conc., 2 mL dioxane. Compound **58** (20 mg, 85.8 % yield) was isolated as an off-yellow colorless oil (insoluble in diethyl ether). ^1H NMR (500 MHz, Methanol- d_4) δ 7.27 – 7.22 (m, 3H), 7.21 – 7.13 (m, 4H), 7.01 (d, $J = 8.4$ Hz, 1H), 4.59 (q, $J = 6.6$ Hz, 1H), 3.93 (s, 2H), 3.89 (s, 3H), 1.59 (d, $J = 6.8$ Hz, 3H). ^{13}C NMR (126 MHz, Methanol- d_4) δ 155.3, 141.3, 134.1, 130.4, 128.4, 128.1, 127.5, 125.7, 125.3, 111.0, 54.8, 40.5, 17.6.

(S)-1-((3-benzylbenzyl)amino)-3-(4-hydroxy-2,6-dimethylphenyl)-1-oxopropan-2-aminium trifluoroacetate (59): See Procedure D: Step 1: 16 mg (0.068 mmol) of **43**, 120 μ L (89 mg, 0.69 mmol, 10.1 eq.) of N,N-diisopropylethylamine, 39 mg (0.075 mmol, 1.1 eq.) of PyBOP, 12 mg (0.071 mmol, 1.0 eq.) of 6-Cl-HOBt, 28 mg (0.068 mmol, 1.0 eq.) of Boc-O-Boc-L-2',6'-dimethyltyrosine, 3+1.5 mL of DMF. Step 2: 2 mL TFA and 2 mL DCM. Compound **59** (10 mg, 29.1 % yield) was isolated as a white solid. ^1H NMR (400 MHz, Methanol- d_4) δ 7.25-7.21 (m, 2H), 7.18-7.12 (m, 4H), 7.06 (d, $J = 7.7$ Hz, 1H), 6.93 (s, 1H), 6.78 (d, $J = 7.8$ Hz, 1H), 6.46 (s, 2H), 4.30 (d, $J = 14.7$ Hz, 1H), 4.11 (d, $J = 14.7$ Hz, 1H), 3.92 (s, 2H), 3.83 (dd, $J = 11.3, 4.8$ Hz, 1H), 3.19 (dd, $J = 13.6, 11.5$ Hz, 1H), 2.96 (dd, $J = 13.8, 4.8$ Hz, 1H), 2.18 (s, 6H). No ^{13}C Data Acquired. ESI-MS: 389.3 $[\text{M} + \text{H}]^+$, HPLC (gradient A): Retention Time: 36.25 min.

(S)-1-(((R)-1-(3-benzylphenyl)ethyl)amino)-3-(4-hydroxy-2,6-dimethylphenyl)-1-oxopropan-2-aminium trifluoroacetate (60): See Procedure D: Step 1: 14 mg (0.057 mmol) of **44**, 100 μ L (74 mg, 0.57 mmol, 10.2 eq.) of N,N-diisopropylethylamine, 31 mg (0.060 mmol, 1.1 eq.) of PyBOP, 11 mg (0.065 mmol, 1.2 eq.) of 6-Cl-HOBt, 26 mg (0.063 mmol, 1.1 eq.) of Boc-O-Boc-L-2',6'-dimethyltyrosine, 3+1.5 mL of DMF. Step 2: 2 mL TFA and 2 mL DCM. Compound **60** (14.4 mg, 49.3 % yield) was isolated as a white solid. ^1H NMR (500 MHz, Methanol- d_4) δ 7.27 – 7.20 (m, 2H), 7.21 – 7.11 (m, 4H), 7.11 (s, 1H), 7.07 (d, $J = 7.8$ Hz, 1H), 7.03 (d, $J = 7.5$ Hz, 1H), 6.54 (s, 2H), 4.79 (q, $J = 6.7$ Hz, 1H), 3.91 (s, 2H), 3.79 (dd, $J = 11.5, 4.6$ Hz, 1H), 3.21 (dd, $J = 13.7, 11.6$ Hz, 1H), 3.01 (dd, $J = 13.8, 4.7$ Hz, 1H), 2.28 (s, 6H), 1.10 (d, $J = 7.0$ Hz, 3H). No ^{13}C Data Acquired. ESI-MS: 403.2 $[\text{M} + \text{H}]^+$, HPLC (gradient A): Retention Time: 38.26 min.

(S)-1-(((R)-1-(3-benzylphenyl)propyl)amino)-3-(4-hydroxy-2,6-dimethylphenyl)-1-oxopropan-2-aminium trifluoroacetate (61): See Procedure D: Step 1: 18 mg (0.069 mmol) of

45, 140 μ L (103 mg, 0.80 mmol, 11.7 eq.) of N,N-diisopropylethylamine, 45 mg (0.086 mmol, 1.3 eq.) of PyBOP, 14 mg (0.083 mmol, 1.2 eq.) of 6-Cl-HOBt, 30 mg (0.073 mmol, 1.1 eq.) of Boc-O-Boc-L-2',6'-dimethyltyrosine, 3+1.5 mL of DMF. Step 2: 2 mL TFA and 2 mL DCM. Compound **61** (10 mg, 27.4 % yield) was isolated as a white solid. ^1H NMR (500 MHz, Methanol- d_4) δ 8.12 (d, J = 8.0 Hz, 1H), 7.25 – 7.11 (m, 6H), 7.10 (s, 1H), 7.09 – 7.00 (m, 2H), 6.52 (s, 2H), 4.51 (dd, J = 8.8, 6.5 Hz, 1H), 3.92 (s, 2H), 3.83 (dd, J = 11.5, 4.6 Hz, 1H), 3.23 (dd, J = 13.8, 11.5 Hz, 1H), 2.98 (dd, J = 13.8, 4.6 Hz, 1H), 2.29 (s, 6H), 1.47 (tt, J = 9.2, 4.6 Hz, 2H), 0.56 (t, J = 7.4 Hz, 3H). No ^{13}C Data Acquired. ESI-MS: 417.3 $[\text{M} + \text{H}]^+$, HPLC (gradient A): Retention Time: 40.94 min.

(S)-1-((5-benzyl-2-methylbenzyl)amino)-3-(4-hydroxy-2,6-dimethylphenyl)-1-oxopropan-2-aminium trifluoroacetate (62): See Procedure D: Step 1: 20 mg (0.081 mmol) of **46**, 170 μ L (126 mg, 0.98 mmol, 12.1 eq.) of N,N-diisopropylethylamine, 54 mg (0.10 mmol, 1.3 eq.) of PyBOP, 20 mg (0.12 mmol, 1.5 eq.) of 6-Cl-HOBt, 39 mg (0.095 mmol, 1.3 eq.) of Boc-O-Boc-L-2',6'-dimethyltyrosine, 3+1.5 mL of DMF. Step 2: 2 mL TFA and 2 mL DCM. Compound **62** (6 mg, 14.4 % yield) was isolated as a white solid. ^1H NMR (500 MHz, Methanol- d_4) δ 7.99 (s, 1H), 7.23 (t, J = 7.5 Hz, 2H), 7.14 (dd, J = 15.9, 7.6 Hz, 3H), 7.03 (d, J = 7.8 Hz, 1H), 6.99 (d, J = 7.6 Hz, 1H), 6.94 (s, 1H), 6.41 (s, 2H), 4.25 (dd, J = 14.7, 4.7 Hz, 1H), 4.16 (dd, J = 14.5, 5.0 Hz, 1H), 3.88 (s, 2H), 3.82 (dd, J = 11.3, 4.7 Hz, 1H), 3.15 (dd, J = 13.5, 11.5 Hz, 1H), 2.93 (dd, J = 13.7, 4.7 Hz, 1H), 2.10 (s, 6H), 2.03 (s, 3H). No ^{13}C Data Acquired. ESI-MS: 403.3 $[\text{M} + \text{H}]^+$, HPLC (gradient A): Retention Time: 38.13 min.

(S)-1-((5-benzyl-2-chlorobenzyl)amino)-3-(4-hydroxy-2,6-dimethylphenyl)-1-oxopropan-2-aminium trifluoroacetate (63): See Procedure D: Step 1: 20 mg (0.075 mmol) of **47**, 150 μ L (111 mg, 0.86 mmol, 11.5 eq.) of N,N-diisopropylethylamine, 47 mg (0.090 mmol, 1.2

eq.) of PyBOP, 16 mg (0.094 mmol, 1.3 eq.) of 6-Cl-HOBt, 39 mg (0.095 mmol, 1.3 eq.) of Boc-O-Boc-L-2',6'-dimethyltyrosine, 3+1.5 mL of DMF. Step 2: 2 mL TFA and 2 mL DCM. Compound **63** (18 mg, 44.9 % yield) was isolated as a white solid. ¹H NMR (400 MHz, Methanol-*d*₄) δ 7.69-7.66 (m, 3H), 7.61-7.58 (m, 3H), 7.53 – 7.44 (m, 2H), 6.81 (s, 2H), 4.82 (d, *J* = 14.9 Hz, 1H), 4.67 (d, *J* = 14.8 Hz, 1H), 4.35 (s, 2H), 4.30 (dd, *J* = 11.4, 4.8 Hz, 1H), 3.57 (dd, *J* = 13.4, 11.6 Hz, 1H), 3.36 (dd, *J* = 13.9, 5.0 Hz, 1H), 2.53 (s, 6H). No ¹³C Data Acquired. ESI-MS: 423.2 [M + H]⁺, HPLC (gradient A): Retention Time: 38.05 min.

(S)-1-((5-benzyl-2-hydroxybenzyl)amino)-3-(4-hydroxy-2,6-dimethylphenyl)-1-oxopropan-2-aminium trifluoroacetate (64): See Procedure D: Step 1: 12 mg (0.041 mmol) of **48**, 90 μL (67 mg, 0.52 mmol, 12.7 eq.) of N,N-diisopropylethylamine, 26 mg (0.050 mmol, 1.2 eq.) of PyBOP, 9 mg (0.053 mmol, 1.3 eq.) of 6-Cl-HOBt, 20 mg (0.049 mmol, 1.2 eq.) of Boc-O-Boc-L-2',6'-dimethyltyrosine, 3+1.5 mL of DMF. Step 2: 2 mL TFA and 2 mL DCM. Compound **64** (7 mg, 28.1 % yield) was isolated as a white solid. ¹H NMR (500 MHz, Methanol-*d*₄) δ 7.88 (t, *J* = 5.7 Hz, 1H), 7.23 (t, *J* = 7.5 Hz, 2H), 7.18 – 7.07 (m, 3H), 6.92 (dd, *J* = 8.2, 2.2 Hz, 1H), 6.80 (d, *J* = 2.2 Hz, 1H), 6.66 (d, *J* = 8.2 Hz, 1H), 6.39 (s, 2H), 4.20 (d, *J* = 3.8 Hz, 2H), 3.89 – 3.81 (m, 3H), 3.14 (dd, *J* = 14.0, 11.2 Hz, 1H), 2.94 (dd, *J* = 13.9, 4.8 Hz, 1H), 2.12 (s, 6H). No ¹³C Data Acquired. ESI-MS: 405.3 [M + H]⁺, HPLC (gradient A): Retention Time: 33.69 min.

(S)-1-((2-acetamido-5-benzylbenzyl)amino)-3-(4-hydroxy-2,6-dimethylphenyl)-1-oxopropan-2-aminium trifluoroacetate (65): See Procedure D: Step 1: 31 mg (0.11 mmol) of **49**, 190 μL (141 mg, 1.1 mmol, 10.2 eq.) of N,N-diisopropylethylamine, 58 mg (0.11 mmol, 1.0 eq.) of PyBOP, 19 mg (0.11 mmol, 1.1 eq.) of 6-Cl-HOBt, 44 mg (0.11 mmol, 1.0 eq.) of Boc-O-Boc-L-2',6'-dimethyltyrosine, 3+1.5 mL of DMF. Step 2: 2 mL TFA and 2 mL DCM. Compound **65** (12 mg, 20.1 % yield) was isolated as a white solid. ¹H NMR (500 MHz, Methanol-*d*₄) δ 7.42

(d, $J = 8.2$ Hz, 1H), 7.27 – 7.20 (m, 2H), 7.20 – 7.09 (m, 4H), 6.89 (d, $J = 2.0$ Hz, 1H), 6.42 (s, 2H), 4.14 (d, $J = 2.8$ Hz, 2H), 3.93 (d, $J = 2.9$ Hz, 2H), 3.80 (dd, $J = 11.2, 4.9$ Hz, 1H), 3.15 (dd, $J = 13.9, 11.2$ Hz, 1H), 2.96 (dd, $J = 13.9, 5.0$ Hz, 1H), 2.16 (s, 3H), 2.13 (s, 6H). No ^{13}C Data Acquired. ESI-MS: 446.3 $[\text{M} + \text{H}]^+$, HPLC (gradient A): Retention Time: 31.27 min.

(S)-1-((5-benzyl-2-(ethylamino)benzyl)amino)-3-(4-hydroxy-2,6-dimethylphenyl)-1-oxopropan-2-aminium trifluoroacetate (66): See Procedure D: Step 1: 0.072 mmol of **50**, 130 μL (96 mg, 0.75 mmol, 10.3 eq.) of N,N-diisopropylethylamine, 40 mg (0.077 mmol, 1.1 eq.) of PyBOP, 14 mg (0.083 mmol, 1.1 eq.) of 6-Cl-HOBt, 30 mg (0.073 mmol, 1.0 eq.) of Boc-O-Boc-L-2',6'-dimethyltyrosine, 3+1.5 mL of DMF. Step 2: 2 mL TFA and 2 mL DCM. Compound **66** (15.9 mg, 40.4 % yield) was isolated as a white solid. ^1H NMR (400 MHz, Methanol- d_4) δ 7.42 – 7.32 (m, 2H), 7.31 – 7.22 (m, 2H), 7.23 – 7.14 (m, 3H), 7.00 (d, $J = 1.8$ Hz, 1H), 6.35 (s, 2H), 4.22 (d, $J = 15.0$ Hz, 1H), 4.12 (d, $J = 15.0$ Hz, 1H), 4.03 (d, $J = 3.4$ Hz, 2H), 3.88 (dd, $J = 11.4, 4.9$ Hz, 1H), 3.48 (qd, $J = 7.2, 1.7$ Hz, 2H), 3.12 (dd, $J = 13.9, 11.5$ Hz, 1H), 2.99 (dd, $J = 13.9, 5.0$ Hz, 1H), 2.03 (s, 6H), 1.45 (t, $J = 7.2$ Hz, 3H). No ^{13}C Data Acquired. ESI-MS: 432.3 $[\text{M} + \text{H}]^+$, HPLC (gradient A): Retention Time: 28.11 min.

(S)-1-((5-benzyl-2-propionamidobenzyl)amino)-3-(4-hydroxy-2,6-dimethylphenyl)-1-oxopropan-2-aminium trifluoroacetate (67): See Procedure D: Step 1: 6 mg (0.020 mmol) of **51**, 40 μL (30 mg, 0.23 mmol, 11.3 eq.) of N,N-diisopropylethylamine, 12 mg (0.023 mmol, 1.1 eq.) of PyBOP, 11 mg (0.065 mmol, 3.2 eq.) of 6-Cl-HOBt, 11 mg (0.027 mmol, 1.3 eq.) of Boc-O-Boc-L-2',6'-dimethyltyrosine, 3+1.5 mL of DMF. Step 2: 2 mL TFA and 2 mL DCM. Compound **67** (6.4 mg, 56.7 % yield) was isolated as a white solid. ^1H NMR (500 MHz, Methanol- d_4) δ 8.20 (t, $J = 6.1$ Hz, 1H), 7.42 (d, $J = 8.2$ Hz, 1H), 7.24 (t, $J = 7.6$ Hz, 2H), 7.18 – 7.11 (m, 4H), 6.87 (d, $J = 2.0$ Hz, 1H), 6.41 (s, 2H), 4.12 (d, $J = 3.1$ Hz, 2H), 3.93 (d, $J = 3.1$ Hz, 2H), 3.80

(dd, $J = 11.2, 4.9$ Hz, 1H), 3.15 (dd, $J = 13.9, 11.3$ Hz, 1H), 2.96 (dd, $J = 13.9, 4.9$ Hz, 1H), 2.44 (q, $J = 7.6$ Hz, 2H), 2.11 (s, 6H), 1.23 (t, $J = 7.6$ Hz, 3H). No ^{13}C Data Acquired. ESI-MS: 460.3 $[\text{M} + \text{H}]^+$, HPLC (gradient A): Retention Time: 32.89 min.

(S)-1-((5-benzyl-2-methoxybenzyl)amino)-3-(4-hydroxy-2,6-dimethylphenyl)-1-oxopropan-2-aminium trifluoroacetate (68): See Procedure D: Step 1: 22 mg (0.083 mmol) of **52**, 170 μL (126 mg, 0.98 mmol, 11.8 eq.) of N,N-diisopropylethylamine, 51 mg (0.098 mmol, 1.2 eq.) of PyBOP, 19 mg (0.11 mmol, 1.4 eq.) of 6-Cl-HOBt, 43 mg (0.11 mmol, 1.3 eq.) of Boc-O-Boc-L-2',6'-dimethyltyrosine, 3+1.5 mL of DMF. Step 2: 2 mL TFA and 2 mL DCM. Compound **68** (18 mg, 40.5 % yield) was isolated as a white solid. ^1H NMR (500 MHz, Methanol- d_4) δ 7.63 (t, $J = 5.9$ Hz, 1H), 7.25 (t, $J = 7.6$ Hz, 2H), 7.21 – 7.17 (m, 2H), 7.15 (tt, $J = 7.2, 1.3$ Hz, 1H), 7.10 (dd, $J = 8.4, 2.3$ Hz, 1H), 6.96 (d, $J = 2.2$ Hz, 1H), 6.81 (d, $J = 8.4$ Hz, 1H), 6.31 (s, 2H), 4.37 – 4.26 (m, 1H), 4.12 (dd, $J = 14.2, 4.6$ Hz, 1H), 3.89 – 3.83 (m, 3H), 3.67 (s, 3H), 3.10 (dd, $J = 13.8, 11.6$ Hz, 1H), 2.92 (dd, $J = 13.8, 4.5$ Hz, 1H), 2.03 (s, 6H). No ^{13}C Data Acquired. ESI-MS: 419.3 $[\text{M} + \text{H}]^+$, HPLC (gradient A): Retention Time: 37.07 min.

(S)-1-((5-benzyl-2-(trifluoromethoxy)benzyl)amino)-3-(4-hydroxy-2,6-dimethylphenyl)-1-oxopropan-2-aminium trifluoroacetate (69): See Procedure D: Step 1: 19 mg (0.060 mmol) of **53**, 110 μL (82 mg, 0.63 mmol, 10.5 eq.) of N,N-diisopropylethylamine, 32 mg (0.061 mmol, 1.0 eq.) of PyBOP, 11 mg (0.065 mmol, 1.1 eq.) of 6-Cl-HOBt, 29 mg (0.071 mmol, 1.2 eq.) of Boc-O-Boc-L-2',6'-dimethyltyrosine, 3+1.5 mL of DMF. Step 2: 2 mL TFA and 2 mL DCM. Compound **69** (19 mg, 54.2 % yield) was isolated as a white solid. ^1H NMR (500 MHz, Methanol- d_4) δ 8.10 (t, $J = 5.7$ Hz, 1H), 7.29 – 7.22 (m, 2H), 7.20 – 7.12 (m, 5H), 7.01 (s, 1H), 6.43 (s, 2H), 4.39 (dd, $J = 15.1, 6.4$ Hz, 1H), 4.23 (dd, $J = 15.2, 4.7$ Hz, 1H), 3.95 (d, $J = 3.7$ Hz, 2H), 3.89 (dd, $J = 11.1, 5.0$ Hz, 1H), 3.16 (dd, $J = 13.9, 11.1$ Hz, 1H), 2.97 (dd, $J = 13.9, 5.0$

Hz, 1H), 2.15 (s, 6H). No ^{13}C Data Acquired. ESI-MS: 473.3 $[\text{M} + \text{H}]^+$, HPLC (gradient A): Retention Time: 42.11 min.

(S)-1-((5-benzyl-2-ethoxybenzyl)amino)-3-(4-hydroxy-2,6-dimethylphenyl)-1-oxopropan-2-aminium trifluoroacetate (70): See Procedure D: Step 1: 18 mg (0.065 mmol) of **54**, 120 μL (89 mg, 0.69 mmol, 10.6 eq.) of N,N-diisopropylethylamine, 38 mg (0.073 mmol, 1.1 eq.) of PyBOP, 13 mg (0.077 mmol, 1.2 eq.) of 6-Cl-HOBt, 26 mg (0.063 mmol, 0.98 eq.) of Boc-O-Boc-L-2',6'-dimethyltyrosine, 3+1.5 mL of DMF. Step 2: 2 mL TFA and 2 mL DCM. Compound **70** (15 mg, 42.4 % yield) was isolated as a white solid. ^1H NMR (500 MHz, Methanol- d_4) δ 7.35 (t, $J = 5.7$ Hz, 1H), 7.23 (t, $J = 7.5$ Hz, 2H), 7.21 – 7.16 (m, 2H), 7.13 (t, $J = 7.2$ Hz, 1H), 7.07 (dd, $J = 8.4, 2.3$ Hz, 1H), 6.93 (d, $J = 2.2$ Hz, 1H), 6.78 (d, $J = 8.4$ Hz, 1H), 6.30 (s, 2H), 4.33 (dd, $J = 14.3, 7.0$ Hz, 1H), 4.14 (dd, $J = 14.3, 4.6$ Hz, 1H), 3.93 – 3.84 (m, 5H), 3.08 (dd, $J = 13.8, 11.6$ Hz, 1H), 2.91 (dd, $J = 13.8, 4.6$ Hz, 1H), 2.01 (s, 6H), 1.27 (t, $J = 7.0$ Hz, 3H). No ^{13}C Data Acquired. ESI-MS: 433.3 $[\text{M} + \text{H}]^+$, HPLC (gradient A): Retention Time: 39.20 min.

(S)-1-((5-benzyl-2-propoxybenzyl)amino)-3-(4-hydroxy-2,6-dimethylphenyl)-1-oxopropan-2-aminium trifluoroacetate (71): See Procedure D: Step 1: 24 mg (0.065 mmol) of **55**, 110 μL (82 mg, 0.63 mmol, 9.7 eq.) of N,N-diisopropylethylamine, 37 mg (0.071 mmol, 1.1 eq.) of PyBOP, 14 mg (0.083 mmol, 1.3 eq.) of 6-Cl-HOBt, 30 mg (0.073 mmol, 1.1 eq.) of Boc-O-Boc-L-2',6'-dimethyltyrosine, 3+1.5 mL of DMF. Step 2: 2 mL TFA and 2 mL DCM. Compound **71** (17 mg, 46.7 % yield) was isolated as a white solid. ^1H NMR (500 MHz, Methanol- d_4) δ 7.31 (t, $J = 5.8$ Hz, 1H), 7.25-7.22 (m, 2H), 7.20 – 7.16 (m, 2H), 7.13 (t, $J = 7.1$ Hz, 1H), 7.06 (dd, $J = 8.4, 2.2$ Hz, 1H), 6.92 (d, $J = 2.2$ Hz, 1H), 6.78 (d, $J = 8.3$ Hz, 1H), 6.30 (s, 2H), 4.36 (dd, $J = 14.4, 7.0$ Hz, 1H), 4.15 (dd, $J = 14.4, 4.4$ Hz, 1H), 3.89 – 3.85 (m, 3H), 3.80 (td, $J = 6.6, 4.5$ Hz, 2H), 3.08 (dd, $J = 13.8, 11.6$ Hz, 1H), 2.92 (dd, $J = 13.8, 4.6$ Hz, 1H), 2.02 (s, 6H), 1.67

(h, $J = 7.1$ Hz, 2H), 0.99 (t, $J = 7.4$ Hz, 3H). No ^{13}C Data Acquired. ESI-MS: 447.3 $[\text{M} + \text{H}]^+$, HPLC (gradient A): Retention Time: 42.13 min.

(S)-1-((5-benzyl-2-(cyclopropylmethoxy)benzyl)amino)-3-(4-hydroxy-2,6-dimethylphenyl)-1-oxopropan-2-aminium trifluoroacetate (72): See Procedure D: Step 1: 17 mg (0.045 mmol) of **56**, 140 μL (104 mg, 0.80 mmol, 18.0 eq.) of N,N-diisopropylethylamine, 35 mg (0.067 mmol, 1.5 eq.) of PyBOP, 13 mg (0.077 mmol, 1.7 eq.) of 6-Cl-HOBt, 28 mg (0.068 mmol, 1.5 eq.) of Boc-O-Boc-L-2',6'-dimethyltyrosine, 3+1.5 mL of DMF. Step 2: 2 mL TFA and 2 mL DCM. Compound **72** (4 mg, 12.5 % yield) was isolated as a white solid. ^1H NMR (500 MHz, Methanol- d_4) δ 7.23 (t, $J = 7.6$ Hz, 2H), 7.20 – 7.16 (m, 2H), 7.13 (t, $J = 7.3$ Hz, 1H), 7.06 (dd, $J = 8.4, 2.2$ Hz, 1H), 6.92 (d, $J = 2.2$ Hz, 1H), 6.76 (d, $J = 8.4$ Hz, 1H), 6.29 (s, 2H), 4.37 (d, $J = 14.4$ Hz, 1H), 4.18 (d, $J = 14.4$ Hz, 1H), 3.87 (s, 2H), 3.84 (dd, $J = 11.7, 4.8$ Hz, 1H), 3.74 – 3.61 (m, 2H), 3.08 (dd, $J = 13.8, 11.5$ Hz, 1H), 2.90 (dd, $J = 13.8, 4.6$ Hz, 1H), 2.03 (s, 6H), 1.12 (ddd, $J = 12.7, 8.0, 5.6$ Hz, 1H), 0.56 (d, $J = 7.5$ Hz, 2H), 0.27 (dd, $J = 7.1, 5.0$ Hz, 2H). No ^{13}C Data Acquired. ESI-MS: 459.3 $[\text{M} + \text{H}]^+$, HPLC (gradient A): Retention Time: 42.68 min.

(S)-1-((5-benzyl-2-(benzyloxy)benzyl)amino)-3-(4-hydroxy-2,6-dimethylphenyl)-1-oxopropan-2-aminium trifluoroacetate (73): See Procedure D: Step 1: 17 mg (0.050 mmol) of **57**, 100 μL (74 mg, 0.57 mmol, 11.5 eq.) of N,N-diisopropylethylamine, 31 mg (0.060 mmol, 1.2 eq.) of PyBOP, 10 mg (0.059 mmol, 1.2 eq.) of 6-Cl-HOBt, 24 mg (0.059 mmol, 1.2 eq.) of Boc-O-Boc-L-2',6'-dimethyltyrosine, 3+1.5 mL of DMF. Step 2: 2 mL TFA and 2 mL DCM. Compound **73** (11 mg, 36.1 % yield) was isolated as a white solid. ^1H NMR (400 MHz, Methanol- d_4) δ 7.44 – 7.38 (m, 1H), 7.36 (d, $J = 4.4$ Hz, 4H), 7.32 – 7.27 (m, 1H), 7.26 – 7.21 (m, 2H), 7.21 – 7.16 (m, 2H), 7.13 (t, $J = 7.2$ Hz, 1H), 7.08 (dd, $J = 8.3, 2.2$ Hz, 1H), 6.95 (d, $J = 2.2$ Hz, 1H), 6.87 (d, $J = 8.4$ Hz, 1H), 6.29 (s, 2H), 4.95 (d, $J = 4.3$ Hz, 2H), 4.40 (dd, $J = 14.4, 7.0$ Hz, 1H),

4.17 (dd, $J = 14.4, 4.3$ Hz, 1H), 3.88 (s, 2H), 3.80 (dd, $J = 11.4, 4.6$ Hz, 1H), 3.06 (dd, $J = 13.4, 11.8$ Hz, 1H), 2.89 (dd, $J = 13.8, 4.7$ Hz, 1H), 1.98 (s, 6H). No ^{13}C Data Acquired. ESI-MS: 495.3 $[\text{M} + \text{H}]^+$, HPLC (gradient A): Retention Time: 44.98 min.

(S)-1-(((R)-1-(5-benzyl-2-methoxyphenyl)ethyl)amino)-3-(4-hydroxy-2,6-dimethylphenyl)-1-oxopropan-2-aminium trifluoroacetate (74): See Procedure D: Step 1: 12 mg (0.043 mmol) of **58**, 76 μL (56 mg, 0.44 mmol, 10.1 eq.) of N,N-diisopropylethylamine, 24 mg (0.046 mmol, 1.1 eq.) of PyBOP, 8 mg (0.047 mmol, 1.1 eq.) of 6-Cl-HOBt, 19 mg (0.046 mmol, 1.1 eq.) of Boc-O-Boc-L-2',6'-dimethyltyrosine, 3+1.5 mL of DMF. Step 2: 2 mL TFA and 2 mL DCM. Compound **74** (7 mg, 29.6 % yield) was isolated as a white solid. ^1H NMR (500 MHz, Methanol- d_4) δ 7.52 (d, $J = 8.0$ Hz, 1H), 7.22 (dd, $J = 8.2, 7.0$ Hz, 2H), 7.16 – 7.09 (m, 3H), 7.02 – 6.94 (m, 2H), 6.82 (d, $J = 8.3$ Hz, 1H), 6.55 (s, 2H), 5.08 (p, $J = 6.9$ Hz, 1H), 3.87 (dd, $J = 11.6, 4.7$ Hz, 1H), 3.84 (s, 2H), 3.76 (s, 3H), 3.20 (dd, $J = 13.7, 11.7$ Hz, 1H), 3.02 (dd, $J = 13.8, 4.8$ Hz, 1H), 2.29 (s, 6H), 1.06 (d, $J = 6.9$ Hz, 3H). No ^{13}C Data Acquired. ESI-MS: 433.4 $[\text{M} + \text{H}]^+$, HPLC (gradient A): Retention Time: 40.43 min.

***In Vitro* Pharmacology**

Cell Lines and Membrane Preparations.

All opioid *in vitro* assays were performed by Nicholas Griggs, Thomas Fernandez, and Jessica Anand. Tissue culture reagents were purchased from Gibco Life Sciences (Grand Island, NY, U.S.) unless otherwise noted. C6-rat glioma cells stably expressing rat MOR (C6-MOR) or rat DOR (C6-DOR) and Chinese hamster ovary (CHO) cells stably expressing human DOR (CHO-DOR) or human KOR (CHO-KOR) were used for all *in vitro* assays. Cells were grown to confluence at 37 °C in 5 % CO_2 in Dulbecco's modified Eagle medium (DMEM) containing 10 % fetal bovine serum and 5 % penicillin/streptomycin. Membranes were prepared by washing

confluent cells three times with ice cold phosphate buffered saline (0.9 % NaCl, 0.61 mM Na₂HPO₄, 0.38 mM KH₂PO₄, pH 7.4). Cells were detached from the plates by incubation in warm harvesting buffer (20 mM HEPES, 150 mM NaCl, 0.68 mM EDTA, pH 7.4) and pelleted by centrifugation at 1600 rpm for 3 min. The cell pellet was suspended in ice-cold 50 mM Tris- HCl buffer, pH 7.4, and homogenized with a Tissue Tearor (Biospec Products, Inc., Bartlesville, OK, U.S.) for 20 s. The homogenate was centrifuged at 15,000 rpm for 20 min at 4 °C. The pellet was rehomogenized in 50 mM Tris-HCl with a Tissue Tearor for 10 s, followed by recentrifugation. The final pellet was resuspended in 50 mM Tris-HCl and frozen in aliquots at -80 °C. Protein concentration was determined via a BCA protein assay (Thermo Scientific Pierce, Waltham, MA, U.S.) using bovine serum albumin as the standard.

Radioligand Competition Binding Assays.

Radiolabeled compounds were purchased from Perkin-Elmer (Waltham, MA, U.S.). Opioid ligand binding assays were performed by competitive displacement of 0.2 nM [³H]-diprenorphine (250 µCi, 1.85 TBq/mmol) by the peptidomimetic from membrane preparations containing opioid receptors as described above. The assay mixture, containing membranes (20 µg protein/tube) in 50 mM Tris-HCl buffer (pH 7.4), 0.2 nM [³H]-diprenorphine, and various concentrations of test peptidomimetic, was incubated at room temperature on a shaker for 1 h to allow binding to reach equilibrium. The samples were rapidly filtered through Whatman GF/C filters using a Brandel harvester (Brandel, Gaithersburg, MD, U.S.) and washed three times with 50 mM Tris-HCl buffer, pH 7.4. Bound radioactivity on dried filters was determined by liquid scintillation counting, after saturation with EcoLume liquid scintillation cocktail, in a Wallac 1450 MicroBeta (Perkin-Elmer, Waltham, MA, U.S.). Nonspecific binding was determined using 10 µM naloxone. The results presented are the mean ± standard error (S.E.M.) from at least three

separate assays performed in duplicate. K_i (nM) values were calculated using nonlinear regression analysis to fit a logistic equation to the competition data using GraphPad Prism, version 6.0c, (GraphPad Software Inc., La Jolla, CA).

[³⁵S]-GTP γ S Binding Assays.

Agonist stimulation of [³⁵S]guanosine 5'-O-[γ -thio]triphosphate ([³⁵S]-GTP γ S, 1250 Ci, 46.2 TBq/mmol) binding to G protein was measured as described previously.⁸² Briefly, membranes (10 μ g of protein/well) were incubated for 1 h at 25°C in GTP γ S buffer (50 mM Tris-HCl, 100 mM NaCl, 5 mM MgCl₂, 1 mM EDTA, pH 7.4) containing 0.1 nM [³⁵S]-GTP γ S, 30 μ M guanosine diphosphate (GDP), and varying concentrations of test peptidomimetic. G protein activation following receptor activation by peptidomimetic was compared with 10 μ M of the standard compounds [D-Ala²,N-MePhe⁴,Gly-ol]enkephalin (DAMGO) at MOR, D-Pen^{2,5}-enkephalin (DPDPE) at DOR, or U69,593 at KOR. The reaction was terminated by vacuum filtration through GF/C filters that were washed 5 times with GTP γ S buffer. Bound radioactivity was measured as described above. The results are presented as the mean \pm standard error (S.E.M.) from at least three separate assays performed in duplicate; potency (EC₅₀ (nM)) and percent stimulation were determined using nonlinear regression analysis with GraphPad Prism 6, as above.

K_e Determination.

Agonist stimulation of [³⁵S]GTP γ S binding by the known standard agonist DPDPE at delta opioid receptor was measured as described above. This was then compared to [³⁵S]GTP γ S binding stimulated by DPDPE in the presence of test compound. Both conditions produced 100% stimulation relative to DPDPE. The fold difference between the EC₅₀ of DPDPE alone and in the presence of test compound is defined as the shift in dose response. The K_e was then calculated as $K_e = (\text{concentration of test compound}) / (\text{Dose response shift} - 1)$. The results presented are the

mean \pm SEM from three individual assays performed in duplicate and then averaged. The data were fitted to a non-linear regression curve (sigmoidal dose response curve for agonist stimulation) using GraphPad Prism v8.01.

Mouse Liver Microsome Stability Assays

All liver microsome assays were performed by Quintara Biosciences. Metabolic stability of testing compounds was evaluated using mouse liver microsomes to predict intrinsic clearance. Mouse liver microsome tissue fractions were obtained from Corning or BioreclamationIVT. The assay was carried out in 96-well microtiter plates at 37 °C. Reaction mixtures (25 μ L) contained a final concentration of 1 μ M test compound, 0.1 mg/mL liver microsome protein, and 1 mM NADPH in 100 mM potassium phosphate, pH 7.4 buffer with 3 mM MgCl₂. At each of the time points (0, 15, 30, and 60 minutes), 150 μ L of quench solution (acetonitrile with 0.1% formic acid) with internal standard (bucetin) was transferred to each well. Verapamil was included as a positive control to verify assay performance. Plates were sealed, vortexed, and centrifuged at 4 °C for 15 minutes at 4000 rpm. The supernatant was transferred to fresh plates for LC/MS/MS analysis. All samples were analyzed on LC/MS/MS using an AB Sciex API 4000 instrument, coupled to a Shimadzu LC-20AD LC Pump system. Analytical samples were separated using a Waters Atlantis T3 dC18 reverse phase HPLC column (20 mm x 2.1 mm) at a flow rate of 0.5 mL/min. The mobile phase consists of 0.1% formic acid in water (solvent A) and 0.1% formic acid in acetonitrile (solvent B). The extent of metabolism was calculated as the disappearance of the test compound, compared to the 0-min time incubation. Initial rates were calculated for the compound concentration and used to determine $t_{1/2}$ values and subsequently, the intrinsic clearance.

Molecular Modeling

All *in silico* studies were performed by Irina Pogozeva. Modeling of three-dimensional (3D) structures of receptor-ligand complexes was based on available X-ray structures of the mouse MOR (PDB ID: 5c1m).⁸³ Structures of peptidomimetic ligands were generated using the 3D-Builder Application of QUANTA (Accelrys, Inc) followed by Conformational Search included in the program package. Low-energy ligand conformations (within 2 kcal/mol) that demonstrated the best superposition of aromatic substituents of the ligand core with the pharmacophore elements (DMT and benzyl pendant) of receptor-bound conformations of peptidomimetics were selected for docking into the receptor binding pocket. Ligands were positioned inside the receptor binding cavity to reproduce the binding modes of peptidomimetics and co-crystalized ligands in MOR X-ray structures. The docking pose of each ligand was subsequently refined using the solid docking module of QUANTA.

Chapter 3: Further Derivatization of the Aromatic Core

3.1 Introduction

The conversion to the monocyclic core described in the previous chapter was an important first step in improving the metabolic stability of our MOR-agonist/DOR-antagonist peptidomimetic series. However, there exists a lot of room for improvement both in terms of their metabolic stability and in their ability to activate MOR. We therefore opted to introduce small modifications aimed at blocking sites of CYP metabolism and observe their effects on our MOR-agonist/DOR-antagonist profile (**Figure 9**). Two different ligands from the previous studies were selected for these purposes. These ligands were selected as they possessed the best MOR-efficacy of the two different modifications types, namely the best benzylic position analogue (Compound **60**), and the best aromatic position analogue (Compound **70**).

Diversification here consisted of small changes on each respective analogue. For derivatives of **60**, these modifications consisted of inversion of stereochemistry of the benzylic position aimed at determining if this can block binding to the active site of the CYP enzyme. This was also followed by similar analogues containing a methyl ether, or those containing a nitrogen within the aromatic ring system aimed at decreasing the cLogP of these ligands and reducing the electron density of the aromatic ring. Finally, the benzylic methyl group was converted to a trifluoromethyl group to probe the effect of electronics on the stability of the benzylic position. Derivative of **70** followed a similar design philosophy as those of **60**, with the focus here being solely on the aromatic ring. This included the addition of simple fluoro groups to block potential

sites of metabolism on the core aromatic ring. For the purposes of this chapter, the data will be grouped based on these two different lead analogues.

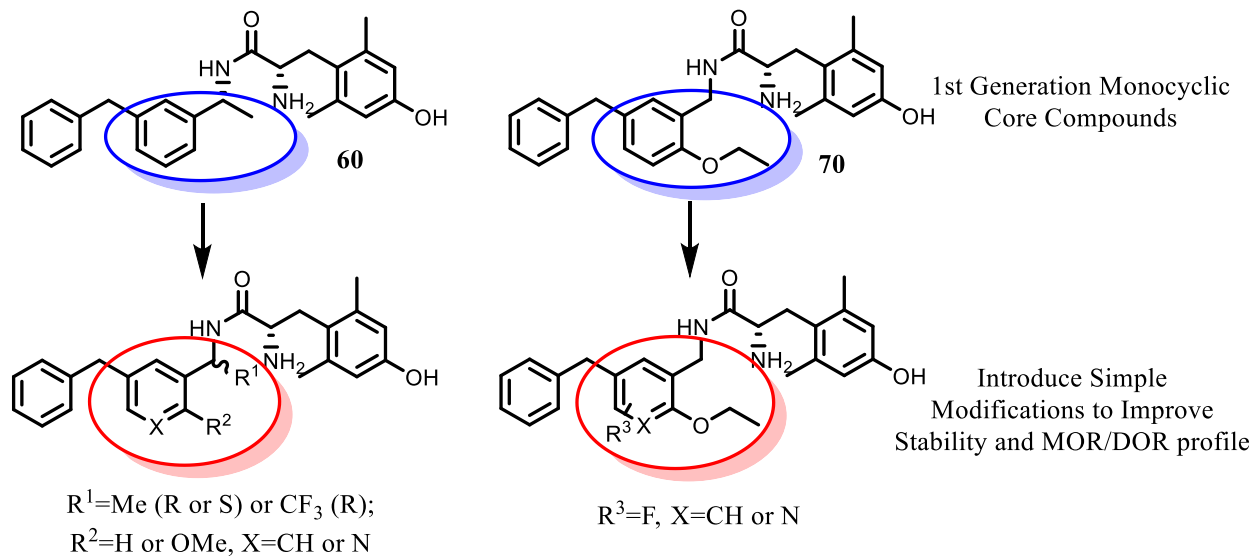


Figure 9: Further derivatization of compounds **60** and **70**. These analogues were selected as they were the best in their respective sites of functionalization. New substituents were selected on the grounds that they either block metabolism sterically through manipulation of appropriate stereocenters, or electronically using fluorine and nitrogen atoms.

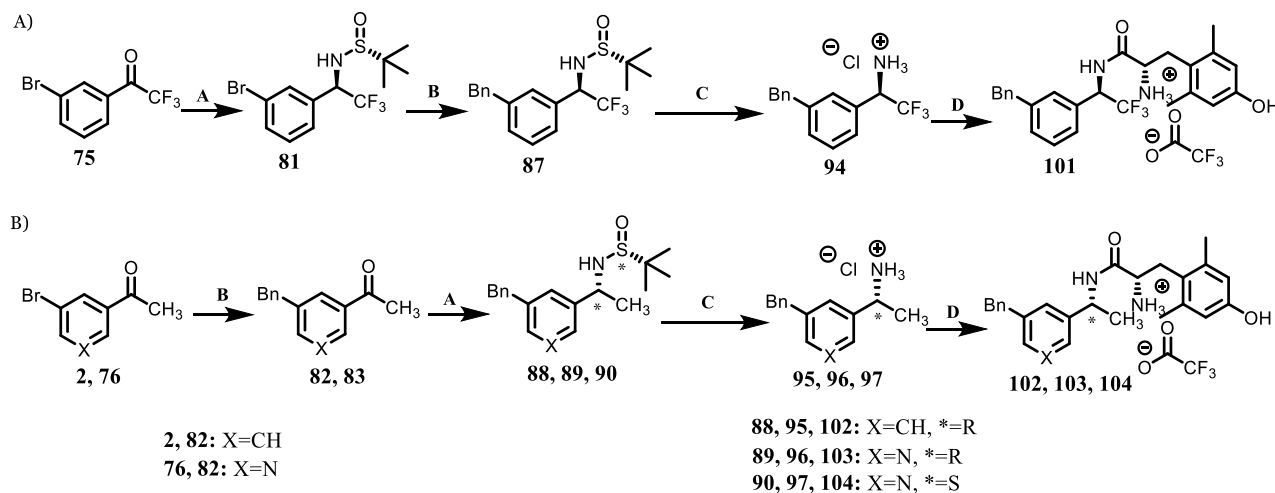
3.2 Results

General Chemistry: The bulk of the benzylic core modifications are described in **Scheme 3**. They largely use the same synthetic steps, though the order of the steps varies to enable diversification in later stages of the synthesis. **Scheme 3A** is concerned with the synthesis of the trifluoromethyl analogue **101**. This was synthesized by first subjecting the trifluoromethyl ketone to Ellman's chiral auxiliary, followed by sodium borohydride, yielding the reduced and protected amine. It should be noted that this stereochemistry is inverted when using the R-enantiomer of Ellman's chiral auxiliary. It is hypothesized that this is a result of electrostatic repulsion between the lone pair of the sulfinamide and the trifluoromethyl group,⁸⁴ which results in an inversion of the more stable transition state when compared to the simple ketones in the previous chapter.⁸⁵ It should be

noted that this intermediate is poorly UV active, so care must be taken during purification by chromatography. This was followed by Suzuki coupling with benzyl boronic acid pinacol ester, and deprotection of the Ellman auxiliary with concentrated HCl and dioxane. Finally, the liberated amine was coupled to Boc-protected DMT, of which, the Boc groups were removed using TFA and DCM.

The simple methyl analogues **102-104** described in **Scheme 3B** were synthesized using similar methods as the trifluoromethyl analogue **101** described above. However, the order of the Suzuki coupling, and the introduction of the chiral amine was inverted. This was to allow for the diversification of these analogues to occur later in the synthesis, reducing the total number of steps and thus time needed to synthesize each analogue. This diversification consisted of the use of either the *S* or *R* enantiomer of Ellman's chiral auxiliary, yielding either the *R* or *S* stereocenter on the chiral amine.

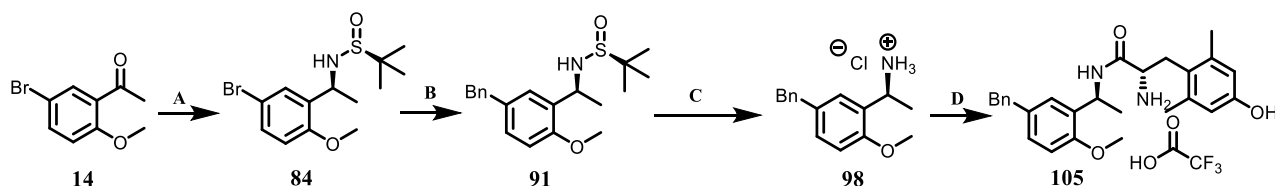
Scheme 3: Synthesis of Analogues 101-104.



- A) 1. (R)-(+)-2-methyl-propane-2-sulfinamide or (S)-(-)-2-methyl-propane-2-sulfinamide, Ti(OEt)₄, THF, 75 °C 2. NaBH₄. B) BnBPIn, K₂CO₃, Pd(dppf)Cl₂, 3:1 Acetone:Water, 80-100 °C. C) HCl conc., Dioxane. D) 1. DiBocDMT, DIEA, PyBOP, 6-Cl-HOBt, DMF. 2. TFA, DCM.

Finally, we were interested in synthesizing analogue **105**, which is a diastereomer of **74**. This is described in **Scheme 4** and used the same synthetic steps as those described in **Scheme 3**. The only difference here is the use of the S isomer of Ellman's chiral auxiliary.

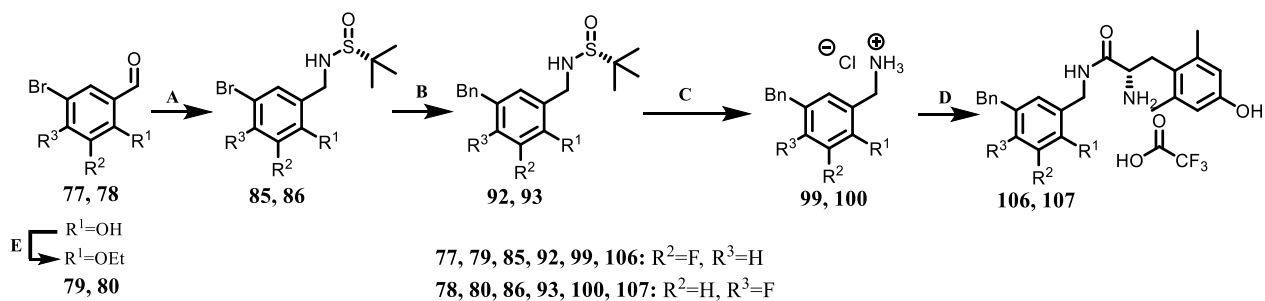
Scheme 4: Synthesis of Analogue 105.



- A) 1. (S)-(-)-2-methyl-propane-2-sulfinamide, $\text{Ti}(\text{OEt})_4$, THF, 75 °C 2. NaBH_4 . B) BnBPIn, K_2CO_3 , $\text{Pd}(\text{dppf})\text{Cl}_2$, 3:1 Acetone:Water, 80-100 °C. C) HCl conc., Dioxane. D) 1. DiBocDMT, DIEA, PyBOP, 6-Cl-HOBt, DMF. 2. TFA, DCM.

In addition to the benzylic analogues described above, we also opted to look at modifications focusing only on the aromatic core. The synthesis of the fluorinated analogues is described in **Scheme 5**. These analogues also used the same synthetic steps described above; however, they included an initial alkylation step to incorporate the ethyl ether, akin to that described in the previous chapter.

Scheme 5: Synthesis of Analogues 106-107.

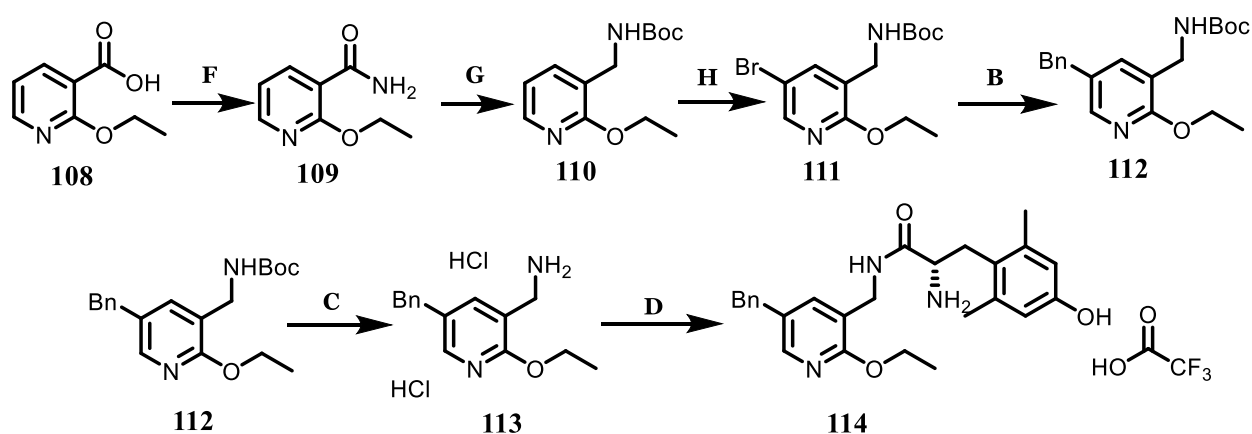


- A) 1. (R)-(+)-2-methyl-propane-2-sulfinamide, $\text{Ti}(\text{OEt})_4$, THF, 75 °C 2. NaBH_4 . B) BnBPIn, K_2CO_3 , $\text{Pd}(\text{dppf})\text{Cl}_2$, 3:1 Acetone:Water, 80-100 °C. C) HCl conc., Dioxane. D) 1. DiBocDMT, DIEA, PyBOP, 6-Cl-HOBt, DMF. 2. TFA, DCM. E) EtBr, K_2CO_3 , DMF.

Finally, the conversion of the core benzene ring of **70** into the pyridine ring of **114** was not as straight forward as the other analogues. As similar starting materials were unavailable, this

required the alternative synthesis as describe in **Scheme 6**. 2-ethoxynicotinic acid was first converted to 2-ethoxynicotinamide using PyBOP and NH₄Cl. This primary amide was then subject to reduction using BH₃*Me₂S at 75 °C, and the subsequent amine was then protected with a Boc group. This was in preparation for aromatic bromination using NBS, though the yields here were low. This can be explained both by how electron poor the pyridine ring is, and by competition with benzylic bromination on the position adjacent to the protected amine. The brominated intermediate was then subject to similar chemistry as described above, namely, Suzuki coupling, Boc-deprotection with concentrated HCl and dioxane, and peptide coupling to Boc-protected DMT and subsequent deprotection with TFA.

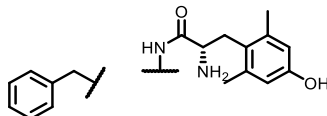
Scheme 6: Synthesis of Analogue 114.



B) BnBPIn, K₂CO₃, Pd(dppf)Cl₂, 3:1 Acetone:Water, 80-100 °C. C) HCl conc., Dioxane. D) 1. DiBocDMT, DIEA, PyBOP, 6-Cl-HOBt, DMF. 2. TFA, DCM. F) NH₄Cl, PyBOP, NMM, DMF. G) 1. BH₃*Me₂S, THF, 75 °C. 2. Boc₂O, TEA, THF. H) NBS, MeCN, 80 °C

SAR: Our analyses started with the benzylic analogues **101-105**, the binding affinity of which at MOR, DOR, and KOR are described in **Table 5**. Included are the previously described analogues **60** and **74** for comparison. As a technical note, some of these analogues were tested against human MOR and DOR as well as rat MOR and DOR. These analogues were screened during a transition period within our laboratory where we moved away from rat MOR and DOR to human MOR and

DOR to better model the performance of these analogues in human patients. These distinctions are thus made where necessary in the following data tables. If the stereochemistry of the methyl group of **60** is inverted to that of **102**, then approximately a single log unit loss in binding affinity is observed at each receptor. Notably, the MOR selectivity of **60** is lost in **102**. Attachment of fluoro groups to this methyl as in **101** resulted in further 6-fold loss in binding affinity at MOR and a further 2-fold loss in binding at DOR compared to **101**.



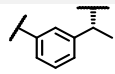
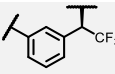
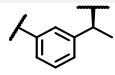
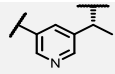
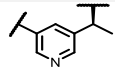
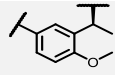
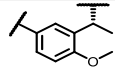
<i>Name</i>	<i>Structure</i>	<i>Binding Affinity, K_i (nM)</i>			<i>Selectivity</i>
		MOR	DOR	KOR	MOR:DOR:KOR
60		1.1±0.3	46±10	201±36	1:42:180
101		560±120	279±83	ND	1:0.50:-
102		96±37	122±46	1133±83*	1:1.3:11.8
103		0.53±0.03 ^a	8.0±1.9 ^a	143±60	1:15.1:270
104		238±16 ^{*a}	540±120 ^{*a}	>975	1:2.3:4.1
105		580±360	6.5±0.9*	1380**	1:0.011:2.4
74		8.0±0.8	6.8±1.1	330±150	1:0.85:41

Table 5: Binding affinity of 2nd generation benzylic derivatives at MOR, DOR, and KOR.

Binding affinities (K_i) were obtained by competitive displacement of radiolabeled [³H] diprenorphine in membrane preparations. Included are analogues **60** and **74** for comparison. All data were from three separate experiments, performed in duplicate unless otherwise noted. These data are reported as the average ± standard error of the mean. Selectivity was calculated by dividing the K_i of each receptor by the K_i at MOR for a given compound. DNS=Does Not

Stimulate. ND =No Data. * N=2, ** N=1. ^aData are from assays using human MOR and DOR instead of rat MOR and DOR.

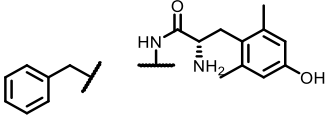
Conversion to the pyridine core structure appears to have divergent effects. Analogue **103**, with the same stereochemistry as **60**, appears to have improved binding affinity at each of the three receptors, whereas **104** had a 2-fold loss compared to **102**. Finally, the diastereomer of **74** (**105**) had significantly reduced binding affinity at MOR and KOR. Curiously, the binding affinity at DOR was not affected upon this conversion.

Name	Structure	Potency, EC_{50} (nM)			Efficacy, (% Stimulation)		
		MOR	DOR	KOR	MOR	DOR	KOR
60		44.4±7.5	DNS	>1700	41±12	DNS	>40
101		DNS**	DNS*	DNS**	DNS**	DNS*	DNS**
102		333**	DNS	>6720*	30.7**	DNS	>65.9*
103		38±19 ^a	DNS ^a	DNS	55.6±6.3 ^a	DNS ^a	DNS
104		DNS ^{**a}	DNS ^a	DNS	DNS ^{**a}	DNS ^a	DNS
105		DNS	DNS**	DNS**	DNS	DNS**	DNS**
74		296±69	DNS	DNS	20.2±1.4	DNS	DNS

Table 6: Potency and efficacy of 2nd generation benzylic derivatives at MOR, DOR, and KOR. Potency and efficacy data were obtained using agonist induced stimulation of [³⁵S] GTP γ S binding. Potency is represented as EC_{50} (nM) and efficacy as percent maximal stimulation relative to standard agonist DAMGO (MOR), DPDPE (DOR), or U69,593 (KOR) at 10 μ M. Included are analogues **60** and **74** for comparison. All data were from three separate experiments, performed in duplicate unless otherwise noted. These data are reported as the average \pm standard

error of the mean. DNS=Does Not Stimulate. * N=2, ** N=1. ^aData are from assays using human MOR and DOR instead of rat MOR and DOR.

The efficacy and potency of analogues **101-105** were also examined, with analogues **60** and **74** shown for comparison and are shown in **Table 6**. The trifluoromethyl analogue **101** did not stimulate any of the three opioid receptors. Furthermore, inverting the stereochemistry of **60** reduced potency at MOR and KOR. The pyridine analogue **103** produced no significant change compared to **60**, but the inverted stereocenter of **104** eliminated any agonism that may have been present in **102**. A similar trend was observed upon the inversion of **74** to **105**, namely that the ligand's ability to stimulate MOR is lost.



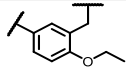
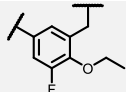
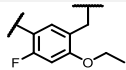
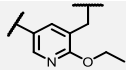
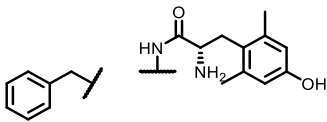
<i>Name</i>	Structure	<u><i>Binding Affinity, K_i (nM)</i></u>			<u><i>Selectivity</i></u>
		MOR	DOR	KOR	MOR:DOR:KOR
70		2.8±0.5	23.8±3.3	1180±120	1:8.4:415
106		0.32±0.14	1.7±0.7	ND	1:5.3:-
107		5.5±2.2	4.4±0.2	234**	1:0.80:43
114		13.8±1.0 ^a	1.8±0.4 ^a	>393	1:0.16:>28

Table 7: Binding affinity of 2nd generation aromatic derivatives at MOR, DOR, and KOR.

Binding affinities (K_i) were obtained by competitive displacement of radiolabeled [³H] diprenorphine in membrane preparations. All data were from three separate experiments, performed in duplicate unless otherwise noted. Included is analogue **70** for comparison. These data are reported as the average ± standard error of the mean. Selectivity was calculated by dividing the K_i of each receptor by the K_i at MOR for a given compound. DNS=Does Not Stimulate. ND =No Data. ** N=1. ^aData are from assays using human MOR and DOR instead of rat MOR and DOR.

Table 7 describes the binding affinity of the aromatic derivatives of analogue **70**. Here, the ortho-fluoro analogue **106** possessed improved binding affinity at MOR and DOR by a log unit as compared to **70**. Similarly, the meta-fluoro analogue **107** had improved binding affinity at DOR and KOR, but not MOR, and was therefore less selective for MOR over DOR and KOR. Interestingly, the pyridine analogue **114** improved binding affinity at DOR only, and reduced affinity at MOR compared to **70**.



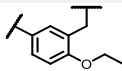
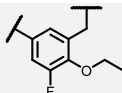
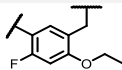
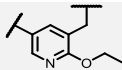
<i>Name</i>	<i>Structure</i>	<i>Potency, EC₅₀ (nM)</i>			<i>Efficacy, (% Stimulation)</i>		
		MOR	DOR	KOR	MOR	DOR	KOR
70		77±10	DNS	DNS	65.9±5.2	DNS	DNS
106		10.9±3.0	DNS	DNS**	74.8±2.8	DNS	DNS**
107		340±140	1.87**	ND	64±11	13.0**	ND
114		216±87 ^a	43±20 ^a	DNS	80.5±9.4 ^a	54.6±3.4 ^a	DNS

Table 8: Potency and efficacy of 2nd generation aromatic derivatives at MOR, DOR, and KOR. Potency and efficacy data were obtained using agonist induced stimulation of [³⁵S] GTPγS binding. Potency is represented as EC₅₀ (nM) and efficacy as percent maximal stimulation relative to standard agonist DAMGO (MOR), DPDPE (DOR), or U69,593 (KOR) at 10 μM.

Included is analogue **70** for comparison. All data were from three separate experiments, performed in duplicate unless otherwise noted. These data are reported as the average ± standard error of the mean. DNS=Does Not Stimulate. ND =No Data. ** N=1. ^aData are from assays using human MOR and DOR instead of rat MOR and DOR.

These aromatic modifications also yielded interesting changes in potency and efficacy at MOR and DOR as illustrated in **Table 8**. The best appears to be the ortho-fluoro analogue **106**, which yielded a 7-fold improvement in potency at MOR compared to **70** without stimulating DOR. Interestingly, moving the fluoro group to the meta-position in **107** had the reverse effect, yielding

a 5-fold loss in potency compared to **70** with some residual DOR agonism. The pyridine analogue **114** behaved similarly to the meta-fluoro analogue **107** at MOR. However, this analogue had a much greater efficacy at DOR. None of these new analogues were able to stimulate KOR.

Metabolic Stability: A few benzylic modifications were then subjected to stability analyses in MLM. These were the trifluoromethyl analogue **101** and the diastereomer of **74** (**105**) and are found in **Table 9**. The conversion from the methyl group of **60** to the trifluoromethyl of **101** and inverting this stereochemistry managed to improve the metabolic stability by a factor of 3, despite increasing the cLogP of this ligand by a quarter unit. Furthermore, inverting the benzylic stereochemistry of **74** produced a 6-fold improvement in metabolic stability as illustrated by compound **105**.

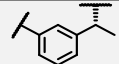
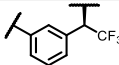
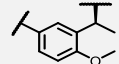
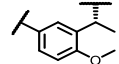
<i>Name</i>	<i>Structure</i>	<i>T_{1/2} (min)</i>	<i>Verapamil T_{1/2} (min)</i>	<i>Stability Ratio</i>	<i>cLogP</i>
60		8.5± 0.8	22.6±1.4	0.38±0.04	4.75
101		29.0±2.2	19.6±1.3	1.4±0.2	5.07
105		26.4±0.3	14.6±1.0	1.8±0.1	4.53
74		4.3±0.0	14.6±1.0	0.30±0.02	4.53

Table 9: Metabolic stability of 2nd generation benzylic derivatives in MLM. Included are the compound half-life ($T_{1/2}$), the half-life of the positive control verapamil, and the stability ratio between the compound and the positive control. The stability ratio was calculated by dividing the half-life of the analogue of interest by the half-life of the positive control in that assay. Individual compounds were tested once, with errors representing the SE in the decay curve regressed onto the data collected in 15-minute intervals. Finally, the cLogP of these analogues are included and were calculated using PerkinElmer's ChemDraw® Professional Software.

Likewise, the simple aromatic core modifications of **70** were examined for their effects on the metabolic stability of our ligands (**Table 10**). Curiously, the ortho-fluoro modification in **106**

and its pyridine counterpart **114** managed to cut the stability of these ligands in half. The meta-fluoro analogue **107** yielded no significant improvements in stability.

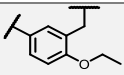
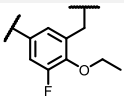
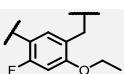
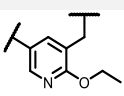
<i>Name</i>	<i>Structure</i>	<i>T_{1/2} (min)</i>	<i>Verapamil T_{1/2} (min)</i>	<i>Stability Ratio</i>	<i>cLogP</i>
70		23.7±5.9	14.6±1.0	1.6±0.4	4.75
106		17.5±0.9	19.6±1.3	0.89±0.07	4.83
107		23.9±1.6	19.6±1.3	1.2±0.1	5.03
114		20.3±2.6	29.9±4.7	0.7±0.1	4.15

Table 10: Metabolic stability of 2nd generation aromatic derivatives in MLM. Included are the compound half-life ($T_{1/2}$), the half-life of the positive control verapamil, and the stability ratio between the compound and the positive control. The stability ratio was calculated by dividing the half-life of the analogue of interest by the half-life of the positive control in that assay. Individual compounds were tested once, with errors representing the SE in the decay curve regressed onto the data collected in 15-minute intervals. Finally, the cLogP of these analogues are included and were calculated using PerkinElmer's ChemDraw® Professional Software.

3.3 Discussion and Conclusion

SAR: Modest modifications to analogue **60** had profound effects on our opioid profile. A simple inversion in stereochemistry from **60** to **102** yielded significant losses in binding at all three receptors. Given the size of the methyl substituent, this suggests that significant steric factors are coming into play and the inversion of this stereocenter is causing the ligand to enter a much less favorable conformation that impedes receptor binding. This trend is reflected in the change in potency upon this conversion, as the ligand's ability to induce the receptor's active state is also impaired. The incorporation of fluoro groups (**101**) onto this methyl group only exacerbates this

problem, as its larger size amplifies steric effects and no electronic effects are present to compensate and recover the lost binding affinity and potency.

Curiously, the conversion to a pyridine ring in the core had varying effects on these ligands. Comparisons here, however, should be made with caution, as the pyridine analogues **103** and **104** were tested against human MOR and DOR, whereas their phenyl analogues were tested against rat MOR and DOR. Nevertheless, conversion from **60** to **103** resulted in improvements in DOR binding and in selectivity of MOR and DOR over KOR. This may be attributed to electronic interactions between the pyridine ring of the ligand and DOR. This interaction may translate to the improved efficacy of this ligand at MOR, as this pyridine ring can enable MOR to assume a more active state. In DOR, this has the reverse effect, enabling binding, but still preventing the adoption of the active state. Inversion of the methyl group to **104** has a disruptive effect, possibly due to the ligand's inability to adopt a conformation that can both accommodate the negative steric effects of the new stereocenter and the electronic effects of the pyridine ring. As such, these two factors instead work against each other, causing losses in binding affinity across at DOR, and converting **104** into a MOR antagonist.

Finally, this loss in binding affinity and potency was further illustrated by the inversion of **74** to **105**. This is true for binding affinity at MOR and KOR, as well as what little potency was present in MOR. However, no difference in binding affinity at DOR was observed between these two ligands. In fact, **105** is a very selective DOR antagonist. This may be attributed to the methoxy group, which may interact with the receptor in a manner that can counteract the effect of the inverted stereocenter. It should be noted that within those other analogues that were tested against rat DOR (**60**, **101**, and **102**), DOR binding was the least affected upon these structural

transformations where data is available. Thus, only modest interactions between DOR and the methoxy group may be necessary to prevent losses in binding affinity.

The aromatic core modifications also yielded some interesting effects on the binding affinity of these ligands. The ortho-fluoro analogue **106** produced a log improvement in binding affinity at MOR and DOR over the unfunctionalized analogue **70**. This contrasts with the meta-fluoro analogue **107** and the ortho pyridine analogue **114**, which improved DOR binding, but not MOR binding. The large differences in affinity between the ortho- and meta-fluoro analogues at MOR suggests that the ortho-analogue is picking up a specific interaction with this receptor rather than a more general interaction mediated by lipophilicity or the electronics of the core aromatic ring. This contrasts with the binding of these two analogues at DOR, which are more similar to each other than to analogue **70**, suggesting that the improvement in binding at DOR is a product of electronics or lipophilicity.

The pyridine analogue **114** clarifies whether electronics or lipophilicity is responsible for binding at DOR. Since the pyridine analogue is more polar than the two fluoro analogues, differences in binding affinity would be expected if lipophilicity is the dominate force. This is not the case, as the fluoro analogues and the pyridine analogue have very similar binding affinity to each other at DOR. However, since both pyridine rings and fluoro groups make the aromatic core more electron poor, it appears that these differences in binding affinity at DOR are driven by electronics.

Many of these trends that are observed at MOR for these ethyl ether analogues are also reflected in the efficacy and potency of these ligands. The ortho-fluoro analogue (**106**) possesses a near 8-fold improvement in potency and a 10 % improvement in efficacy compared to **70**. When compared to the meta-fluoro (**107**) and pyridine analogues (**114**), these data suggest that **106** is

picking up a specific interaction with the receptor rather than manipulating the electronics or polarity of the core aromatic ring. Indeed, fluorine is highly electronegative, and therefore is capable of engaging in dipole-dipole interactions.⁸⁶

DOR stimulation with the fluoro analogues is practically nonexistent, whereas substantial DOR agonism is acquired in the pyridine analogue. This could be a product of the different DOR homologs, or the pyridine ring may be picking up a specific interaction with DOR needed to activate the receptor. Under this hypothesis, the ortho-fluoro analogue (**106**) would not be able to interact with this receptor in the same way as the pyridine analogue (**114**) due to the position of these groups in space.

Metabolic Stability: The ligands within this brief series that were subject to metabolism studies yielded some surprising results. Regarding the benzylic analogues, metabolism appears to be sensitive to the stereochemistry of the benzylic modification. This is illustrated in the difference in stability of analogues **74** and **105**, which only differ in the stereochemistry of the benzylic methyl group. Here, inversion of the stereocenter yields a 6-fold improvement in metabolic stability as measured by the stability ratio. This trend is reinforced with the metabolism of analogues **60** and **101**, which contain different stereocenters. The presence of the trifluoromethyl group in **101** does not appear to be a factor in stability in this specific case. These data suggest that the methyl group can block metabolism by cytochrome P450 enzymes due to steric effects if it has the appropriate stereochemistry. Conversely, when the stereocenter is inverted, the steric effect is removed, and the methyl group instead facilitates metabolism through stabilization of the free radical intermediate.

Curiously, the aromatic core analogues did not yield the stability improvements we anticipated. Blocking possible metabolic sites with fluoro groups in **106** and **107** appeared to

instead reduce stability as compared to **70**. This suggests that the aromatic core is not a site of further metabolism and that losses in stability may be a product of increased cLogP. However, this is inconsistent with the reduced stability of the pyridine analogue **114**, which possesses a lower cLogP than **70**. The reduced stability here may instead be explained by electronic effects on the adjacent ethyl ether. In the previous chapter, we postulated that the ethers improved stability in part by sterically blocking metabolism on the benzylic position linking the dimethyltyrosine residue to the rest of the peptidomimetic. This did not mean that the ether itself was not labile, as metabolism here could be mitigated through the incorporation of a cyclopropyl methyl group (analogue **72**). If the ethyl ether then is still metabolically labile, it is possible that the fluoro and pyridine groups are facilitating metabolism of the adjacent ether through stabilization of the phenol as illustrated in **Figure 10**.

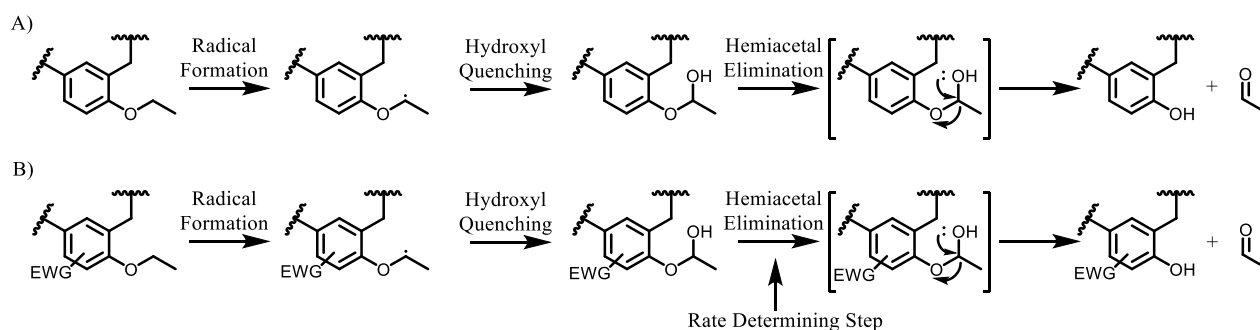


Figure 10: Proposed CYP450 reaction mechanism on both A) **70** and B) analogues that possess an electron-withdrawing group (**106**, **107**, **114**).

Conclusion: The exploration of these simple modifications to analogues **60** and **70** yielded new insights into the opioid SAR of this series, in addition to their metabolic stability. We further confirmed that the benzylic position is a metabolic hotspot, and that metabolism at this position differs based on the stereochemistry of substituents at this position as illustrated by analogues **74** and **105**. However, any improvements in stability through modulation of this stereochemistry are associated with losses in the capability of these ligands to stimulate MOR. The introduction of

electron withdrawing groups into the core aromatic ring proved to be tolerated in terms of maintaining the ability to stimulate MOR. This is particularly true for the ortho-fluoro analogue **106**, which produced a near log improvement in MOR-potency and affinity over analogue **70**. However, these electron withdrawing groups surprisingly reduced the metabolic stability of these ligands where tested, likely through facilitation of cleavage of the adjacent ethyl ether.

While the derivatives presented here provided some valuable insights into SAR profile both in terms of improving stability or improving MOR stimulation, these two effects did not occur simultaneously. Improvements in stability here resulted in losses in MOR stimulation, and improvements in MOR stimulation resulted in losses in stability. These data suggest that further modifications to the aromatic core of these peptidomimetics are unlikely to be fruitful for both improving MOR stimulation and metabolic stability. As such, we sought instead to pursue further derivatization elsewhere in our peptidomimetics in the next chapter.

3.4 Experimental

Chemistry

General Methods: All reagents and solvents were obtained commercially and were used without further purification. Intermediates were purified by flash chromatography using a Biotage Isolera One instrument. Most purification methods utilized a hexanes/ethyl acetate solvent system in a Biotage SNAP KP-Sil column, with a linear gradient between 0 and 100% ethyl acetate. Reverse phase column chromatography using a linear gradient of 0 % to 100 % solvent B (0.1 % TFA in acetonitrile) in solvent A (0.1 % TFA in water) using a Biotage SNAP Ultra C18 column was utilized for some intermediate amine salts. Purification of final compounds was performed using a Waters semipreparative HPLC with a Vydac protein and peptide C18 reverse phase

column, using a linear gradient of 0 % to 100 % solvent B in solvent A at a rate 1 % per minute, monitoring UV absorbance at 230 nm. The purity of final compounds was assessed using a Waters Alliance 2690 analytical HPLC instrument with a Vydac protein and peptide C18 reverse phase column. A linear gradient (gradient A) of 0 % to 70 % solvent B in solvent A in 70 min, measuring UV absorbance at 230 nm was used to determine purity. All final compounds used for testing were ≥ 95 % pure, as determined by analytical HPLC. ^1H NMR and ^{13}C NMR data were obtained on a 500 or 400 MHz Varian spectrometer using CDCl_3 or CD_3OD solvents. The identities of final compounds were verified by mass spectrometry using an Agilent 6130 LC-MS mass spectrometer in the positive ion mode, or an Agilent 6230 TOF HPLC-MS in the positive ion mode. Suzuki couplings using microwave irradiation were performed on a Discover S-class (CEM) microwave in a closed vessel with maximum power input of 300 W and temperature set to 100 °C for 30 min under the standard method using their Synergy software.

General Procedure for Ellman Reductions (Procedure A): A flamed-dried round bottom flask containing 1 equivalent of aldehyde or ketone and 1.5 or 3 equivalents of (R)-(+)-2-methylpropane-2-sulfinamide was attached to a reflux condenser and flushed with argon. 4 mL of THF was added and cooled to 0 °C. 3.8, 6, or 7.5 equivalents of titanium (IV) ethoxide was added, followed by an additional 4 mL of THF. The solution was stirred and heated to 75 °C overnight with TLC monitoring until all ketone or aldehyde was consumed. A separate flame-dried flask containing 6 or 6.5 equivalents of sodium borohydride was flushed with argon. 4 mL of THF was added, at which point the solution was cooled to -78 °C. The solution containing Ellman adduct was cooled to room temperature and slowly transferred to the sodium borohydride solution via syringe. This final solution was then allowed to warm to room temperature and stirred for 2 hours, at which point the reaction mixture was quenched with methanol to consume the sodium

borohydride, followed by DI water to precipitate the titanium. The solution was vacuum filtered, and the precipitate was washed with ethyl acetate. The filtrate was then concentrated in vacuo and purified via column chromatography (0-100 % EtOAc in Hexanes).

General Procedure for Suzuki Couplings Using Microwave Irradiation (Procedure Ba):

To a microwave vessel containing the protected amine was added 1.7 equivalents of benzylboronic acid pinacol ester, 2.8 equivalents of potassium carbonate, and 0.11 equivalents of 1,1'-bis(diphenylphosphino)ferrocene] dichloropalladium. The vessel was purged with argon and 2.5 mL of degassed 3:1 acetone:water was added. The vessel was then subject to microwave irradiation to a temperature of 100 °C for 30 min. The solution was cooled, partitioned between brine and ethyl acetate, and extracted with ethyl acetate. The organic layer was then dried with magnesium sulfate, filtered, and concentrated in vacuo. Column chromatography was then performed (0-100 % ethyl acetate in hexanes), yielding the desired Suzuki coupled derivatives.

General Procedure for Suzuki Couplings without Microwave Irradiation (Procedure Bb):

To a round bottom flask containing protected amine, 1.8 equivalents of potassium carbonate, and 0.1 equivalents of 1,1'-bis(diphenylphosphino)ferrocene] dichloropalladium was added 1.3 equivalents of benzylboronic acid pinacol ester. The flask was equipped with a reflux condenser, purged with argon, and 5 mL of degassed 3:1 acetone:water was added. The vessel was then heated to a temperature of 80 °C overnight. The solution was cooled, partitioned between brine and ethyl acetate, and extracted with ethyl acetate. The organic layer was then dried with magnesium sulfate, filtered, and concentrated in vacuo. Column chromatography was then performed (0-100 % ethyl acetate in hexanes), yielding the desired Suzuki coupled derivatives.

General Procedure for Removal of Ellman's chiral sulfonamide or Boc groups (Procedure C): To a flask containing Ellman or Boc protected amine was added 2 mL of Dioxane and 0.2 mL concentrated HCl. The solution was stirred at room temperature for 1 minute and concentrated in vacuo. The ensuing salt was then purified via one of two methods. If the product is insoluble in diethyl ether, it was triturated with diethyl ether, and the precipitate was concentrated in vacuo to dryness, yielding the product as an HCl salt.

General Procedure for the Coupling of 2',6'-Dimethyltyrosine to Functionalized Amine Salt (Procedure D): To a dried flask containing the amine salt under argon was added 3 mL of DMF and 10 equivalents of Hunig's base. 1 equivalent of PyBOP and 1 equivalent of 6-Cl-HOBt was added, followed by 1 equivalent of N-Boc-O-Boc-2',6'-dimethyl-L-tyrosine in 1.5 mL DMF. The solution was stirred overnight at room temperature and concentrated in vacuo. 2 mL of TFA and 2 mL of DCM were then added, and the solution was stirred for an additional hour. The reaction mixture was concentrated in vacuo and purified via semipreparative reverse phase HPLC (0.1% TFA in water: 0.1% TFA in acetonitrile). The product was concentrated in vacuo and lyophilized overnight to yield the final peptidomimetic.

General Procedure for the Synthesis of 6-position Ethers (Procedure E): To a flame dried flask containing phenolic aldehyde or ketone was added 2 or 3 equivalents of potassium carbonate. The flask was purged with argon and 4 mL of DMF was added. 3 or 4 equivalents of an alkyl iodide or bromide was then added, and the solution was stirred at room temperature overnight. The solution was then concentrated in vacuo, partitioned between ethyl acetate and saturated sodium bicarbonate, and extracted with ethyl acetate. The organic layers were combined, dried with magnesium sulfate, filtered, and concentrated in vacuo, yielding the desired ether.

General Procedure for the Synthesis of 2-ethoxynicotinamide (Procedure F): To a flame dried flask containing **2-ethoxynicotinic acid** was added 1.2 equivalents of PyBOP and 1.1 equivalents of NH₄Cl. The flask was flushed with argon, at which point 4.1 mL of DMF and 9.9 equivalents of NMM were added. The reaction was allowed to stir overnight and was concentrated in vacuo. The residue was then partitioned between sat. NaHCO₃ and EtOAc and extracted with EtOAc. The organic layers were combined, dried with MgSO₄, filtered and concentrated in vacuo. The residue was then purified via column chromatography (0 to 100 % EtOAc in Hexanes) yielding the desired amide.

General Procedure for the Synthesis of tert-butyl ((2-ethoxypyridin-3-yl)methyl)carbamate (Procedure G): To a flame dried flask under argon equipped with a reflux condenser containing **2-ethoxynicotinamide** was added 7 equivalents of 2 M BH₃*Me₂S in THF and 4 mL of THF. The solution was heated to 75 °C for 3 hours, at which point the reaction was quenched with methanol and heated for an additional 15 minutes. The solution was concentrated in vacuo, acidified using 1 M HCl, and concentrated in vacuo again. The residue was dried in the same pot in a vacuum desiccator, at which point 1.2 equivalents of Boc₂O was added and the flask was purged with argon. 3.3 equivalents of TEA and 4 mL of THF were added and the reaction was stirred overnight. An additional 2.4 equivalents of Boc₂O were added and the reaction was stirred for an additional day. The solution was then partitioned between sat. NaHCO₃ and EtOAc and extracted with EtOAc. The organic layers were then collected, dried with MgSO₄, filtered, and concentrated in vacuo. The residue was then purified yielding column chromatography (2:1 Hexanes:EtOAc), yielding the Boc-protected amine.

General Procedure for the Synthesis of tert-butyl ((5-bromo-2-ethoxypyridin-3-yl)methyl)carbamate (Procedure H): To a flame dried flask equipped with **tert-butyl ((2-ethoxypyridin-3-yl)methyl)carbamate** was added 1 equivalent of NBS. The flask was equipped with a condenser and purged under argon. 5 mL of MeCN was added and the solution was heated to 80 °C overnight. The solution was cooled and concentrated in vacuo. The residue was then purified using column chromatography (2:1 Hexanes:EtOAc), yielding the brominated compound.

5-bromo-2-ethoxy-3-fluorobenzaldehyde (79): See Procedure E: 106 mg (0.48 mmol) **5-bromo-3-fluoro-2-hydroxybenzaldehyde (77)**, 271 mg (2.0 mmol, 4.1 eq.) of K₂CO₃, 0.11 mL (161 mg, 1.5 mmol, 3.0 eq.) of EtBr, 4 mL of DMF. Compound **79** (107 mg, 86 % yield) was isolated as a light brown oil. ¹H NMR (500 MHz, Chloroform-*d*) δ 10.32 (s, 1H), 7.70 (dd, *J* = 2.5, 1.5 Hz, 1H), 7.45 (dd, *J* = 10.9, 2.5 Hz, 1H), 4.31 (qd, *J* = 7.1, 1.8 Hz, 2H), 1.42 (td, *J* = 7.0, 0.8 Hz, 3H). ¹³C NMR (126 MHz, Chloroform-*d*) δ 187.55, 187.52, 156.11, 154.08, 148.68, 148.60, 130.99, 130.97, 126.16, 126.13, 125.79, 125.62, 115.17, 115.10, 71.08, 71.03, 15.37, 15.36.

5-bromo-2-ethoxy-4-fluorobenzaldehyde (80): See Procedure E: 150 mg (0.68 mmol) **5-bromo-4-fluoro-2-hydroxybenzaldehyde (78)**, 289 mg (2.1 mmol, 3.1 eq.) of K₂CO₃, 0.15 mL (219 mg, mmol, 2.0 eq.) of EtBr, 4 mL of DMF. Compound **80** (136 mg, 80 % yield) was isolated as a white solid. ¹H NMR (400 MHz, Chloroform-*d*) δ 10.31 (s, 1H), 8.00 (d, *J* = 8.1 Hz, 1H), 6.75 (d, *J* = 10.2 Hz, 1H), 4.12 (q, *J* = 7.0 Hz, 2H), 1.49 (t, *J* = 7.0 Hz, 3H). ¹³C NMR (101 MHz, Chloroform-*d*) δ 187.17, 187.16, 187.15, 187.14, 164.65, 162.10, 161.90, 161.81, 133.25, 133.23, 133.21, 133.20, 101.81, 101.79, 101.54, 101.52, 100.55, 100.32, 65.08, 65.07, 14.39.

(R)-N-((R)-1-(3-bromophenyl)-2,2,2-trifluoroethyl)-2-methylpropane-2-sulfonamide (81): See Procedure A: Step 1: 60 μL (98 mg, 0.39 mmol) of **1-(3-bromophenyl)-2,2,2-**

trifluoroethan-1-one (75), 78 mg (0.64 mmol, 1.7 eq.) of (R)-(+)-2-methyl-propane-2-sulfinamide, 310 μ L (337 mg, 1.5 mmol, 3.8 eq.) of Ti(OEt)₄, and 3+3 mL THF. Step 2: 94 mg (2.5 mmol, 6.4 eq.) of sodium borohydride in 3 mL THF. Compound **81** (69 mg) was isolated as a colorless oil and continued without further purification.

(S)-N-((S)-1-(3-benzylphenyl)ethyl)-2-methylpropane-2-sulfinamide (88): See Procedure A: Step 1: 63 mg (0.30 mmol) of **82**, 114 mg (0.94 mmol, 3.1 eq.) of (S)-(-)-2-methylpropane-2-sulfinamide, 380 μ L (413 mg, 1.8 mmol, 6.0 eq.) of Ti(OEt)₄, and 3+3 mL THF. Step 2: 68 mg (1.8 mmol, 6.0 eq.) of sodium borohydride in 3 mL THF. Compound **88** (76 mg, 80 % yield) was isolated as a colorless oil. ¹H NMR (500 MHz, Chloroform-*d*) δ 7.32 – 7.25 (m, 3H), 7.23 – 7.16 (m, 5H), 7.12 (d, *J* = 7.6 Hz, 1H), 4.52 (qd, *J* = 6.5, 2.6 Hz, 1H), 3.99 (s, 2H), 3.41 (d, *J* = 2.6 Hz, 1H), 1.50 (d, *J* = 6.5 Hz, 3H), 1.22 (s, 9H). ¹³C NMR (126 MHz, Chloroform-*d*) δ 144.31, 141.68, 140.77, 128.93, 128.88, 128.50, 128.35, 127.23, 126.15, 124.22, 55.43, 53.79, 41.88, 22.79, 22.63.

(S)-N-((S)-1-(5-benzylpyridin-3-yl)ethyl)-2-methylpropane-2-sulfinamide (89): See Procedure A: Step 1: 61 mg (0.29 mmol) of **83**, 111 mg (0.92 mmol, 3.2 eq.) of (S)-(-)-2-methylpropane-2-sulfinamide, 370 μ L (403 mg, 1.8 mmol, 6.1 eq.) of Ti(OEt)₄, and 3+3 mL THF. Step 2: 68 mg (1.8 mmol, 6.2 eq.) of sodium borohydride in 3 mL THF. Compound **89** (52 mg, 57 % yield) was isolated as a yellow oil. ¹H NMR (500 MHz, Chloroform-*d*) δ 8.43 (s, 1H), 8.38 (s, 1H), 7.70 (s, 1H), 7.37 – 7.30 (m, 2H), 7.30 – 7.24 (m, 1H), 7.19 – 7.12 (m, 2H), 4.55 (qd, *J* = 6.7, 4.8 Hz, 1H), 4.02 (s, 2H), 3.49 (d, *J* = 4.3 Hz, 1H), 1.53 (d, *J* = 6.7 Hz, 3H), 1.20 (s, 9H). ¹³C NMR (126 MHz, Chloroform-*d*) δ 146.76, 143.83, 141.85, 139.53, 138.06, 137.57, 129.11, 128.87, 127.24, 56.03, 51.93, 38.73, 22.59, 22.50.

(R)-N-((R)-1-(5-benzylpyridin-3-yl)ethyl)-2-methylpropane-2-sulfinamide (90): See Procedure A: Step 1: 38 mg (0.18 mmol) of **83**, 67 mg (0.55 mmol, 3.1 eq.) of (R)-(+)-2-methylpropane-2-sulfinamide, 230 μ L (250 mg, 1.1 mmol, 6.1 eq.) of Ti(OEt)₄, and 3+3 mL THF. Step 2: 44 mg (1.2 mmol, 6.5 eq.) of sodium borohydride in 3 mL THF. Compound **90** (10 mg, 17 % yield) was isolated as a colorless oil. ¹H NMR (500 MHz, Chloroform-*d*) δ 8.44 (s, 1H), 8.39 (s, 1H), 7.70 (s, 1H), 7.37 – 7.32 (m, 2H), 7.30 – 7.27 (m, 1H), 7.19 – 7.13 (m, 2H), 4.56 (qd, *J* = 6.6, 4.4 Hz, 1H), 4.03 (s, 2H), 3.42 (d, *J* = 4.2 Hz, 1H), 1.54 (d, *J* = 6.7 Hz, 3H), 1.21 (s, 9H). ¹³C NMR (126 MHz, Chloroform-*d*) δ 146.80, 143.83, 141.83, 139.54, 138.04, 137.53, 129.12, 128.87, 127.27, 56.02, 51.90, 38.74, 22.58, 22.49.

(S)-N-((S)-1-(5-bromo-2-methoxyphenyl)ethyl)-2-methylpropane-2-sulfinamide (84): See Procedure A: Step 1: 208 mg (0.91 mmol) of **14**, 336 mg (2.8 mmol, 3.1 eq.) of (S)-(-)-2-methylpropane-2-sulfinamide, 1450 μ L (1578 mg, 6.9 mmol, 7.6 eq.) of Ti(OEt)₄, 4+4 mL THF. Step 2: 206 mg (5.4 mmol, 6.0 eq.) of sodium borohydride in 4 mL THF. Compound **84** (242 mg, 80 % yield) was isolated as a colorless oil. ¹H NMR (500 MHz, Chloroform-*d*) δ 7.34 (d, *J* = 2.4 Hz, 1H), 7.28 (dd, *J* = 8.7, 2.5 Hz, 1H), 6.71 (d, *J* = 8.7 Hz, 1H), 4.71 (p, *J* = 6.5 Hz, 1H), 3.78 (s, 3H), 1.41 (d, *J* = 6.7 Hz, 3H), 1.17 (s, 9H). ¹³C NMR (126 MHz, Chloroform-*d*) δ 155.55, 134.51, 131.05, 129.70, 113.02, 112.60, 55.58, 49.54, 23.62, 22.55, 21.73.

(R)-N-(5-bromo-2-ethoxy-3-fluorobenzyl)-2-methylpropane-2-sulfinamide (85): See Procedure A: Step 1: 105 mg (0.43 mmol) of **77**, 156 mg (1.3 mmol, 3.0 eq.) of (R)-(+)-2-methylpropane-2-sulfinamide, 670 μ L (729 mg, 3.2 mmol, 7.5 eq.) of Ti(OEt)₄, and 3+3 mL THF. Step 2: 97 mg (2.6 mmol, 6.0 eq.) of sodium borohydride in mL 3 THF. Compound **85** (91 mg, 60 % yield) was isolated as a white solid on standing. ¹H NMR (400 MHz, Chloroform-*d*) δ 7.23 (td, *J*

= 1.6, 0.7 Hz, 1H), 7.18 (dd, $J = 10.8, 2.4$ Hz, 1H), 4.37 (dd, $J = 14.4, 5.5$ Hz, 1H), 4.23 – 4.13 (m, 3H), 3.64 (t, $J = 6.7$ Hz, 1H), 1.38 (td, $J = 7.0, 0.8$ Hz, 3H), 1.23 (s, 9H). ^{13}C NMR (101 MHz, Chloroform-*d*) δ 156.21, 153.71, 143.75, 134.92, 134.89, 127.49, 127.46, 119.86, 119.63, 114.65, 114.56, 69.73, 56.05, 44.43, 44.40, 22.61, 15.70.

(R)-N-(5-bromo-2-ethoxy-4-fluorobenzyl)-2-methylpropane-2-sulfinamide (86): See Procedure A: Step 1: 122 mg (0.50 mmol) of **78**, 89 mg (0.73 mmol, 1.5 eq.) of (R)-(+)-2-methylpropane-2-sulfinamide, 390 μL (424 mg, 1.9 mmol, 3.8 eq.) of $\text{Ti}(\text{OEt})_4$, and 3+3 mL THF. Step 2: 112 mg (3.0 mmol, 6.0 eq.) of sodium borohydride in 3 mL THF. Compound **86** (111 mg, 64 % yield) was isolated as a waxy white solid. ^1H NMR (500 MHz, Chloroform-*d*) δ 7.39 (d, $J = 7.8$ Hz, 1H), 6.63 (d, $J = 10.2$ Hz, 1H), 4.30 (dd, $J = 14.4, 5.7$ Hz, 1H), 4.12 (dd, $J = 14.3, 7.4$ Hz, 1H), 4.00 (q, $J = 6.9$ Hz, 2H), 3.70 (t, $J = 6.8$ Hz, 1H), 1.42 (t, $J = 6.8$ Hz, 3H), 1.21 (s, 9H). ^{13}C NMR (126 MHz, Chloroform-*d*) δ 159.96, 158.00, 156.97, 156.90, 132.88, 132.87, 124.76, 124.73, 100.84, 100.63, 98.35, 98.19, 64.34, 55.94, 44.54, 22.58, 14.61.

(R)-N-((R)-1-(3-benzylphenyl)-2,2,2-trifluoroethyl)-2-methylpropane-2-sulfinamide (87): See Procedure Ba: 67 mg (0.19 mmol) of **81**, 70 μL (69 mg, 0.31 mmol, 1.7 eq.) of benzyl boronic acid pinacol ester, 74 mg (0.54 mmol, 2.9 eq.) of potassium carbonate, 14 mg (0.019 mmol, 0.10 eq.) of 1,1'-bis(diphenylphosphino)ferrocene]dichloropalladium, 1.8 mL of acetone, and 0.6 mL of water. Compound **87** (32 mg, 46 % yield) was isolated as a yellow oil. ^1H NMR (500 MHz, Chloroform-*d*) δ 7.38 – 7.13 (m, 9H), 4.82 (qd, $J = 7.3, 3.8$ Hz, 1H), 4.00 (s, 2H), 1.23 (s, 9H). ^{13}C NMR (126 MHz, Chloroform-*d*) δ 141.77, 140.40, 131.70, 130.35, 129.77, 128.94, 128.83, 128.52, 128.51, 127.14, 126.24, 60.81, 60.57, 60.32, 60.08, 56.36, 53.79, 41.67, 22.30.

1-(3-benzylphenyl)ethan-1-one (82): See Procedure Bb: 150 μL (226 mg, 1.1 mmol) of **1-(3-bromophenyl)ethan-1-one (2)**, 320 μL (314 mg, 1.4 mmol, 1.3 eq.) of benzyl boronic acid pinacol ester, 280 mg (2.0 mmol, 1.8 eq.) of potassium carbonate, 77 mg (0.11 mmol, 0.093 eq.) of 1,1'-bis(diphenylphosphino)ferrocene]dichloropalladium, 4 mL of 3:1 Acetone:Water. Compound **82** (176 mg, 74 % yield) was isolated as a colorless oil. ^1H NMR (500 MHz, Chloroform-*d*) δ 7.86 (s, 1H), 7.82 (dt, $J = 6.8, 1.9$ Hz, 1H), 7.43 – 7.37 (m, 2H), 7.32 (dd, $J = 8.2, 6.9$ Hz, 2H), 7.26 – 7.20 (m, 3H), 4.06 (s, 2H), 2.59 (s, 3H). ^{13}C NMR (126 MHz, Chloroform-*d*) δ 198.17, 141.74, 140.45, 137.41, 133.74, 128.91, 128.76, 128.67, 128.65, 126.38, 126.37, 41.80, 26.69.

1-(5-benzylpyridin-3-yl)ethan-1-one (83): See Procedure Bb: 146 mg (0.73 mmol) of **1-(5-bromopyridin-3-yl)ethan-1-one (76)**, 210 μL (206 mg, 0.94 mmol, 1.3 eq.) of benzyl boronic acid pinacol ester, 179 mg (1.3 mmol, 1.8 eq.) of potassium carbonate, 50 mg (0.068 mmol, 0.094 eq.) of 1,1'-bis(diphenylphosphino)ferrocene]dichloropalladium, 5 mL of 3:1 acetone:water. Compound **83** (141 mg, 91 % yield) was isolated as an orange oil. ^1H NMR (500 MHz, Chloroform-*d*) δ 8.96 (d, $J = 2.1$ Hz, 1H), 8.62 (d, $J = 2.2$ Hz, 1H), 8.00 (t, $J = 2.2$ Hz, 1H), 7.26 (dd, $J = 8.1, 6.7$ Hz, 2H), 7.19 (tt, $J = 7.1, 1.4$ Hz, 1H), 7.17 – 7.11 (m, 2H), 4.00 (s, 2H), 2.55 (s, 3H). ^{13}C NMR (126 MHz, Chloroform-*d*) δ 196.79, 153.84, 147.75, 138.99, 136.89, 135.55, 132.14, 128.82, 128.76, 126.74, 38.84, 26.78.

(S)-N-((S)-1-(5-benzyl-2-methoxyphenyl)ethyl)-2-methylpropane-2-sulfinamide (91): See Procedure Ba: 142 mg (0.43 mmol) of **84**, 160 μL (157 mg, 0.72 mmol, 1.7 eq.) of benzyl boronic acid pinacol ester, 160 mg (1.2 mmol, 2.7 eq.) of potassium carbonate, 31 mg (0.042 mmol, 0.10 eq.) of 1,1'-bis(diphenylphosphino)ferrocene]dichloropalladium, 2.4 mL of 3:1

acetone:water. Compound **91** (87 mg, 59 % yield) was isolated as a colorless oil. ^1H NMR (500 MHz, Chloroform-*d*) δ 7.30 – 7.25 (m, 2H), 7.20 – 7.15 (m, 3H), 7.10 (d, $J = 2.2$ Hz, 1H), 7.03 (dd, $J = 8.2, 2.2$ Hz, 1H), 6.79 (d, $J = 8.4$ Hz, 1H), 4.77 (p, $J = 6.3$ Hz, 1H), 3.93 (s, 2H), 3.81 (s, 3H), 3.79 (d, $J = 5.2$ Hz, 1H), 1.45 (d, $J = 6.7$ Hz, 3H), 1.19 (s, 9H). ^{13}C NMR (126 MHz, Chloroform-*d*) δ 154.88, 141.34, 133.29, 132.20, 128.96, 128.59, 128.40, 127.36, 125.97, 110.85, 55.44, 55.39, 49.85, 41.09, 22.60, 21.81.

(R)-N-(5-benzyl-2-ethoxy-3-fluorobenzyl)-2-methylpropane-2-sulfinamide (92): See Procedure Bb: 67 mg (0.20 mmol) of **85**, 60 μL (59 mg, 0.27 mmol, 1.3 eq.) of benzyl boronic acid pinacol ester, 52 mg (0.38 mmol, 1.9 eq.) of potassium carbonate, 14 mg (0.019 mmol, 0.095 eq.) of 1,1'-bis(diphenylphosphino)ferrocene]dichloropalladium, 5 mL of 3:1 acetone:water. Compound **92** (42 mg, 61 % yield) was isolated as a white solid on standing. ^1H NMR (500 MHz, Chloroform-*d*) δ 7.29 (t, $J = 7.4$ Hz, 2H), 7.21 (tt, $J = 6.5, 1.4$ Hz, 1H), 7.17 (d, $J = 6.9$ Hz, 2H), 6.90 (s, 1H), 6.83 (dd, $J = 12.2, 2.1$ Hz, 1H), 4.38 (dd, $J = 13.9, 5.1$ Hz, 1H), 4.21 – 4.07 (m, 3H), 3.90 (s, 2H), 3.65 (dd, $J = 8.0, 5.1$ Hz, 1H), 1.38 (t, $J = 7.1$ Hz, 3H), 1.19 (s, 10H). ^{13}C NMR (126 MHz, Chloroform-*d*) δ 156.08, 154.11, 142.78, 142.69, 140.25, 136.91, 136.86, 133.05, 133.03, 128.89, 128.57, 126.34, 124.77, 124.75, 116.61, 116.46, 69.62, 69.57, 55.88, 44.83, 44.80, 41.14, 41.12, 22.60, 15.74.

(R)-N-(5-benzyl-2-ethoxy-4-fluorobenzyl)-2-methylpropane-2-sulfinamide (93): See Procedure Ba: 65 mg (0.19 mmol) of **86**, 70 μL (69 mg, 0.31 mmol, 1.7 eq.) of benzyl boronic acid pinacol ester, 72 mg (0.52 mmol, 2.8 eq.) of potassium carbonate, 15 mg (0.021 mmol, 0.11 eq.) of 1,1'-bis(diphenylphosphino)ferrocene]dichloropalladium, 2.5 mL of 3:1 acetone:water. Compound **93** (49 mg, 73 % yield) was isolated as a yellow oil. ^1H NMR (500 MHz, Chloroform-*d*) δ 7.29 – 7.26 (m, 2H), 7.22 – 7.16 (m, 3H), 7.01 (d, $J = 8.6$ Hz, 1H), 6.57 (d, $J = 11.6$ Hz, 1H), 4.32 (dd, $J = 13.9, 5.4$ Hz, 1H), 4.08 (dd, $J = 13.9, 7.9$ Hz, 1H), 4.00 (q, $J = 7.0$ Hz, 2H), 3.91 (s,

2H), 3.62 (dd, $J = 8.0, 5.4$ Hz, 1H), 1.42 (t, $J = 7.0$ Hz, 3H), 1.17 (s, 9H). ^{13}C NMR (126 MHz, Chloroform- d) δ 161.66, 159.70, 156.23, 156.15, 140.17, 131.25, 131.19, 128.66, 128.47, 126.13, 122.81, 119.10, 118.97, 99.73, 99.52, 63.99, 55.76, 44.96, 34.08, 34.06, 22.57, 14.75.

(R)-1-(3-benzylphenyl)-2,2,2-trifluoroethan-1-aminium chloride (94): See Procedure C: 32 mg (0.087 mmol) of **87**, 0.4 mL HCl conc., 2 mL dioxane. Compound **94** (21 mg, 80 % yield) was isolated as a white solid. ^1H NMR (500 MHz, Methanol- d_4) δ 7.48 – 7.39 (m, 4H), 7.30 – 7.25 (m, 2H), 7.23 – 7.16 (m, 3H), 5.32 (q, $J = 7.5$ Hz, 1H), 4.05 (s, 2H). ^{13}C NMR (126 MHz, Methanol- d_4) δ 143.20, 140.40, 131.19, 129.29, 128.72, 128.48, 128.21, 125.97, 125.80, 55.37, 55.11, 48.43, 41.11.

(S)-1-(3-benzylphenyl)ethan-1-aminium chloride (95): See Procedure C: 76 mg (0.24 mmol) of **88**, 0.2 mL HCl conc., 2 mL dioxane. Compound **95** (56 mg, 94 % yield) was isolated as a white solid. ^1H NMR (500 MHz, Methanol- d_4) δ 7.39 – 7.34 (m, 2H), 7.31 (dt, $J = 7.7, 1.5$ Hz, 1H), 7.28 – 7.20 (m, 5H), 7.19 – 7.14 (m, 1H), 4.42 (q, $J = 6.9$ Hz, 1H), 4.01 (s, 2H), 1.61 (d, $J = 7.1$ Hz, 3H). ^{13}C NMR (126 MHz, Methanol- d_4) δ 142.63, 140.82, 138.44, 129.29, 129.01, 128.51, 128.14, 126.84, 125.82, 123.91, 50.96, 41.30, 19.43.

(S)-3-(1-ammonioethyl)-5-benzylpyridin-1-ium chloride (96): See Procedure C: 52 mg (0.16 mmol) of **89**, 0.2 mL HCl conc., 2 mL dioxane. Compound **96** was isolated as a tan oil and used without further purification. ^1H NMR (500 MHz, Methanol- d_4) δ 8.98 (s, 1H), 8.84 (s, 1H), 8.77 (s, 1H), 7.38 – 7.26 (m, 5H), 4.84 (s, 1H), 4.32 (s, 2H), 1.75 (d, $J = 5.4$ Hz, 3H). ^{13}C NMR (126 MHz, Methanol- d_4) δ 145.64, 143.10, 141.48, 138.76, 138.26, 137.54, 128.98, 128.87, 127.02, 37.86, 20.11, 18.48.

(R)-3-(1-ammonioethyl)-5-benzylpyridin-1-ium chloride (97): See Procedure C: 10 mg (0.18 mmol) of **90**, 0.2 mL HCl conc., 2 mL dioxane. Compound **97** (6 mg, 67 % yield) was isolated as a colorless oil. ^1H NMR (500 MHz, Methanol- d_4) δ 8.92 (s, 1H), 8.84 (s, 1H), 8.66 (s, 1H), 7.42 – 7.32 (m, 4H), 7.32 – 7.22 (m, 1H), 4.80 (q, $J = 6.9$ Hz, 1H), 4.30 (s, 2H), 1.72 (d, $J = 6.9$ Hz, 3H). ^{13}C NMR (126 MHz, Methanol- d_4) δ 146.66, 145.01, 143.01, 141.76, 138.84, 137.48, 128.85, 128.83, 127.04, 37.74, 20.04, 18.27.

(S)-1-(5-benzyl-2-methoxyphenyl)ethan-1-aminium chloride (98): See Procedure D: 87 mg (0.25 mmol) of **91**, 0.4 mL HCl conc., 2 mL dioxane. Compound **98** was continued without further purification.

(5-benzyl-2-ethoxy-3-fluorophenyl)methanaminium chloride (99): See Procedure C: 42 mg (mmol) of **92**, 0.2 mL HCl conc., 2 mL dioxane. Compound **99** (30 mg, 88 % yield) was isolated as a white solid. ^1H NMR (500 MHz, Methanol- d_4) δ 7.30 – 7.26 (m, 2H), 7.23 – 7.17 (m, 3H), 7.09 – 7.04 (m, 2H), 4.24 (qd, $J = 7.1, 1.6$ Hz, 2H), 4.11 (s, 2H), 3.94 (s, 2H), 1.40 (td, $J = 7.0, 0.7$ Hz, 3H). ^{13}C NMR (126 MHz, Methanol- d_4) δ 155.56, 153.59, 140.31, 138.02, 137.96, 128.46, 128.23, 126.01, 125.50, 125.48, 118.12, 117.97, 69.60, 69.54, 40.36, 40.35, 38.24, 38.22, 14.52.

(5-benzyl-2-ethoxy-4-fluorophenyl)methanaminium chloride (100): See Procedure C: 49 mg (mmol) of **93**, 0.4 mL HCl conc., 2 mL dioxane. Compound **100** (36 mg, 90 % yield) was isolated as an off white solid. ^1H NMR (500 MHz, $-d_4$) δ 7.28 – 7.22 (m, 3H), 7.20 (d, $J = 7.5$ Hz, 2H), 7.16 (t, $J = 7.1$ Hz, 1H), 6.86 (d, $J = 11.7$ Hz, 1H), 4.13 (q, $J = 6.9$ Hz, 2H), 4.04 (s, 2H), 3.93 (s, 2H), 1.45 (t, $J = 7.0$ Hz, 3H). ^{13}C NMR (126 MHz, Methanol- d_4) δ 162.93,

160.97, 156.91, 156.82, 140.02, 132.76, 132.70, 128.22, 128.11, 125.85, 119.90, 119.76, 116.87, 116.85, 99.85, 99.63, 64.34, 38.23, 33.39, 33.37, 13.42.

(S)-1-(((R)-1-(3-benzylphenyl)-2,2,2-trifluoroethyl)amino)-3-(4-hydroxy-2,6-dimethylphenyl)-1-oxopropan-2-aminium trifluoroacetate (101): See Procedure D: Step 1: 20 mg (0.066 mmol) of **94**, 140 μ L (104 mg, 0.80 mmol, 12 eq.) of N,N-diisopropylethylamine, 42 mg (0.081 mmol, 1.2 eq.) of PyBOP, 15 mg (0.088 mmol, 1.3 eq.) of 6-Cl-HOBt, 34 mg (0.083 mmol, 1.3 eq.) of Boc-O-Boc-L-2',6'-dimethyltyrosine, 3+1.5 mL of DMF. Step 2: 2 mL TFA and 2 mL DCM. Compound **101** (4 mg, 11 % yield) was isolated as a white solid. ^1H NMR (500 MHz, Methanol- d_4) δ 7.29 – 7.22 (m, 4H), 7.21 – 7.14 (m, 3H), 6.98 (s, 1H), 6.85 – 6.79 (m, 1H), 6.13 (s, 2H), 5.59 (q, $J = 8.3, 7.4$ Hz, 1H), 4.05 – 3.93 (m, 4H), 3.09 (dd, $J = 13.8, 11.7$ Hz, 1H), 2.93 (dd, $J = 13.8, 4.2$ Hz, 1H), 1.94 (s, 6H). No ^{13}C Data Acquired. ESI-MS: 457.3 $[\text{M} + \text{H}]^+$, HPLC (gradient A): Retention Time: 40.42 min.

(S)-1-(((S)-1-(3-benzylphenyl)ethyl)amino)-3-(4-hydroxy-2,6-dimethylphenyl)-1-oxopropan-2-aminium trifluoroacetate (102): See Procedure D: Step 1: 27 mg (0.11 mmol) of **95**, 190 μ L (141 mg, 1.1 mmol, 10 eq.) of N,N-diisopropylethylamine, 61 mg (0.12 mmol, 1.1 eq.) of PyBOP, 20 mg (0.12 mmol, 1.1 eq.) of 6-Cl-HOBt, 47 mg (0.11 mmol, 1.1 eq.) of Boc-O-Boc-L-2',6'-dimethyltyrosine, 3+1 mL of DMF. Step 2: 2 mL TFA and 2 mL DCM. Compound **102** (mg, % yield) was isolated as a white solid. ^1H NMR (400 MHz, DMSO- d_6) δ 9.10 (s, 1H), 8.43 (d, $J = 8.1$ Hz, 1H), 8.32 (br s, 3H), 7.29 – 7.22 (m, 2H), 7.21 – 7.13 (m, 3H), 7.10 (t, $J = 7.6$ Hz, 1H), 7.02 (d, $J = 7.6$ Hz, 1H), 6.90 (s, 1H), 6.51 (d, $J = 7.5$ Hz, 1H), 6.34 (s, 2H), 4.85 (p, $J = 6.7$ Hz, 1H), 3.91 (d, $J = 14.6$ Hz, 1H), 3.85 (d, $J = 14.6$ Hz, 1H), 3.72 (br s, 1H), 3.15 (s, 1H), 2.97

(dd, $J = 13.5, 11.1$ Hz, 1H), 2.76 (dd, $J = 13.8, 4.2$ Hz, 1H), 2.01 (s, 6H), 1.26 (d, $J = 6.9$ Hz, 3H). No ^{13}C Data Acquired. ESI-MS: 457.3 $[\text{M} + \text{H}]^+$, HPLC (gradient A): Retention Time: 37.48 min.

(S)-1-(((S)-1-(5-benzylpyridin-3-yl)ethyl)amino)-3-(4-hydroxy-2,6-dimethylphenyl)-1-oxopropan-2-aminium trifluoroacetate (103): See Procedure D: Step 1: 24 mg (0.084 mmol) of **96**, 150 μL (111 mg, 0.86 mmol, 10 eq.) of N,N-diisopropylethylamine, 47 mg (0.090 mmol, 1.1 eq.) of PyBOP, 17 mg (0.10 mmol, 1.2 eq.) of 6-Cl-HOBt, 35 mg (0.085 mmol, 1.0 eq.) of Boc-O-Boc-L-2',6'-dimethyltyrosine, 3+1.5 mL of DMF. Step 2: 2 mL TFA and 2 mL DCM. Compound **103** (9.5 mg, 19 % yield) was isolated as a white solid. ^1H NMR (500 MHz, Methanol- d_4) δ 8.62 (s, 1H), 8.38 (s, 1H), 7.99 (s, 1H), 7.38 – 7.33 (m, 2H), 7.32 – 7.24 (m, 3H), 6.22 (s, 2H), 5.15 (q, $J = 6.9$ Hz, 1H), 4.26 (d, $J = 15.5$ Hz, 1H), 4.20 (d, $J = 15.5$ Hz, 1H), 3.88 (dd, $J = 11.5, 5.1$ Hz, 1H), 3.08 (dd, $J = 13.7, 11.5$ Hz, 1H), 2.92 (dd, $J = 13.8, 5.2$ Hz, 1H), 2.02 (s, 6H), 1.39 (d, $J = 7.1$ Hz, 3H). No ^{13}C Data Acquired. ESI-MS: 403.2 $[\text{M} + \text{H}]^+$, HPLC (gradient A): Retention Time: 20.45 min.

(S)-1-(((R)-1-(5-benzylpyridin-3-yl)ethyl)amino)-3-(4-hydroxy-2,6-dimethylphenyl)-1-oxopropan-2-aminium trifluoroacetate (104): See Procedure D: Step 1: 5 mg (0.018 mmol) of **97**, μL (30 mg, 0.23 mmol, 13 eq.) of N,N-diisopropylethylamine, 12 mg (0.023 mmol, 1.3 eq.) of PyBOP, 5 mg (0.029 mmol, 1.7 eq.) of 6-Cl-HOBt, 7 mg (0.017 mmol, 0.98 eq.) of Boc-O-Boc-L-2',6'-dimethyltyrosine, 3+1.5 mL of DMF. Step 2: 2 mL TFA and 2 mL DCM. Compound **104** (5.6 mg, 54 % yield) was isolated as a white solid. ^1H NMR (500 MHz, Methanol- d_4) δ 8.60 (s, 1H), 8.56 (s, 1H), 8.33 (s, 1H), 7.37 – 7.30 (m, 2H), 7.29 – 7.23 (m, 3H), 6.54 (s, 2H), 4.96 (q, $J = 7.1$ Hz, 1H), 4.19 (s, 2H), 3.84 (dd, $J = 11.6, 4.8$ Hz, 1H), 3.20 (dd, $J = 13.8, 11.6$ Hz, 1H), 3.06

(dd, $J = 13.8, 4.9$ Hz, 1H), 2.27 (s, 6H), 1.18 (d, $J = 7.1$ Hz, 3H). No ^{13}C Data Acquired. ESI-MS: 404.2 $[\text{M} + \text{H}]^+$, HPLC (gradient A): Retention Time: 21.64 min.

(S)-1-(((S)-1-(5-benzyl-2-methoxyphenyl)ethyl)amino)-3-(4-hydroxy-2,6-dimethylphenyl)-1-oxopropan-2-aminium trifluoroacetate (105): See Procedure D: Step 1: 27 mg (0.097 mmol) of **98**, 170 μL (126 mg, 0.98 mmol, 10 eq.) of N,N-diisopropylethylamine, 54 mg (0.10 mmol, 1.1 eq.) of PyBOP, 18 mg (0.11 mmol, 1.1 eq.) of 6-Cl-HOBt, 40 mg (0.098 mmol, 1.0 eq.) of Boc-O-Boc-L-2',6'-dimethyltyrosine, 3+1.5 mL of DMF. Step 2: 2 mL TFA and 2 mL DCM. Compound **105** (6 mg, 11 % yield) was isolated as a white solid. ^1H NMR (500 MHz, Methanol- d_4) δ 7.63 (d, $J = 9.1$ Hz, 1H), 7.29 – 7.16 (m, 4H), 7.15 – 7.07 (m, 2H), 6.79 (dd, $J = 5.3, 3.1$ Hz, 2H), 6.14 (s, 2H), 5.19 – 5.11 (m, 1H), 3.87 (dd, $J = 9.3, 4.6$ Hz, 3H), 3.63 (s, 3H), 3.01 (dd, $J = 13.8, 11.5$ Hz, 1H), 2.84 (dd, $J = 13.9, 4.4$ Hz, 1H), 1.92 (s, 6H), 1.31 (d, $J = 7.0$ Hz, 3H). No ^{13}C Data Acquired. ESI-MS: 433.3 $[\text{M} + \text{H}]^+$, HPLC (gradient A): Retention Time: 38.04 min.

(S)-1-((5-benzyl-2-ethoxy-3-fluorobenzyl)amino)-3-(4-hydroxy-2,6-dimethylphenyl)-1-oxopropan-2-aminium trifluoroacetate (106): See Procedure D: Step 1: 13 mg (0.044 mmol) of **99**, 80 μL (59 mg, 0.46 mmol, 10 eq.) of N,N-diisopropylethylamine, 25 mg (0.048 mmol, 1.1 eq.) of PyBOP, 8 mg (0.047 mmol, 1.1 eq.) of 6-Cl-HOBt, 18 mg (0.044 mmol, 1.0 eq.) of Boc-O-Boc-L-2',6'-dimethyltyrosine, 3+1.5 mL of DMF. Step 2: 2 mL TFA and 2 mL DCM. Compound **106** (20.1 mg, 81 % yield) was isolated as a white solid. ^1H NMR (400 MHz, Methanol- d_4) δ 7.80 (t, $J = 5.7$ Hz, 1H), 7.30 – 7.21 (m, 2H), 7.19 – 7.11 (m, 3H), 6.81 (dd, $J = 12.5, 2.1$ Hz, 1H), 6.70 (s, 1H), 6.42 (s, 2H), 4.41 – 4.15 (m, 2H), 4.07 – 3.92 (m, 2H), 3.91 – 3.80 (m, 3H), 3.15

(dd, $J = 13.8, 11.2$ Hz, 1H), 2.95 (dd, $J = 13.9, 4.8$ Hz, 1H), 2.14 (s, 6H), 1.27 (t, $J = 7.0$ Hz, 3H). No ^{13}C Data Acquired. ESI-MS: 451.3 $[\text{M} + \text{H}]^+$, HPLC (gradient A): Retention Time: 40.46 min.

(S)-1-((5-benzyl-2-ethoxy-4-fluorobenzyl)amino)-3-(4-hydroxy-2,6-dimethylphenyl)-1-oxopropan-2-aminium trifluoroacetate (107): See Procedure D: Step 1: 18 mg (0.061 mmol) of **100**, 130 μL (96 mg, 0.75 mmol, 12 eq.) of N,N-diisopropylethylamine, 39 mg (0.075 mmol, 1.2 eq.) of PyBOP, 14 mg (0.083 mmol, 1.4 eq.) of 6-Cl-HOBt, 30 mg (0.073 mmol, 1.2 eq.) of Boc-O-Boc-L-2',6'-dimethyltyrosine, 2.5+2 mL of DMF. Step 2: 2 mL TFA and 2 mL DCM. Compound **107** (15 mg, 44 % yield) was isolated as a white solid. ^1H NMR (400 MHz, Methanol- d_4) δ 7.41 (t, $J = 5.8$ Hz, 1H), 7.27 – 7.17 (m, 4H), 7.13 (tt, $J = 6.1, 1.7$ Hz, 1H), 6.97 (d, $J = 8.7$ Hz, 1H), 6.64 (d, $J = 11.9$ Hz, 1H), 6.29 (s, 2H), 4.35 – 4.25 (m, 1H), 4.05 (dd, $J = 14.3, 4.3$ Hz, 1H), 3.95 – 3.78 (m, 5H), 3.06 (dd, $J = 13.7, 11.6$ Hz, 1H), 2.90 (dd, $J = 13.8, 4.6$ Hz, 1H), 1.98 (s, 6H), 1.27 (t, $J = 7.0$ Hz, 3H). No ^{13}C Data Acquired. ESI-MS: 451.2 $[\text{M} + \text{H}]^+$, HPLC (gradient A): Retention Time: 40.24 min.

2-ethoxynicotinamide (109): See Procedure F: 117 mg (0.70 mmol) of **2-ethoxynicotinic acid (108)**, 426 mg (0.82 mmol, 1.2 eq.) of PyBOP, 41 mg (0.77 mmol, 1.1 eq.) of ammonium chloride, 760 μL (699 mg, 6.9 mol, 9.9 eq.) of NMM, and 4.1 mL of DMF. Compound **109** (85 mg, 73 % yield) was isolated as a white solid. ^1H NMR (400 MHz, Chloroform- d) δ 8.44 (dd, $J = 7.5, 2.1$ Hz, 1H), 8.20 (dd, $J = 4.9, 2.1$ Hz, 1H), 7.83 (br s, 1H), 7.16 (br s, 1H), 6.97 (dd, $J = 7.6, 4.9$ Hz, 1H), 4.48 (q, $J = 7.1$ Hz, 2H), 1.40 (t, $J = 7.1$ Hz, 3H). ^{13}C NMR (101 MHz, Chloroform- d) δ 166.33, 160.74, 150.06, 141.62, 117.45, 115.25, 62.87, 14.58.

tert-butyl ((2-ethoxypyridin-3-yl)methyl)carbamate (110): See Procedure G: 84 mg (0.51 mmol) of **109**, 3.5 mL of 2M $\text{BH}_3 \cdot \text{Me}_2\text{S}$ in THF (7.0 mmol, 14 eq.) and 4 mL THF. 132 mg

(0.60 mmol, 1.2 eq.) of Boc₂O, 230 μ L (167 mg, 1.6 mmol, 3.3 eq.) of triethylamine and 4 mL of THF. An additional 261 mg (1.2 mmol, 2.4 eq.) of Boc₂O was added. Compound **110** (32 mg, 25 % yield) was isolated a yellow oil that solidified on standing. ¹H NMR (500 MHz, Chloroform-*d*) δ 8.04 (dd, *J* = 5.1, 1.9 Hz, 1H), 7.52 (d, *J* = 7.2 Hz, 1H), 6.82 (dd, *J* = 7.2, 5.0 Hz, 1H), 5.04 (br s, 1H), 4.40 (q, *J* = 7.1 Hz, 2H), 4.25 (d, *J* = 6.3 Hz, 2H), 1.44 (s, 9H), 1.40 (t, *J* = 7.0 Hz, 3H). ¹³C NMR (126 MHz, Chloroform-*d*) δ 161.57, 155.85, 145.58, 137.10, 121.33, 116.56, 79.45, 61.62, 39.92, 28.39, 14.71.

tert-butyl ((5-bromo-2-ethoxypyridin-3-yl)methyl)carbamate (111): See Procedure H: 42 mg (0.17 mmol) of **109**, 31 mg (0.17 mmol, 1.0 eq.) of NBS, and 5 mL of MeCN. Compound **111** (13 mg, 24 % yield) was isolated as a colorless oil. ¹H NMR (500 MHz, Chloroform-*d*) δ 8.07 (d, *J* = 2.4 Hz, 1H), 7.61 (s, 1H), 5.00 (br s, 1H), 4.36 (q, *J* = 7.1 Hz, 2H), 4.23 (d, *J* = 6.4 Hz, 2H), 1.45 (s, 9H), 1.38 (t, *J* = 7.1 Hz, 3H). ¹³C NMR (126 MHz, Chloroform-*d*) δ 160.25, 152.28, 145.94, 139.12, 123.36, 117.00, 62.19, 39.42, 28.37, 14.58.

tert-butyl ((5-benzyl-2-ethoxypyridin-3-yl)methyl)carbamate (112): See Procedure Bb: 22 mg (0.066 mmol) of **111**, 30 μ L (29 mg, 0.13 mmol, 2.0 eq.) of benzyl boronic acid pinacol ester, 20 mg (0.14 mmol, 2.2 eq.) of potassium carbonate, 12 mg (0.016 mmol, 0.25 eq.) of 1,1'-bis(diphenylphosphino)ferrocene]dichloropalladium, 4 mL of 3:1 acetone:water. Compound **112** (13 mg, 57 % yield) was isolated as a colorless oil and used without further purification.

3-(ammoniomethyl)-5-benzyl-2-ethoxypyridin-1-ium chloride (113): See Procedure C: 13 mg (mmol) of **112**, 0.2 mL HCl conc., 2 mL dioxane. No trituration was performed. Compound **113** (12 mg, Quantitative yield) was isolated as a colorless oil. ¹H NMR (500 MHz, Methanol-*d*₄) δ 8.10 (d, *J* = 2.3 Hz, 1H), 7.74 (d, *J* = 2.3 Hz, 1H), 7.32 – 7.26 (m, 2H), 7.26 – 7.17 (m, 3H), 4.49

(q, $J = 7.0$ Hz, 2H), 4.08 (s, 2H), 3.98 (s, 2H), 1.46 (t, $J = 7.0$ Hz, 3H). ^{13}C NMR (126 MHz, Methanol- d_4) δ 159.54, 144.71, 141.70, 139.91, 130.84, 128.44, 128.36, 126.18, 63.46, 37.91, 37.13, 13.33.

(S)-1-(((5-benzyl-2-ethoxypyridin-3-yl)methyl)amino)-3-(4-hydroxy-2,6-dimethylphenyl)-1-oxopropan-2-aminium trifluoroacetate (114): See Procedure D: Step 1: 5 mg (0.016 mmol) of **113**, 40 μL (30 mg, 0.23 mmol, 14 eq.) of N,N-diisopropylethylamine, 11 mg (0.021 mmol, 1.3 eq.) of PyBOP, 5 mg (0.029 mmol, 1.9 eq.) of 6-Cl-HOBt, 11 mg (0.027 mmol, 1.7 eq.) of Boc-O-Boc-L-2',6'-dimethyltyrosine, 3+1.5 mL of DMF. Step 2: 2 mL TFA and 2 mL DCM. Compound **114** (3.8 mg, 39 % yield) was isolated as a white solid. ^1H NMR (500 MHz, Methanol- d_4) δ 7.89 (d, $J = 2.3$ Hz, 1H), 7.68 (t, $J = 6.0$ Hz, 1H), 7.30 – 7.23 (m, 3H), 7.24 – 7.19 (m, 2H), 7.16 (t, $J = 7.3$ Hz, 1H), 6.31 (s, 2H), 4.37 – 4.30 (m, 1H), 4.23 (qq, $J = 10.3, 7.0$ Hz, 2H), 4.03 (dd, $J = 14.8, 4.5$ Hz, 1H), 3.89 (s, 2H), 3.86 (dd, $J = 11.5, 4.7$ Hz, 1H), 3.07 (dd, $J = 13.8, 11.5$ Hz, 1H), 2.91 (dd, $J = 13.8, 4.7$ Hz, 1H), 2.00 (s, 6H), 1.27 (t, $J = 7.0$ Hz, 3H). No ^{13}C Data Acquired. ESI-MS: 434.3 $[\text{M} + \text{H}]^+$, HPLC (gradient A): Retention Time: 31.87 min.

***In Vitro* Pharmacology**

Cell Lines and Membrane Preparations.

All opioid *in vitro* assays were performed by Nicholas Griggs, Thomas Fernandez, and Jessica Anand. Tissue culture reagents were purchased from Gibco Life Sciences (Grand Island, NY, U.S.) unless otherwise noted. C6-rat glioma cells stably expressing rat MOR, Chinese hamster ovary cells human (CHO) stably expressing human MOR, C6 for rat DOR, CHO for human DOR and CHO for human KOR were used for all *in vitro* assays. Cells were grown to confluence at 37 $^\circ\text{C}$ in 5 % CO_2 in Dulbecco's modified Eagle medium (DMEM) containing 10 % fetal bovine

serum and 5 % penicillin/streptomycin. Membranes were prepared by washing confluent cells three times with ice cold phosphate buffered saline (0.9 % NaCl, 0.61 mM Na₂HPO₄, 0.38 mM KH₂PO₄, pH 7.4). Cells were detached from the plates by incubation in warm harvesting buffer (20 mM HEPES, 150 mM NaCl, 0.68 mM EDTA, pH 7.4) and pelleted by centrifugation at 1600 rpm for 3 min. The cell pellet was suspended in ice-cold 50 mM Tris- HCl buffer, pH 7.4, and homogenized with a Tissue Tearor (Biospec Products, Inc., Bartlesville, OK, U.S.) for 20 s. The homogenate was centrifuged at 15,000 rpm for 20 min at 4 °C. The pellet was rehomogenized in 50 mM Tris-HCl with a Tissue Tearor for 10 s, followed by recentrifugation. The final pellet was resuspended in 50 mM Tris-HCl and frozen in aliquots at -80 °C. Protein concentration was determined via a BCA protein assay (Thermo Scientific Pierce, Waltham, MA, U.S.) using bovine serum albumin as the standard.

Radioligand Competition Binding Assays.

Radiolabeled compounds were purchased from Perkin-Elmer (Waltham, MA, U.S.). Opioid ligand binding assays were performed by competitive displacement of 0.2 nM [³H]-diprenorphine (250 µCi, 1.85 TBq/mmol) by the peptidomimetic from membrane preparations containing opioid receptors as described above. The assay mixture, containing membranes (20 µg protein/tube) in 50 mM Tris-HCl buffer (pH 7.4), 0.2 nM [³H]-diprenorphine, and various concentrations of test peptidomimetic, was incubated at room temperature on a shaker for 1 h to allow binding to reach equilibrium. The samples were rapidly filtered through Whatman GF/C filters using a Brandel harvester (Brandel, Gaithersburg, MD, U.S.) and washed three times with 50 mM Tris-HCl buffer, pH 7.4. Bound radioactivity on dried filters was determined by liquid scintillation counting, after saturation with EcoLume liquid scintillation cocktail, in a Wallac 1450 MicroBeta (Perkin-Elmer, Waltham, MA, U.S.). Nonspecific binding was determined using 10

μM naloxone. The results presented are the mean \pm standard error (S.E.M.) from at least three separate assays performed in duplicate. K_i (nM) values were calculated using nonlinear regression analysis to fit a logistic equation to the competition data using GraphPad Prism, version 6.0c, (GraphPad Software Inc., La Jolla, CA).

[^{35}S]-GTP γS Binding Assays.

Agonist stimulation of [^{35}S]guanosine 5'-O-[γ -thio]triphosphate ([^{35}S]-GTP γS , 1250 Ci, 46.2 TBq/mmol) binding to G protein was measured as described previously.⁸² Briefly, membranes (10 μg of protein/well) were incubated for 1 h at 25°C in GTP γS buffer (50 mM Tris-HCl, 100 mM NaCl, 5 mM MgCl₂, 1 mM EDTA, pH 7.4) containing 0.1 nM [^{35}S]-GTP γS , 30 μM guanosine diphosphate (GDP), and varying concentrations of test peptidomimetic. G protein activation following receptor activation by peptidomimetic was compared with 10 μM of the standard compounds [D-Ala²,N-MePhe⁴,Gly-ol]enkephalin (DAMGO) at MOR, D-Pen^{2,5}-enkephalin (DPDPE) at DOR, or U69,593 at KOR. The reaction was terminated by vacuum filtration through GF/C filters that were washed 5 times with GTP γS buffer. Bound radioactivity was measured as described above. The results are presented as the mean \pm standard error (S.E.M.) from at least three separate assays performed in duplicate; potency (EC₅₀ (nM)) and percent stimulation were determined using nonlinear regression analysis with GraphPad Prism 6, as above.

Mouse Liver Microsome Stability Assays

All liver microsome assays were performed by Quintara Biosciences. Metabolic stability of testing compounds was evaluated using mouse liver microsomes to predict intrinsic clearance. Mouse liver microsome tissue fractions were obtained from Corning or BioreclamationIVT. The assay was carried out in 96-well microtiter plates at 37°C. Reaction mixtures (25 μL) contained a final concentration of 1 μM test compound, 0.1 mg/mL liver microsome protein, and 1 mM

NADPH in 100 mM potassium phosphate, pH 7.4 buffer with 3 mM MgCl₂. At each of the time points (0, 15, 30, and 60 minutes), 150 µL of quench solution (acetonitrile with 0.1% formic acid) with internal standard (bucetin) was transferred to each well. Verapamil was included as a positive control to verify assay performance. Plates were sealed, vortexed, and centrifuged at 4°C for 15 minutes at 4000 rpm. The supernatant was transferred to fresh plates for LC/MS/MS analysis. All samples were analyzed on LC/MS/MS using an AB Sciex API 4000 instrument, coupled to a Shimadzu LC-20AD LC Pump system. Analytical samples were separated using a Waters Atlantis T3 dC18 reverse phase HPLC column (20 mm x 2.1 mm) at a flow rate of 0.5 mL/min. The mobile phase consists of 0.1% formic acid in water (solvent A) and 0.1% formic acid in acetonitrile (solvent B). The extent of metabolism was calculated as the disappearance of the test compound, compared to the 0-min time incubation. Initial rates were calculated for the compound concentration and used to determine $t_{1/2}$ values and subsequently, the intrinsic clearance.

Chapter 4: Amine Pendants as MOR Pharmacophores with Improved Stability

4.1 Introduction

The conversion from a bicyclic core to a monocyclic core structure as described in Chapter 2 yielded MOR-agonist/DOR-antagonists with improved metabolic stability. While this was a useful first step, there was room for improvement on both fronts. Unfortunately, further core modifications described in Chapter 3 did not yield simultaneous improvements in both parameters. Therefore, we opted to shift our focus onto different areas of our peptidomimetic that may be more amenable to further derivatization. DMT is very sensitive to modification, and typically is optimal for affinity and potency at all three opioid receptors.⁵³ As such, we decided to ignore this region and focus instead on the benzyl pendant, which is more amenable to modification as illustrated by our previous bicyclic core series. Here, successful derivatives in this bicyclic series were used to help guide the design of our new analogues.

The monocyclic ligands that possess MOR-agonism while improving metabolic stability thus far have a cLogP of 4.75 or higher. Therefore, we sought to make analogues that would reduce cLogP in order to reduce their liability to CYP metabolism.⁸⁰ In our original tetrahydroquinoline core peptidomimetics, we reported that cyclic amine pendants are either tolerated or show improved efficacy and potency at MOR (**Figure 11**).⁶⁴ These amine pendants also have a lower cLogP than their benzyl pendant precursor. As such, we opted to introduce these polar amine pendants into our previously described monocyclic core system. This was hypothesized to retain or improve already established opioid activity while further improving metabolic stability through reduced cLogP. Herein, the results of an SAR campaign aimed at combining these two structural elements will be discussed.

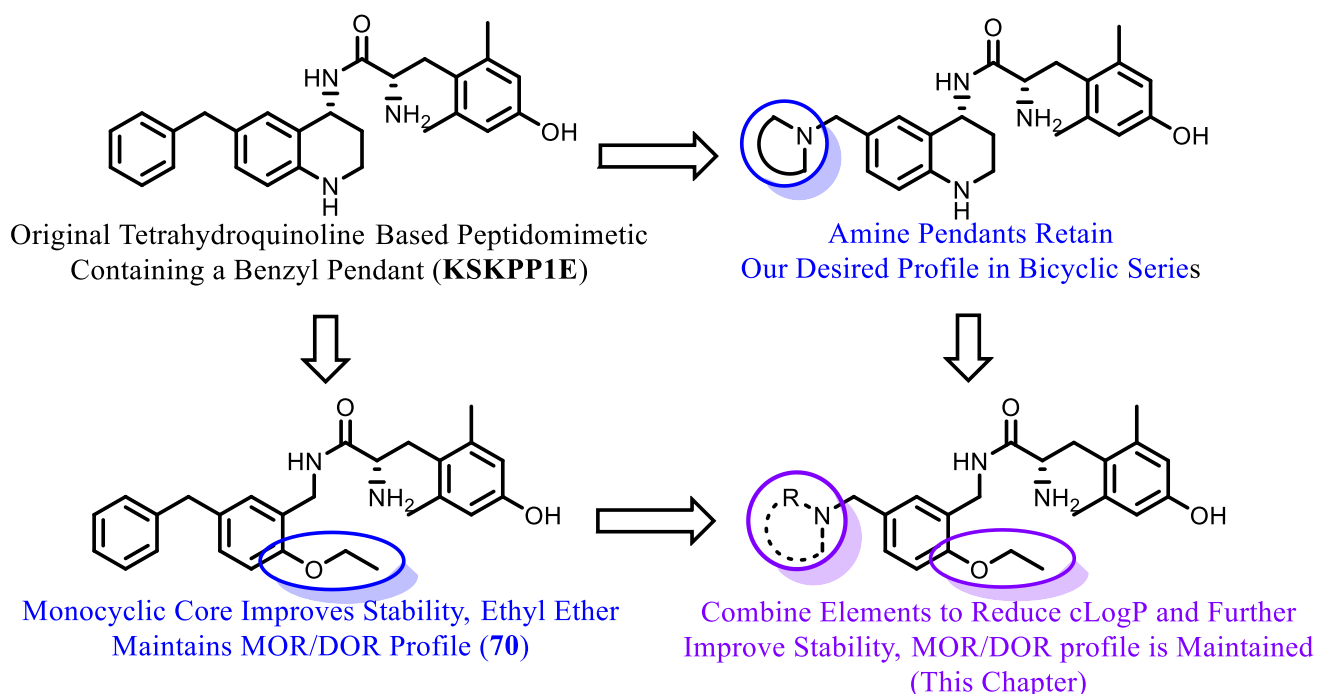
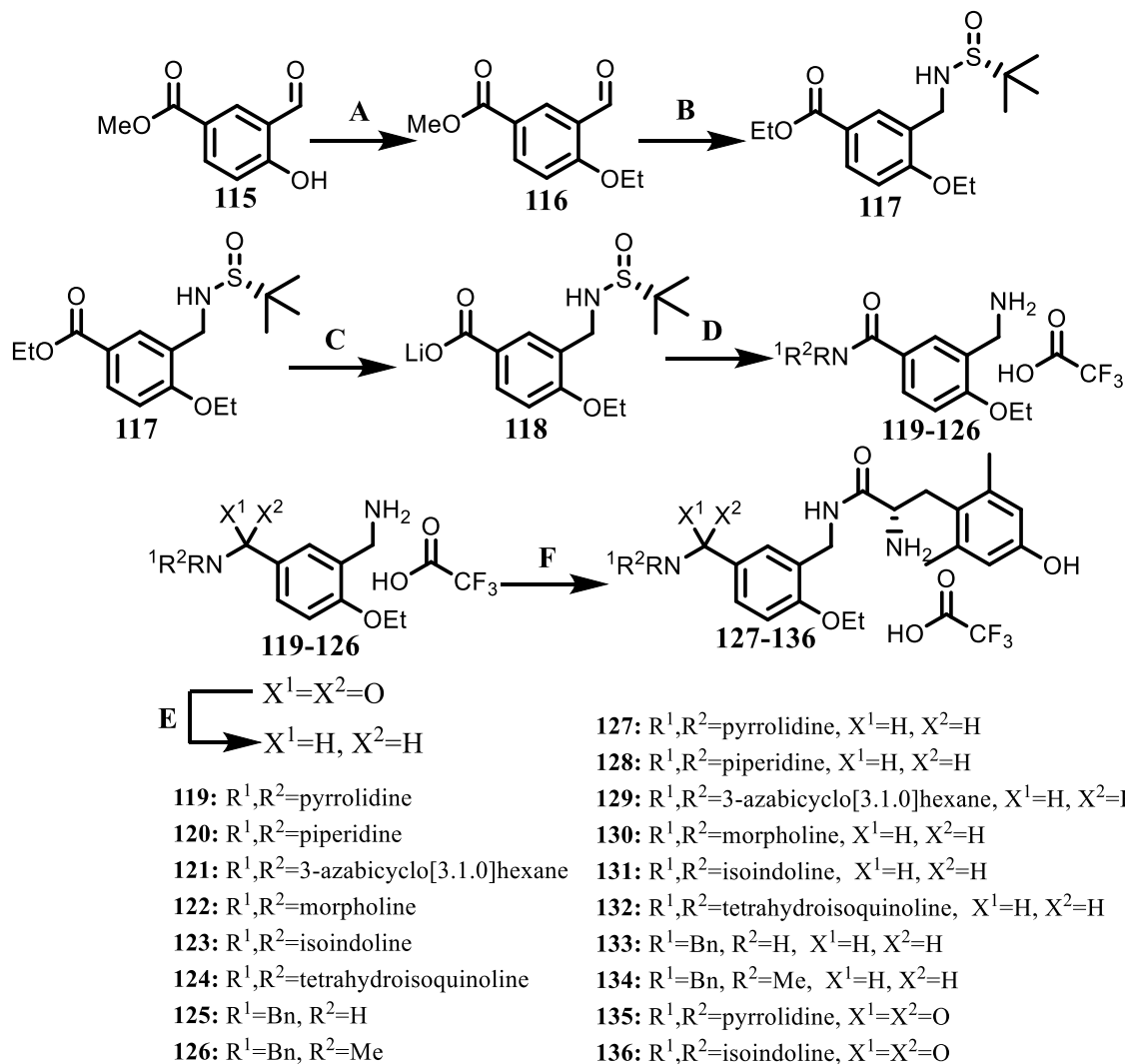


Figure 11: Design path leading to more stable peptidomimetics with amine pendants. Blue indicates previously reported SAR. Purple indicates combined strategies reported in this chapter.

4.2 Results

General Chemistry: In order to incorporate basic amine pendants into our series, we first opted to introduce the ethyl ether into the scaffold using **Scheme 7**. This was done by taking commercially available methyl 3-formyl-4-hydroxybenzoate and alkylating the phenol with ethyl bromide and potassium carbonate. The aldehyde was then subject to a reductive amination using an Ellman auxiliary as an amine source. The auxiliary was left on the scaffold, as it served as a protecting group for the subsequent LiOH mediated saponification and attachment of the amine pendant using PyBOP. The carboxylate was not reduced before the pendant attachment because we were interested in producing analogues that tested the effect an amide would have on our SAR. This amide was then deprotected with conc. HCl and reduced with borane at elevated temperatures if desired. Finally, the intermediate was coupled to Boc-protected DMT and the Boc groups were removed with TFA.

Scheme 7: Synthesis of Amine or Amide Pendant Analogues Containing an Ethyl Ether.

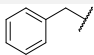


A) EtBr, K₂CO₃, DMF. B) 1. (R)-(+)-2-methyl-2-propanesulfonamide, Ti(OEt)₄, THF 2. NaBH₄.
 C) LiOH, THF, EtOH, H₂O D) 1. NHR¹R², NMM, PyBOP, DMF. 2. conc. HCl, Dioxane. E) BH₃*Me₂S, THF, 75 C° F) 1. DiBocDMT, DIEA, PyBOP, 6-Cl-HOBt, DMF. 2. TFA, DCM.

SAR: Our studies began by selecting the monocyclic analogue from the previous series with the best MOR/DOR profile, namely that containing the ethyl ether (**70**). We were further encouraged by the stability of this analogue, as this was one of the most stable derivatives synthesized thus far. We proceeded by replacing the benzyl pendant with various cyclic amines, some of which were previously reported in our THQ series.⁶⁴ These included piperidine (**128**), morpholine (**130**), isoindoline (**131**), and tetrahydroisoquinoline (THIQ) (**132**) pendants. A few novel pendants for

this series were also synthesized and screened, namely the pyrrolidine (**127**) and 3-azabicyclo[3.1.0]hexane (**129**) heterocycles, and two analogues that possessed conformationally flexible benzyl amines (**133** and **134**). Finally, these derivatives were complemented with the amide analogues of the pyrrolidine (**135**) and isoindoline (**136**) pendants.

Conversion to the monocyclic amine analogues (**127**, **129-130**) generally came with a loss in MOR binding, in contrast to the bicyclic amine analogues (**131-132**) which showed improvements in binding affinity at this receptor (**Table 11**). The monocyclic amines also caused losses in DOR binding affinity, whereas the bicyclic amines produced no change in affinity at this receptor. Neither the benzyl amines (**133-134**) nor the amides (**135-136**) were significantly different from their bicyclic amine counterparts at MOR or DOR. KOR affinity was generally higher with each of these amine pendant analogues, the only exception here being the morpholine pendant (**130**). The highest binding affinity at KOR comes from the benzyl amine pendant analogues (**133-134**), with binding affinity in the low double-digit nanomolar range. The selectivity ratio was also determined for each of these analogues. In general, good binding affinity balance was maintained between MOR and DOR, the only exceptions being the THIQ analogue **132** and the isoindoline amide analogue **136**. Selectivity of MOR over KOR was reduced for most analogues, though good selectivity was maintained with the bicyclic analogues **131**, **132**, and **136**.

<i>Name</i>	<i>R</i>	<i>Binding Affinity, K_i (nM)</i>			<i>Selectivity</i>
		MOR	DOR	KOR	MOR:DOR:KOR
70		3.6±0.5 ^a	4.8±0.9 ^a	1200±120	1:1.3:333

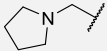
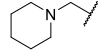
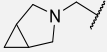
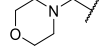
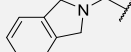
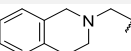
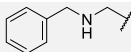
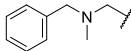
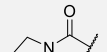
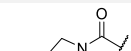
127		15.0±1.8	44.4±7.9	430±16	1:3.0:29
128		5.0±1.5	15.7±4.3	101±14	1:3.1:20
129		19.6±6.1	50±10	247±51	1:2.6:13
130		38.0±9.9	76.0±4.5	>1870	1:2.0:>49
131		0.80±0.22	2.7±0.6	243±53	1:3.4:304
132		0.23±0.04	2.4±0.5	44.2±4.6	1:10:192
133		0.45±0.13	0.82±0.27	23.2±7.6	1:1.2:52
134		0.48±0.13	1.9±0.4	12.4±0.5	1:4.0:26
135		33±11	74±23	760±100	1:2.2:23
136		0.29±0.05	5.9±2.0	261±12	1:20:900

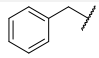
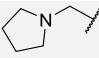
Table 11: Binding affinity of amine or amide pendant analogues at MOR, DOR, and KOR.

Binding affinities (K_i) were obtained by competitive displacement of radiolabeled [^3H] diprenorphine in membrane preparations. Included is **70** for comparison. Selectivity was calculated by dividing the K_i of each receptor by the K_i at MOR for a given compound. All data were from three separate experiments, performed in duplicate unless otherwise noted. These data are reported as the average \pm standard error of the mean. * N=2. ^aData are from assays using human MOR and DOR instead of rat MOR and DOR as reported in Chapter 2.

With regards to potency at MOR, a variety of effects were observed (**Table 12**). The pyrrolidine (**127**) and piperidine (**128**) had potency lower than **70**. Incorporation of a cyclopropyl group (**129**) onto the pyrrolidine, or conversion from a piperidine to a morpholine pendant (**130**) only reduced this potency further. Analogues that reincorporated an aromatic ring (**131-134**) showed improvements in potency, which was especially true if the ring was locked in a bicyclic structure (**131-132**). Variable levels of DOR activity were observed in these amine pendants. Some were partial DOR agonists, having either weak potency and 40-50 % efficacy (**127-129**), or were

moderately potent (**131**). The morpholine (**130**), THIQ (**132**), N-methyl benzyl amine (**134**), and the amides (**135-136**) did not stimulate DOR. Finally, none of these compounds had any appreciable potency at KOR up to 1.3 μ M.

The most interesting data that came from this series was the efficacy of these ligands at MOR. Notably, every analogue discussed thus far had the same or greater efficacy compared to **70**, apart from the amides (**135-136**). This high efficacy was true regardless of the size or presence of a cyclic amine ring. The greatest improvements in efficacy were with the bicyclic amine pendants (**131-132**), which were full agonists at MOR compared to DAMGO.

<i>Name</i>	R	<i>Potency, EC₅₀ (nM)</i>			<i>Efficacy (% Stimulation)</i>		
		MOR	DOR	KOR	MOR	DOR	KOR
70		72±13 ^a	DNS ^a	DNS	75.5±5.8 ^a	DNS ^a	DNS
127		168±42	1360±96	>6000	85.9±9.7	55±11	>40

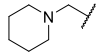
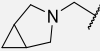
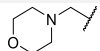
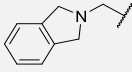
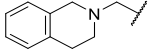
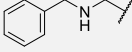
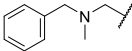
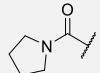
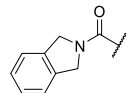
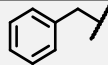
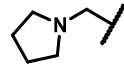
128		585±73	129±20	DNS	77.5±5.8	36.8±6.7	DNS
129		990±160	460±100	>10000	88±16	52.1±7.0	>36.4
130		1020±290	DNS	DNS	72.2±8.3	DNS	DNS
131		8.4±1.2	43±13	Not Tested	98.1±6.7	35.7±2.8	Not Tested
132		1.9±0.5	DNS	DNS	94.6±3.9	DNS	DNS
133		16.7±4.8	4.8±2.0	>1000	77.9±3.0	26.1±2.0	>20
134		33.9±4.3	DNS	DNS	72.2±6.2	DNS	DNS
135		DNS	DNS	Not Tested	DNS	DNS	Not Tested
136		15.0±3.3	DNS	DNS	27.8±0.7	DNS	DNS

Table 12: Potency and efficacy of amine or amide pendant analogues at MOR, DOR, and KOR. Potency and efficacy data were obtained using agonist induced stimulation of [³⁵S] GTPγS binding. Potency is represented as EC₅₀ (nM) and efficacy as percent maximal stimulation relative to standard agonist DAMGO (MOR), DPDPE (DOR), or U69,593 (KOR) at 10 μM. Included is **70** for comparison. All data were from three separate experiments, performed in duplicate unless otherwise noted. These data are reported as the average ± standard error of the mean. DNS=Does Not Stimulate. * N=2, ** N=1. ^aData are from assays using human MOR and DOR instead of rat MOR and DOR as reported in Chapter 2.

Metabolic Stability: Since improving metabolic stability is one of our goals, most of the ligands described above were examined for stability in MLM (**Table 13**). For comparison, our previously reported benzyl pendant (**70**) is again included, as well as the ratio in stability between each

Name	R ¹	T _{1/2} (min)	Verapamil T _{1/2} (min)	Stability Ratio	cLogP
70		23.7±5.9	14.6±1.0	1.6±0.4	4.75
127		199±79	29.9±4.7	6.6±2.8	3.15

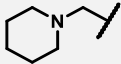
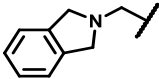
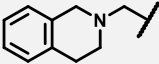
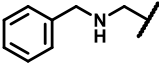
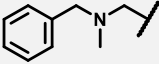
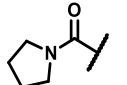
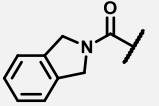
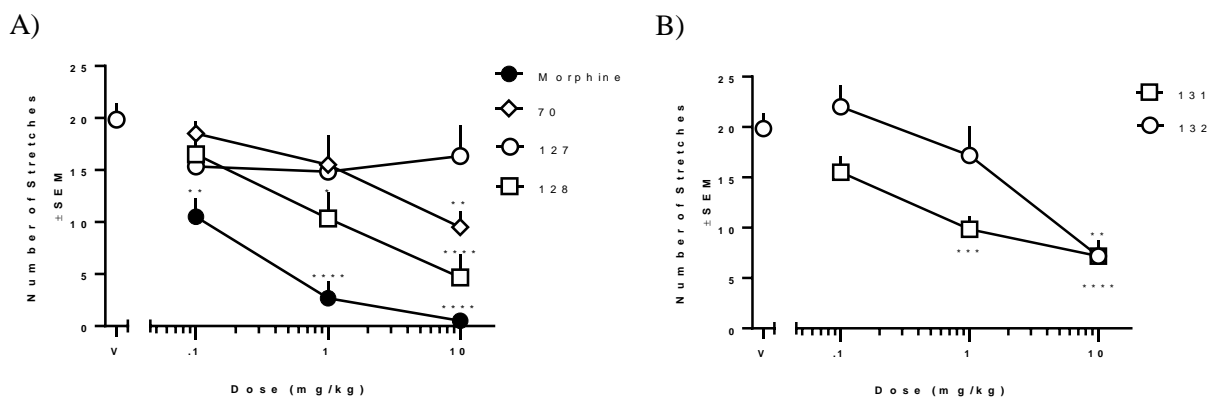
128		99.2±4.3	29.9±4.7	3.3±0.5	3.71
131		70.4±7.5	25.7±1.7	2.7±0.3	4.11
132		52.9±8.3	29.9±4.7	1.8±0.4	4.57
133		51.5±1.8	27.6±4.9	1.9±0.3	3.21
134		39.2±1.5	27.6±4.9	1.4±0.2	4.28
135		137±47	25.7±1.7	5.3±1.9	2.08
136		97±12	29.9±4.7	3.3±0.6	3.56

Table 13: Metabolic stability of amine or amide pendant analogues in MLM. Included are the compound half-life ($T_{1/2}$), the half-life of the positive control verapamil, and the stability ratio between the compound and the positive control. The stability ratio was calculated by dividing the half-life of the analogue of interest by the half-life of the positive control in that assay. Included is compound **70** for comparison. Individual compounds were tested once, with errors representing the SE in the decay curve regressed onto the data collected in 15-minute intervals. Finally, the cLogP of these analogues are included and were calculated using PerkinElmer's ChemDraw® Professional Software.

compound and the positive control verapamil. Immediate conversion to the simple pyrrolidine (**127**) or piperidine (**128**) pendants produced a significant boost in metabolic stability, providing half-lives of 199 and 99 min respectively. The attachment of aromatic rings to form the isoindoline (**131**) and THIQ (**132**) pendants attenuates these stability improvements, however their stability is greater than or equal to that of the original benzyl pendant. Breaking the THIQ pendant of **132** produces differential effects, as the benzylamine analogue (**133**) shows no change in stability, while the N-methyl benzylamine (**134**) causes stability loss. Finally, the amide analogues of **127**

and **131** either produce a minor loss, or a minor gain in stability compared to their amine counterparts.

Antinociceptive Activity: The analogues presented in this work were also screened for *in vivo* antinociceptive activity using the acetic acid stretch assay (AASA). Analogues **127-128** and **131-134** were tested for their antinociceptive activity and are described in **Figure 12A-C**. Morphine was used as a positive control. Additional details for this assay are found in the experimental section. Two analogues were inactive in this assay, namely the pyrrolidine analogue **127** and the N-methylbenzyl amine analogue **134**. Three analogues showed antinociception at 10 mg/kg (**70**, **132**, and **133**) when administered sc. Finally, the piperidine (**128**) and isoindoline (**131**) analogues were both active at 1 mg/kg.



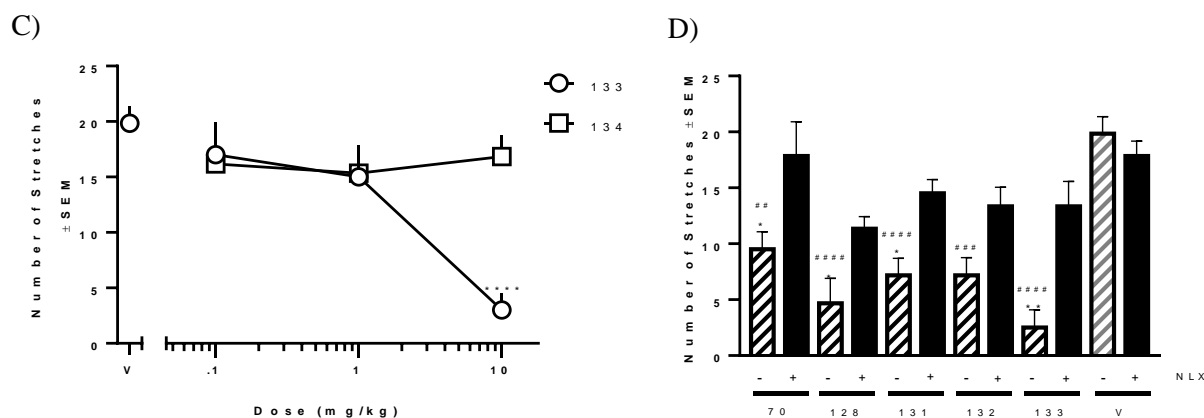


Figure 12: Antinociceptive activity of **70** and analogues **127-128**, and **131-134** using the AASA. Included is morphine as positive control. Panels A-C represent dose-response curves with the ligands: A) **70** and monocyclic amine analogues **127** and **128**, B) bicyclic amine analogues **131** and **132** C) benzyl amine analogues **133** and **134**. * $P < 0.05$ compared to vehicle. ** $P < 0.01$ compared to vehicle. *** $P < 0.001$ compared to vehicle. **** $P < 0.0001$ compared to vehicle. D) Competition assays between each analogue active at 10 mg/kg and the opioid antagonist naloxone in the AASA. ## $P < 0.01$ (drug - nlx) vs (vehicle - nlx). ### $P < 0.001$ (drug - nlx) vs (vehicle - nlx). #### $P < 0.0001$ (drug - nlx) vs (vehicle - nlx). * $P < 0.05$ (drug - nlx) vs (drug + nlx). ** $P < 0.01$ (drug - nlx) vs (drug + nlx).

We next sought to confirm that antinociception was mediated through the opioid receptors. Each mouse was pretreated with a 10 mg/kg dose of the nonselective opioid receptor antagonist naloxone (NLX) (**Figure 12D**) before treatment with 10 mg/kg of an active ligand from above. If the antinociception here is opioid mediated, it will be attenuated. For each analogue tested, the administration of naloxone inhibited the antinociceptive response induced in the AASA, confirming that the antinociception observed for these analogues is opioid receptor mediated.

Next, we opted to test these analogues in another assay for antinociception, namely the warm water tail withdrawal assay (WWTW). Unfortunately, none of the analogues that showed activity in the AASA were active at doses up to 32 mg/kg in the WWTW.

4.3 Discussion and Conclusion

SAR: Within the analogues found in **Table 11**, it appears that most of the monocyclic amine pendants produce a marked loss in binding at MOR, the only exception being the piperidine **128**.

Those that contain an aromatic ring (**131-134**, **136**) instead show improved binding at MOR. Conversion of the amine to an amide (**127** to **135**, **131** to **136**) produced no significant difference in this binding affinity. This suggests that the aromatic ring is an important component for MOR binding, whereas the amine is not. Similar trends can be observed for DOR binding as well.

In general, increases in binding affinity to KOR were observed for these analogues. This is possibly a result of polarity around the attachment point of the pendant to the rest of the molecule, as conversion between the amine and the amides of the pyrrolidine (**127** and **135**) and the isoindoline (**131** and **136**) produce similar affinities. The greatest binding affinity comes with the benzyl amine analogues (**133-134**), and suggests that additional conformational flexibility enables higher binding as compared to their conformationally restricted counterparts (**131-132**)

Consistent with the binding affinity at MOR is the potency. Aromatic rings appear to be important in these new pendants for potency, whereas the amine does not appear to be vital (as exemplified by **131** and **136**). Concerning efficacy at MOR, every compound containing an amine group had at least 72 % stimulation compared to DAMGO. Converting the amine into an amide drastically reduces this efficacy, but had little effect on potency, as evidenced by **131** and **136**. This suggests either that this amine is an important pharmacophore element for activation of MOR, or that the conjugation of the amide with the aromatic ring prevents the pendant from adopting an orientation necessary to activate MOR. While these amines may provide efficacy at MOR, alone they reduce potency. However, attachment of an aromatic ring greatly improves this potency, and in most cases, improves potency compared to the original benzyl pendant. It then appears that the amine in these pendants is important for maintaining high efficacy, whereas the aromatic ring is important for high potency. This combination may therefore be a useful pharmacophore for producing future MOR-agonists.

Interestingly, half of these amine compounds produced some residual agonism at DOR. As with MOR, this residual agonism at DOR is abolished upon conversion to the amide, suggesting the amine is contributing to this activity. The incorporation of an aromatic ring also appears to improve the potency of these compounds at DOR (when applicable), namely through comparison between **127** and **131**. However, it should be noted that the efficacy here decreases with these aromatic rings, and the only MOR-agonist/DOR-antagonists in this series possess an aromatic ring. As such, it appears that the additional aromatic ring can reduce the efficacy at DOR of these compounds. Finally, none of these compounds had any appreciable ability to activate KOR, though the N-methyl benzylamine analogue (**134**) was a weak partial agonist at 1.3 μM .

Metabolic Stability: The conversion from the benzyl pendant to the pyrrolidine and piperidine pendants produced a marked improvement in metabolic stability. This can be attributed to the reduced cLogP of these two pendants, which is known to reduce binding affinity to cytochrome P450 enzymes.⁸⁰ In fact, regression analyses of the stability ratio of the cyclic amines (**127-132**) against their cLogP follows a linear relationship with an R^2 value of 0.89 as shown in **Figure 13 (blue)**. Two different groups of exceptions exist. The first are the benzyl amine analogues **133** and **134 (Figure 13, orange)**, which have lower stability than predicted by their cLogP. This could be attributed to their increased conformational flexibility in relation to the amine and the aromatic ring, allowing for more binding orientations within the CYP enzyme. Furthermore, the amides **135** and **136** also have reduced stability than predicted by their cLogP (**Figure 13, grey**). These amides are conjugated to the ethyl ether through the aromatic core and could facilitate elimination of the ethyl group at the end of the CYP catalytic cycle akin to analogues described in Chapter 3. Overall, the stability improvements of this series are primarily inversely related to their cLogP, and secondarily are predicted by their state of cyclization.

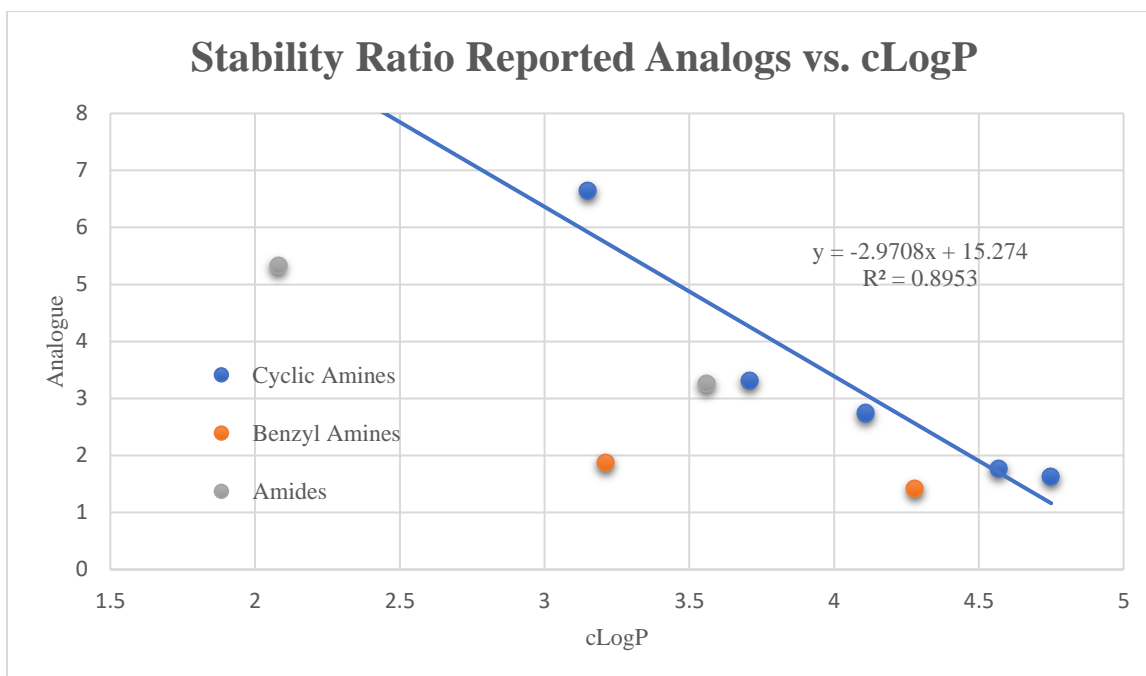


Figure 13: Stability ratio of analogues **127-128** and **131-136** against their cLogP. These ligands are divided into group based on their structure, with cyclic amines in blue, benzyl amines in orange, and amides in grey. The cyclic amines were also subject to linear regression.

Antinociceptive Activity: Of the analogues synthesized that possess high MOR agonism, only the pyrrolidine (**127**) and the N-methylbenzyl (**134**) amine pendants did not express antinociceptive activity. In fact, the piperidine (**128**) and the isoindoline (**131**) analogues were active at 1 mg/kg. Within this set of analogues, there appear to be no obvious trends that dictate what would be active. *In vitro* MOR potency does not appear to be a driving force, as the piperidine **128** has a potency value of 585 nM. The presence of an aromatic ring also does not appear to be a factor from these analogues, as the piperidine analogue **128** is active and the N-methylbenzyl analogue **134** is inactive. More analogues would need to be synthesized in order to allow trends in *in vivo* activity to emerge.

Unlike in the acetic acid stretch assay, none of these analogues were active in the warm water tail withdrawal assay. This difference in activity may be a result of both the type of nociception and the location upon which the opioids are operating. Abdominal writhing in the

AASA can be inhibited by the action of opioids in the periphery, whereas the tail flick in the WWTW is centrally mediated.⁸⁷ This suggests that these molecules are having trouble crossing the blood-brain barrier (BBB) and their action may be peripherally mediated.

Fortunately, the nociception in the AASA is presumed to be a result of inflammation,⁸⁸ and opioid receptor agonists have been found to induce stronger antinociceptive responses in inflamed tissue.⁸⁹ This inflammation can appear in many different disease syndromes, including cancer, arthritis, and chronic injuries.⁸⁹ Given the long duration of these health conditions, the use of peripheral opioids may be beneficial for treating various forms of chronic pain. This can be of great benefit, as drug-seeking behavior is a centrally mediated effect and other side-effects can be bypassed through peripheral action. An example of this peripheral activity in action is a series of fluorinated fentanyl derivatives designed to be active in the low pH of inflamed tissue. Analogues in this series were found to produce antinociception without respiratory depression, constipation, or addiction.⁹⁰

Conclusion: In comparison to Chapter 3, the analogues synthesized in this chapter represent a more promising direction for further derivatization. It appears thus far that the amine in the pendant can induce high levels of efficacy at MOR, whereas the incorporation of an aromatic ring back into the pendant can induce high levels of potency at MOR. This is largely insensitive to flexibility in the pendant, as illustrated by the two benzyl amine analogues. For the purposes of our initial goals, the metabolic stability of these ligands was much greater than those of previous chapters. This is noteworthy, as the isoindoline analogue produced improved stability with improved MOR-agonism. The only drawback in the SAR thus far appears to be a lurking partial DOR-agonism that appears in some analogues. This may not be a huge problem, as bifunctional MOR-agonist/DOR-agonist ligands have been shown to display reduced opioid side effect profiles as

described in Chapter 1. Finally, we can also show that these compounds can express antinociceptive activity *in vivo* through the acetic acid stretch assay and that this antinociception is mediated through opioid receptors. Though not active in the warm water tail withdrawal assay, the fact that these analogues may only be active peripherally may help us eliminate some negative side-effects associated with opioids. Given the progress that these pendants have provided us, future analogues will use these as a key element in their design.

4.4 Experimental

Chemistry

General Methods: All reagents and solvents were obtained commercially and were used without further purification. Intermediates were purified by flash chromatography using a Biotage Isolera One instrument. Most purification methods utilized a hexanes/ethyl acetate solvent system in a Biotage SNAP KP-Sil column, with a linear gradient between 0 and 100% ethyl acetate. Reverse phase column chromatography using a linear gradient of 0 % to 100 % solvent B (0.1 % TFA in acetonitrile) in solvent A (0.1 % TFA in water) using a Biotage SNAP Ultra C18 column was utilized for some intermediate amine salts. Purification of final compounds was performed using a Waters semipreparative HPLC with a Vydac protein and peptide C18 reverse phase column, using a linear gradient of 0 % to 100 % solvent B in solvent A at a rate 1 % per minute, monitoring UV absorbance at 230 nm. The purity of final compounds was assessed using a Waters Alliance 2690 analytical HPLC instrument with a Vydac protein and peptide C18 reverse phase column. A linear gradient (gradient A) of 0 % to 70 % solvent B in solvent A in 70 min, measuring UV absorbance at 230 nm was used to determine purity. All final compounds used for testing were ≥ 95 % pure, as determined by analytical HPLC. ^1H NMR and ^{13}C NMR data were obtained on a 500 or 400 MHz Varian spectrometer using CDCl_3 , CD_3OD , $\text{DMSO-}d_6$, or D_2O as solvents. The

identities of final compounds were verified by mass spectrometry using an Agilent 6130 LC–MS mass spectrometer in the positive ion mode, or an Agilent 6230 TOF HPLC-MS in the positive ion mode.

General Procedure for the Synthesis of 6-position Ethyl Ethers (Procedure A): To a flame dried flask containing **methyl 3-formyl-4-hydroxybenzoate (115)** was added 3 equivalents of potassium carbonate. The flask was purged with argon and 4 mL of DMF was added. 3 equivalents of an alkyl iodide or bromide was then added, and the solution was stirred at room temperature overnight. The solution was then concentrated in vacuo, partitioned between ethyl acetate and saturated sodium carbonate, and extracted with ethyl acetate. The organic layers were combined, dried with magnesium sulfate, filtered, and concentrated in vacuo, yielding the desired ethyl ether **(116)**.

General Procedure for Ellman Reductions (Procedure B): A flamed-dried round bottom flask containing 1 equivalent of aldehyde **(116)** and 3 equivalents of (R)-(+)-2-methyl-2-propanesulfonamide was attached to a reflux condenser and flushed with argon. 4 mL of THF was added and cooled to 0 °C. 6 equivalents of titanium (IV) ethoxide was added, followed by an additional 4 mL of THF. The solution was stirred and heated to 75 °C overnight with TLC monitoring until all ketone or aldehyde was consumed. A separate flame-dried flask containing 6 equivalents of sodium borohydride was flushed with argon. 4 mL of THF was added, at which point the solution was cooled to -78 °C. The solution containing Ellman adduct was cooled to room temperature and slowly transferred to the sodium borohydride solution via syringe. This final solution was then allowed to warm to room temperature and stirred for 2 hours, at which point the reaction mixture was quenched with methanol to consume the sodium borohydride, followed by DI water to precipitate the titanium. The solution was vacuum filtered, and the precipitate was

washed with ethyl acetate. The filtrate was concentrated in vacuo and purified via column chromatography (0-100% EtOAc in Hexanes), yielding the desired sulfonamide (**117**).

General Procedure for the Saponification of Esters (Procedure C): To a flask containing 1 equivalent of the ester (**117**) was added 7 equivalents of LiOH, 2 mL of THF, 2 mL of EtOH, and 2 mL of H₂O. The reaction was stirred overnight under ambient atmosphere and temperature. Upon completion, the solvent was concentrated in vacuo, suspended in acetone, and filtered. The precipitate was washed with additional acetone, and the filtrate was concentrated in vacuo, yielding the saponified product as a lithium carboxylate (**118**).

General Procedure for Amine Pendant Attachment and Cleavage of Ellman Auxiliaries (Procedure D): To a flask containing 1 equivalent of the lithium carboxylate (**118**) was added 1 equivalent of PyBOP and 1 equivalent of the desired amine. The flask was flushed with argon, DMF was added as solvent, and 10 equivalents of N-methylmorpholine was added. The reaction was stirred overnight, at which point it was concentrated in vacuo and purified via column chromatography (0-10% methanol in DCM). To the protected amine was immediately added 2 mL of Dioxane and 0.2 mL concentrated HCl. The solution was stirred at room temperature for 1 minute and concentrated in vacuo. The ensuing salt was triturated with diethyl ether, and then was purified using a reverse phase chromatography (0-100% B in A), yielding the product as a TFA salt.

General Procedure for the Reduction of Pendant Amides (Procedure E): To a dried flask containing 1 equivalent of the desired amide under argon was added THF and 7 equivalents of 2 M BH₃*Me₂S complex in THF. The reaction was heated at 75 °C for 3 hours, at which point the reaction was quenched with MeOH and heated for an additional 15 minutes. The reaction was then cooled, concentrated in vacuo, and was used in Procedure F without further purification.

General Procedure for the Coupling of 2',6'-Dimethyltyrosine to Functionalized Amine Salt (Procedure F): To a dried flask containing the amine under argon was added 3 mL of DMF and 10 equivalents of Hunig's base. 1 equivalent of PyBOP and 1 equivalent of 6-Cl-HOBt was added, followed by a 1 equivalent of doubly Boc protected 2',6'-Dimethyltyrosine in 1.5 mL DMF. The solution was stirred overnight at room temperature, concentrated in vacuo, and purified via semipreparative reverse phase HPLC (0.1% TFA in water: 0.1% TFA in acetonitrile). 2 mL of TFA and 2 mL of DCM were then added, and the solution was stirred for an additional hour. The reaction mixture was concentrated in vacuo and purified via an additional semipreparative reverse phase HPLC (0.1% TFA in water: 0.1% TFA in acetonitrile). The product was concentrated in vacuo and lyophilized overnight to yield the final peptidomimetic.

Methyl 4-ethoxy-3-formylbenzoate (116): See Procedure A: 149 mg (0.83 mmol) of **methyl 3-formyl-4-hydroxybenzoate (115)**, 342 mg (2.47 mmol, 2.99 eq.) of K₂CO₃, 190 μ L (277 mg, 2.55 mmol, 3.08 eq) of EtBr, 4 mL of DMF. Compound **116** (162 mg, Yield=94 %) was isolated as a white solid. ¹H NMR (500 MHz, Chloroform-*d*) δ 10.46 (s, 1H), 8.47 (d, *J* = 2.3 Hz, 1H), 8.19 (dd, *J* = 8.8, 2.3 Hz, 1H), 7.00 (d, *J* = 8.8 Hz, 1H), 4.21 (q, *J* = 7.0 Hz, 2H), 3.88 (s, 3H), 1.50 (t, *J* = 7.0 Hz, 3H). ¹³C NMR (126 MHz, Chloroform-*d*) δ 188.93, 166.00, 164.25, 137.01, 130.35, 124.33, 122.63, 112.22, 64.68, 52.07, 14.49.

Ethyl (R)-3-(((tert-butylsulfinyl)amino)methyl)-4-ethoxybenzoate (117): See Procedure B: Step 1: 149 mg (0.72 mmol) of **116**, 262 mg (2.16 mmol, 3.02 eq.) of (R)-(+)-2-methyl-2-propanesulfinamide, 900 μ L (979 mg, 4.3 mmol, 6.0 eq.) of Ti(OEt)₄, 4+4 mL THF. Step 2: 165 mg (4.4 mmol, 6.1 eq.) of sodium borohydride in 4 mL THF. Compound **117** (232 mg, Yield= 99 %) was isolated as a colorless oil. ¹H NMR (500 MHz, Chloroform-*d*) δ 7.95 (m, 2H),

6.85 (d, $J = 9.1$ Hz, 1H), 4.41 (dd, $J = 14.3, 5.5$ Hz, 1H), 4.32 (q, $J = 7.1$ Hz, 2H), 4.20 (dd, $J = 14.3, 7.8$ Hz, 1H), 4.11 (q, $J = 7.0$ Hz, 2H), 3.74 (dd, $J = 7.8, 5.6$ Hz, 1H), 1.44 (t, $J = 7.0$ Hz, 3H), 1.36 (t, $J = 7.1$ Hz, 3H), 1.21 (s, 9H). ^{13}C NMR (126 MHz, Chloroform- d) δ 166.26, 160.35, 131.05, 130.61, 127.10, 122.49, 110.50, 63.94, 60.67, 55.87, 45.18, 22.60, 14.73, 14.34.

Lithium (R)-3-(((tert-butylsulfinyl)amino)methyl)-4-ethoxybenzoate (118): See Procedure C: 208 mg (0.64 mmol) of **117**, 198 mg (8.27 mmol, 12.9 eq.) of LiOH, 2 mL of THF, 2 mL of EtOH, and 2 mL of H₂O. Compound **118** (172 mg, Yield= 89 %) was isolated as a white solid. ^1H NMR (500 MHz, Methanol- d_4) δ 7.91 (d, $J = 2.2$ Hz, 1H), 7.88 (dd, $J = 8.5, 2.2$ Hz, 1H), 6.91 (d, $J = 8.5$ Hz, 1H), 4.34 (d, $J = 14.3$ Hz, 1H), 4.23 (d, $J = 14.3$ Hz, 1H), 4.12 (q, $J = 7.0$ Hz, 2H), 1.44 (t, $J = 7.0$ Hz, 3H), 1.22 (s, 9H). ^{13}C NMR (126 MHz, Methanol- d_4) δ 173.90, 158.48, 130.37, 130.12, 129.54, 125.96, 109.79, 63.44, 55.64, 44.31, 21.73, 13.81.

(2-ethoxy-5-(pyrrolidine-1-carbonyl)phenyl)methanaminium trifluoroacetate (119): See Procedure D: Step 1: 28 mg (0.092 mmol) of **118**, 49 mg (0.094 mmol, 1.0 eq.) of PyBOP, 20 μL (17 mg, 0.24 mmol, 2.7 eq.) of pyrrolidine, 100 μL (92 mg, 0.91 mmol, 9.9 eq.) of NMM, and 4 mL of DMF. Step 2: 2 mL of dioxane and 0.2 mL conc. HCl. Compound **118** (33 mg, Quant Yield) was isolated as a yellow oil. ^1H NMR (500 MHz, Methanol- d_4) δ 7.61 (dd, $J = 8.6, 2.2$ Hz, 1H), 7.54 (d, $J = 2.3$ Hz, 1H), 7.13 (d, $J = 8.6$ Hz, 1H), 4.22 (q, $J = 6.9$ Hz, 2H), 4.15 (s, 2H), 3.57 (t, $J = 7.0$ Hz, 2H), 3.51 (t, $J = 6.7$ Hz, 2H), 1.99 (p, $J = 6.8$ Hz, 2H), 1.89 (p, $J = 6.2$ Hz, 2H), 1.47 (t, $J = 6.9$ Hz, 3H). ^{13}C NMR (126 MHz, Methanol- d_4) δ 169.75, 158.69, 130.16, 129.66, 128.32, 126.99, 111.15, 64.29, 49.81, 46.41, 38.49, 25.88, 23.92, 13.52.

(2-ethoxy-5-(piperidine-1-carbonyl)phenyl)methanaminium trifluoroacetate (120): See Procedure D: Step 1: 27 mg (0.088 mmol) of **118**, 46 mg (0.088 mmol, 1.0 eq.) of PyBOP,

20 μL (17 mg, 0.20 mmol, 2.3 eq.) of piperidine, 100 μL (92 mg, 0.91 mmol, 10.3 eq.) of NMM, and 4 mL of DMF. Step 2: 2 mL of dioxane and 0.2 mL conc. HCl. Compound **120** (28 mg, Yield=84 %) was isolated as a colorless oil. ^1H NMR (500 MHz, Methanol- d_4) δ 7.47 (dd, $J = 8.5, 2.2$ Hz, 1H), 7.41 (d, $J = 2.2$ Hz, 1H), 7.14 (d, $J = 8.4$ Hz, 1H), 4.22 (q, $J = 7.0$ Hz, 2H), 4.14 (s, 2H), 3.68 (br s, 2H), 3.44 (br s, 2H), 1.76 – 1.68 (m, 2H), 1.64 (br s, 2H), 1.57 (br s, 2H), 1.48 (t, $J = 7.0$ Hz, 3H). ^{13}C NMR (126 MHz, Methanol- d_4) δ 170.20, 158.22, 129.74, 129.42, 127.91, 121.26, 111.19, 64.17, 38.48, 24.02, 20.05, 13.41.

(5-(3-azabicyclo[3.1.0]hexane-3-carbonyl)-2-ethoxyphenyl)methanaminium

trifluoroacetate (121): See Procedure D: Step 1: 25 mg (0.082 mmol) of **118**, 41 mg (0.079 mmol, 0.96 eq.) of PyBOP, 12 mg, (0.10 mmol, 1.2 eq.) of 3-azabicyclo[3.1.0]hexane hydrochloride, 90 μL (83 mg, 0.82 mmol, 10.0 eq.) of NMM, and 4 mL of DMF. Step 2: 2 mL of dioxane and 0.2 mL conc. HCl. Compound **121** (21 mg, Yield=69 %) was isolated as a colorless oil. ^1H NMR (500 MHz, Methanol- d_4) δ 7.54 (dd, $J = 8.6, 2.3$ Hz, 1H), 7.47 (d, $J = 2.2$ Hz, 1H), 7.12 (d, $J = 8.6$ Hz, 1H), 4.22 (q, $J = 7.0$ Hz, 2H), 4.14 (s, 2H), 4.07 (d, $J = 12.0$ Hz, 1H), 3.75 (dd, $J = 10.9, 4.1$ Hz, 1H), 3.51 – 3.42 (m, 2H), 1.60 (ddt, $J = 20.4, 7.1, 3.6$ Hz, 2H), 1.48 (t, $J = 7.0$ Hz, 3H), 0.72 (td, $J = 7.7, 5.2$ Hz, 1H), 0.10 (q, $J = 4.3$ Hz, 1H). ^{13}C NMR (126 MHz, Methanol- d_4) δ 170.61, 158.46, 130.07, 129.60, 128.61, 126.97, 111.01, 64.19, 51.35, 38.45, 20.05, 15.41, 13.73, 13.41, 7.57.

(2-ethoxy-5-(morpholine-4-carbonyl)phenyl)methanaminium trifluoroacetate (122):

See Procedure D: Step 1: 29 mg (0.095 mmol) of **118**, 50 mg (0.096 mmol, 1.0 eq.) of PyBOP, 20 μL (20 mg, 0.23 mmol, 2.4 eq.) of morpholine, 110 μL (101 mg, 1.0 mmol, 10.5 eq.) of NMM, and 4 mL of DMF. Step 2: 2 mL of dioxane and 0.2 mL conc. HCl. Compound **122** (28 mg, Yield=78 %) was isolated as a colorless oil. ^1H NMR (500 MHz, Methanol- d_4) δ 7.51 (dd, $J = 8.5, 2.2$

Hz, 1H), 7.45 (d, $J = 2.1$ Hz, 1H), 7.15 (d, $J = 8.5$ Hz, 1H), 4.23 (q, $J = 7.0$ Hz, 2H), 4.15 (s, 2H), 3.78 – 3.50 (m, 8H), 1.48 (t, $J = 7.0$ Hz, 3H). ^{13}C NMR (126 MHz, Methanol- d_4) δ 170.37, 158.48, 130.22, 129.77, 126.97, 121.33, 111.27, 66.35, 64.21, 38.44, 20.05, 13.40.

(2-ethoxy-5-(isoindoline-2-carbonyl)phenyl)methanaminium trifluoroacetate (123):

See Procedure D: Step 1: 40 mg (0.13 mmol) of **118**, 70 mg (0.13 mmol, 1.0 eq.) of PyBOP, 22 mg (0.14 mmol, 1.1 eq.) of isoindoline hydrochloride, 150 μL (138 mg, 1.4 mol, 10.4 eq.) of NMM, and 4 mL of DMF. Step 2: 2 mL of dioxane and 0.2 mL conc. HCl. Compound **123** (39 mg, Yield=73 %) was isolated as a colorless oil. ^1H NMR (500 MHz, Methanol- d_4) δ 7.74 (dd, $J = 8.5, 2.2$ Hz, 1H), 7.64 (d, $J = 2.2$ Hz, 1H), 7.37 (d, $J = 7.3$ Hz, 1H), 7.35 – 7.25 (m, 2H), 7.23 (d, $J = 7.4$ Hz, 1H), 7.19 (d, $J = 8.5$ Hz, 1H), 4.96 (s, 2H), 4.88 (s, 5H), 4.26 (q, $J = 7.0$ Hz, 2H), 4.18 (s, 2H), 1.50 (t, $J = 7.0$ Hz, 3H). ^{13}C NMR (126 MHz, Methanol- d_4) δ 170.15, 158.61, 136.31, 135.58, 130.08, 129.61, 128.19, 127.51, 127.33, 122.44, 122.15, 121.20, 111.20, 64.24, 54.70, 52.29, 38.49, 13.43.

(2-ethoxy-5-(1,2,3,4-tetrahydroisoquinoline-2-carbonyl)phenyl)methanaminium

trifluoroacetate (124): Step 1: See Procedure D: 26 mg (0.085 mmol) of **118**, 44 mg (0.085 mmol, 0.99 eq.) of PyBOP, 20 μL (21 mg, 0.16 mmol, 1.9 eq.) of 1,2,3,4-tetrahydroquinoline, 90 μL (83 mg, 0.82 mmol, 9.6 eq.) of NMM, and 4 mL of DMF. Step 2: 2 mL of dioxane and 0.2 mL conc. HCl. Compound **124** (22 mg, Yield=61 %) was isolated as a colorless oil. ^1H NMR (400 MHz, 50 $^\circ\text{C}$, Methanol- d_4) δ 7.54 (dd, $J = 8.5, 2.2$ Hz, 1H), 7.48 (d, $J = 2.1$ Hz, 1H), 7.16 (d, $J = 8.2$ Hz, 4H), 7.07 (s, 1H), 4.74 (s, 2H), 4.25 (q, $J = 7.0$ Hz, 2H), 4.17 (s, 2H), 3.81 (s, 2H), 2.93 (t, $J = 6.0$ Hz, 2H), 1.49 (t, $J = 7.0$ Hz, 3H). ^{13}C NMR (101 MHz, 50 $^\circ\text{C}$, Methanol- d_4) δ 158.48, 134.19, 132.61, 129.93, 129.54, 128.32, 127.96, 126.54, 126.15, 121.39, 111.44, 64.33, 38.61, 13.38.

(5-(benzylcarbamoyl)-2-ethoxyphenyl)methanaminium trifluoroacetate (125): See Procedure D: Step 1: 30 mg (0.098 mmol) of **118**, 52 mg (0.10 mmol, 1.02 eq.) of PyBOP, 20 μ L (20 mg, 0.183 mmol, 1.86 eq.) of benzylamine, 110 μ L (101 mg, 1.00 mmol, 10.2 eq.) of NMM, and 4 mL of DMF. Step 2: 2 mL of dioxane and 0.2 mL conc. HCl. Compound **125** (27 mg, Yield=69 %) was isolated as a colorless oil. ^1H NMR (500 MHz, Methanol- d_4) δ 7.94 (dd, $J = 8.6, 2.3$ Hz, 1H), 7.89 (d, $J = 2.3$ Hz, 1H), 7.35 – 7.22 (m, 5H), 7.14 (d, $J = 8.7$ Hz, 1H), 4.57 (s, 2H), 4.23 (q, $J = 7.0$ Hz, 2H), 4.15 (s, 2H), 1.48 (t, $J = 7.0$ Hz, 3H). ^{13}C NMR (126 MHz, Methanol- d_4) δ 167.60, 159.69, 138.80, 130.02, 129.99, 128.10, 127.15, 127.09, 126.78, 126.77, 126.40, 121.10, 111.07, 64.29, 43.12, 38.63, 13.40.

(5-(benzyl(methyl)carbamoyl)-2-ethoxyphenyl)methanaminium trifluoroacetate (126): See Procedure D: Step 1: 30 mg (0.098 mmol) of **118**, 52 mg (0.10 mmol, 1.02 eq.) of PyBOP, 20 μ L (19 mg, 0.155 mmol, 1.58 eq.) of N-methylbenzylamine, 110 μ L (101 mg, 1.00 mmol, 10.2 eq.) of NMM, and 4 mL of DMF. Step 2: 2 mL of dioxane and 0.2 mL conc. HCl. Compound **126** (28 mg, Yield=69 %) was isolated as a colorless oil. ^1H NMR (400 MHz, 50 $^\circ\text{C}$, Methanol- d_4) δ 7.53 (dd, $J = 8.5, 2.2$ Hz, 1H), 7.49 (d, $J = 2.1$ Hz, 1H), 7.39 – 7.19 (m, 5H), 7.12 (d, $J = 8.5$ Hz, 1H), 4.68 (s, 2H), 4.23 (q, $J = 7.0$ Hz, 2H), 4.15 (s, 2H), 2.97 (s, 3H), 1.47 (t, $J = 7.0$ Hz, 3H). ^{13}C NMR (101 MHz, 50 $^\circ\text{C}$, Methanol- d_4) δ 158.31, 136.67, 129.84, 129.54, 129.48, 128.41, 128.12, 127.27, 121.29, 111.39, 64.31, 38.63, 13.38.

(S)-1-((2-ethoxy-5-(pyrrolidin-1-ylmethyl)benzyl)amino)-3-(4-hydroxy-2,6-dimethylphenyl)-1-oxopropan-2-aminium trifluoroacetate (127): See Procedure E and F: 32 mg (0.088 mmol) of **119**, 320 μ L (0.64 mmol, 7.25 eq.) of 2 M $\text{BH}_3^*\text{Me}_2\text{S}$ in THF, and 4 mL of THF. Step 1 of F: 155 μ L (115 mg, 0.89 mmol, 10.1 eq.) of N,N-diisopropylethylamine, 52 mg

(0.10 mmol, 1.13 eq.) of PyBOP, 17 mg (0.10 mmol, 1.14 eq.) of 6-Cl-HOBt, 36 mg (0.088 mmol, 1.00 eq.) of Boc-O-Boc-L-2',6'-dimethyltyrosine, 3+1.5 mL of DMF. Step 2 of F: 2 mL TFA and 2 mL DCM. Compound **127** (12.4 mg, Yield= 26 %) was isolated as a white solid. ¹H NMR (500 MHz, Methanol-*d*₄) δ 7.67 (t, *J* = 5.8 Hz, 1H), 7.40 (dd, *J* = 8.6, 2.3 Hz, 1H), 7.14 (d, *J* = 2.3 Hz, 1H), 6.98 (d, *J* = 8.4 Hz, 1H), 6.34 (s, 2H), 4.39 (dd, *J* = 14.7, 6.3 Hz, 1H), 4.26 (q, *J* = 13.0 Hz, 2H), 4.15 (dd, *J* = 14.5, 4.7 Hz, 1H), 3.98 (p, *J* = 7.1 Hz, 2H), 3.91 (dd, *J* = 11.8, 4.4 Hz, 1H), 3.53 – 3.38 (m, 2H), 3.22 – 3.06 (m, 3H), 2.94 (dd, *J* = 13.8, 4.4 Hz, 1H), 2.18 (br s, 2H), 2.03 (s, 8H), 1.30 (t, *J* = 6.9 Hz, 3H). No ¹³C Data Acquired. ESI-MS: 426.3 [M + H]⁺, HPLC (gradient A): Retention Time: 17.62 min.

(S)-1-((2-ethoxy-5-(piperidin-1-ylmethyl)benzyl)amino)-3-(4-hydroxy-2,6-dimethylphenyl)-1-oxopropan-2-aminium trifluoroacetate (128): See Procedure E and F: 30 mg (0.080 mmol) of **120**, 280 μL (0.56 mmol, 7.03 eq.) of 2 M BH₃*Me₂S in THF, and 4 mL of THF. Step 1 of F: 140 μL (104 mg, 0.80 mmol, 10.1 eq.) of N,N-diisopropylethylamine, 44 mg (0.085 mmol, 1.1 eq.) of PyBOP, 14 mg (0.083 mmol, 1.0 eq.) of 6-Cl-HOBt, 34 mg (0.083 mmol, 1.0 eq.) of Boc-O-Boc-L-2',6'-dimethyltyrosine, 3+1.5 mL of DMF. Step 2 of F: 2 mL TFA and 2 mL DCM. Compound **128** (11 mg, Yield= 25 %) was isolated as a white solid. ¹H NMR (500 MHz, Methanol-*d*₄) δ 7.73 (t, *J* = 5.8 Hz, 1H), 7.38 (dd, *J* = 8.4, 2.2 Hz, 1H), 7.13 (d, *J* = 2.2 Hz, 1H), 6.98 (d, *J* = 8.4 Hz, 1H), 6.35 (s, 2H), 4.36 (dd, *J* = 14.7, 6.8 Hz, 1H), 4.21-4.15 (m, 3H), 4.04 – 3.94 (m, 2H), 3.92 (dd, *J* = 11.8, 4.4 Hz, 1H), 3.42 (t, *J* = 11.9 Hz, 2H), 3.12 (dd, *J* = 13.7, 11.8 Hz, 1H), 3.00 – 2.90 (m, 2H), 2.87 (td, *J* = 13.2, 12.4, 2.8 Hz, 1H), 2.04 (s, 6H), 1.93 (d, *J* = 13.8 Hz, 2H), 1.83 (d, *J* = 13.8 Hz, 1H), 1.79 – 1.63 (m, 2H), 1.50 (qt, *J* = 12.8, 3.3 Hz, 1H), 1.31 (t, *J* = 7.0 Hz, 3H). No ¹³C Data Acquired. ESI-MS: 440.3 [M + H]⁺, HPLC (gradient A): Retention Time: 18.64 min.

(2S)-1-((5-((3-azabicyclo[3.1.0]hexan-3-yl)methyl)-2-ethoxybenzyl)amino)-3-(4-hydroxy-2,6-dimethylphenyl)-1-oxopropan-2-aminium trifluoroacetate (129): See Procedure E and F: 9 mg (0.024 mmol) of **121**, 220 μ L (0.44 mmol, 18.3 eq.) of 2 M $\text{BH}_3 \cdot \text{Me}_2\text{S}$ in THF, and 3 mL of THF. Step 1 of F: 60 μ L (44 mg, 0.34 mmol, 14.3 eq.) of N,N-diisopropylethylamine, 17 mg (0.033 mmol, 1.36 eq.) of PyBOP, 6 mg (0.035 mmol, 1.47 eq.) of 6-Cl-HOBt, 14 mg (0.034 mmol, 1.42 eq.) of Boc-O-Boc-L-2',6'-dimethyltyrosine, 3+1.5 mL of DMF. Step 2 of F: 2 mL TFA and 2 mL DCM. Compound **129** (1.0 mg, Yield=8 %) was isolated as a white solid. ^1H NMR (500 MHz, Methanol- d_4) δ 7.38 (dd, $J = 8.4, 2.4$ Hz, 1H), 7.15 (d, $J = 2.2$ Hz, 1H), 6.97 (d, $J = 8.4$ Hz, 1H), 6.34 (s, 2H), 4.39 (dd, $J = 14.5, 4.4$ Hz, 1H), 4.28 (d, $J = 12.6$ Hz, 1H), 4.24 (d, $J = 12.8$ Hz, 1H), 4.15 (dd, $J = 14.6, 4.3$ Hz, 1H), 3.98 (qd, $J = 9.4, 7.3$ Hz, 2H), 3.90 (dd, $J = 11.8, 4.4$ Hz, 1H), 3.51 – 3.38 (m, 4H), 3.11 (dd, $J = 13.8, 11.9$ Hz, 1H), 2.94 (dd, $J = 13.8, 4.5$ Hz, 1H), 2.03 (s, 6H), 1.86 (s, 2H), 1.30 (t, $J = 6.9$ Hz, 3H), 0.85 (q, $J = 7.7$ Hz, 1H), 0.65 (q, $J = 4.9$ Hz, 1H). No ^{13}C Data Acquired. ESI-MS: 438.3 $[\text{M} + \text{H}]^+$, HPLC (gradient A): Retention Time: 18.41 min.

(S)-1-((2-ethoxy-5-(morpholinomethyl)benzyl)amino)-3-(4-hydroxy-2,6-dimethylphenyl)-1-oxopropan-2-aminium trifluoroacetate (130): See Procedure E and F: 27 mg (0.071 mmol) of **122**, 250 μ L (0.50 mmol, 7.0 eq.) of 2 M $\text{BH}_3 \cdot \text{Me}_2\text{S}$ in THF, and 4 mL of THF. Step 1 of F: 130 μ L (96 mg, 0.75 mmol, 10.5 eq.) of N,N-diisopropylethylamine, 38 mg (0.073 mmol, 1.0 eq.) of PyBOP, 13 mg (0.077 mmol, 1.1 eq.) of 6-Cl-HOBt, 29 mg (0.071 mmol, 0.99 eq.) of Boc-O-Boc-L-2',6'-dimethyltyrosine, 3+1.5 mL of DMF. Step 2 of F: 2 mL TFA and 2 mL DCM. Compound **130** (12.9 mg, Yield= 33 %) was isolated as a white solid. ^1H NMR (500 MHz, Methanol- d_4) δ 7.72 (t, $J = 5.7$ Hz, 1H), 7.40 (dd, $J = 8.4, 2.3$ Hz, 1H), 7.15 (d, $J = 2.2$ Hz, 1H), 6.99 (d, $J = 8.4$ Hz, 1H), 6.35 (s, 2H), 4.38 (dd, $J = 14.8, 4.6$ Hz, 1H), 4.28 (d, $J = 13.1$ Hz, 1H), 4.24 (d, $J = 13.0$ Hz, 1H), 4.17 (dd, $J = 14.7, 4.6$ Hz, 1H), 4.08 – 3.95 (m, 4H), 3.92 (dd, $J =$

11.8, 4.4 Hz, 1H), 3.73 (t, $J = 12.6$ Hz, 2H), 3.38 – 3.32 (m, 2H), 3.21 – 3.07 (m, 3H), 2.95 (dd, $J = 13.8, 4.5$ Hz, 1H), 2.05 (s, 6H), 1.31 (t, $J = 6.9$ Hz, 3H). No ^{13}C Data Acquired. ESI-MS: 442.3 $[\text{M} + \text{H}]^+$, HPLC (gradient A): Retention Time: 15.94 min.

(S)-1-((2-ethoxy-5-(isoindolin-2-ylmethyl)benzyl)amino)-3-(4-hydroxy-2,6-dimethylphenyl)-1-oxopropan-2-aminium trifluoroacetate (131): See Procedure E and F: 16 mg (0.039 mmol) of **123**, 140 μL (0.28 mmol, 7.18 eq.) of 2 M $\text{BH}_3 \cdot \text{Me}_2\text{S}$ in THF, and 4 mL of THF. Step 1 of F: 80 μL (59 mg, 0.46 mmol, 11.8 eq.) of N,N-diisopropylethylamine, 22 mg (0.042 mmol, 1.08 eq.) of PyBOP, 9 mg (0.053 mmol, 1.36 eq.) of 6-Cl-HOBt, 17 mg (0.042 mmol, 1.06 eq.) of Boc-O-Boc-L-2',6'-dimethyltyrosine, 3+1.5 mL of DMF. Step 2 of F: 2 mL TFA and 2 mL DCM. Compound **131** (6.1 mg, Yield=27 %) was isolated as a white solid. ^1H NMR (500 MHz, Methanol- d_4) δ 7.74 – 7.62 (m, 1H), 7.46 (dd, $J = 8.5, 2.3$ Hz, 1H), 7.44 – 7.37 (m, 4H), 7.22 (d, $J = 2.3$ Hz, 1H), 7.02 (d, $J = 8.5$ Hz, 1H), 6.32 (s, 2H), 4.66 (s, 2H), 4.64 (s, 2H), 4.52 (d, $J = 3.2$ Hz, 2H), 4.45 – 4.35 (m, 1H), 4.17 (dd, $J = 14.5, 4.6$ Hz, 1H), 4.07 – 3.94 (m, 2H), 3.91 (dd, $J = 11.7, 4.4$ Hz, 1H), 3.11 (dd, $J = 13.5, 12.2$ Hz, 1H), 2.94 (dd, $J = 13.8, 4.4$ Hz, 1H), 2.02 (s, 6H), 1.31 (t, $J = 7.0$ Hz, 3H). No ^{13}C Data Acquired. ESI-MS: 474.2 $[\text{M} + \text{H}]^+$, HPLC (gradient A): Retention Time: 22.43 min.

(S)-1-((5-((3,4-dihydroisoquinolin-2(1H)-yl)methyl)-2-ethoxybenzyl)amino)-3-(4-hydroxy-2,6-dimethylphenyl)-1-oxopropan-2-aminium trifluoroacetate (132): See Procedure E and F: 32 mg (0.075 mmol) of **124**, 270 μL (0.54 mmol, 7.16 eq.) of 2 M $\text{BH}_3 \cdot \text{Me}_2\text{S}$ in THF, and 4 mL of THF. Step 1 of F: 140 μL (103 mg, 0.80 mmol, 10.6 eq.) of N,N-diisopropylethylamine, 41 mg (0.079 mmol, 1.04 eq.) of PyBOP, 15 mg (0.088 mmol, 1.17 eq.) of 6-Cl-HOBt, 33 mg (0.081 mmol, 1.07 eq.) of Boc-O-Boc-L-2',6'-dimethyltyrosine, 3+1.5 mL of

DMF. Step 2 of F: 2 mL TFA and 2 mL DCM. Compound **132** (6.3 mg, Yield=14 %) was isolated as a white solid. ¹H NMR (400 MHz, Methanol-*d*₄) δ 7.78 (t, *J* = 5.7 Hz, 1H), 7.46 (dd, *J* = 8.4, 2.3 Hz, 1H), 7.36 – 7.20 (m, 4H), 7.18 (d, *J* = 7.4 Hz, 1H), 7.02 (d, *J* = 8.5 Hz, 1H), 6.33 (s, 2H), 4.38 (d, *J* = 12.8 Hz, 5H), 4.17 (dd, *J* = 14.5, 4.3 Hz, 1H), 4.00 (p, *J* = 7.4 Hz, 2H), 3.91 (dd, *J* = 11.8, 4.4 Hz, 1H), 3.77 (br s, 1H), 3.39 (br s, 1H), 3.24 – 3.15 (m, 2H), 3.10 (t, *J* = 12.7 Hz, 1H), 2.94 (dd, *J* = 13.8, 4.3 Hz, 1H), 2.01 (s, 6H), 1.30 (t, *J* = 6.9 Hz, 3H). No ¹³C Data Acquired. ESI-MS: 488.3 [M + H]⁺, HPLC (gradient A): Retention Time: 23.36 min.

(S)-1-((5-((benzylamino)methyl)-2-ethoxybenzyl)amino)-3-(4-hydroxy-2,6-dimethylphenyl)-1-oxopropan-2-aminium trifluoroacetate (133): See Procedure E and F: 26 mg (0.065 mmol) of **125**, 230 μL (0.46 mmol, 7.04 eq.) of 2 M BH₃*Me₂S in THF, and 4 mL of THF. Step 1 of F: 120 μL (89 mg, 0.69 mmol, 10.5 eq.) of N,N-diisopropylethylamine, 34 mg (0.065 mmol, 1.00 eq.) of PyBOP, 11 mg (0.065 mmol, 0.99 eq.) of 6-Cl-HOBt, 30 mg (0.073 mmol, 1.12 eq.) of Boc-O-Boc-L-2',6'-dimethyltyrosine, 3+1.5 mL of DMF. Step 2 of F: 2 mL TFA and 2 mL DCM. Compound **133** (13.5 mg, Yield= 36%) was isolated as a white solid. ¹H NMR (500 MHz, Methanol-*d*₄) δ 7.69 (t, *J* = 5.9 Hz, 1H), 7.54 – 7.42 (m, 5H), 7.38 (dd, *J* = 8.4, 2.4 Hz, 1H), 7.18 (d, *J* = 2.3 Hz, 1H), 6.96 (d, *J* = 8.4 Hz, 1H), 6.34 (s, 2H), 4.35 (dd, *J* = 14.5, 4.8 Hz, 1H), 4.24 – 4.12 (m, 5H), 3.97 (dddd, *J* = 16.3, 9.3, 7.0, 2.4 Hz, 3H), 3.92 (dd, *J* = 11.8, 4.4 Hz, 1H), 3.10 (dd, *J* = 13.8, 11.7 Hz, 1H), 2.95 (dd, *J* = 13.8, 4.5 Hz, 1H), 2.03 (s, 6H), 1.30 (t, *J* = 6.9 Hz, 3H). No ¹³C Data Acquired. ESI-MS: 462.3 [M + H]⁺, HPLC (gradient A): Retention Time: 22.58 min.

(S)-1-((5-((benzyl(methyl)amino)methyl)-2-ethoxybenzyl)amino)-3-(4-hydroxy-2,6-dimethylphenyl)-1-oxopropan-2-aminium trifluoroacetate (134): See Procedure E and F: 26

mg (0.063 mmol) of **126**, 220 μ L (0.44 mmol, 7.18 eq.) of 2 M $\text{BH}_3 \cdot \text{Me}_2\text{S}$ in THF, and 4 mL of THF. Step 1 of F: 110 μ L (82 mg, 0.63 mmol, 10.0 eq.) of N,N-diisopropylethylamine, 37 mg (0.071 mmol, 1.13 eq.) of PyBOP, 11 mg (0.065 mmol, 1.03 eq.) of 6-Cl-HOBt, 28 mg (0.068 mmol, 1.09 eq.) of Boc-O-Boc-L-2',6'-dimethyltyrosine, 3+1.5 mL of DMF. Step 2 of F: 2 mL TFA and 2 mL DCM. Compound **134** (14.4 mg, Yield= 39%) was isolated as a white solid. ^1H NMR (400 MHz, Methanol- d_4) δ 7.50 (s, 5H), 7.39 (dd, $J = 8.4, 2.3$ Hz, 1H), 7.18 (s, 1H), 7.00 (d, $J = 8.5$ Hz, 1H), 6.35 (s, 2H), 4.53 – 4.29 (m, 3H), 4.29 – 4.11 (m, 3H), 4.05 – 3.95 (m, 2H), 3.92 (dd, $J = 11.7, 4.4$ Hz, 1H), 3.10 (dd, $J = 13.6, 12.0$ Hz, 1H), 2.94 (dd, $J = 13.8, 4.4$ Hz, 1H), 2.67 (s, 3H), 2.03 (s, 6H), 1.31 (t, $J = 7.0$ Hz, 3H). No ^{13}C Data Acquired. ESI-MS: 476.3 $[\text{M} + \text{H}]^+$, HPLC (gradient A): Retention Time: 23.30 min.

(S)-1-((2-ethoxy-5-(pyrrolidine-1-carbonyl)benzyl)amino)-3-(4-hydroxy-2,6-dimethylphenyl)-1-oxopropan-2-aminium trifluoroacetate (135): See Procedure F: Step 1: 36 mg (0.099 mmol) of **119**, 180 μ L (133 mg, 1.03 mmol, 10.4 eq.) of N,N-diisopropylethylamine, 55 mg (0.11 mmol, 1.06 eq.) of PyBOP, 17 mg (0.10 mmol, 1.01 eq.) of 6-Cl-HOBt, 41 mg (0.10 mmol, 1.01 eq.) of Boc-O-Boc-L-2',6'-dimethyltyrosine, 3+1.5 mL of DMF. Step 2: 2 mL TFA and 2 mL DCM. Compound **135** (9.7 mg, Yield=18 %) was isolated as a yellow solid. ^1H NMR (500 MHz, Methanol- d_4) δ 7.63 (t, $J = 5.9$ Hz, 1H), 7.48 (dd, $J = 8.5, 2.2$ Hz, 1H), 7.35 (d, $J = 2.2$ Hz, 1H), 6.94 (d, $J = 8.5$ Hz, 1H), 6.33 (s, 2H), 4.31 (dd, $J = 14.6, 5.0$ Hz, 1H), 4.21 (dd, $J = 14.6, 4.7$ Hz, 1H), 4.01 (dtt, $J = 16.3, 8.9, 6.9$ Hz, 2H), 3.89 (dd, $J = 11.6, 4.5$ Hz, 1H), 3.59 (t, $J = 7.0$ Hz, 2H), 3.52 (t, $J = 6.7$ Hz, 2H), 3.11 (dd, $J = 13.7, 11.7$ Hz, 1H), 2.94 (dd, $J = 13.8, 4.5$ Hz, 1H), 2.06 (s, 6H), 1.99 (p, $J = 6.7$ Hz, 2H), 1.90 (p, $J = 6.4$ Hz, 2H), 1.32 (t, $J = 6.3$ Hz, 3H). No ^{13}C Data Acquired. ESI-MS: 440.3 $[\text{M} + \text{H}]^+$, HPLC (gradient A): Retention Time: 25.21 min.

(S)-1-((2-ethoxy-5-(isoindoline-2-carbonyl)benzyl)amino)-3-(4-hydroxy-2,6-dimethylphenyl)-1-oxopropan-2-aminium trifluoroacetate (136): See Procedure F: Step 1: 7 mg (0.021 mmol) of **123** as HCl salt, 40 μ L (30 mg, 0.23 mmol, 10.9 eq.) of N,N-diisopropylethylamine, 14 mg (0.027 mmol, 1.28 eq.) of PyBOP, 4 mg (0.024 mmol, 1.12 eq.) of 6-Cl-HOBt, 11 mg (0.027 mmol, 1.28 eq.) of Boc-O-Boc-L-2',6'-dimethyltyrosine, 3+1.5 mL of DMF. Step 2: 2 mL TFA and 2 mL DCM. Compound **136** (4.2 mg, Yield=41 %) was isolated as a white solid. ^1H NMR (500 MHz, DMSO- d_6) δ 8.99 (s, 1H), 8.29 (d, J = 5.4 Hz, 3H), 8.10 (t, J = 5.9 Hz, 1H), 7.52 (dd, J = 8.5, 2.2 Hz, 1H), 7.38 (d, J = 6.9 Hz, 1H), 7.35 – 7.21 (m, 4H), 6.98 (d, J = 8.6 Hz, 1H), 6.31 (s, 2H), 4.85 (s, 2H), 4.73 (d, J = 8.4 Hz, 2H), 4.29 (dd, J = 15.3, 6.1 Hz, 1H), 4.11 – 3.99 (m, 3H), 3.82 – 3.73 (m, 1H), 2.96 (dd, J = 13.9, 11.0 Hz, 1H), 2.81 (dd, J = 14.0, 4.6 Hz, 1H), 2.07 (s, 6H), 1.30 (t, J = 6.9 Hz, 3H). No ^{13}C Data Acquired. ESI-MS: 488.3 [M + H] $^+$, HPLC (gradient A): Retention Time: 32.75 min.

***In Vitro* Pharmacology**

Cell Lines and Membrane Preparations.

All opioid *in vitro* assays were performed by Ashley Brinkel, Jack Twarozynski, and Jessica Anand. Tissue culture reagents were purchased from Gibco Life Sciences (Grand Island, NY, U.S.) unless otherwise noted. C6-rat glioma cells stably expressing rat MOR (C6-MOR) or rat DOR (C6-DOR) and Chinese hamster ovary (CHO) cells stably expressing human KOR (CHO-KOR) were used for all *in vitro* assays. Cells were grown to confluence at 37 $^{\circ}\text{C}$ in 5 % CO_2 in Dulbecco's modified Eagle medium (DMEM) containing 10 % fetal bovine serum and 5 % penicillin/streptomycin. Membranes were prepared by washing confluent cells three times with ice cold phosphate buffered saline (0.9 % NaCl, 0.61 mM Na_2HPO_4 , 0.38 mM KH_2PO_4 , pH 7.4). Cells were detached from the plates by incubation in warm harvesting buffer (20 mM HEPES, 150 mM

NaCl, 0.68 mM EDTA, pH 7.4) and pelleted by centrifugation at 1600 rpm for 3 min. The cell pellet was suspended in ice-cold 50 mM Tris- HCl buffer, pH 7.4, and homogenized with a Tissue Tearor (Biospec Products, Inc., Bartlesville, OK, U.S.) for 20 s. The homogenate was centrifuged at 15,000 rpm for 20 min at 4 °C. The pellet was rehomogenized in 50 mM Tris-HCl with a Tissue Tearor for 10 s, followed by recentrifugation. The final pellet was resuspended in 50 mM Tris-HCl and frozen in aliquots at -80 °C. Protein concentration was determined via a BCA protein assay (Thermo Scientific Pierce, Waltham, MA, U.S.) using bovine serum albumin as the standard.

Radioligand Competition Binding Assays.

Radiolabeled compounds were purchased from Perkin-Elmer (Waltham, MA, U.S.). Opioid ligand binding assays were performed by competitive displacement of 0.2 nM [³H]-diprenorphine (250 µCi, 1.85 TBq/mmol) by the peptidomimetic from membrane preparations containing opioid receptors as described above. The assay mixture, containing membranes (20 µg protein/tube) in 50 mM Tris-HCl buffer (pH 7.4), 0.2 nM [³H]-diprenorphine, and various concentrations of test peptidomimetic, was incubated at room temperature on a shaker for 1 h to allow binding to reach equilibrium. The samples were rapidly filtered through Whatman GF/C filters using a Brandel harvester (Brandel, Gaithersburg, MD, U.S.) and washed three times with 50 mM Tris-HCl buffer, pH 7.4. Bound radioactivity on dried filters was determined by liquid scintillation counting, after saturation with EcoLume liquid scintillation cocktail, in a Wallac 1450 MicroBeta (Perkin-Elmer, Waltham, MA, U.S.). Nonspecific binding was determined using 10 µM naloxone. The results presented are the mean ± standard error (S.E.M.) from at least three separate assays performed in duplicate. K_i (nM) values were calculated using nonlinear regression analysis to fit a logistic equation to the competition data using GraphPad Prism, version 6.0c, (GraphPad Software Inc., La Jolla, CA).

[³⁵S]-GTPγS Binding Assays.

Agonist stimulation of [³⁵S]guanosine 5'-O-[γ-thio]triphosphate ([³⁵S]-GTPγS, 1250 Ci, 46.2 TBq/mmol) binding to G protein was measured as described previously.⁸² Briefly, membranes (10 μg of protein/well) were incubated for 1 h at 25°C in GTPγS buffer (50 mM Tris-HCl, 100 mM NaCl, 5 mM MgCl₂, 1 mM EDTA, pH 7.4) containing 0.1 nM [³⁵S]-GTPγS, 30 μM guanosine diphosphate (GDP), and varying concentrations of test peptidomimetic. G protein activation following receptor activation by peptidomimetic was compared with 10 μM of the standard compounds [D-Ala²,N-MePhe⁴,Gly-ol]enkephalin (DAMGO) at MOR, D-Pen^{2,5}-enkephalin (DPDPE) at DOR, or U69,593 at KOR. The reaction was terminated by vacuum filtration through GF/C filters that were washed 5 times with GTPγS buffer. Bound radioactivity was measured as described above. The results are presented as the mean ± standard error (S.E.M.) from at least three separate assays performed in duplicate; potency (EC₅₀ (nM)) and percent stimulation were determined using nonlinear regression analysis with GraphPad Prism 6, as above.

Mouse Liver Microsome Stability Assays

All liver microsome assays were performed by Quintara Biosciences. Metabolic stability of testing compounds was evaluated using mouse liver microsomes to predict intrinsic clearance. Mouse liver microsome tissue fractions were obtained from Corning or BioreclamationIVT. The assay was carried out in 96-well microtiter plates at 37 °C. Reaction mixtures (25 μL) contained a final concentration of 1 μM test compound, 0.1 mg/mL liver microsome protein, and 1 mM NADPH in 100 mM potassium phosphate, pH 7.4 buffer with 3 mM MgCl₂. At each of the time points (0, 15, 30, and 60 minutes), 150 μL of quench solution (acetonitrile with 0.1% formic acid) with internal standard (bucetin) was transferred to each well. Verapamil was included as a positive control to verify assay performance. Plates were sealed, vortexed, and centrifuged at 4°C for 15

minutes at 4000 rpm. The supernatant was transferred to fresh plates for LC/MS/MS analysis. All samples were analyzed on LC/MS/MS using an AB Sciex API 4000 instrument, coupled to a Shimadzu LC-20AD LC Pump system. Analytical samples were separated using a Waters Atlantis T3 dC18 reverse phase HPLC column (20 mm x 2.1 mm) at a flow rate of 0.5 mL/min. The mobile phase consists of 0.1% formic acid in water (solvent A) and 0.1% formic acid in acetonitrile (solvent B). The extent of metabolism was calculated as the disappearance of the test compound, compared to the 0-min time incubation. Initial rates were calculated for the compound concentration and used to determine $T_{1/2}$ values.

Animals and *In Vivo* Solutions

All *in vivo* opioid assays were performed by Bryan Sears. Animal care and experimental procedures complied with the US National Research Council's Guide for the Care and Use of Laboratory Animals.⁹¹ Animal studies are reported in compliance with the ARRIVE guidelines.^{92,93} Mice were group-housed with a maximum of five animals per cage in clear polypropylene cages with corn cob bedding and nestlets as enrichment. Mice had free access to food and water at all times. Animals were housed in pathogen-free rooms maintained between 68 and 79 °F and humidity between 30 and 70 % humidity with a 12 h light/dark cycle with lights on at 07:00 h. Experiments were conducted in the housing room during the light cycle. All studies utilize male C57BL/6 mice from Envigo laboratories. Wild type mice weighing between 20-30 g at 7-15 weeks old, were used for behavioral experiments. All drug solutions were injected at a volume of 10 ml/kg. All drugs were dissolved in 9:1 DMSO/saline solution except for morphine sulphate and 0.6 % acetic acid which were dissolved in saline and water, respectively. All drugs were given sc. except for 0.6 % acetic acid which was given ip.

Acetic Acid Stretch Assay (AASA)

Antinociceptive effects were evaluated in the mouse acetic acid stretch assay in which a noxious stimulus is administered ip. that induces a stretching behavior characterized by constriction of the abdomen followed by extension of the hind limbs. Mice received an injection of 0.6 % acetic acid, placed individually in clear plastic observation cages (10 x 6 x 8 in) with bedding, and the number of stretches were recorded for 20 min. Antinociceptive effects were determined with a 30 min pretreatment dose of compound sc. followed by 0.6 % acetic acid ip. A 5 min latency period after acetic acid injection was establish and total number of stretches were recorded for the following 20 min. For the competition assays, a dose of 10 mg/kg naloxone was administered ip. 15 min. before administration of test drug. The assay was resumed as described above. Statistical comparison of the number of stretches recorded were assessed using a two-way ANOVA.

Warm Water Tail Withdrawal Assay (WWTW)

Antinociceptive effects were evaluated in the mouse warm water tail withdrawal (WWTW) assay. Mice were placed in cylindrical plastic restrainers and 2-3 cm of their tail were immersed in a water bath maintained at 50 °C. Latency to a tail withdrawal or a rapid flick of the tail from the water bath was recorded for a maximum cut-off time of 20 s. Acute antinociceptive effects were determined by a single bolus injection. Each mouse received an injection of saline ip. and then 30 min later their baseline withdrawal latencies were recorded. Mice were then administered a 32 mg/kg dose ip. and withdrawal latencies were recorded every 30 min for 150 min.

Chapter 5: Discovery of Aromatic-Amine Pharmacophore

5.1 Introduction

In the previous chapter, we had determined that replacing the benzyl pendant with an aromatic-amine pendant was capable of greatly improving MOR affinity, efficacy, and potency, while providing improvements in metabolic stability. These improvements in MOR effects occur regardless of whether the amine is attached to the aromatic group through a simple methylene

group (such as the benzyl amines), or through an aromatic-aliphatic bicyclic system (such as with an isoindoline or tetrahydroisoquinoline pendant). Furthermore, the amine alone was capable of greatly improving metabolic stability while stimulating MOR, though at the cost of reduced MOR potency.

These amine pendant analogues therefore show promise in our new series, and we were interested in exploring the scope with which these pendants can yield MOR-agonists. While it was feasible to begin to introduce additional functional groups around both the aromatic core and these amine pendants, we instead opted for a tighter SAR campaign that sought to combine these new pendants with elements from Chapter 2 that improved stability. This allowed us to ask multiple questions simultaneously in our series, opens the door for structural simplification rather than complication, and uses the same chemistry developed in Chapter 4.

Four structural elements from Chapter 2 were selected to complement the ethyl ether derivatives described in Chapter 4. These include the methyl, n-propyl and cyclopropyl methyl ethers, as well as the unfunctionalized aromatic core. The ethers were selected due to their capacity to improve stability and due to the range of MOR efficacy they elicit with modest differences in alkyl chain length and structure. The unfunctionalized core was also selected because it was the simplest structure and because it produced no stimulation at MOR. This provided a wide range of MOR efficacy and metabolic stability values through very simple structural changes upon which the introduction of amine pendants can reveal the degree to which the pendants can improve these parameters. These modifications can thus allow us to determine the scope of MOR-agonism and stability the amine pendants can provide in our series.

Regarding the amine pendants, four were selected. The bicyclic aromatic-amine pendants (isoindoline and tetrahydroisoquinoline) were selected due to their ability to greatly improve MOR

efficacy and potency, with the possibility of improving stability. Two monocyclic amine pendants (pyrrolidine and piperidine) were selected due to their capacity to greatly improve metabolic stability and MOR efficacy.

The overall design of these ligands is summarized in **Figure 14**. These four amine pendants and the additional four aromatic core structural elements were used to construct an SAR matrix pairing each amine pendant with each core element. This resulted in sixteen additional analogues that were combined with their respective ethyl ether analogues described in Chapter 4 and used to ask the several questions. To what degree can these new amine pendants stimulate MOR? How dependent is this activity on their respective aromatic core modifications? Do the stability gains described thus far with the amine pendants translate across different core modifications?

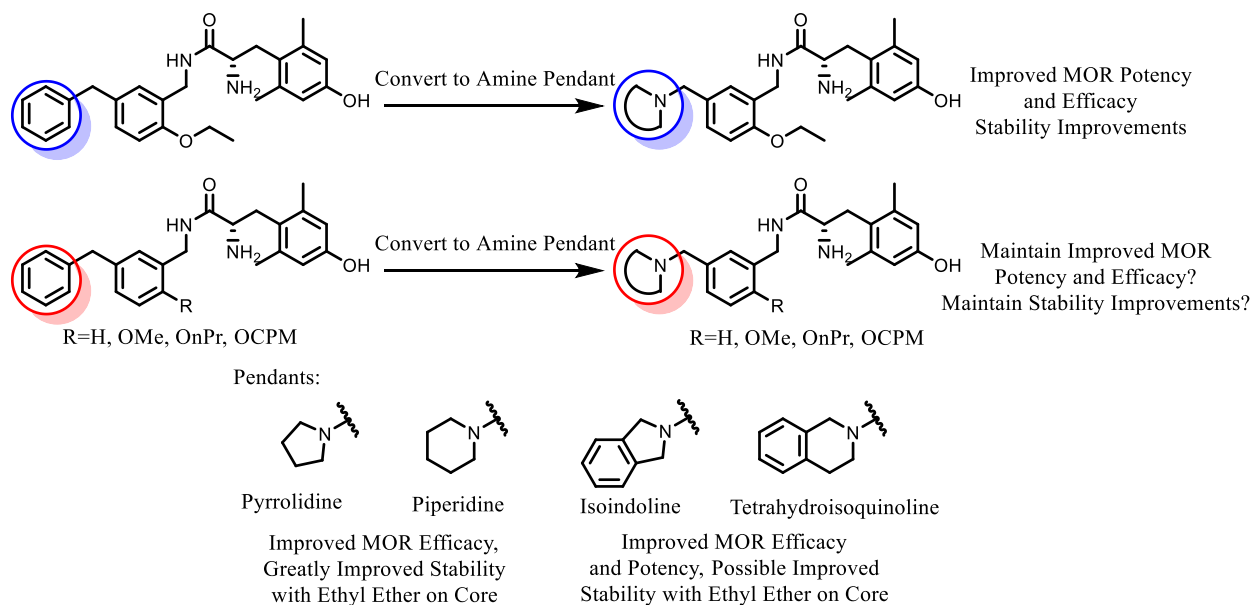


Figure 14: Design of amine pendant analogues with different aromatic core modifications. Pendants were selected based on their improved metabolic stability, MOR-efficacy, and MOR-potency. Core modifications were selected based on their improved stability and variability in MOR-agonism with minor changes in structure.

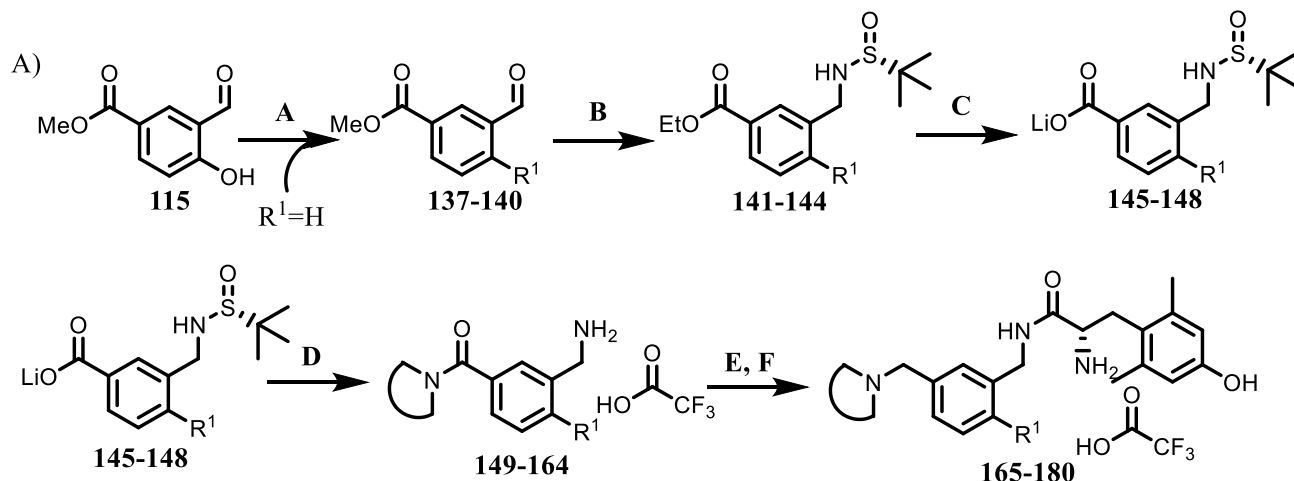
The answers to these questions can give us valuable insight into the SAR of these structures, allowing us to determine the ability and degree to which these pharmacophore elements

can produce our desired MOR-agonist/DOR-antagonist profile. This will also enable more efficient design of future analogues by reducing the number of ligands synthesized that do not stimulate MOR, as opposed to exploring moieties that produce unknown results.

5.2 Results

General Chemistry: The synthesis of these new analogues followed the same synthetic pathway described in Chapter 4 and are described in **Scheme 8A**. Here, the different ethers were introduced by alkylating methyl 3-formyl-4-hydroxybenzoate (**115**) using different alkyl iodides or bromides. These ethers, in addition to methyl 3-formylbenzoate (**137**), were then treated with Ellman's chiral auxiliary to introduce a protected amine onto the aldehyde. The subsequent ethyl ester was then cleaved using LiOH and used as a common intermediate for incorporation of the amine analogues to construct our desired matrix (**Scheme 8B**). Pyrrolidine, piperidine, isoindoline, and tetrahydroisoquinoline pendants were incorporated into each aromatic core scaffold using PyBOP,

Scheme 8: A) Synthesis of aromatic core analogues containing amine pendants to produce SAR matrices. B) Analogue codes for the intermediate amides and final compounds for each aromatic core modification and amine pendant in matrices.



B)

	R ¹ =H	R ¹ =OMe	R ¹ =OnPr	R ¹ =OCPM
	149, 165	153, 169	157, 173	161, 177
	150, 166	154, 170	158, 174	162, 178
	151, 167	155, 171	159, 175	163, 179
	152, 168	156, 172	160, 176	164, 180

A) MeI or Alk-Br, K₂CO₃, DMF. B) 1. (R)-(+)-2-methyl-2-propanesulfinamide, Ti(OEt)₄, THF
 2. NaBH₄. C) LiOH, THF, EtOH, H₂O D) 1. Cyclic amine, NMM, PyBOP, DMF. 2. conc. HCl,
 Dioxane. E) BH₃*Me₂S, THF, 75 C° F) 1. DiBocDMT, DIEA, PyBOP, 6-Cl-HOBt, DMF. 2.
 TFA, DCM.

and the Ellman auxiliary was removed with conc. HCl and purified by reverse phase, yielding the intermediate as a TFA salt. The subsequent tertiary amide was then reduced with BH₃*Me₂S at 75 °C and the primary amine was coupled to Boc-protected 2',6'-dimethyltyrosine. The synthesis was completed by deprotection of the Boc group using TFA.

SAR: The analogues synthesized using **Scheme 8** were sorted into matrices based on their affinity, selectivity, potency, and efficacy at MOR, DOR, and KOR respectively. The binding affinity matrix for MOR and DOR are described in **Table 14**, and for the sake of space, the binding affinity at KOR and selectivity are described in **Table 15**. These matrices will be used to describe the general effects of each pendant and core modification on our *SAR*.

With regards to MOR-binding affinity (**Table 14**), several noteworthy trends are revealed from these matrices. The monocyclic amines possess low double-digit to single-digit nanomolar binding affinity depending on the presence and size of the ether chain. The pyrrolidine achieves an affinity maximum at the methyl ether (**169**) and gets close to but does not achieve similar levels of binding affinity as their benzyl pendant counterparts. The piperidine pendant in general, possesses higher levels of binding affinity than the pyrrolidine pendant and is in the single-digit nanomolar range independent of ether chain size. These piperidine analogues are often similar to their benzyl pendant counterparts.

The binding affinity of the aromatic-amine analogues at MOR produce very flat *SAR* landscapes. These affinity values are similar and consistently sub-nanomolar, with the greatest affinity found with the cyclopropyl methyl ethers (**179-180**). These analogues generally possess a log improvement in binding affinity over the benzyl and piperidine analogues and upwards of a 2-fold log improvement over the pyrrolidine depending on the core modification.

The trends observed in DOR binding affinity (**Table 14**) with these analogues are similar to those observed in MOR. Conversion to the pyrrolidine ring consistently yielded a log loss in binding affinity compared to the benzyl pendant and was optimized at the ethyl (**127**) and n-propyl ethers (**173**). The piperidine pendant had a near 2 log range in binding affinity, which improves with increasing size of the ether. The isoindoline and tetrahydroquinoline pendants were also

insensitive to changes to the aromatic core, and in contrast to MOR binding affinity, DOR binding affinity rested in the low single-digit nanomolar range.

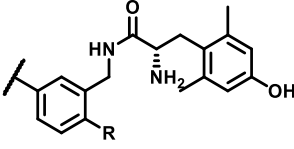
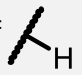
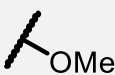
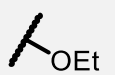
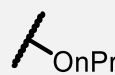
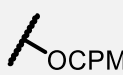
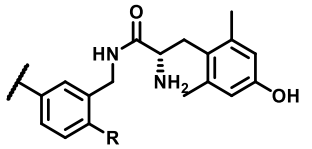
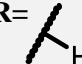
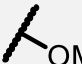
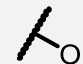
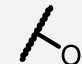
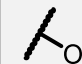
			59, 165-168	68, 169-172	70, 127-128, 131-132	71, 173-176	72, 177-180
R=							
MOR	58, 68, 70, 71, 72	Benzyl	1.0±0.2 ^a	3.6±0.1 ^a	3.60±0.52	0.91±0.06 ^a	2.7±0.6 ^a
	165, 169, 127, 173, 177	Pyrrolidine	39.7±7.0	8.40**	15.0±1.8	53±19*	29.4±4.2*
	166, 170, 128, 174, 178	Piperidine	12.1±5.6	7.5±2.2	5.0±1.5	4.6±0.2	2.5±1.3*
	167, 171, 131, 175, 179	isoindoline	0.30±0.07	0.44±0.08	0.80±0.22	0.33±0.00*	0.05**
	168, 172, 132, 176, 180	Tetrahydro-isoquinoline	0.23±0.02	0.16±0.05	0.23±0.04	0.22±0.04	0.05±0.0
DOR	58, 68, 70, 71, 72	Benzyl	14.7±0.6 ^a	21.5±4.5 ^a	4.81±0.89	5.3±1.4 ^a	13.9±1.8 ^a
	165, 169, 127, 173, 177	Pyrrolidine	212±75	184**	44.4±7.9	39.8±7.8	92.1**
	166, 170, 128, 174, 178	Piperidine	143±25	175±82*	15.7±4.3	20.1±2.1	3.32**
	167, 171, 131, 175, 179	isoindoline	6.1±1.7	0.87±0.14	2.7±0.6	1.6±0.2	2.00**
	168, 172, 132, 176, 180	Tetrahydro-isoquinoline	4.8±1.0	1.85**	2.4±0.5	1.4±0.3	2.33**

Table 14: Binding affinity matrix (K_i (nM)) of amine analogues of benzylic core structures from Chapter 2 at MOR and DOR. Included are the original benzylic core structures containing the benzyl pendant. Binding affinities were obtained by competitive displacement of radiolabeled [³H] diprenorphine in membrane preparations. All data were from three separate experiments, performed in duplicate unless otherwise noted. These data are reported as the average ± standard error of the mean. ^aData are from assays using rat MOR and DOR instead of human MOR and DOR used for all other assays. ** N=1, * N=2.

KOR binding affinity (**Table 15**) was subject to a greater variety of trends within these structural matrices. In general, each of the amine pendants yielded higher binding affinity compared to the original benzyl pendant. The exception exists when the pyrrolidine pendant is combined with the n-propyl ether (**173**), which had the lowest KOR affinity in the amine series and was the affinity minimum for the pyrrolidine pendant. The piperidine pendant had its affinity minimum with the n-propyl ether (**174**) as well. In fact, only the isoindoline did not possess an

affinity minimum with the n-propyl ether (**175**), which was instead located with the ethyl ether (**131**). Conversely, affinity maximums, if anywhere, appear to occur consistently with the methyl ether across all four pendants (**169-172**). Finally, the aromatic-amine pendants generally had mid double-digit nanomolar affinity at KOR, a trend which broke with the ethyl ether and isoindoline pendant analogue (**131**), and with the n-propyl ether with both aromatic-amine pendants.

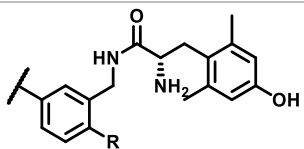
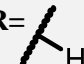
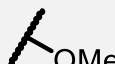
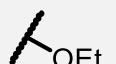
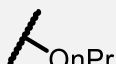
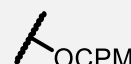
In general, the amine pendants yielded reduced selectivity of MOR over KOR, and variable affinity balance between MOR and DOR. The monocyclic analogues possessing smaller modifications (**165-166**, **169-170**) had very poor selectivity for MOR over KOR. For the piperidine and isoindoline pendants, MOR-selectivity over KOR was at its highest with the larger cyclopropyl methyl ethers (**178-179**). For the pyrrolidine, the greatest selectivity was with the ethyl ether (**127**), and for the THIQ pendant, the greatest selectivity was with the n-propyl ether (**176**). MOR binding affinity was most balanced with DOR binding affinity at different ethers within each pendant type. The pyrrolidine and piperidine pendants possessed the most affinity balance ranging from the ethyl ether to the cyclopropyl methyl ether. The aromatic-amine analogues generally had their affinity balance between MOR and DOR ranging from the methyl to n-propyl ethers. Interestingly, a loss of MOR/DOR balance was observed on the aromatic-amine pendants with the cyclopropyl methyl ethers (**179-180**). This, in conjunction with the improved selectivity of MOR over KOR, is likely a product of the improved binding affinity at MOR with these two analogues.

		59, 165-168	68, 169-172	70, 127-128, 131-132	71, 173-176	72, 177-180	
		R= 					
KOR	58, 68, 70, 71, 72	Benzyl	410±47	610±100	1180±120	390±150	319±51
	165, 169, 127, 173, 177	Pyrrolidine	159±24*	71±18*	430±16	>721	340±120*

	166, 170, 128, 174, 178	Piperidine	84±10*	28.4±7.7*	101±14	460±170	273.20**
	167, 171, 131, 175, 179	Isoindoline	37.5±2.4*	33.4±9.9*	243±53	139±39	40.3±6.5*
	168, 172, 132, 176, 180	Tetrahydro- isoquinoline	46.3±9.7	28.4±3.1	44.2±4.6	202±18	26.2**
MOR:DOR:KOR	58, 68, 70, 71, 72	Benzyl	1:15:410	1:6.0:170	1:8.5:420	1:5.8:430	1:5.1:120
	165, 169, 127, 173, 177	Pyrrolidine	1:5.3:4.0	1:22:8.5	1:3.0:29	1:0.75:>14	1:3.1:17
	166, 170, 128, 174, 178	Piperidine	1:12:6.9	1:23:3.8	1:3.1:20	1:4.4:100	1:1.3:110
	167, 171, 131, 175, 179	Isoindoline	1:20:125	1:2.0:76	1:3.4:304	1:4.8:421	1:40:960
	168, 172, 132, 176, 180	Tetrahydro- isoquinoline	1:21:201	1:8.8:178	1:10:192	1:6.4:918	1:47:520

Table 15: Binding affinity (K_i (nM)) matrices of amine analogues of benzylic core structures from Chapter 2 at KOR and the selectivity of each analogue across all three receptors standardized to MOR. Included are the original benzylic core structures containing the benzyl pendant. Binding affinities were obtained by competitive displacement of radiolabeled [^3H] diprenorphine in membrane preparations. All data were from three separate experiments, performed in duplicate unless otherwise noted. These data are reported as the average \pm standard error of the mean. ** N=1, * N=2.

The potency matrices across MOR, DOR, and KOR are described in **Table 16**. The pyrrolidine analogues in general had micromolar potency at MOR, the only exception here is with the ethyl ether (**70**), which was in the low triple-digit nanomolar range. The piperidine also possessed poor MOR potency, with the maximum being with the n-propyl ether (**174**). In general, these monocyclic amines were less potent than their benzyl pendant counterparts. Interestingly, the aromatic-amine pendant analogues possessed improved potency at MOR across all core modifications as compared to their benzyl pendant precursors. Like MOR-binding affinity, potency here varied little and was in the single-digit nanomolar range, the only exception being the isoindoline pendant with no ether on the core (**167**).

	59, 165-168	68, 169-172	70, 127-128, 131-132	71, 173-176	72, 177-180
	R= 				

MOR	58, 68, 70, 71, 72	Benzyl	DNS ^a	264±21 ^a	72±14	67.5±9.9 ^a	71±13 ^a
	165, 169, 170, 171, 172, 173, 177	Pyrrolidine	>1630	951**	168±42	>4290	1520**
	166, 169, 170, 171, 172, 173, 177	Piperidine	>737	>1390**	585±73	183±46	715**
	167, 171, 172, 173, 177	Isoindoline	28.1±6.9	2.40**	8.4±1.2	5.0±1.0	4.28**
	168, 172, 173, 176, 180	Tetrahydroisoquinoline	8.9±2.9	2.90±0.50	1.9±0.5	3.3±1.5*	3.9±2.3
DOR	58, 68, 70, 71, 72	Benzyl	DNS ^a	DNS ^a	DNS	DNS ^a	DNS ^a
	165, 169, 170, 171, 172, 173, 177	Pyrrolidine	DNS*	DNS**	1360±96	>2770	DNS**
	166, 169, 170, 171, 172, 173, 177	Piperidine	DNS	97.70**	129±20	117±45	85.1**
	167, 171, 172, 173, 177	Isoindoline	DNS	>2000**	43±13	200±120	DNS*
	168, 172, 173, 176, 180	Tetrahydroisoquinoline	490±170	25±21	DNS	DNS	DNS
KOR	58, 68, 70, 71, 72	Benzyl	DNS	DNS	DNS	DNS	DNS
	165, 169, 170, 171, 172, 173, 177	Pyrrolidine	474**	>5000**	>6000	DNS	DNS**
	166, 169, 170, 171, 172, 173, 177	Piperidine	>5420*	DNS**	DNS**	DNS	DNS**
	167, 171, 172, 173, 177	Isoindoline	>10000**	DNS**	DNS**	DNS	DNS**
	168, 172, 173, 176, 180	Tetrahydroisoquinoline	DNS	>1000	DNS**	DNS	DNS

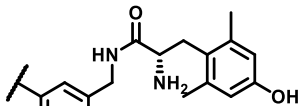
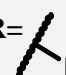

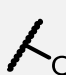
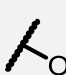
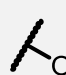
Table 16: Potency matrices of amine and analogues of previously reported benzylic core structures from Chapter 2 at MOR, DOR, and KOR. Included are the original benzylic core structures containing the benzyl pendant. Potency data were obtained using agonist induced stimulation of [³⁵S] GTPγS binding assay. Potency is represented as EC₅₀ (nM). All data were from three separate experiments, performed in duplicate unless otherwise noted. ** N=1, * N=2. These data are reported as the average ± standard error of the mean. DNS=Does Not Stimulate. ^aData are from assays using rat MOR and DOR instead of human MOR and DOR used for all other assays.

In this series, a mixture of DOR effects was observed. Whereas the benzyl pendant consistently did not stimulate DOR, regions of DOR-agonism were found in the matrices. In fact, it is simpler to describe which regions did not have any DOR-agonism in this series. No agonism was observed for analogues that possessed no ether modification on the core except with the tetrahydroisoquinoline pendant (**168**). The tetrahydroquinoline pendant did not yield DOR-agonism when combined with the ethyl or larger ethers. Finally, the pyrrolidine combined with the methyl ether also did not stimulate DOR (**169**). KOR-agonism in this series appears to be

consistently very low. In most cases, no observed KOR-stimulation was observed over the assay concentrations, and when efficacy was present, the potency was weak at values no less than 474 nM.

Efficacy matrices were also produced across MOR, DOR, and KOR and are shown in **Table 17**. The efficacy data collected at MOR revealed some promising trends. In the benzyl pendant series from Chapter 2, the efficacy at MOR ranged from no stimulation to 75.6 % stimulation. Here, across nearly all the amine pendant analogues, high levels of efficacy were observed. The exceptions here were with the monocyclic pendants with the unmodified core (**165-166**), which may be a result of the poor potency of these analogues, and the pyrrolidine with the cyclopropyl methyl ether (**177**), which still had double the efficacy of its benzyl pendant counterpart (**72**). More importantly, most of these analogues were full agonists compared to DAMGO, and two analogues were superagonists compared to DAMGO, namely **168** and **175**.

With regard to DOR-efficacy when present, efficacy decreased with increasing size of the ether and efficacy also dropped with increasing amine pendant size. None of these analogues produced more than 55 % efficacy as compared to DPDPE. KOR-efficacy was largely poor when present. Of those that activated KOR, only one analogue produced efficacy greater than 40 % over the assay range (**127**).

		59, 165-168	68, 169-172	70, 127-128, 131-132	71, 173-176	72, 177-180	
		R= 	R= 	R= 	R= 	R= 	
MOR	58, 68, 70, 71, 72	Benzyl	DNS ^a	37.2±1.7 ^a	75.6±5.8	54.9±4.0 ^a	37.5±1.3 ^a
	165, 169, 127, 173, 177	Pyrrolidine	>13	72.1**	85.9±9.7	92±11	68.1**
	166, 170, 128, 174, 178	Piperidine	>49	>89.4**	77.5±5.8	98.0±3.5	105**
	167, 171, 131, 175, 179	Isoindoline	106±8	94.1**	98.1±6.7	129±10	81.6**

	168, 172, 132, 176, 180	Tetrahydro-isoquinoline	148±13	102±7	94.6±3.9	113±3*	93.7±3.5
DOR	58, 68, 70, 71, 72	Benzyl	DNS ^a	DNS ^a	DNS	DNS ^a	DNS ^a
	165, 169, 127, 173, 177	Pyrrolidine	DNS*	DNS**	55±11	>27.7	DNS**
	166, 170, 128, 174, 178	Piperidine	DNS	49.50**	36.8±6.7	39.9±6.5	26.4**
	167, 171, 131, 175, 179	Isoindoline	DNS	>40**	35.7±2.8	29.4±3.0	DNS*
	168, 172, 132, 176, 180	Tetrahydro-isoquinoline	57.9±6.0	29.8±3.5	DNS	DNS	DNS
KOR	58, 68, 70, 71, 72	Benzyl	DNS	DNS	DNS	DNS	DNS
	165, 169, 127, 173, 177	Pyrrolidine	23.5**	>20**	>40	DNS	DNS**
	166, 170, 128, 174, 178	Piperidine	>13*	DNS**	DNS**	DNS	DNS**
	167, 171, 131, 175, 179	Isoindoline	>18.5**	DNS**	DNS**	DNS	DNS**
	168, 172, 132, 176, 180	Tetrahydro-isoquinoline	DNS	>15	DNS**	DNS	DNS

Table 17: Efficacy matrices of amine analogues of previously reported benzylic core structures from Chapter 2 at MOR, DOR, and KOR. Included are the original benzylic core structures containing the benzyl pendant. Efficacy data were obtained using agonist induced stimulation of [³⁵S] GTPγS binding assay. Efficacy was measured as percent maximal stimulation relative to standard agonist DAMGO (MOR), DPDPE (DOR), or U69,593 (KOR) at 10 μM. All data were from three separate experiments, performed in duplicate unless otherwise noted. These data are reported as the average ± standard error of the mean. ** N=1, * N=2. DNS=Does Not Stimulate. ^aData are from assays using rat MOR and DOR instead of human MOR and DOR used for all other assays.

Metabolic Stability: In keeping with our goals of maintaining improved metabolic stability, these stability values were determined for many of these analogues and compiled into a matrix found in **Table 18**. Many of these analogues possessed enhanced stability compared to their respective benzyl pendant counterparts. Where tested, the monocyclic amines still showed the greatest stability, which improved significantly when the ether on the core was removed. The stability here reached half-lives upwards of 5 hours in this assay. Curiously, the aromatic-amine pendants followed a different trend than that of the benzyl or monocyclic amine pendants. Here, they expressed stability optima at the ethyl ether, and stability dropped on either side of the ether chain length. The least stable molecule was analogue **167**, which possessed an isoindoline pendant and no ether, and was worse than the positive control verapamil.

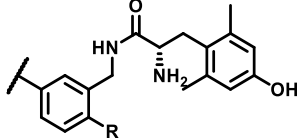
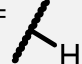
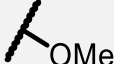

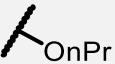
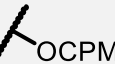
		59, 165-168	68, 169-172	70, 127-128, 131-132	71, 173-176	72, 177-180
		R= 				
58, 68, 70-72	Benzyl	13.0±2.6 (14.6±1.0) [0.89±0.19]	19.7±2.0 (13.8±1.6) [1.4±0.2]	23.7±5.9 (14.6±1.0) [1.6±0.4]	33.1±2.8 (19.6±2.3) [1.7±0.2]	56±10 (22.6±1.4) [2.5±0.5]
165, 169, 127, 173, 177	Pyrrolidine	310±130 (25.7±1.7) [12.1±1.3]	ND	199±79 (29.9±4.7) [6.6±2.8]	ND	ND
166, 170, 128, 174, 178	Piperidine	167±38 (25.7±1.7) [6.5±1.6]	ND	99.2±4.3 (29.9±4.7) [3.3±0.5]	ND	ND
167, 171, 131, 175, 179	Isoindoline	20.3±3.6 (25.7±1.7) [0.79±0.15]	47.0±1.8 (27.6±4.9) [1.7±0.3]	70.4±7.5 (25.7±1.7) [2.7±0.3]	39.1±6.8 (25.7±1.7) [1.5±0.3]	43.2±5.3 (27.6±4.9) [1.6±0.3]
168, 172, 132, 176, 180	Tetrahydro- isoquinoline	34.9±4.7 (25.7±1.7) [1.4±0.2]	46.5±5.0 (27.6±4.9) [1.7±0.3]	52.9±8.3 (29.9±4.7) [1.8±0.4]	49.8±1.0 (28.1±7.4) [1.8±0.5]	29.7±2.1 (27.6±4.9) [1.1±0.2]

Table 18: Metabolic stability matrix of amine analogues of previously reported benzylic core structures from Chapter 2. Included are the original benzylic core structures containing the benzyl pendant for comparison. The compound half-life ($T_{1/2}$) is in bold, the half-life of the positive control verapamil is in parentheses, and the stability ratio between the compound and the positive control is in brackets. The stability ratio was calculated by dividing the half-life of the analogue of interest by the half-life of the positive control in that assay. Individual compounds were tested once, with errors representing the SE in the decay curve regressed onto the data collected in 15-minute intervals. ND= No Data

Molecular Modeling: To elucidate how the aromatic-amine pharmacophore is producing the *in vitro* effects described above, molecular docking studies of superagonist **168** were performed at MOR, DOR, and KOR (**Figure 15**). At MOR, a couple of notable interactions can be observed. It appears that the aromatic ring is interacting with Trp133, and while at a distance, Asn127 may be interacting with the tertiary amine. At DOR, another tryptophan residue (Trp114) interacts with the aromatic ring, though the primary interaction with this ring appears to be a charge- π interaction

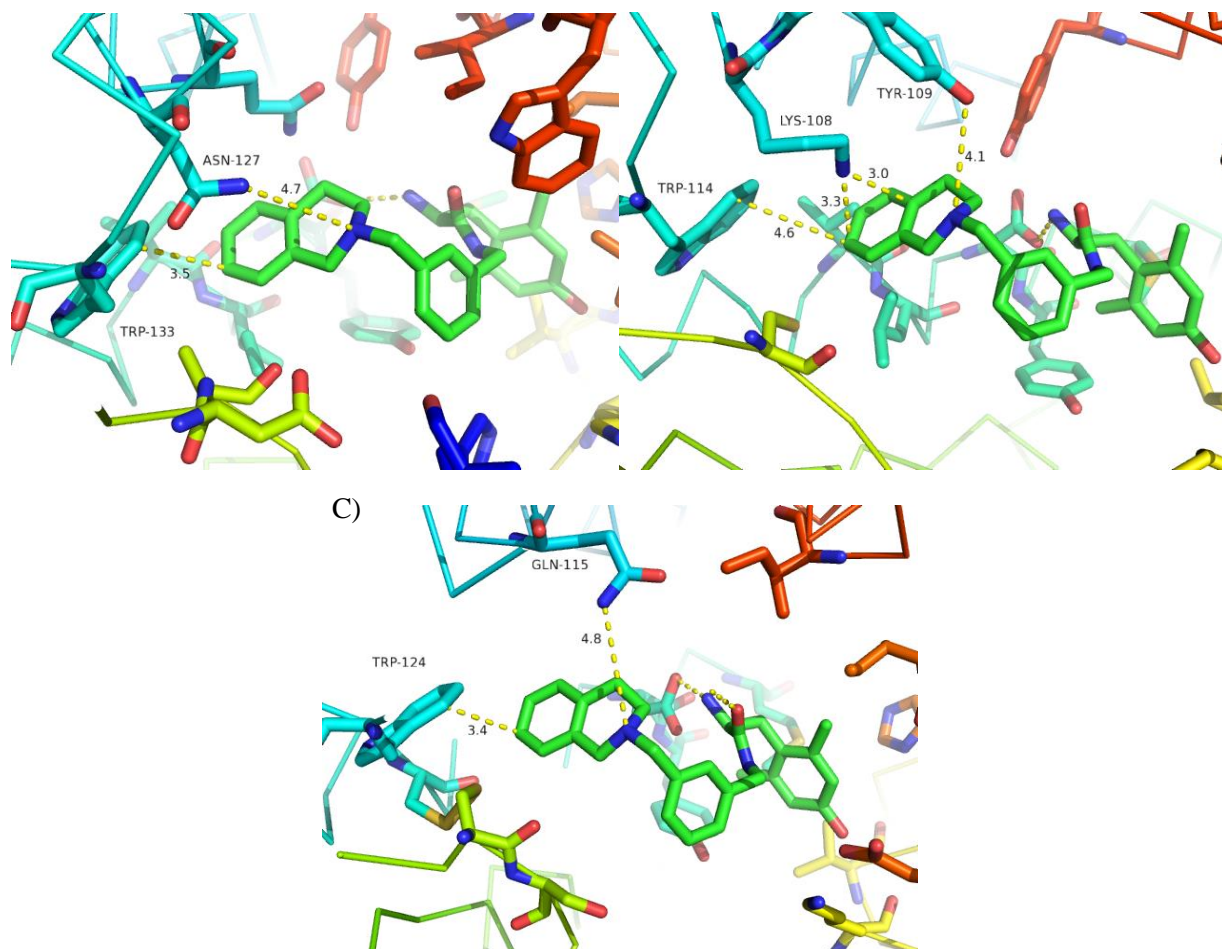


Figure 15: Molecular docking of superagonist **168** at the three opioid receptors. Shown are interactions of the tetrahydroisoquinoline pendant with A) MOR in the active state, B) DOR in the inactive state, and C) KOR in the inactive state.

with Lys108. Finally, the tertiary amine may interact with the phenol of Tyr109. Lastly, the aromatic ring of the pharmacophore again interacts with the indole of Trp124, and the amine may interact with the primary amide of Gln115.

Antinociceptive Activity: Several of the tetrahydroquinoline pendant analogues were then subject to *in vivo* screening in the AASA (**Figure 16**). For comparison, the ethyl ether analogue **132** is included and morphine was used as the positive control. Since the screening of these analogues is currently in progress, no data points at 0.1 mg/kg are available. Each of the ether analogues

produced antinociception at a dose of at least 10 mg/kg, and the n-propyl ether analogue **176** was also active at 1 mg/kg. Unfortunately, the superagonist **168** was inactive at 10 mg/kg.

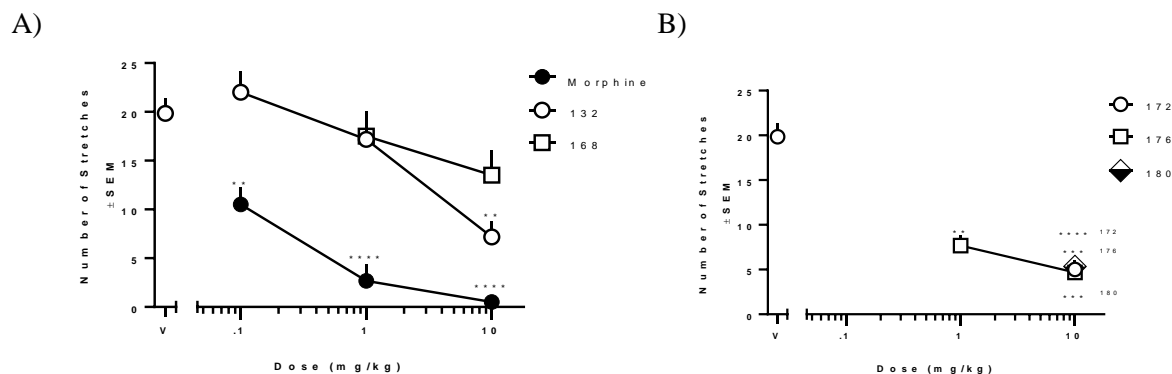


Figure 16: Antinociceptive activity of **132** and analogues **168**, **172**, **176**, and **180** using the AASA. Included is morphine as positive control. Panels A-B represent dose-response curves with the ligands: A) **132** and the superagonist **168**, B) ether analogues **172**, **176**, and **180**. ** $P < 0.01$ compared to vehicle. *** $P < 0.001$ compared to vehicle. **** $P < 0.0001$ compared to vehicle. Codes by asterisks in panel B represent P-values for overlapping analogues. N's are between 2 and 6 for each data point.

5.3 Discussion and Conclusions

SAR: The data presented in the above matrices reveal some very useful SAR trends, particularly in their effects at MOR. Monocyclic amine pendants generally appear to be dependent on their aromatic core modifications for binding affinity and potency, but not high efficacy. Conversely, the aromatic-amine pendants are largely insensitive to changes on the aromatic core and consistently possess very good binding affinity and potency. These data point out two important SAR characteristics on the nature of the amine pendants. Amines can produce high MOR-efficacy on their own, a trend that is supported by the amide analogues **135** and **136** of the previous chapter, which lose all MOR-efficacy. When these amines are combined with an aromatic ring in the pendant, then high MOR-binding affinity and potency are achieved independent of changes to the aromatic core. In some cases, this aromatic-amine pharmacophore can produce potent superagonists, as evidenced by analogues **168** and **175**. These data suggest that the aromatic-amine

can be a valuable pharmacophore for producing MOR-agonists, which is a necessary component in our desired bifunctional profile.

With regard to DOR-binding, aromatic-amine analogues generally possessed between a one to two log improvement in binding affinity over their monocyclic amine counterparts. This can be attributed to the aromatic ring, as the original benzyl pendant analogues also possessed good binding affinity at this receptor. DOR-potency and efficacy occurred frequently and was typically weak. If the analogue was relatively potent at DOR compared to the other analogues, then it was not as efficacious and vice versa. This points to weak interactions within DOR that come from a combination of core and pendant modifications. This is supported by the fact that within each amine pendant and core modification, there exist analogues which do not stimulate DOR. Ergo no single amine pendant or core modification consistently stimulates DOR.

KOR-binding was generally improved upon conversion to the amine pendants, and the addition of the aromatic ring to the amine pharmacophore either further improved binding affinity or had no appreciable effect. This suggests that the aromatic-amine pharmacophore generally improves binding compared to the benzyl pendant, though exceptions do exist. This points toward the possibility that KOR-binding can be reduced with appropriate core modifications. When selectivity is incorporated, the aromatic-amine pendants generally possess greater selectivity for MOR over KOR, mostly through improved MOR-binding. The aromatic-amine analogues also possessed the best MOR/DOR balance, particularly with the isoindolines. These data suggest that the aromatic-amines will be better pharmacophores for our desired opioid profile. Finally, KOR-agonism was always low, which is consistent with our desired profile.

Metabolic Stability: The stability data acquired here revealed some interesting trends. Unlike the benzyl pendant, the monocyclic amines possess improved stability with no ether on the core (**165-**

166). This may be attributed to a combination of two things. The monocyclic amines are more polar than the benzyl pendant and are less metabolically labile. Conversion then away from this benzyl pendant therefore reduces the cLogP of the entire ligand and removes a metabolically labile aromatic ring. Since the ethers increase cLogP and are metabolically labile, removal of these structures when the monocyclic amines are present result in further stability improvements.

Curiously, the aromatic-amine pendants result in different stability trends compared to the benzyl and monocyclic amine pendants. The stability optimum exists in both cases with the ethyl ethers, though the tetrahydroisoquinoline pendant with an n-propyl ether was just as stable as the ethyl ether. Here, it appears that a balance of cLogP and blocking metabolic sites is important for the stability of these ligands. The cyclopropyl group, which may sterically block metabolism at the adjacent benzylic position that connects to DMT, also happens to increase cLogP. This increase in cLogP can facilitate metabolism on the aromatic-amine pendant, which is more metabolically liable than the monocyclic amine or benzyl pendants. The steric effects of these ethers are still relevant, as reduction to a methyl ether or removal of the ether entirely enables metabolism at the adjacent benzylic position. This is more prevalent in the aromatic-amine series than in the monocyclic amine series likely due to their greater cLogP.

Molecular Modeling: The molecular modeling shown in this chapter may allow us to explain the superagonist activity enabled by the pharmacophore at MOR, any residual DOR agonism present, and the enhanced binding at KOR. Consistent across all of the opioid receptors is an interaction between the aromatic ring of the pharmacophore and the indole of a tryptophan residue. This interaction can explain the enhanced binding at MOR and DOR, though the lack of a trend in the KOR-binding data with and without the aromatic ring suggests this interaction is not a deciding

factor at this receptor. At MOR, the closest residue to the amine is an asparagine residue, which may activate the receptor through the formation of a hydrogen bond.

At DOR, there appears to be a clear charge- π interaction between the aromatic ring of the peptidomimetic and Lys108 and can explain the enhanced binding affinity that occurs with the aromatic rings. On either side of this residue is a tyrosine residue (Tyr109), and a tryptophan residue (Trp114). The phenol of the tyrosine residue may interact with the tertiary amine of the ligand, and thus facilitate activation of this receptor. Receptor activation though, appears to be a bit sensitive to both the identity of the pendant and the identity of the ether modification. It is feasible that the ligand needs to position this amine in just the right way to interact with this tyrosine residue. If this ligand is too big (eg a large ether with a large pendant), the amine may be pushed closer to Trp114 and unable to interact with the phenol. If too small (eg no ether and a small pendant), the amine is too close to the DMT pharmacophore in space and can't interact with the phenol. This may explain diagonal line of DOR-stimulation that bisects the DOR-efficacy matrix.

Finally, the amine of analogue **168** may interact with Gln115 at KOR. Though this possesses an amide, like Asn127 in MOR, it should be noted that any KOR-stimulation that exists is extremely weak, if present at all. In MOR, the residues Trp133 and Asn127 that interact with the pharmacophore are only six residues apart. In KOR, Trp124 and Gln115 are nine residues apart. This difference in distance may have important implications for receptor activation, as it may not be possible for the pharmacophore to adequately interact with both residues such that the receptor is activated, especially if the core of the ligand is tied into an aromatic ring. However, given the large distance between some of these key residues and the tetrahydroisoquinoline pendant, additional *in silico* studies will be needed to verify these interactions.

Antinociceptive Activity: The additional analogues screened for their *in vivo* activity, while limited, allows for a possible trend to emerge. It appears that the ether on the aromatic core may be important for activity, as the only analogue without this ether (**168**) was inactive. It should be noted here that **168** is a superagonist at MOR. While this high efficacy did not translate in this case to *in vivo* activity, it is possible that this may be a product of pharmacokinetic factors rather than pharmacodynamic ones. Short of synthesizing additional analogues that may yield an *in vivo* active superagonist, it may be more feasible to administer this compound via intracerebral ventricular injection. This may allow for the pharmacological effects of a MOR-superagonist to be elucidated in future studies.

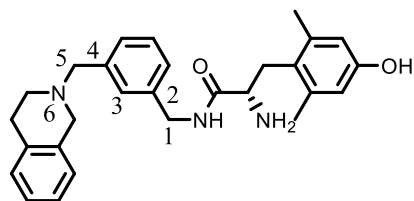
Broader Implications: This aromatic-amine pharmacophore appears to have great potential in producing bifunctional MOR/DOR ligands. As such, we were curious to determine if a similar pharmacophore was utilized in previously described opioids outside of our peptidomimetic series. The aromatic activity of this pharmacophore is unsurprising, as it still mimics the phenylalanine side chain of the opioid peptides. An overview of the literature of similar peptides and peptidomimetics suggests that the most similar analogues rely upon aromatic-amides instead of our aromatic-amines (**Figure 17A**), with the superagonist analogue **168** shown for comparison. Most notable are the DMT-Tic pharmacophore series^{94–101} their structurally related DMT-Aba derivatives^{102,103} and the DMT-Xxx-Aba derivatives,^{104–110} though a screen of a peptide library also produced a cyclic peptides with a similar amide.^{111,112} Bifunctional ligands connecting the DMT-Tic pharmacophore to a fentanyl scaffold have also been reported.¹¹³ Finally, a series of endomorphin derivatives have also been reported.^{114–120}

The closest structures that utilize amines possess the amine in a different relative position compared to the dimethyl tyrosine residue (**Figure 17B**). For instance, the MOR-agonist/DOR

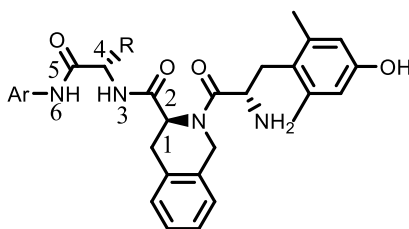
antagonist DIPP[Ψ]-NH₂ in the TIPP series of analogues¹²¹ possesses an amine in the peptide chain, albeit at the 3rd heavy atom away from the DMT residue instead of ours which is the 6th heavy atom. A few similar ligands have also been described.^{77,122}

There are a few opioid peptides that express a nitrogen heterocycle at similar positions to our newly synthesized peptidomimetics without the aromatic ring (**Figure 17C**). The nitrogen in these systems are noticeably at different distances from the DMT or Tyr residues, and they are conjugated into either an amide¹²³ or guanidine system.¹²⁴

A)

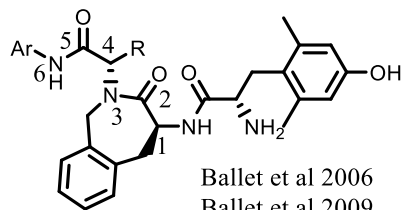


Analog **168**



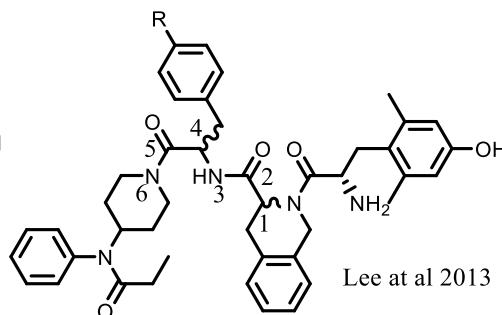
DMT-Tic pharmacophore series

Balboni et al 2002
Balboni et al 2003
Balboni et al 2006
Balboni et al 2007
Balboni et al 2008
Balboni et al 2010
Dietis et al 2012
Dietis et al 2018

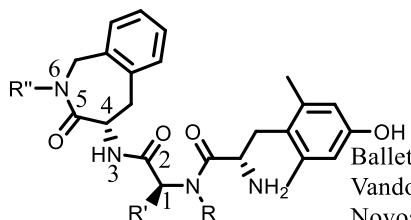


DMT-Aba series

Ballet et al 2006
Ballet et al 2009

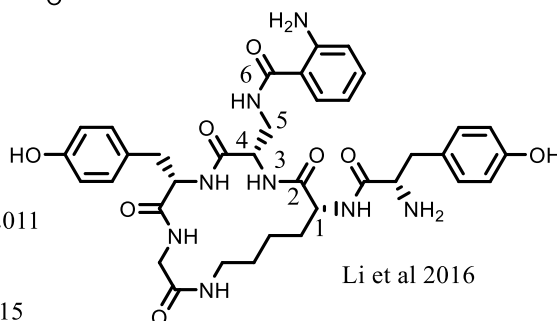


Lee et al 2013

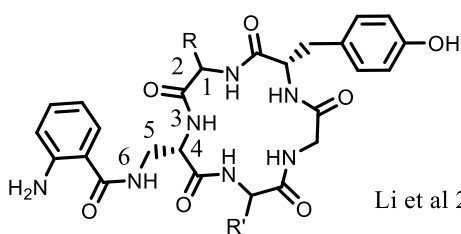


DMT-Xxx-Aba series

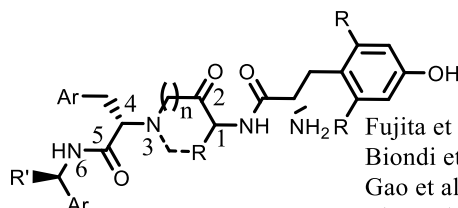
Ballet et al 2011
Vandormael et al 2011
Novoa et al 2012
Betti et al 2015
Guillemyn et al 2015
Guillemyn et al 2016
Starnowska et al 2017



Li et al 2016



Li et al 2012



Endomorphin Analogues

Fujita et al 2004
Biondi et al 2006
Gao et al 2006
Liu et al 2013
Nair et al 2015
Liu et al 2017
Wang et al 2017

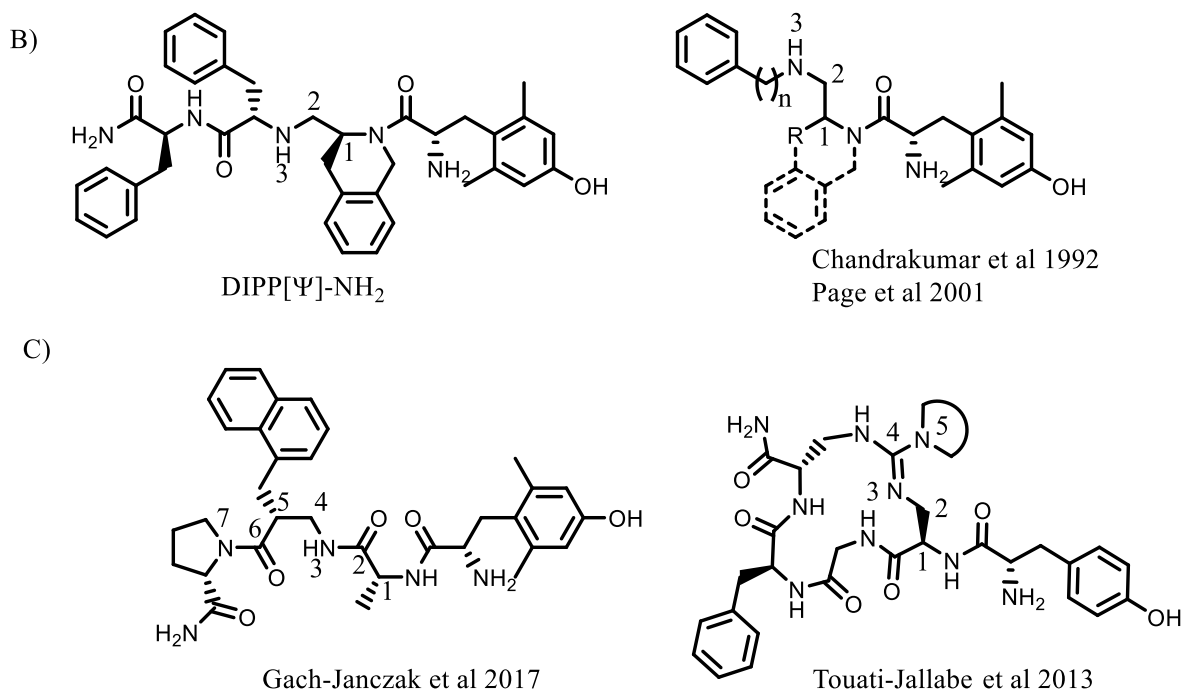


Figure 17: Literature structures that are close to our discovered aromatic-amine pharmacophore outside of our previously reported peptidomimetic series. A) Opioid peptides and peptidomimetics that contain the benzyl pharmacophore, but have the amine trapped as an amide. B) Opioid peptides and small molecules that contain an amine pharmacophore with variability in the distance to the aromatic portion of the pharmacophore and in the distance from the dimethyltyrosine residue if applicable. C) Opioid peptides that contain a nitrogen heterocycle without the corresponding aromatic ring.

Notably, each of the unnatural peptides reported previously have a much higher molecular weight than our peptidomimetics, and many of these are incapable of stimulating MOR. With this aromatic-amine pharmacophore, we believe that this structure can be incorporated into the opioid peptides and their analogues to produce potent MOR-agonists. This pharmacophore in turn may allow for structural simplification of these peptides, through removal of bulky core elements, such as the large ring systems produced through peptide cyclization, or the use of large amino acids, such as Tic, Phe, and their other unnatural amino acid counterparts.

Conclusions: The data collected in this chapter provide valuable information necessary to address the questions asked in the beginning of this chapter. Amines in the pendant are capable of

consistently stimulating MOR, independent of modifications to the core. The addition of an aromatic ring onto the amine pendant consistently improves potency at MOR, also independent of modifications to the core. As such, this aromatic-amine pendant pharmacophore may be used in future ligands to produce MOR-agonists out of a wide variety of structures. In this series, DOR-affinity is maintained, and while some residual DOR-agonism may be present in some ligands, they may still be used as leads to further develop non-addictive opioids. Finally, the monocyclic amines maintain high levels of metabolic stability, whereas the stability of the aromatic-amine pendant analogues are dependent on the structures attached to the core.

Finally, it should be noted that this series produced two MOR-superagonists (**168** and **175**). Not only does this reinforce the utility of this new pharmacophore, but it may also yield some novel pharmacological results, as there are few ligands that possess efficacy at MOR this high. As such, further pharmacological studies should be pursued with these analogues, and additional derivatives that use this aromatic-amine pendant are likely to be fruitful.

5.4 Experimental

Chemistry

General Methods: All reagents and solvents were obtained commercially and were used without further purification. Intermediates were purified by flash chromatography using a Biotage Isolera One instrument. Most purification methods utilized a hexanes/ethyl acetate solvent system in a Biotage SNAP KP-Sil column, with a linear gradient between 0 and 100% ethyl acetate. Reverse phase column chromatography using a linear gradient of 0% to 100% solvent B (0.1% TFA in acetonitrile) in solvent A (0.1% TFA in water) using a Biotage SNAP Ultra C18 column was utilized for some intermediate amine salts. Purification of final compounds was performed

using a Waters semipreparative HPLC with a Vydac protein and peptide C18 reverse phase column, using a linear gradient of 0% to 100% solvent B in solvent A at a rate 1% per minute, monitoring UV absorbance at 230 nm. The purity of final compounds was assessed using a Waters Alliance 2690 analytical HPLC instrument with a Vydac protein and peptide C18 reverse phase column. A linear gradient (gradient A) of 0% to 70% solvent B in solvent A in 70 min, measuring UV absorbance at 230 nm was used to determine purity. All final compounds used for testing were $\geq 95\%$ pure, as determined by analytical HPLC. ^1H NMR and ^{13}C NMR data were obtained on a 500 or 400 MHz Varian spectrometer using CDCl_3 , CD_3OD , $\text{DMSO}-d_6$, or D_2O as solvents. The identities of final compounds were verified by mass spectrometry using an Agilent 6130 LC-MS mass spectrometer in positive ion mode, or an Agilent 6230 TOF HPLC-MS in the positive ion mode.

General Procedure for the Synthesis of 6-position Ethers (Procedure A): To a flame dried flask containing **methyl 3-formyl-4-hydroxybenzoate (115)** was added 3 equivalents of potassium carbonate. The flask was purged with argon and 4 mL of DMF was added. 3 equivalents of an alkyl iodide or bromide was then added, and the solution was stirred at room temperature overnight. The solution was then concentrated in vacuo, partitioned between ethyl acetate and saturated sodium carbonate, and extracted with ethyl acetate. The organic layers were combined, dried with magnesium sulfate, filtered, and concentrated in vacuo, yielding the desired ether.

General Procedure for Ellman Reductions (Procedure B): A flamed-dried round bottom flask containing 1 equivalent of aldehyde and 3 equivalents of (R)-(+)-2-methyl-2-propanesulfonamide was attached to a reflux condenser and flushed with argon. 4 mL of THF was added and cooled to 0 °C. 6 equivalents of titanium (IV) ethoxide was added, followed by an additional 4 mL of THF. The solution was stirred and heated to 75 °C overnight with TLC

monitoring until all ketone or aldehyde was consumed. A separate flame-dried flask containing 6 equivalents of sodium borohydride was flushed with argon. 4 mL of THF was added, at which point the solution was cooled to -78 °C. The solution containing Ellman adduct was cooled to room temperature and slowly transferred to the sodium borohydride solution via syringe. This final solution was then allowed to warm to room temperature and stirred for 2 hours, at which point the reaction mixture was quenched with methanol to consume the sodium borohydride, followed by DI water to precipitate the titanium. The solution was vacuum filtered, and the precipitate was washed with ethyl acetate. The filtrate was concentrated in vacuo and purified via column chromatography (0-100% EtOAc in Hexanes).

General Procedure for the Saponification of Esters (Procedure C): To a flask containing 1 equivalent of the desired ester was added 7 equivalents of LiOH, 2 mL of THF, 2 mL of EtOH, and 2 mL of H₂O. The reaction was stirred overnight under ambient atmosphere and temperature. Upon completion, the solvent was concentrated in vacuo, suspended in acetone, and filtered. The precipitate was washed with additional acetone, and the filtrate was concentrated in vacuo, yielding the saponified product as a lithium carboxylate.

General Procedure for Amine Pendant Attachment and Cleavage of Ellman auxiliaries (Procedure D): To a flask containing 1 equivalent of the lithium carboxylate was added 1 equivalent of PyBOP and 1 equivalent of the desired amine. The flask was flushed with argon, DMF was added as solvent, and 10 equivalents of N-methylmorpholine was added. The reaction was stirred overnight, at which point it was concentrated in vacuo and purified via column chromatography (0-10% methanol in DCM). To the protected amine was immediately added 2 mL of Dioxane and 0.2 mL concentrated HCl. The solution was stirred at room temperature for 1 minute and concentrated in vacuo. The ensuing salt was triturated with diethyl ether, and then was

purified using a reverse phase chromatography (0-100% B in A), yielding the product as a TFA salt.

General Procedure for the Reduction of Pendant Amides (Procedure E): To a dried flask containing 1 equivalent of the desired amide under argon was added THF and 7 equivalents of 2 M $\text{BH}_3 \cdot \text{Me}_2\text{S}$ complex in THF. The reaction was heated at 75 °C for 3 hours, at which point the reaction was quenched with MeOH and heated for an additional 15 minutes. The reaction was then cooled, concentrated in vacuo, and was used in Procedure F without further purification.

General Procedure for the Coupling of 2',6'-Dimethyltyrosine to Functionalized Amine Salts (Procedure F): To a dried flask containing the amine under argon was added 3 mL of DMF and 10 equivalents of Hunig's base. 1 equivalent of PyBOP and 1 equivalent of 6-Cl-HOBt was added, followed by a 1 equivalent of doubly Boc protected 2',6'-Dimethyltyrosine in 1.5 mL DMF. The solution was stirred overnight at room temperature, concentrated in vacuo, and purified via semipreparative reverse phase HPLC (0.1% TFA in water: 0.1% TFA in acetonitrile). 2 mL of TFA and 2 mL of DCM were then added, and the solution was stirred for an additional hour. The reaction mixture was concentrated in vacuo and purified via an additional semipreparative reverse phase HPLC (0.1% TFA in water: 0.1% TFA in acetonitrile). The product was concentrated in vacuo and lyophilized overnight to yield the final peptidomimetic.

Methyl 4-methoxy-3-formylbenzoate (138): See Procedure A: 160 mg (0.88 mmol) of **methyl 3-formyl-4-hydroxybenzoate (115)**, 368 mg (2.66 mmol, 3.00 eq.) of K_2CO_3 , 170 μL (388 mg, 2.73 mmol, 3.08 eq) of MeI, 4 mL of DMF. Compound **138** (162 mg, Yield=94 %) was isolated as a yellow solid. ^1H NMR (500 MHz, Chloroform-*d*) δ 10.44 (s, 1H), 8.49 (d, $J = 2.3$ Hz, 1H), 8.23 (dd, $J = 8.8, 2.3$ Hz, 1H), 7.04 (d, $J = 8.8$ Hz, 1H), 4.00 (s, 3H), 3.90 (s, 3H). ^{13}C NMR

(126 MHz, Chloroform-*d*) δ 188.84, 165.96, 164.71, 137.10, 130.67, 124.44, 122.92, 111.54, 56.06, 52.12.

Methyl 4-propoxy-3-formylbenzoate (139): See Procedure A: 168 mg (0.93 mmol) of **methyl 3-formyl-4-hydroxybenzoate (115)**, 388 mg (2.81 mmol, 3.01 eq.) of K_2CO_3 , 260 μ L (352 mg, 2.86 mmol, 3.07 eq) of *n*PrBr, 4 mL of DMF. Compound **139** (188 mg, Yield=91 %) was isolated as a colorless oil that turns to a white solid on standing. 1H NMR (500 MHz, Chloroform-*d*) δ 10.44 (s, 1H), 8.43 (d, $J = 2.3$ Hz, 1H), 8.15 (dd, $J = 8.8, 2.3$ Hz, 1H), 6.98 (d, $J = 8.8$ Hz, 1H), 4.07 (t, $J = 6.4$ Hz, 2H), 3.86 (s, 3H), 1.87 (h, $J = 7.2$ Hz, 2H), 1.05 (t, $J = 7.4$ Hz, 3H). ^{13}C NMR (126 MHz, Chloroform-*d*) δ 188.78, 165.94, 164.41, 136.98, 130.24, 124.36, 122.56, 112.27, 70.44, 52.03, 22.30, 10.41.

Methyl 4-(cyclopropylmethoxy)-3-formylbenzoate (140): See Procedure A: See Procedure A: 181 mg (1.00 mmol) of **methyl 3-formyl-4-hydroxybenzoate (115)**, 417 g (3.02 mmol, 3.00 eq.) of K_2CO_3 , 290 μ L (404 mg, 2.99 mmol, 2.98 eq) of cyclopropylmethyl bromide, 4 mL of DMF. Compound **140** (233 mg, Yield=99 %) was isolated as a yellow oil. 1H NMR (500 MHz, Chloroform-*d*) δ 10.41 (s, 1H), 8.35 (d, $J = 2.3$ Hz, 1H), 8.07 (dd, $J = 8.8, 2.3$ Hz, 1H), 6.90 (d, $J = 8.8$ Hz, 1H), 3.91 (d, $J = 6.9$ Hz, 2H), 3.80 (s, 3H), 1.31 – 1.20 (m, 1H), 0.65 – 0.56 (m, 2H), 0.32 (dt, $J = 6.2, 4.8$ Hz, 2H). ^{13}C NMR (126 MHz, Chloroform-*d*) δ 188.81, 165.84, 164.29, 136.86, 130.06, 124.34, 122.48, 112.43, 73.58, 51.97, 9.83, 3.18.

Ethyl (R)-3-(((tert-butylsulfinyl)amino)methyl)benzoate (141): See Procedure B: Step 1: 220 mg (1.34 mmol) of **methyl 3-formylbenzoate (137)**, 490 mg (4.04 mmol, 3.02 eq.) of (R)-(+)-2-methyl-2-propanesulfinamide, 1.7 mL (1.8 g, 8.1 mmol, 6.1 eq.) of $Ti(OEt)_4$, 5+5 mL THF. Step 2: 331 mg (8.75 mmol, 6.08 eq.) of sodium borohydride in 5 mL THF. Compound **141** (278

mg, Yield= 73 %) was isolated as a colorless oil. ^1H NMR (500 MHz, Chloroform-*d*) δ 7.93 (t, J = 1.8 Hz, 1H), 7.86 (dt, J = 7.8, 1.5 Hz, 1H), 7.46 (dt, J = 7.7, 1.4 Hz, 1H), 7.32 (td, J = 7.7, 2.5 Hz, 1H), 4.33 – 4.18 (m, 4H), 3.80 (dd, J = 6.9, 4.6 Hz, 1H), 1.30 (t, J = 7.1 Hz, 3H), 1.17 (d, J = 1.4 Hz, 9H). ^{13}C NMR (126 MHz, Chloroform-*d*) δ 166.24, 139.00, 132.41, 130.68, 128.97, 128.66, 128.57, 60.95, 55.94, 48.79, 22.63, 14.24.

Ethyl (R)-3-(((tert-butylsulfinyl)amino)methyl)-4-methoxybenzoate (142): See Procedure B: Step 1: 234 mg (1.21 mmol) of **138**, 441 mg (3.64 mmol, 3.02 eq.) of (R)-(+)-2-methyl-2-propanesulfinamide, 1.55 mL (1.69 g, 7.39 mmol, 6.14 eq.) of $\text{Ti}(\text{OEt})_4$, 4+4 mL THF. Step 2: 274 mg (7.24 mmol, 6.01 eq.) of sodium borohydride in 4 mL THF. Compound **142** (374 mg, Yield=99 %) was isolated as a colorless oil. ^1H NMR (500 MHz, Chloroform-*d*) δ 7.96 – 7.90 (m, 2H), 6.84 (d, J = 9.3 Hz, 1H), 4.36 (dd, J = 14.3, 5.6 Hz, 1H), 4.28 (q, J = 7.1 Hz, 2H), 4.16 (dd, J = 14.3, 7.6 Hz, 1H), 3.85 (s, 3H), 3.73 (t, J = 6.6 Hz, 1H), 1.32 (t, J = 7.1 Hz, 3H), 1.17 (s, 9H). ^{13}C NMR (126 MHz, Chloroform-*d*) δ 166.19, 160.92, 131.07, 130.63, 127.08, 122.66, 109.83, 60.65, 55.88, 55.58, 44.92, 22.56, 21.94, 14.31.

Ethyl (R)-3-(((tert-butylsulfinyl)amino)methyl)-4-propoxybenzoate (143): See Procedure B: Step 1: 181 mg (0.81 mmol) of **139**, 299 mg (2.5 mmol, 3.0 eq.) of (R)-(+)-2-methyl-2-propanesulfinamide, 1025 μL (1115 mg, 4.9 mmol, 6.0 eq.) of $\text{Ti}(\text{OEt})_4$, 4+4 mL THF. Step 2: 187 mg (4.9 mmol, 6.1 eq.) of sodium borohydride in 4 mL THF. Compound **143** (272 mg, Yield= 98 %) was isolated as a yellow oil. ^1H NMR (500 MHz, Chloroform-*d*) δ 7.89 (d, J = 2.2 Hz, 1H), 7.86 (dd, J = 8.5, 2.3 Hz, 1H), 6.77 (d, J = 8.6 Hz, 1H), 4.32 (dd, J = 14.4, 5.5 Hz, 1H), 4.23 (q, J = 7.0 Hz, 2H), 4.13 (dd, J = 14.3, 7.7 Hz, 1H), 3.91 (t, J = 6.4 Hz, 2H), 3.76 (t, J = 6.6 Hz, 1H), 1.75 (h, J = 7.4 Hz, 2H), 1.27 (t, J = 7.1 Hz, 3H), 1.13 (s, 9H), 0.97 (t, J = 7.4 Hz, 3H). ^{13}C NMR

(126 MHz, Chloroform-*d*) δ 166.11, 160.35, 130.90, 130.46, 127.11, 122.34, 110.40, 69.73, 60.20, 55.74, 44.88, 22.52, 22.40, 14.25, 10.52.

Ethyl (R)-3-(((tert-butylsulfinyl)amino)methyl)-4-(cyclopropylmethoxy)benzoate

(144): See Procedure B: Step 1: 230 mg (0.98 mmol) of **140**, 359 mg (2.96 mmol, 3.02 eq.) of (R)-(+)-2-methyl-2-propanesulfonamide, 1.25 mL (1.36 g, 5.96 mmol, 6.07 eq.) of Ti(OEt)₄, 4+4 mL THF. Step 2: 225 mg (4.26 mmol, 5.95 eq.) of sodium borohydride in 4 mL THF. Compound **144** (333 mg, Yield= 96 %) was isolated as a colorless oil. ¹H NMR (500 MHz, Chloroform-*d*) δ 7.97 – 7.87 (m, 2H), 6.79 (d, *J* = 8.5 Hz, 1H), 4.42 (dd, *J* = 14.3, 5.7 Hz, 1H), 4.29 (q, *J* = 7.1 Hz, 2H), 4.20 (dd, *J* = 14.3, 7.8 Hz, 1H), 3.91 – 3.81 (m, 3H), 1.34 (t, *J* = 7.1 Hz, 4H), 1.29 – 1.20 (m, 2H), 1.19 (s, 10H), 0.66 – 0.58 (m, 2H), 0.36 – 0.29 (m, 2H). ¹³C NMR (126 MHz, Chloroform-*d*) δ 166.23, 160.41, 131.01, 130.59, 127.24, 122.48, 110.58, 72.99, 60.65, 55.83, 45.46, 22.59, 14.33, 10.10, 3.24, 3.20.

Lithium (R)-3-(((tert-butylsulfinyl)amino)methyl)benzoate (145): See Procedure C: 285 mg (1.01 mmol) of **141**, 143 mg (5.97 mmol, 5.94 eq.) of LiOH, 2 mL of THF, 2 mL of EtOH, and 2 mL of H₂O. The compound was suspended and filtered in EtOH instead of acetone. Compound **145** (240 mg, Yield= 91 %) was isolated as a white solid. ¹H NMR (400 MHz, Methanol-*d*₄) δ 7.92 (d, *J* = 1.8 Hz, 1H), 7.85 (dt, *J* = 7.7, 1.5 Hz, 1H), 7.45 – 7.39 (m, 1H), 7.33 (t, *J* = 7.6 Hz, 1H), 4.34 (d, *J* = 14.4 Hz, 1H), 4.26 (d, *J* = 14.4 Hz, 1H), 1.24 (s, 9H). ¹³C NMR (101 MHz, Methanol-*d*₄) δ 173.83, 138.51, 137.91, 129.60, 128.53, 127.93, 127.48, 55.72, 48.76, 21.79.

Lithium (R)-3-(((tert-butylsulfinyl)amino)methyl)-4-methoxybenzoate (146): See Procedure C: 181 mg (0.58 mmol) of **142**, 86 mg (3.59 mmol, 6.21 eq.) of LiOH, 2 mL of THF, 2

mL of EtOH, and 2 mL of H₂O. Compound **146** (128 mg, Yield= 76 %) was isolated as a white solid. ¹H NMR (500 MHz, Methanol-*d*₄) δ 7.95 – 7.88 (m, 2H), 6.93 (d, *J* = 8.4 Hz, 1H), 4.32 (d, *J* = 14.4 Hz, 1H), 4.22 (d, *J* = 14.4 Hz, 1H), 3.87 (s, 3H), 1.22 (s, 9H). ¹³C NMR (126 MHz, Methanol-*d*₄) δ 173.83, 159.18, 130.41, 130.20, 129.69, 125.95, 109.03, 55.64, 54.63, 44.23, 21.74.

Lithium (R)-3-(((tert-butylsulfinyl)amino)methyl)-4-propoxybenzoate (147): See Procedure C: 272 mg (0.80 mmol) of **143**, 114 mg (4.76 mmol, 6.0 eq.) of LiOH, 2 mL of THF, 2 mL of EtOH, and 2 mL of H₂O. Compound **147** (226 mg, Yield= 89 %) was isolated as a colorless oil. ¹H NMR (400 MHz, Methanol-*d*₄) δ 7.92 (d, *J* = 2.2 Hz, 1H), 7.87 (dd, *J* = 8.5, 2.2 Hz, 1H), 6.91 (d, *J* = 8.6 Hz, 1H), 4.35 (d, *J* = 14.3 Hz, 1H), 4.23 (d, *J* = 14.3 Hz, 1H), 4.01 (t, *J* = 6.4 Hz, 2H), 1.85 (h, *J* = 7.4 Hz, 2H), 1.22 (s, 9H), 1.08 (t, *J* = 7.4 Hz, 3H). ¹³C NMR (101 MHz, Methanol-*d*₄) δ 173.91, 158.57, 130.34, 130.11, 129.48, 125.96, 109.75, 69.35, 55.63, 44.22, 22.32, 21.73, 9.67.

Lithium (R)-3-(((tert-butylsulfinyl)amino)methyl)-4-(cyclopropylmethoxy)benzoate (148): See Procedure C: 333 mg (0.94 mmol) of **144**, 135 mg (5.64 mmol, 5.98 eq.) of LiOH, 2 mL of THF, 2 mL of EtOH, and 2 mL of H₂O. Compound **148** (271 mg, Yield=87 %) was isolated as a white amorphous solid. ¹H NMR (500 MHz, Methanol-*d*₄) δ 7.93 (d, *J* = 2.2 Hz, 1H), 7.88 (dd, *J* = 8.5, 2.2 Hz, 1H), 6.89 (d, *J* = 8.6 Hz, 1H), 4.37 (d, *J* = 14.3 Hz, 1H), 4.25 (d, *J* = 14.4 Hz, 1H), 3.90 (d, *J* = 7.2 Hz, 2H), 1.30 (dddd, *J* = 11.6, 8.0, 4.7, 1.2 Hz, 2H), 1.23 (s, 12H), 0.67 – 0.59 (m, 2H), 0.41 – 0.35 (m, 2H). ¹³C NMR (126 MHz, Methanol-*d*₄) δ 173.84, 158.58, 130.38, 130.15, 129.60, 126.06, 110.05, 72.54, 55.65, 44.55, 21.77, 9.87, 2.28, 2.27.

(3-(pyrrolidine-1-carbonyl)phenyl)methanaminium trifluoroacetate (149): See Procedure D: Step 1: 24 mg (0.092 mmol) of **145**, 49 mg (0.094 mmol, 1.02 eq.) of PyBOP, 20 μ L (17 mg, 0.24 mmol, 2.6 eq.) of pyrrolidine, 100 μ L (92 mg, 0.91 mmol, 9.89 eq.) of NMM, and 4 mL of DMF. The compound was suspended in DCM and sat. Na_2CO_3 , extracted with DCM, and filtered after column chromatography. Step 2: 2 mL of dioxane and 0.2 mL conc. HCl. Compound **149** (12 mg, Yield=41 %) was isolated as a colorless oil. ^1H NMR (500 MHz, Methanol- d_4) δ 7.61 – 7.51 (m, 4H), 4.17 (s, 2H), 3.60 (t, $J = 7.0$ Hz, 2H), 3.45 (t, $J = 6.7$ Hz, 2H), 2.00 (p, $J = 6.5, 6.1$ Hz, 2H), 1.91 (p, $J = 6.7$ Hz, 2H). ^{13}C NMR (126 MHz, Methanol- d_4) δ 169.56, 137.54, 133.57, 130.29, 129.00, 127.28, 127.15, 49.36, 46.07, 42.52, 25.78, 23.90.

(3-(piperidine-1-carbonyl)phenyl)methanaminium trifluoroacetate (150): See Procedure D: Step 1: 20 mg (0.077 mmol) of **145**, 41 mg (0.079 mmol, 1.03 eq.) of PyBOP, 20 μ L (17 mg, 0.20 mmol, 2.6 eq.) of piperidine, 90 μ L (83 mg, 0.82 mmol, 10.7 eq.) of NMM, and 4 mL of DMF. Step 2: 2 mL of dioxane and 0.2 mL conc. HCl. Compound **150** (15 mg, Yield=59 %) was isolated as a colorless oil. ^1H NMR (500 MHz, Methanol- d_4) δ 7.60 – 7.51 (m, 2H), 7.47 (d, $J = 1.8$ Hz, 1H), 7.44 (dt, $J = 7.1, 1.6$ Hz, 1H), 3.72 (d, $J = 5.9$ Hz, 2H), 3.37 (t, $J = 5.4$ Hz, 2H), 1.76 – 1.63 (m, 4H), 1.54 (s, 2H). ^{13}C NMR (126 MHz, Methanol- d_4) δ 170.04, 136.87, 133.77, 129.94, 129.13, 126.96, 126.91, 48.62, 42.94, 42.53, 26.13, 25.28, 23.97.

(3-(isoindoline-2-carbonyl)phenyl)methanaminium trifluoroacetate (151): See Procedure D: Step 1: 21 mg (0.080 mmol) of **145**, 45 mg (0.086 mmol, 1.08 eq.) of PyBOP, 14 mg (0.090 mmol, 1.12 eq.) of isoindoline hydrochloride, 90 μ L (83 mg, 0.82 mmol, 10.2 eq.) of NMM, and 4 mL of DMF. Step 2: 2 mL of dioxane and 0.2 mL conc. HCl. Compound **151** (19 mg, Yield=65 %) was isolated as a colorless oil. ^1H NMR (500 MHz, DMSO- d_6) δ 8.29 (br s, 3H),

7.70 (t, $J = 1.6$ Hz, 1H), 7.62 (dt, $J = 7.4, 1.5$ Hz, 1H), 7.57 (dt, $J = 7.8, 1.6$ Hz, 1H), 7.52 (t, $J = 7.5$ Hz, 1H), 7.40 (d, $J = 6.5$ Hz, 1H), 7.34 – 7.21 (m, 3H), 4.87 (s, 2H), 4.76 (s, 2H), 4.11 (q, $J = 5.8$ Hz, 2H). ^{13}C NMR (126 MHz, DMSO- d_6) δ 168.97, 158.86, 158.58, 137.40, 137.21, 136.35, 134.74, 130.74, 129.20, 127.97, 127.87, 127.84, 127.38, 123.41, 123.12, 54.63, 52.49, 42.47.

(3-(1,2,3,4-tetrahydroisoquinoline-2-carbonyl)phenyl)methanaminium

trifluoroacetate (152): See Procedure D: Step 1: 16 mg (0.061 mmol) of **145**, 36 mg (0.069 mmol, 1.13 eq.) of PyBOP, 20 μL (21 mg, 0.16 mmol, 2.6 eq.) of 1,2,3,4-tetrahydroisoquinoline, 80 μL (74 mg, 0.73 mmol, 11.9 eq.) of NMM, and 5 mL of DMF. Step 2: 2 mL of dioxane and 0.2 mL conc. HCl. Compound **152** (17 mg, Yield=73 %) was isolated as a colorless oil. ^1H NMR (400 MHz, 50 $^\circ\text{C}$, Methanol- d_4) δ 7.62 – 7.41 (m, 5H), 7.17 (s, 3H), 4.77 (br s, 2H), 4.18 (s, 2H), 3.68 (br s, 2H), 2.92 (br s, 2H). ^{13}C NMR (101 MHz, 50 $^\circ\text{C}$, Methanol- d_4) δ 170.64, 136.84, 133.78, 132.44, 130.11, 129.20, 128.32, 127.16, 127.00, 126.57, 126.18, 42.63.

(2-methoxy-5-(pyrrolidine-1-carbonyl)phenyl)methanaminium trifluoroacetate

(153): See Procedure D: Step 1: 20 mg (0.069 mmol) of **146**, 37 mg (0.071 mmol, 1.03 eq.) of PyBOP, 20 μL (17 mg, 0.24 mmol, 3.5 eq.) of pyrrolidine, 80 μL (74 mg, 0.73 mmol, 10.6 eq.) of NMM, and 4 mL of DMF. Step 2: 2 mL of dioxane and 0.2 mL conc. HCl. Compound **153** (21 mg, Yield=88 %) was isolated as a colorless oil. ^1H NMR (500 MHz, Methanol- d_4) δ 7.65 (dd, $J = 8.5, 2.2$ Hz, 1H), 7.55 (d, $J = 2.3$ Hz, 1H), 7.15 (d, $J = 8.6$ Hz, 1H), 4.14 (s, 2H), 3.97 (s, 3H), 3.58 (t, $J = 7.0$ Hz, 2H), 3.51 (t, $J = 6.6$ Hz, 2H), 1.98 (p, $J = 6.9$ Hz, 2H), 1.91 (p, $J = 6.7$ Hz, 2H). ^{13}C NMR (126 MHz, Methanol- d_4) δ 169.44, 159.24, 130.20, 129.76, 128.82, 110.28, 55.09, 49.60, 46.25, 38.67, 25.89, 23.89.

(2-methoxy-5-(piperidine-1-carbonyl)phenyl)methanaminium trifluoroacetate (154):

See Procedure D: Step 1: 23 mg (0.079 mmol) of **146**, 42 mg (0.081 mmol, 1.02 eq.) of PyBOP, 20 μ L (17 mg, 0.20 mmol, 2.5 eq.) of piperidine, 90 μ L (83 mg, 0.82 mmol, 10.4 eq.) of NMM, and 4 mL of DMF. Step 2: 2 mL of dioxane and 0.2 mL conc. HCl. Compound **154** (23 mg, Yield=80 %) was isolated as a colorless oil. ^1H NMR (500 MHz, Methanol- d_4) δ 7.49 (dd, J = 8.5, 2.2 Hz, 1H), 7.41 (d, J = 2.1 Hz, 1H), 7.16 (d, J = 8.5 Hz, 1H), 4.13 (s, 2H), 3.97 (s, 3H), 3.69 (br s, 2H), 3.44 (br s, 2H), 1.74 – 1.51 (m, 6H). ^{13}C NMR (126 MHz, Methanol- d_4) δ 170.18, 158.97, 129.82, 129.49, 128.10, 121.24, 110.47, 55.08, 48.43, 38.67, 24.01, 20.05.

(5-(isoindoline-2-carbonyl)-2-methoxyphenyl)methanaminium trifluoroacetate (155):

See Procedure D: Step 1: 21 mg (0.072 mmol) of **146**, 39 mg (0.075 mmol, 1.04 eq.) of PyBOP, 12 mg (0.077 mmol, 1.07 eq.) of isoindoline hydrochloride, 80 μ L (74 mg, 0.73 mmol, 10.1 eq.) of NMM, and 4 mL of DMF. Step 2: 2 mL of dioxane and 0.2 mL conc. HCl. Compound **155** (26 mg, Yield=91 %) was isolated as a colorless oil. ^1H NMR (500 MHz, Methanol- d_4) δ 7.76 (dd, J = 8.5, 2.2 Hz, 1H), 7.64 (d, J = 2.2 Hz, 1H), 7.37 (d, J = 7.3 Hz, 1H), 7.34 – 7.26 (m, 2H), 7.22 (t, J = 7.3 Hz, 2H), 4.96 (s, 2H), 4.88 (s, 2H), 4.17 (s, 2H), 4.00 (s, 3H). ^{13}C NMR (126 MHz, Methanol- d_4) δ 170.13, 159.36, 136.29, 135.57, 130.16, 129.68, 128.39, 127.51, 127.33, 122.44, 122.15, 121.19, 110.48, 55.13, 54.69, 52.29, 38.66.

(2-methoxy-5-(1,2,3,4-tetrahydroisoquinoline-2-carbonyl)phenyl)methanaminium trifluoroacetate (156): See Procedure D: Step 1: 19 mg (0.065 mmol) of **146**, 34 mg (0.065 mmol, 1.0 eq.) of PyBOP, 40 μ L (42 mg, 0.32 mmol, 4.8 eq.) of 1,2,3,4-tetrahydroisoquinoline, 75 μ L (69 mg, 0.68 mmol, 10.0 eq.) of NMM, and 4 mL of DMF. Step 2: 2 mL of dioxane and 0.2 mL conc. HCl. Compound **156** (23 mg, Yield=86 %) was isolated as a colorless oil. ^1H NMR (400

MHz, 50 °C, Methanol-*d*₄) δ 7.56 (dd, $J = 8.5, 2.2$ Hz, 1H), 7.47 (d, $J = 2.1$ Hz, 1H), 7.20 – 7.13 (m, 4H), 7.07 (br s, 1H), 4.74 (br s, 2H), 4.15 (s, 2H), 3.98 (s, 3H), 3.80 (br s, 2H), 2.92 (t, $J = 6.1$ Hz, 2H). ¹³C NMR (101 MHz, 50 °C, Methanol-*d*₄) δ 159.24, 134.20, 132.60, 130.00, 129.60, 128.31, 128.17, 126.52, 126.14, 121.34, 110.66, 55.13, 38.75.

(2-propoxy-5-(pyrrolidine-1-carbonyl)phenyl)methanaminium trifluoroacetate

(157): See Procedure D: Step 1: 20 mg (0.063 mmol) of **147**, 33 mg (0.063 mmol, 1.01 eq.) of PyBOP, 20 μ L (17 mg, 0.24 mmol, 3.8 eq.) of pyrrolidine, 70 μ L (64 mg, 0.64 mmol, 10.2 eq.) of NMM, and 4 mL of DMF. Step 2: 2 mL of dioxane and 0.2 mL conc. HCl. Compound **157** (15 mg, Yield=64 %) was isolated as a colorless oil. ¹H NMR (500 MHz, Methanol-*d*₄) δ 7.63 (dd, $J = 8.5, 2.2$ Hz, 1H), 7.55 (d, $J = 2.2$ Hz, 1H), 7.14 (d, $J = 8.6$ Hz, 1H), 4.15 (s, 2H), 4.12 (t, $J = 6.6$ Hz, 2H), 3.58 (t, $J = 7.0$ Hz, 2H), 3.52 (t, $J = 6.5$ Hz, 2H), 1.99 (p, $J = 6.8$ Hz, 2H), 1.94 – 1.87 (m, 4H), 1.08 (t, $J = 7.4$ Hz, 3H). ¹³C NMR (126 MHz, Methanol-*d*₄) δ 169.54, 158.57, 130.11, 129.57, 128.56, 116.57, 111.10, 70.03, 46.29, 38.34, 25.90, 23.90, 21.90, 9.34.

(5-(piperidine-1-carbonyl)-2-propoxyphenyl)methanaminium trifluoroacetate (158):

See Procedure D: Step 1: 25 mg (0.078 mmol) of **147**, 41 mg (0.079 mmol, 1.0 eq.) of PyBOP, 20 μ L (17 mg, 0.20 mmol, 2.6 eq.) of piperidine, 90 μ L (83 mg, 0.82 mmol, 10.5 eq.) of NMM, and 4 mL of DMF. Step 2: 2 mL of dioxane and 0.2 mL conc. HCl. Compound **158** (24 mg, Yield=79 %) was isolated as a colorless oil. ¹H NMR (500 MHz, Methanol-*d*₄) δ 7.46 (dd, $J = 8.5, 2.2$ Hz, 1H), 7.41 (d, $J = 2.1$ Hz, 1H), 7.14 (d, $J = 8.5$ Hz, 1H), 4.14 (s, 2H), 4.11 (t, $J = 6.6$ Hz, 2H), 3.68 (br s, 2H), 3.44 (br s, 2H), 1.89 (h, $J = 7.4$ Hz, 2H), 1.75 – 1.61 (m, 4H), 1.55 (br s, 2H), 1.08 (t, $J = 7.4$ Hz, 3H). ¹³C NMR (126 MHz, Methanol-*d*₄) δ 170.32, 158.30, 129.73, 129.29, 127.79, 121.27, 111.30, 70.03, 38.34, 23.98, 21.89, 20.07, 9.34.

(5-(isoindoline-2-carbonyl)-2-propoxyphenyl)methanaminium trifluoroacetate (159):

See Procedure D: Step 1: 23 mg (0.072 mmol) of **147**, 39 mg (0.075 mmol, 1.0 eq.) of PyBOP, 15 mg (0.096 mmol, 1.3 eq.) of isoindoline hydrochloride, 80 μ L (74 mg, 0.73 mmol, 10.2 eq.) of NMM, and 4 mL of DMF. Step 2: 2 mL of dioxane and 0.2 mL conc. HCl. Compound **159** (23 mg, Yield=75 %) was isolated as a colorless oil. ^1H NMR (500 MHz, Methanol- d_4) δ 7.73 (dd, J = 8.5, 2.2 Hz, 1H), 7.64 (d, J = 2.2 Hz, 1H), 7.37 (d, J = 7.4 Hz, 1H), 7.30 (dt, J = 15.3, 7.0 Hz, 2H), 7.22 (d, J = 7.4 Hz, 1H), 7.19 (d, J = 8.6 Hz, 1H), 4.96 (s, 2H), 4.18 (s, 2H), 4.15 (t, J = 6.6 Hz, 2H), 1.92 (h, J = 7.4 Hz, 2H), 1.10 (t, J = 7.4 Hz, 3H). ^{13}C NMR (126 MHz, Methanol- d_4) δ 170.17, 158.67, 136.29, 135.57, 130.06, 129.48, 128.17, 127.51, 127.33, 122.44, 122.15, 121.24, 111.27, 70.06, 54.70, 52.30, 38.32, 21.92, 9.32.

(2-propoxy-5-(1,2,3,4-tetrahydroisoquinoline-2-carbonyl)phenyl)methanaminium

trifluoroacetate (160): See Procedure D: Step 1: 30 mg (0.094 mmol) of **147**, 49 mg (0.094 mmol, 1.0 eq.) of PyBOP, 20 μ L (21 mg, 0.16 mmol, 1.7 eq.) of 1,2,3,4-tetrahydroisoquinoline, 110 μ L (101 mg, 1.0 mmol, 10.7 eq.) of NMM, and 4 mL of DMF. Step 2: 2 mL of dioxane and 0.2 mL conc. HCl. Compound **160** (33 mg, Yield=80 %) was isolated as a colorless oil. ^1H NMR (400 MHz, 50 $^\circ\text{C}$, Methanol- d_4) δ 7.53 (dd, J = 8.5, 2.2 Hz, 1H), 7.48 (d, J = 2.1 Hz, 1H), 7.21 – 7.12 (m, 4H), 7.07 (br s, 1H), 4.73 (br s, 2H), 4.17 (s, 2H), 4.14 (t, J = 6.6 Hz, 2H), 3.80 (br s, 2H), 2.92 (br t, J = 6.1 Hz, 2H), 1.90 (h, J = 7.2 Hz, 2H), 1.08 (t, J = 7.4 Hz, 3H). ^{13}C NMR (101 MHz, 50 $^\circ\text{C}$, Methanol- d_4) δ 158.55, 134.20, 132.61, 129.88, 129.46, 128.31, 127.98, 126.53, 126.14, 121.42, 111.50, 70.23, 38.43, 21.90, 9.22.

(2-(cyclopropylmethoxy)-5-(pyrrolidine-1-carbonyl)phenyl)methanaminium

trifluoroacetate (161): See Procedure D: Step 1: 31 mg (0.094 mmol) of **148**, 49 mg (0.094 mmol,

1.01 eq.) of PyBOP, 20 μ L (17 mg, 0.24 mmol, 2.6 eq.) of pyrrolidine, 100 μ L (92 mg, 0.91 mmol, 9.7 eq.) of NMM, and 4 mL of DMF. Step 2: 2 mL of dioxane and 0.2 mL conc. HCl. Compound **161** (32 mg, Yield=88 %) was isolated as a colorless oil. ^1H NMR (500 MHz, Methanol- d_4) δ 7.61 (dd, $J = 8.5, 2.2$ Hz, 1H), 7.56 (d, $J = 2.2$ Hz, 1H), 7.11 (d, $J = 8.6$ Hz, 1H), 4.17 (s, 2H), 4.01 (d, $J = 7.0$ Hz, 2H), 3.58 (t, $J = 7.0$ Hz, 2H), 3.51 (t, $J = 6.7$ Hz, 2H), 1.99 (p, $J = 6.7$ Hz, 2H), 1.90 (p, $J = 6.5$ Hz, 2H), 1.39 – 1.31 (m, 1H), 0.69 – 0.63 (m, 2H), 0.44 – 0.38 (m, 2H). ^{13}C NMR (126 MHz, Methanol- d_4) δ 169.45, 158.58, 130.06, 129.56, 128.67, 121.12, 111.31, 73.29, 49.59, 46.24, 38.45, 25.89, 23.89, 20.05, 9.50, 2.24.

(2-(cyclopropylmethoxy)-5-(piperidine-1-carbonyl)phenyl)methanaminium

trifluoroacetate (162): See Procedure D: Step 1: 31 mg (0.094 mmol) of **148**, 49 mg (0.094 mmol, 1.01 eq.) of PyBOP, 20 μ L (17 mg, 0.20 mmol, 2.2 eq.) of piperidine, 100 μ L (92 mg, 0.91 mmol, 9.7 eq.) of NMM, and 4.5 mL of DMF. Step 2: 2 mL of dioxane and 0.2 mL conc. HCl. Compound **162** (25 mg, Yield=69 %) was isolated as a colorless oil. ^1H NMR (500 MHz, Methanol- d_4) δ 7.45 (d, $J = 8.4$ Hz, 1H), 7.42 (s, 1H), 7.12 (d, $J = 8.4$ Hz, 1H), 4.17 (s, 2H), 4.00 (d, $J = 6.9$ Hz, 2H), 3.68 (br s, 2H), 3.44 (br s, 2H), 1.72 (br s, 2H), 1.64 (br s, 2H), 1.56 (br s, 2H), 1.42 – 1.30 (m, 1H), 0.71 – 0.61 (m, 2H), 0.48 – 0.35 (m, 2H). ^{13}C NMR (126 MHz, Methanol- d_4) δ 170.20, 158.30, 129.68, 129.29, 127.96, 121.38, 111.51, 73.30, 38.45, 24.01, 9.50, 2.24.

(2-(cyclopropylmethoxy)-5-(isoindoline-2-carbonyl)phenyl)methanaminium

trifluoroacetate (163): See Procedure D: Step 1: 24 mg (0.072 mmol) of **148**, 39 mg (0.075 mmol, 1.04 eq.) of PyBOP, 11 mg (0.071 mmol, 0.98 eq.) of isoindoline hydrochloride, 80 μ L (74 mg, 0.73 mmol, 10.1 eq.) of NMM, and 4 mL of DMF. Step 2: 2 mL of dioxane and 0.2 mL conc. HCl. Compound **163** (26 mg, Yield=82 %) was isolated as a colorless oil. ^1H NMR (500 MHz,

Methanol-*d*₄) δ 7.72 (dd, *J* = 8.5, 2.2 Hz, 1H), 7.64 (d, *J* = 2.2 Hz, 1H), 7.37 (d, *J* = 7.4 Hz, 1H), 7.30 (dt, *J* = 15.3, 7.0 Hz, 2H), 7.22 (d, *J* = 7.3 Hz, 1H), 7.18 (d, *J* = 8.6 Hz, 1H), 4.96 (s, 2H), 4.88 (s, 2H), 4.21 (s, 2H), 4.04 (d, *J* = 7.0 Hz, 2H), 1.37 (dddd, *J* = 12.1, 9.9, 7.2, 3.4 Hz, 1H), 0.71 – 0.64 (m, 2H), 0.43 (dt, *J* = 6.2, 4.6 Hz, 2H). ¹³C NMR (126 MHz, Methanol-*d*₄) δ 170.15, 158.70, 136.30, 135.57, 130.02, 129.47, 128.22, 127.51, 127.32, 122.44, 122.15, 121.32, 111.51, 73.34, 54.69, 52.29, 38.45, 9.52, 2.27.

(2-(cyclopropylmethoxy)-5-(1,2,3,4-tetrahydroisoquinoline-2-carbonyl)phenyl)methanaminium trifluoroacetate (164): See Procedure D: Step 1: 28 mg (0.085 mmol) of **148**, 46 mg (0.089 mmol, 1.0 eq.) of PyBOP, 20 μ L (21 mg, 0.16 mmol, 1.9 eq.) of 1,2,3,4-tetrahydroisoquinoline, 100 μ L (92 mg, 0.91 mmol, 10.8 eq.) of NMM, and 4 mL of DMF. Step 2: 2 mL of dioxane and 0.2 mL conc. HCl. Compound **164** (30 mg, Yield=79 %) was isolated as a colorless oil. ¹H NMR (400 MHz, 50 °C, Methanol-*d*₄) δ 7.52 (dd, *J* = 8.5, 2.1 Hz, 1H), 7.48 (d, *J* = 1.9 Hz, 1H), 7.20 – 6.97 (m, 5H), 4.73 (s, 2H), 4.19 (s, 2H), 4.04 (d, *J* = 7.0 Hz, 2H), 3.80 (s, 2H), 2.92 (t, *J* = 6.1 Hz, 2H), 1.41 – 1.29 (m, 1H), 0.77 – 0.60 (m, 2H), 0.42 (qd, *J* = 4.6, 2.3 Hz, 2H). ¹³C NMR (101 MHz, 50 °C, Methanol-*d*₄) δ 158.58, 134.19, 132.61, 129.86, 129.42, 128.31, 128.04, 126.52, 126.14, 121.52, 111.81, 73.45, 38.59, 9.53, 2.22.

(S)-3-(4-hydroxy-2,6-dimethylphenyl)-1-oxo-1-((3-(pyrrolidin-1-ylmethyl)benzyl)amino)propan-2-aminium trifluoroacetate (165): See Procedure E and F: 29 mg (0.091 mmol) of **149**, 320 μ L (0.64 mmol, 7.03 eq.) of 2 M BH₃*Me₂S in THF, and 4 mL of THF. Step 1 of F: 160 μ L (119 mg, 0.92 mmol, 10.1 eq.) of N,N-diisopropylethylamine, 48 mg (0.092 mmol, 1.01 eq.) of PyBOP, 18 mg (0.11 mmol, 1.17 eq.) of 6-Cl-HOBt, 40 mg (0.098 mmol, 1.07 eq.) of Boc-O-Boc-L-2',6'-dimethyltyrosine, 3+1.5 mL of DMF. Step 2 of F: 2 mL

TFA and 2 mL DCM. Compound **165** (4.5 mg, Yield=10 %) was isolated as a white solid. (MS)EI: 382.2 (M+H), Retention Time: 14.47 min. ¹H NMR (500 MHz, Deuterium Oxide) δ 7.32 – 7.23 (m, 2H), 6.96 (s, 1H), 6.87 (d, *J* = 6.4 Hz, 1H), 6.27 (s, 2H), 4.32 (d, *J* = 14.8 Hz, 1H), 4.22 (d, *J* = 13.0 Hz, 1H), 4.15 (d, *J* = 13.0 Hz, 1H), 3.93 – 3.77 (m, 2H), 3.41 – 3.27 (m, 2H), 3.08 – 2.87 (m, 4H), 2.01 (dd, *J* = 12.5, 5.0 Hz, 2H), 1.92 (s, 6H), 1.86 – 1.73 (m, 2H).

(S)-3-(4-hydroxy-2,6-dimethylphenyl)-1-oxo-1-((3-(piperidin-1-ylmethyl)benzyl)amino)propan-2-aminium trifluoroacetate (166): See Procedure E and F: 16 mg (0.048 mmol) of **150**, 170 μL (0.34 mmol, 7.08 eq.) of 2 M BH₃*Me₂S in THF, and 4 mL of THF. Step 1 of F: 90 μL (67 mg, 0.52 mmol, 10.7 eq.) of N,N-diisopropylethylamine, 29 mg (0.056 mmol, 1.16 eq.) of PyBOP, 9 mg (0.053 mmol, 1.10 eq.) of 6-Cl-HOBt, 21 mg (0.051 mmol, 1.07 eq.) of Boc-O-Boc-L-2',6'-dimethyltyrosine, 3+1.5 mL of DMF. Step 2 of F: 2 mL TFA and 2 mL DCM. Compound **166** (11.5 mg, Yield=47 %) was isolated as a white solid. (MS)EI: 396.3 (M+H), Retention Time: 15.67 min. ¹H NMR (500 MHz, Deuterium Oxide) δ 7.95 (t, *J* = 6.0 Hz, 1H), 7.33 – 7.18 (m, 2H), 6.96 (s, 1H), 6.90 (d, *J* = 7.2 Hz, 1H), 6.28 (s, 2H), 4.38 – 4.28 (m, 1H), 4.13 (d, *J* = 13.2 Hz, 1H), 4.06 (d, *J* = 13.2 Hz, 1H), 3.95 – 3.82 (m, 2H), 3.29 (t, *J* = 12.4 Hz, 2H), 3.03 (dd, *J* = 13.9, 11.8 Hz, 1H), 2.94 (dd, *J* = 14.0, 5.0 Hz, 1H), 2.78 (qd, *J* = 13.1, 3.0 Hz, 2H), 1.93 (s, 6H), 1.78 (d, *J* = 12.7 Hz, 2H), 1.67 (dt, *J* = 13.4, 3.3 Hz, 1H), 1.60 – 1.46 (m, 2H), 1.32 (qt, *J* = 12.6, 3.5 Hz, 1H).

(S)-3-(4-hydroxy-2,6-dimethylphenyl)-1-((3-(isoindolin-2-ylmethyl)benzyl)amino)-1-oxopropan-2-aminium trifluoroacetate (167): See Procedure E and F: 16 mg (0.044 mmol) of **151**, 150 μL (0.30 mmol, 6.82 eq.) of 2 M BH₃*Me₂S in THF, and 4 mL of THF. Step 1 of F: 80 μL (59 mg, 0.46 mmol, 10.4 eq.) of N,N-diisopropylethylamine, 25 mg (0.048 mmol, 1.10 eq.) of

PyBOP, 11 mg (0.065 mmol, 1.48 eq.) of 6-Cl-HOBt, 20 mg (0.049 mmol, 1.12 eq.) of Boc-O-Boc-L-2',6'-dimethyltyrosine, 3+1.5 mL of DMF. Step 2 of F: 2 mL TFA and 2 mL DCM. Compound **167** (4.6 mg, Yield=19 %) was isolated as a white solid. (MS)EI: 430.2 (M+H), Retention Time: 19.30 min. ¹H NMR (500 MHz, Methanol-*d*₄) δ 8.31 (t, *J* = 5.7 Hz, 1H), 7.48 – 7.36 (m, 6H), 7.18 (d, *J* = 2.2 Hz, 1H), 7.06 (dt, *J* = 7.1, 1.7 Hz, 1H), 6.44 (s, 2H), 4.65 (s, 4H), 4.59 (d, *J* = 12.9 Hz, 2H), 4.54 (d, *J* = 12.8 Hz, 2H), 4.50 – 4.42 (m, 2H), 4.18 (dd, *J* = 15.2, 4.3 Hz, 1H), 3.91 (dd, *J* = 11.6, 4.7 Hz, 1H), 3.24 (dd, *J* = 13.8, 11.6 Hz, 1H), 3.02 (dd, *J* = 13.8, 4.7 Hz, 1H), 2.19 (s, 6H).

(S)-1-((3-((3,4-dihydroisoquinolin-2(1H)-yl)methyl)benzyl)amino)-3-(4-hydroxy-2,6-dimethylphenyl)-1-oxopropan-2-aminium trifluoroacetate (168): See Procedure E and F: 11 mg (0.029 mmol) of **152**, 100 μL (0.20 mmol, 6.92 eq.) of 2 M BH₃*Me₂S in THF, and 4 mL of THF. Step 1 of F: 50 μL (37 mg, 0.29 mmol, 9.93 eq.) of N,N-diisopropylethylamine, 17 mg (0.033 mmol, 1.13 eq.) of PyBOP, 5 mg (0.029 mmol, 1.02 eq.) of 6-Cl-HOBt, 12 mg (0.029 mmol, 1.01 eq.) of Boc-O-Boc-L-2',6'-dimethyltyrosine, 3+1.5 mL of DMF. Step 2 of F: 2 mL TFA and 2 mL DCM. Compound **168** (5.0 mg, Yield=31 %) was isolated as a white solid. (MS)EI: 444.3 (M+H), Retention Time: 20.66 min. ¹H NMR (500 MHz, Methanol-*d*₄) δ 8.31 (t, *J* = 5.7 Hz, 1H), 7.44 (d, *J* = 6.3 Hz, 2H), 7.37 – 7.25 (m, 3H), 7.20 (s, 1H), 7.16 (d, *J* = 7.4 Hz, 1H), 7.06 (d, *J* = 6.6 Hz, 1H), 6.45 (s, 2H), 4.50 – 4.34 (m, 5H), 4.17 (dd, *J* = 15.1, 4.2 Hz, 1H), 3.89 (dd, *J* = 11.6, 4.7 Hz, 1H), 3.76 (s, 1H), 3.42 (s, 1H), 3.25 – 3.14 (m, 3H), 3.01 (dd, *J* = 13.8, 4.8 Hz, 1H), 2.19 (s, 6H).

(S)-3-(4-hydroxy-2,6-dimethylphenyl)-1-((2-methoxy-5-(pyrrolidin-1-ylmethyl)benzyl)amino)-1-oxopropan-2-aminium trifluoroacetate (169): See Procedure E and F: 18 mg (0.052 mmol) of **153**, 180 μL (0.36 mmol, 6.96 eq.) of 2 M BH₃*Me₂S in THF, and 4

mL of THF. Step 1 of F: 90 μ L (67 mg, 0.52 mmol, 9.99 eq.) of N,N-diisopropylethylamine, 28 mg (0.054 mmol, 1.04 eq.) of PyBOP, 10 mg (0.059 mmol, 1.14 eq.) of 6-Cl-HOBt, 23 mg (0.056 mmol, 1.09 eq.) of Boc-O-Boc-L-2',6'-dimethyltyrosine, 3+1.5 mL of DMF. Step 2 of F: 2 mL TFA and 2 mL DCM. Compound **169** (11.6 mg, Yield=43 %) was isolated as a white solid. 412.3 (M+H), Retention Time: 14.69 min. ^1H NMR (500 MHz, Methanol- d_4) δ 7.95 (t, J = 5.9 Hz, 1H), 7.42 (dd, J = 8.4, 2.3 Hz, 1H), 7.14 (d, J = 2.3 Hz, 1H), 6.99 (d, J = 8.4 Hz, 1H), 6.34 (s, 2H), 4.40 – 4.32 (m, 1H), 4.29 (d, J = 13.0 Hz, 1H), 4.24 (d, J = 13.0 Hz, 1H), 4.14 (dd, J = 14.6, 4.6 Hz, 1H), 3.90 (dd, J = 11.8, 4.3 Hz, 1H), 3.74 (s, 3H), 3.53 – 3.38 (m, 2H), 3.22 – 3.06 (m, 3H), 2.95 (dd, J = 13.8, 4.4 Hz, 1H), 2.17 (br s, 2H), 2.06 (s, 6H), 2.04 – 1.97 (m, 2H).

(S)-3-(4-hydroxy-2,6-dimethylphenyl)-1-((2-methoxy-5-(piperidin-1-ylmethyl)benzyl)amino)-1-oxopropan-2-aminium trifluoroacetate (170): See Procedure E and F: 23 mg (0.063 mmol) of **152**, 220 μ L (0.44 mmol, 6.93 eq.) of 2 M $\text{BH}_3^*\text{Me}_2\text{S}$ in THF, and 4 mL of THF. Step 1 of F: 110 μ L (82 mg, 0.63 mmol, 9.95 eq.) of N,N-diisopropylethylamine, 33 mg (0.063 mmol, 1.00 eq.) of PyBOP, 13 mg (0.077 mmol, 1.21 eq.) of 6-Cl-HOBt, 28 mg (0.068 mmol, 1.08 eq.) of Boc-O-Boc-L-2',6'-dimethyltyrosine, 3+1.5 mL of DMF. Step 2 of F: 2 mL TFA and 2 mL DCM. Compound **170** (9.1 mg, Yield=27 %) was isolated as a white solid. 426.3 (M+H), Retention Time: 16.13 min. ^1H NMR (500 MHz, Methanol- d_4) δ 7.94 (t, J = 6.0 Hz, 1H), 7.41 (dd, J = 8.4, 2.3 Hz, 1H), 7.16 (d, J = 2.3 Hz, 1H), 7.00 (d, J = 8.4 Hz, 1H), 6.33 (s, 2H), 4.35 (dd, J = 14.5, 6.8 Hz, 1H), 4.22 – 4.12 (m, 3H), 3.89 (dd, J = 11.7, 4.4 Hz, 1H), 3.74 (s, 3H), 3.42 (t, J = 12.3 Hz, 2H), 3.12 (dd, J = 13.7, 11.8 Hz, 1H), 2.96 – 2.84 (m, 3H), 2.04 (s, 6H), 1.93 (d, J = 14.9 Hz, 2H), 1.84 (d, J = 13.7 Hz, 1H), 1.78 – 1.66 (m, 2H), 1.50 (qt, J = 12.5, 3.7 Hz, 1H).

(S)-3-(4-hydroxy-2,6-dimethylphenyl)-1-((5-(isoindolin-2-ylmethyl)-2-methoxybenzyl)amino)-1-oxopropan-2-aminium trifluoroacetate (171): See Procedure E and F: 25 mg (0.063 mmol) of **155**, 220 μ L (0.44 mmol, 6.97 eq.) of 2 M $\text{BH}_3 \cdot \text{Me}_2\text{S}$ in THF, and 4 mL of THF. Step 1 of F: 110 μ L (82 mg, 0.63 mmol, 10.0 eq.) of N,N-diisopropylethylamine, 33 mg (0.063 mmol, 1.00 eq.) of PyBOP, 13 mg (0.077 mmol, 1.21 eq.) of 6-Cl-HOBt, 27 mg (0.066 mmol, 1.04 eq.) of Boc-O-Boc-L-2',6'-dimethyltyrosine, 3+1.5 mL of DMF. Step 2 of F: 2 mL TFA and 2 mL DCM. Compound **171** (8.9 mg, Yield=30 %) was isolated as a white solid. (MS)EI: 460.3 (M+H), Retention Time: 19.61 min. ^1H NMR (500 MHz, Methanol- d_4) δ 7.98 (t, $J = 5.9$ Hz, 1H), 7.48 (dd, $J = 8.4, 2.3$ Hz, 1H), 7.45 – 7.36 (m, 4H), 7.21 (d, $J = 2.2$ Hz, 1H), 7.03 (d, $J = 8.4$ Hz, 1H), 6.32 (s, 2H), 4.65 (s, 4H), 4.52 (d, $J = 2.4$ Hz, 2H), 4.38 (dd, $J = 14.6, 6.9$ Hz, 1H), 4.16 (dd, $J = 14.6, 4.6$ Hz, 1H), 3.90 (dd, $J = 11.7, 4.3$ Hz, 1H), 3.76 (s, 3H), 3.12 (dd, $J = 13.7, 11.8$ Hz, 1H), 2.94 (dd, $J = 13.8, 4.4$ Hz, 1H), 2.05 (s, 6H).

(S)-1-((5-((3,4-dihydroisoquinolin-2(1H)-yl)methyl)-2-methoxybenzyl)amino)-3-(4-hydroxy-2,6-dimethylphenyl)-1-oxopropan-2-aminium trifluoroacetate (172): See Procedure E and F: 22 mg (0.054 mmol) of **156**, 190 μ L (0.38 mmol, 7.09 eq.) of 2 M $\text{BH}_3 \cdot \text{Me}_2\text{S}$ in THF, and 4 mL of THF. Step 1 of F: 100 μ L (74 mg, 0.57 mmol, 10.7 eq.) of N,N-diisopropylethylamine, 28 mg (0.054 mmol, 1.00 eq.) of PyBOP, 10 mg (0.059 mmol, 1.10 eq.) of 6-Cl-HOBt, 23 mg (0.056 mmol, 1.05 eq.) of Boc-O-Boc-L-2',6'-dimethyltyrosine, 3+1.5 mL of DMF. Step 2 of F: 2 mL TFA and 2 mL DCM. Compound **172** (3.4 mg, Yield=11 %) was isolated as a white solid. (MS)EI: 474.3 (M+H), Retention Time: 20.56 min. ^1H NMR (500 MHz, Deuterium Oxide) δ 7.39 (dd, $J = 8.5, 2.3$ Hz, 1H), 7.25 – 7.19 (m, 1H), 7.19 – 7.14 (m, 3H), 7.03 (d, $J = 7.5$ Hz, 1H), 6.90 (d, $J = 8.5$ Hz, 1H), 6.11 (s, 2H), 4.32 (d, $J = 13.5$ Hz, 3H), 4.24 (s, 2H), 3.88 (d, $J = 14.1$ Hz, 1H),

3.84 (dd, $J = 11.6, 5.1$ Hz, 1H), 3.52 (s, 5H), 3.07 (t, $J = 6.4$ Hz, 2H), 2.96 – 2.81 (m, 2H), 1.76 (s, 6H).

(S)-3-(4-hydroxy-2,6-dimethylphenyl)-1-oxo-1-((2-propoxy-5-(pyrrolidin-1-ylmethyl)benzyl)amino)propan-2-aminium trifluoroacetate (173): See Procedure E and F: 15 mg (0.040 mmol) of **157**, 140 μ L (0.28 mmol, 7.02 eq.) of 2 M $\text{BH}_3 \cdot \text{Me}_2\text{S}$ in THF, and 4 mL of THF. Step 1 of F: 70 μ L (52 mg, 0.40 mmol, 10.1 eq.) of *N,N*-diisopropylethylamine, 21 mg (0.040 mmol, 1.01 eq.) of PyBOP, 7 mg (0.041 mmol, 1.03 eq.) of 6-Cl-HOBt, 17 mg (0.042 mmol, 1.04 eq.) of Boc-O-Boc-L-2',6'-dimethyltyrosine, 3+1.5 mL of DMF. Step 2 of F: 2 mL TFA and 2 mL DCM. Compound **173** (1.6 mg, Yield=9 %) was isolated as a white solid. (MS)EI: 440.3 (M+H), Retention Time: 20.67 min. ^1H NMR (400 MHz, Methanol- d_4) δ 7.66 (t, $J = 6.0$ Hz, 1H), 7.40 (dd, $J = 8.4, 2.3$ Hz, 1H), 7.12 (d, $J = 2.3$ Hz, 1H), 6.99 (d, $J = 8.4$ Hz, 1H), 6.34 (s, 2H), 4.41 (dd, $J = 14.6, 6.8$ Hz, 1H), 4.26 (q, $J = 13.0$ Hz, 2H), 4.16 (dd, $J = 14.6, 4.5$ Hz, 1H), 3.95 – 3.80 (m, 3H), 3.52 – 3.36 (m, 2H), 3.24 – 3.06 (m, 3H), 2.94 (dd, $J = 13.8, 4.3$ Hz, 1H), 2.18 (br s, 2H), 2.03 (m, 8H), 1.70 (h, $J = 7.0$ Hz, 2H), 1.00 (t, $J = 7.4$ Hz, 3H).

(S)-3-(4-hydroxy-2,6-dimethylphenyl)-1-oxo-1-((5-(piperidin-1-ylmethyl)-2-propoxybenzyl)amino)propan-2-aminium trifluoroacetate (174): See Procedure E and F: 24 mg (0.062 mmol) of **158**, 220 μ L (0.44 mmol, 7.15 eq.) of 2 M $\text{BH}_3 \cdot \text{Me}_2\text{S}$ in THF, and 4 mL of THF. Step 1 of F: 110 μ L (82 mg, 0.63 mmol, 10.3 eq.) of *N,N*-diisopropylethylamine, 28 mg (0.061 mmol, 1.00 eq.) of PyBOP, 11 mg (0.065 mmol, 1.05 eq.) of 6-Cl-HOBt, 26 mg (0.063 mmol, 1.03 eq.) of Boc-O-Boc-L-2',6'-dimethyltyrosine, 3+1.5 mL of DMF. Step 2 of F: 2 mL TFA and 2 mL DCM. Compound **174** (4 mg, Yield=12 %) was isolated as a white solid. (MS)EI: 454.3 (M+H), Retention Time: 21.64 min. ^1H NMR (500 MHz, Methanol- d_4) δ 7.66 (t, $J = 5.8$ Hz,

1H), 7.39 (dd, $J = 8.4, 2.3$ Hz, 1H), 7.12 (d, $J = 2.3$ Hz, 1H), 6.99 (d, $J = 8.4$ Hz, 1H), 6.35 (s, 2H), 4.39 (dd, $J = 14.7, 6.8$ Hz, 1H), 4.24 – 4.11 (m, 3H), 3.98 – 3.82 (m, 3H), 3.41 (d, $J = 13.6$ Hz, 2H), 3.12 (dd, $J = 13.7, 11.9$ Hz, 1H), 2.98 – 2.83 (m, 3H), 2.04 (s, 6H), 1.94 (d, $J = 10.4$ Hz, 2H), 1.84 (d, $J = 13.5$ Hz, 1H), 1.79 – 1.65 (m, 4H), 1.50 (qt, $J = 12.6, 3.4$ Hz, 1H), 1.01 (t, $J = 7.4$ Hz, 3H).

(S)-3-(4-hydroxy-2,6-dimethylphenyl)-1-((5-(isoindolin-2-ylmethyl)-2-propoxybenzyl)amino)-1-oxopropan-2-aminium trifluoroacetate (175): See Procedure E and F: 23 mg (0.061 mmol) of **159**, 220 μ L (0.44 mmol, 7.2 eq.) of 2 M $\text{BH}_3 \cdot \text{Me}_2\text{S}$ in THF, and 4 mL of THF. Step 1 of F: 110 μ L (82 mg, 0.63 mmol, 10.3 eq.) of N,N-diisopropylethylamine, 32 mg (0.061 mmol, 1.01 eq.) of PyBOP, 11 mg (0.065 mmol, 1.06 eq.) of 6-Cl-HOBt, 25 mg (0.061 mmol, 1.00 eq.) of Boc-O-Boc-L-2',6'-dimethyltyrosine, 3+1.5 mL of DMF. Step 2 of F: 2 mL TFA and 2 mL DCM. Compound **175** (4.5 mg, Yield=14 %) was isolated as a white solid. (MS)EI: 488.3 (M+H), Retention Time: 25.13 min. ^1H NMR (400 MHz, Methanol- d_4) δ 7.72 (s, 1H), 7.46 (dd, $J = 8.4, 2.3$ Hz, 1H), 7.41 (d, $J = 2.0$ Hz, 4H), 7.17 (d, $J = 2.3$ Hz, 1H), 7.02 (d, $J = 8.5$ Hz, 1H), 6.32 (s, 2H), 4.65 (s, 2H), 4.63 (s, 2H), 4.51 (d, $J = 3.6$ Hz, 2H), 4.42 (dd, $J = 14.7, 4.5$ Hz, 1H), 4.19 (dd, $J = 14.6, 4.3$ Hz, 1H), 3.95 – 3.81 (m, 3H), 3.12 (dd, $J = 13.8, 12.4$ Hz, 1H), 2.94 (dd, $J = 13.8, 4.5$ Hz, 1H), 2.04 (s, 6H), 1.72 (h, $J = 7.0$ Hz, 2H), 1.01 (t, $J = 7.4$ Hz, 3H).

(S)-1-((5-((3,4-dihydroisoquinolin-2(1H)-yl)methyl)-2-propoxybenzyl)amino)-3-(4-hydroxy-2,6-dimethylphenyl)-1-oxopropan-2-aminium trifluoroacetate (176): See Procedure E and F: 33 mg (0.075 mmol) of **160**, 260 μ L (0.52 mmol, 6.93 eq.) of 2 M $\text{BH}_3 \cdot \text{Me}_2\text{S}$ in THF, and 4 mL of THF. Step 1 of F: 130 μ L (96 mg, 0.75 mmol, 9.95 eq.) of N,N-diisopropylethylamine, 39 mg (0.075 mmol, 1.00 eq.) of PyBOP, 13 mg (0.077 mmol, 1.02 eq.) of 6-Cl-HOBt, 31 mg

(0.076 mmol, 1.01 eq.) of Boc-O-Boc-L-2',6'-dimethyltyrosine, 3+1.5 mL of DMF. Step 2 of F: 2 mL TFA and 2 mL DCM. Compound **176** (7 mg, Yield=15 %) was isolated as a white solid. (MS)EI: 502.3 (M+H), Retention Time: 26.01 min. ¹H NMR (500 MHz, Deuterium Oxide) δ 7.51 (q, $J = 7.5$ Hz, 1H), 7.39 (dt, $J = 8.6, 3.1$ Hz, 1H), 7.27 – 7.15 (m, 4H), 7.05 (t, $J = 7.9$ Hz, 1H), 6.92 (dd, $J = 8.5, 3.0$ Hz, 1H), 6.17 (s, 2H), 4.39 – 4.19 (m, 6H), 3.99 – 3.84 (m, 3H), 3.75 – 3.62 (m, 3H), 3.36 – 3.25 (m, 1H), 3.13 – 3.02 (m, 2H), 2.96 – 2.78 (m, 2H), 1.72 (s, 6H), 1.47 (dtdd, $J = 27.3, 14.1, 6.8, 2.1$ Hz, 2H), 0.81 (t, $J = 7.4$ Hz, 3H).

(S)-1-((2-(cyclopropylmethoxy)-5-(pyrrolidin-1-ylmethyl)benzyl)amino)-3-(4-hydroxy-2,6-dimethylphenyl)-1-oxopropan-2-aminium trifluoroacetate (177): See Procedure E and F: 32 mg (0.082 mmol) of **161**, 290 μ L (0.58 mmol, 7.04 eq.) of 2 M BH₃*Me₂S in THF, and 4 mL of THF. Step 1 of F: 140 μ L (104 mg, 0.80 mmol, 9.75 eq.) of N,N-diisopropylethylamine, 43 mg (0.083 mmol, 1.00 eq.) of PyBOP, 14 mg (0.083 mmol, 1.00 eq.) of 6-Cl-HOBt, 35 mg (0.085 mmol, 1.04 eq.) of Boc-O-Boc-L-2',6'-dimethyltyrosine, 3+1.5 mL of DMF. Step 2 of F: 2 mL TFA and 2 mL DCM. Compound **177** (3.0 mg, Yield=6 %) was isolated as a white solid. (MS)EI: 452.3 (M+H), Retention Time: 20.81 min. ¹H NMR (500 MHz, Methanol-*d*₄) δ 7.66 (t, $J = 5.8$ Hz, 1H), 7.38 (dd, $J = 8.4, 2.4$ Hz, 1H), 7.10 (d, $J = 2.2$ Hz, 1H), 6.97 (d, $J = 8.4$ Hz, 1H), 6.35 (s, 2H), 4.42 (dt, $J = 14.8, 3.5$ Hz, 1H), 4.33 – 4.17 (m, 3H), 3.91 (dd, $J = 11.7, 4.4$ Hz, 1H), 3.78 (d, $J = 6.9$ Hz, 2H), 3.54 – 3.37 (m, 2H), 3.14 (dd, $J = 13.8, 11.8$ Hz, 3H), 2.95 (dd, $J = 13.8, 4.4$ Hz, 1H), 2.18 (s, 2H), 2.06 (s, 6H), 2.01 (s, 2H), 1.17 (tdd, $J = 10.2, 7.3, 3.5$ Hz, 1H), 0.64 – 0.51 (m, 2H), 0.37 – 0.24 (m, 2H).

(S)-1-((2-(cyclopropylmethoxy)-5-(piperidin-1-ylmethyl)benzyl)amino)-3-(4-hydroxy-2,6-dimethylphenyl)-1-oxopropan-2-aminium trifluoroacetate (178): See Procedure

E and F: 25 mg (0.062 mmol) of **162**, 220 μ L (0.44 mmol, 7.10 eq.) of 2 M $\text{BH}_3 \cdot \text{Me}_2\text{S}$ in THF, and 4 mL of THF. Step 1 of F: 110 μ L (82 mg, 0.63 mmol, 10.2 eq.) of N,N-diisopropylethylamine, 32 mg (0.061 mmol, 0.99 eq.) of PyBOP, 12 mg (0.071 mmol, 1.14 eq.) of 6-Cl-HOBt, 25 mg (0.061 mmol, 0.98 eq.) of Boc-O-Boc-L-2',6'-dimethyltyrosine, 3+1.5 mL of DMF. Step 2 of F: 2 mL TFA and 2 mL DCM. Compound **178** (1.8 mg, Yield=5 %) was isolated as a white solid. (MS)EI: 466.3 (M+H), Retention Time: 22.01 min. ^1H NMR (500 MHz, Methanol- d_4) δ 7.63 (t, J = 5.9 Hz, 1H), 7.37 (dd, J = 8.4, 2.3 Hz, 1H), 7.12 (d, J = 2.3 Hz, 1H), 6.97 (d, J = 8.5 Hz, 1H), 6.34 (s, 2H), 4.42 (dd, J = 14.7, 6.8 Hz, 1H), 4.24 – 4.13 (m, 3H), 3.90 (dd, J = 11.7, 4.4 Hz, 1H), 3.78 (d, J = 6.9 Hz, 2H), 3.47 – 3.37 (m, 3H), 3.13 (dd, J = 13.6, 11.9 Hz, 2H), 2.95 (dd, J = 14.1, 4.3 Hz, 2H), 2.93 – 2.82 (m, 2H), 2.05 (s, 6H), 1.97 – 1.91 (m, 2H), 1.84 (d, J = 13.6 Hz, 1H), 1.72 (p, J = 12.7 Hz, 2H), 1.51 (dddd, J = 16.9, 13.0, 8.2, 3.7 Hz, 1H), 1.16 (dddd, J = 15.5, 12.3, 7.6, 4.6 Hz, 1H), 0.59 (dd, J = 8.1, 1.8 Hz, 2H), 0.30 (pd, J = 4.2, 2.8 Hz, 2H).

(S)-1-((2-(cyclopropylmethoxy)-5-(isoindolin-2-ylmethyl)benzyl)amino)-3-(4-hydroxy-2,6-dimethylphenyl)-1-oxopropan-2-aminium trifluoroacetate (179): See Procedure E and F: 18 mg (0.041 mmol) of **163**, 145 μ L (0.29 mmol, 7.03 eq.) of 2 M $\text{BH}_3 \cdot \text{Me}_2\text{S}$ in THF, and 4 mL of THF. Step 1 of F: 70 μ L (52 mg, 0.40 mmol, 9.75 eq.) of N,N-diisopropylethylamine, 22 mg (0.042 mmol, 1.03 eq.) of PyBOP, 6 mg (0.035 mmol, 0.86 eq.) of 6-Cl-HOBt, 17 mg (0.042 mmol, 1.01 eq.) of Boc-O-Boc-L-2',6'-dimethyltyrosine, 3+1.5 mL of DMF. Step 2 of F: 2 mL TFA and 2 mL DCM. Compound **179** (2.2 mg, Yield=9 %) was isolated as a white solid. (MS)EI: 522.3 (M+H), Retention Time: 25.38 min. ^1H NMR (500 MHz, Methanol- d_4) δ 7.68 (t, J = 5.9 Hz, 1H), 7.49 – 7.36 (m, 5H), 7.17 (d, J = 2.2 Hz, 1H), 7.00 (d, J = 8.4 Hz, 1H), 6.32 (s, 2H), 4.66 (s, 2H), 4.63 (s, 2H), 4.53 (d, J = 12.9 Hz, 1H), 4.50 (d, J = 12.9 Hz, 1H), 4.44 (dt, J = 14.8, 3.5 Hz, 1H), 4.23 (dd, J = 14.7, 4.5 Hz, 1H), 3.92 (dd, J = 11.7, 4.4 Hz, 1H), 3.80 (d, J = 6.9 Hz, 2H), 3.13

(dd, $J = 13.8, 11.9$ Hz, 1H), 2.95 (dd, $J = 13.8, 4.4$ Hz, 1H), 2.05 (s, 6H), 1.22 – 1.08 (m, 1H), 0.67 – 0.49 (m, 2H), 0.31 (dq, $J = 5.2, 3.0, 2.4$ Hz, 2H).

(S)-1-((2-(cyclopropylmethoxy)-5-((3,4-dihydroisoquinolin-2(1H)-yl)methyl)benzyl)amino)-3-(4-hydroxy-2,6-dimethylphenyl)-1-oxopropan-2-aminium trifluoro-acetate (180): See Procedure E and F: 30 mg (0.067 mmol) of **164**, 230 μ L (0.46 mmol, 6.91 eq.) of 2 M $\text{BH}_3 \cdot \text{Me}_2\text{S}$ in THF, and 4 mL of THF. Step 1 of F: 120 μ L (89 mg, 0.69 mmol, 10.3 eq.) of N,N-diisopropylethylamine, 35 mg (0.067 mmol, 1.01 eq.) of PyBOP, 11 mg (0.065 mmol, 0.97 eq.) of 6-Cl-HOBt, 27 mg (0.066 mmol, 0.99 eq.) of Boc-O-Boc-L-2',6'-dimethyltyrosine, 3+1.5 mL of DMF. Step 2 of F: 2 mL TFA and 2 mL DCM. Compound **180** (7.0 mg, Yield=17 %) was isolated as a white solid. (MS)EI: 514.3 (M+H), Retention Time: 26.36 min. ^1H NMR (500 MHz, Deuterium Oxide) δ 7.63 (q, $J = 7.3$ Hz, 1H), 7.38 (dq, $J = 8.4, 3.1, 2.7$ Hz, 1H), 7.28 – 7.13 (m, 4H), 7.05 (t, $J = 8.4$ Hz, 1H), 6.89 (dd, $J = 8.5, 2.7$ Hz, 1H), 6.16 (s, 2H), 4.43 – 4.17 (m, 5H), 4.00 (dt, $J = 13.9, 4.1$ Hz, 1H), 3.87 (dt, $J = 10.6, 5.2$ Hz, 1H), 3.71 (dd, $J = 12.3, 5.3$ Hz, 1H), 3.56 (d, $J = 7.1$ Hz, 2H), 3.38 – 3.25 (m, 1H), 3.18 – 3.03 (m, 2H), 3.02 – 2.76 (m, 2H), 1.72 (s, 6H), 0.99 – 0.85 (m, 1H), 0.52 – 0.36 (m, 2H), 0.27 – 0.02 (m, 2H).

***In Vitro* Pharmacology**

Cell Lines and Membrane Preparations.

All *in vitro* opioid assays were performed by Ashley Brinkel, Jack Twarozynski, and Jessica Anand. Tissue culture reagents were purchased from Gibco Life Sciences (Grand Island, NY, U.S.) unless otherwise noted. C6-rat glioma cells stably expressing human MOR (C6-MOR) or human DOR (C6-DOR) and Chinese hamster ovary (CHO) cells stably expressing human KOR (CHO-KOR) were used for all *in vitro* assays. Cells were grown to confluence at 37 °C in 5% CO_2

in Dulbecco's modified Eagle medium (DMEM) containing 10% fetal bovine serum and 5% penicillin/streptomycin. Membranes were prepared by washing confluent cells three times with ice cold phosphate buffered saline (0.9% NaCl, 0.61 mM Na₂HPO₄, 0.38 mM KH₂PO₄, pH 7.4). Cells were detached from the plates by incubation in warm harvesting buffer (20 mM HEPES, 150 mM NaCl, 0.68 mM EDTA, pH 7.4) and pelleted by centrifugation at 1600 rpm for 3 min. The cell pellet was suspended in ice-cold 50 mM Tris- HCl buffer, pH 7.4, and homogenized with a Tissue Tearor (Biospec Products, Inc., Bartlesville, OK, U.S.) for 20 s. The homogenate was centrifuged at 15,000 rpm for 20 min at 4°C. The pellet was rehomogenized in 50 mM Tris-HCl with a Tissue Tearor for 10 s, followed by recentrifugation. The final pellet was resuspended in 50 mM Tris-HCl and frozen in aliquots at -80°C. Protein concentration was determined via a BCA protein assay (Thermo Scientific Pierce, Waltham, MA, U.S.) using bovine serum albumin as the standard.

Radioligand Competition Binding Assays.

Radiolabeled compounds were purchased from Perkin-Elmer (Waltham, MA, U.S.). Opioid ligand binding assays were performed by competitive displacement of 0.2 nM [³H]-diprenorphine (250 µCi, 1.85 TBq/mmol) by the peptidomimetic from membrane preparations containing opioid receptors as described above. The assay mixture, containing membranes (20 µg protein/tube) in 50 mM Tris-HCl buffer (pH 7.4), 0.2 nM [³H]-diprenorphine, and various concentrations of test peptidomimetic, was incubated at room temperature on a shaker for 1 h to allow binding to reach equilibrium. The samples were rapidly filtered through Whatman GF/C filters using a Brandel harvester (Brandel, Gaithersburg, MD, U.S.) and washed three times with 50 mM Tris-HCl buffer, pH 7.4. Bound radioactivity on dried filters was determined by liquid scintillation counting, after saturation with EcoLume liquid scintillation cocktail, in a Wallac 1450 MicroBeta (Perkin-Elmer, Waltham, MA, U.S.). Nonspecific binding was determined using 10

μM naloxone. The results presented are the mean \pm standard error (S.E.M.) from at least three separate assays performed in duplicate. K_i (nM) values were calculated using nonlinear regression analysis to fit a logistic equation to the competition data using GraphPad Prism, version 6.0c, (GraphPad Software Inc., La Jolla, CA).

[^{35}S]-GTP γS Binding Assays.

Agonist stimulation of [^{35}S]guanosine 5'-O-[γ -thio]triphosphate ([^{35}S]-GTP γS , 1250 Ci, 46.2 TBq/mmol) binding to G protein was measured as described previously.⁸² Briefly, membranes (10 μg of protein/well) were incubated for 1 h at 25°C in GTP γS buffer (50 mM Tris-HCl, 100 mM NaCl, 5 mM MgCl₂, 1 mM EDTA, pH 7.4) containing 0.1 nM [^{35}S]-GTP γS , 30 μM guanosine diphosphate (GDP), and varying concentrations of test peptidomimetic. G protein activation following receptor activation by peptidomimetic was compared with 10 μM of the standard compounds [D-Ala²,N-MePhe⁴,Gly-ol]enkephalin (DAMGO) at MOR, D-Pen^{2,5}-enkephalin (DPDPE) at DOR, or U69,593 at KOR. The reaction was terminated by vacuum filtration through GF/C filters that were washed 5 times with GTP γS buffer. Bound radioactivity was measured as described above. The results are presented as the mean \pm standard error (S.E.M.) from at least three separate assays performed in duplicate; potency (EC₅₀ (nM)) and percent stimulation were determined using nonlinear regression analysis with GraphPad Prism, as above.

Mouse Liver Microsome Stability Assays

All liver microsome assays were performed by Quintara Biosciences. Metabolic stability of testing compounds was evaluated using mouse liver microsomes to predict intrinsic clearance. Mouse liver microsome tissue fractions were obtained from Corning or BioreclamationIVT. The assay was carried out in 96-well microtiter plates at 37°C. Reaction mixtures (25 μL) contained a

final concentration of 1 μ M test compound, 0.1 mg/mL liver microsome protein, and 1 mM NADPH in 100 mM potassium phosphate, pH 7.4 buffer with 3 mM MgCl₂. At each of the time points (0, 15, 30, and 60 minutes), 150 μ L of quench solution (acetonitrile with 0.1% formic acid) with internal standard (bucetin) was transferred to each well. Verapamil was included as a positive control to verify assay performance. Plates were sealed, vortexed, and centrifuged at 4°C for 15 minutes at 4000 rpm. The supernatant was transferred to fresh plates for LC/MS/MS analysis. All samples were analyzed on LC/MS/MS using an AB Sciex API 4000 instrument, coupled to a Shimadzu LC-20AD LC Pump system. Analytical samples were separated using a Waters Atlantis T3 dC18 reverse phase HPLC column (20 mm x 2.1 mm) at a flow rate of 0.5 mL/min. The mobile phase consists of 0.1% formic acid in water (solvent A) and 0.1% formic acid in acetonitrile (solvent B). The extent of metabolism was calculated as the disappearance of the test compound, compared to the 0-min time incubation. Initial rates were calculated for the compound concentration and used to determine $t_{1/2}$ values and subsequently, the intrinsic clearance.

Molecular Modeling

All *in silico* experiments were performed by Irina Pogozheva. Modeling of three-dimensional (3D) structures of receptor-ligand complexes was based on available X-ray structures of the mouse MOR (PDB ID: 5c1m)⁸³ in the active conformation, human KOR (PDB IDs: 4djh)¹²⁵ in the inactive conformation, and human DOR in the inactive conformation (PDB IDs: 4rwa)¹²⁶. Structures of peptidomimetic ligands were generated using the 3D-Builder Application of QUANTA (Accelrys, Inc) followed by Conformational Search included in the program package. Low-energy ligand conformations (within 2 kcal/mol) that demonstrated the best superposition of aromatic substituents of the ligand core with the pharmacophore elements (DMT and tetrahydroquinoline pendant) of receptor-bound conformations of peptidomimetics were selected

for docking into the receptor binding pocket. Ligands were positioned inside the receptor binding cavity to reproduce the binding modes of peptidomimetics and co-crystallized ligands in MOR, DOR, and KOR X-ray structures. The docking pose of each ligand was subsequently refined using the solid docking module of QUANTA.

Animals and *In Vivo* Solutions

All *in vivo* assays were performed by Bryan Sears. Animal care and experimental procedures complied with the US National Research Council's Guide for the Care and Use of Laboratory Animals.⁹¹ Animal studies are reported in compliance with the ARRIVE guidelines.^{92,93} Mice were group-housed with a maximum of five animals per cage in clear polypropylene cages with corn cob bedding and nestlets as enrichment. Mice had free access to food and water at all times. Animals were housed in pathogen-free rooms maintained between 68 and 79 °F and humidity between 30 and 70 % humidity with a 12 h light/dark cycle with lights on at 07:00 h. Experiments were conducted in the housing room during the light cycle. All studies utilize male C57BL/6 mice from Envigo laboratories. Wild type mice weighing between 20-30 g at 7-15 weeks old, were used for behavioral experiments. All drug solutions were injected at a volume of 10 ml/kg. All drugs were dissolved in 9:1 DMSO/saline solution except for morphine sulphate and 0.6 % acetic acid which were dissolved in saline and water, respectively. All drugs were given sc. except for 0.6 % acetic acid which was given ip.

Acetic Acid Stretch Assay (AASA)

Antinociceptive effects were evaluated in the mouse acetic acid stretch assay in which a noxious stimulus is administered ip. that induces a stretching behavior characterized by constriction of the abdomen followed by extension of the hind limbs. Mice received an injection

of 0.6 % acetic acid, placed individually in clear plastic observation cages (10 x 6 x 8 in) with bedding, and the number of stretches were recorded for 20 min. Antinociceptive effects were determined with a 30 min pretreatment dose of compound sc. followed by 0.6 % acetic acid ip. A 5 min latency period after acetic acid injection was establish and total number of stretches were recorded for the following 20 min.

Chapter 6: Aromatic-Amine Pharmacophore Enables Removal of Aromatic Core

6.1 Introduction

In the previous chapter, we discovered that incorporation of the aromatic-amine pharmacophore onto our monocyclic core system produced potent and efficacious MOR-agonists whose activity was insensitive to functional changes to the aromatic core. In fact, a core containing a simple aromatic ring in conjunction with a tetrahydroisoquinoline pendant produced a potent superagonist. Since MOR-agonism appears thus far to not be affected negatively by elimination of structural elements on the core, we were interested in the scope upon which these structural elements may be removed (**Figure 18A**). We therefore decided to remove the aromatic core entirely, relying instead on simple alkyl, peptide, ether, or amine groups to hold the peptidomimetic together. This represents a radical change from our original bicyclic core peptidomimetics, and this further structural simplification enables shorter syntheses of novel analogues and more rapid diversification.

It should be noted that this structural simplification will increase the conformational flexibility of these ligands. Previously, our lab reported a series of 4-substituted piperidine and piperazines as bifunctional MOR/DOR ligands.⁷⁰ Despite good binding affinity at MOR and DOR, these ligands possessed poor MOR-efficacy and potency. As such, further derivatization of these ligands was not pursued. However, the discovery of our aromatic-amine pharmacophore has inspired us to return to these analogues. One of the most potent and efficacious analogues in this previous series possessed its aromatic core seven atoms away from the dimethyltyrosine pendant,

the same as that in our aromatic-amine analogues as shown in **Figure 18B**. Since efficacy was an issue with these ligands, we opted to incorporate an amine into the structure in the form of a tetrahydroisoquinoline pendant. This pendant was selected as it produced the most potent MOR analogues and yielded the highest levels of efficacy. This will briefly allow comparisons to the other tetrahydroisoquinoline pendants in this chapter and determine if these more rigid cores are viable for further derivatization.

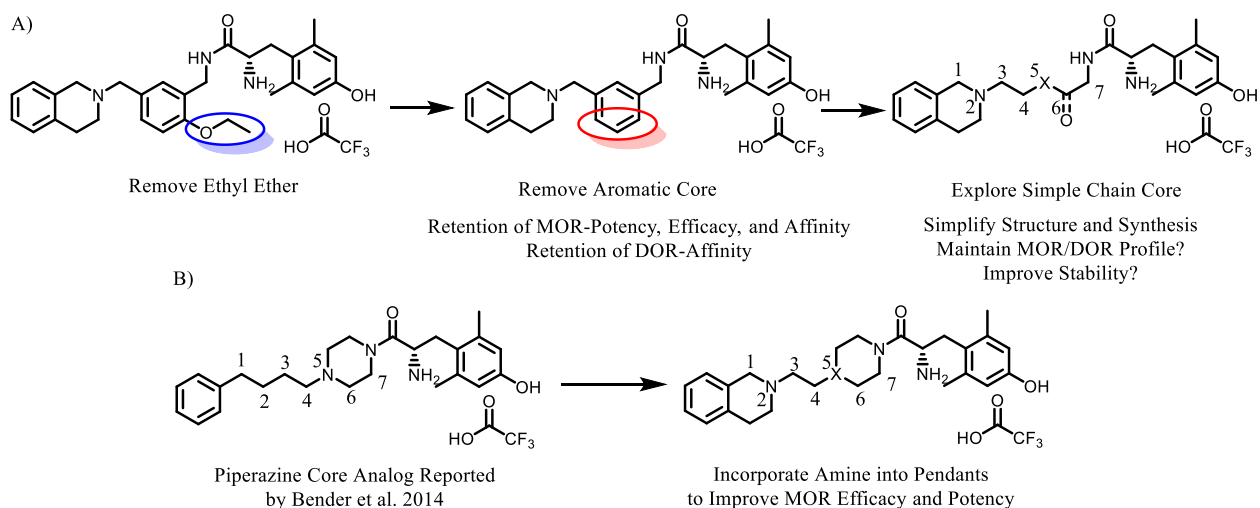


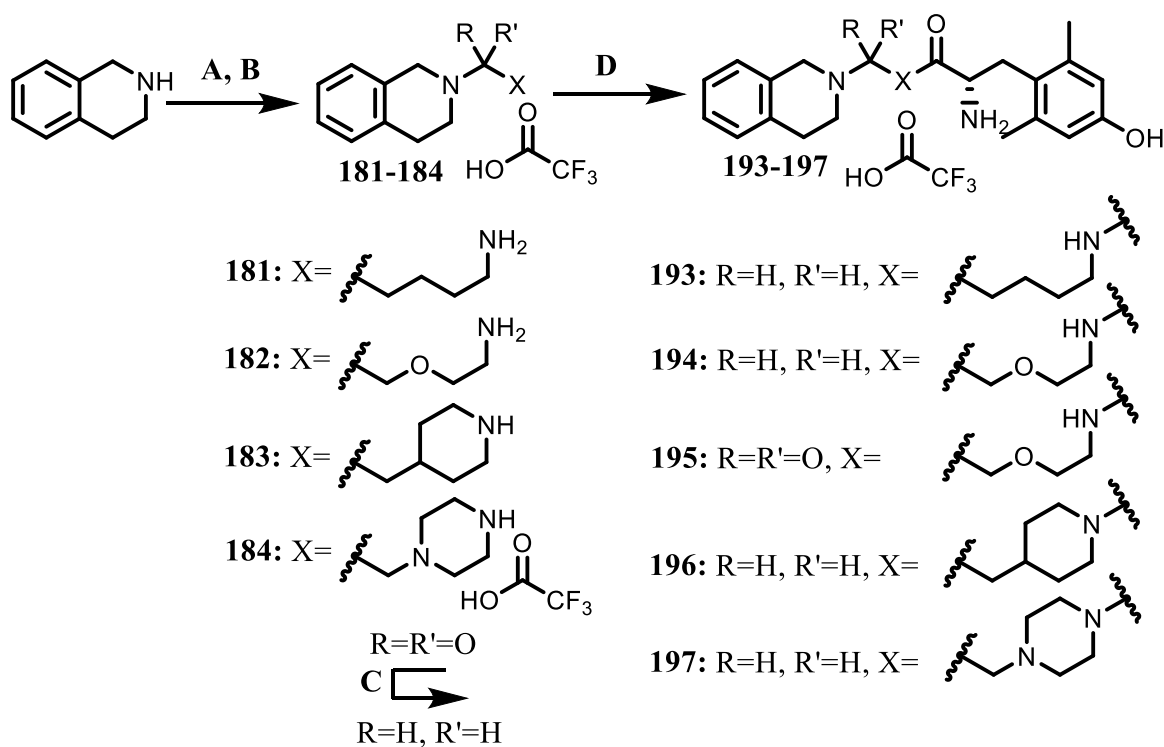
Figure 18: A) Design of analogues possessing greater simplification of core elements. These analogues utilized the tetrahydroisoquinoline pendant, which produced a superagonist at MOR using an unfunctionalized aromatic core. B) Design of more rigid analogues that use the tetrahydroisoquinoline pendant. These were inspired by previously described piperazine core analogues.

6.2 Results

General Chemistry: The synthesis of many of these new analogues required very few steps and most are described in **Scheme 9**. These include a simple alkyl chain, a chain possessing an ether, and the piperidine and piperazine core structures aimed at producing conformational restrictions. An amide analogue was also synthesized to confirm if the efficacy produced at MOR is a product of the amine and not the product of conformational restrictions induced by an amide. The only

amide analogues synthesized thus far are **135** and **136**, of which the amide was conjugated to the aromatic core. The synthesis here began with peptide coupling of tetrahydroisoquinoline to an appropriate Boc-protected δ -amino acid. The Boc group was removed with conc. HCl, and the tertiary amide was reduced with $\text{BH}_3 \cdot \text{Me}_2\text{S}$ at 65 °C if necessary. The primary amine was then coupled to Boc-protected 2',6'-dimethyltyrosine, at which point the Boc-groups were removed with TFA, yielding the final peptidomimetic.

Scheme 9: Synthesis of Analogues 193-197.

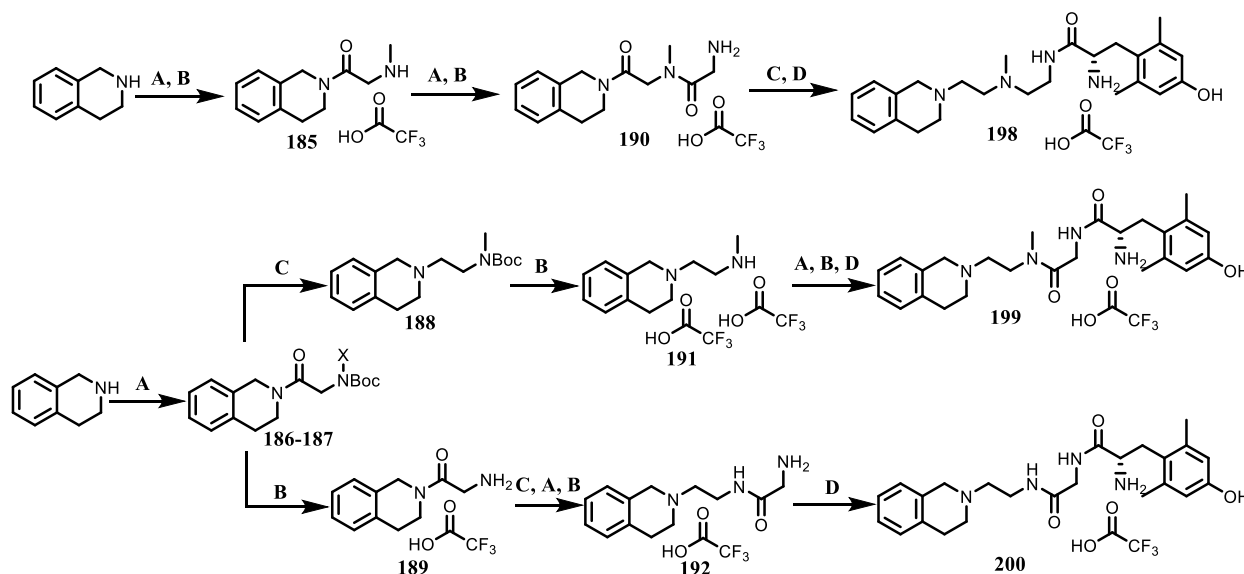


A) 1. $\text{HO}_2\text{C-X-Boc}$, NMM, PyBOP, DMF B) conc. HCl, Dioxane or TFA, DCM. C) $\text{BH}_3 \cdot \text{Me}_2\text{S}$, THF, 65 °C D) 1. DiBocDMT, DIEA, PyBOP, 6-Cl-HOBt, DMF. 2. TFA, DCM.

The analogues that contained a peptide bond or amine in the chain required a slightly modified procedure and are described in **Scheme 10**. Analogue **198**, which possesses a tertiary amine in the chain, was synthesized using peptide coupling of tetrahydroisoquinoline to N-Boc sarcosine using PyBOP, at which point the Boc group was removed with conc. HCl. This was then

coupled to N-Boc glycine and deprotected using the same method. Both peptide bonds were then reduced with $\text{BH}_3 \cdot \text{Me}_2\text{S}$ and the primary amine was then coupled to Boc-protected 2',6'-dimethyltyrosine, at which point the Boc-groups were removed with TFA, yielding **198**.

Scheme 10: Synthesis of Peptide Core Analogues 198-200.



A) 1. $\text{HO}_2\text{C}-\text{CH}_2-\text{NXBoc}$, NMM, PyBOP, DMF B) conc. HCl, Dioxane or TFA, DCM. C) $\text{BH}_3 \cdot \text{Me}_2\text{S}$, THF, $65\text{ }^\circ\text{C}$ D) 1. DiBocDMT, DIEA, PyBOP, 6-Cl-HOBt, DMF. 2. TFA, DCM.

Two additional analogues containing whole peptide bonds in the chain were also synthesized. These two analogues largely used the same steps as those for the simpler analogues above but used slightly different synthetic strategies. As described in **Scheme 10**, tetrahydroisoquinoline was coupled to N-Boc protected glycine or sarcosine. These intermediates were isolated before Boc deprotection, at which point the synthetic schemes diverged. The sarcosine intermediate **186** was then subject to reduction with borane before removal of the Boc group, yielding intermediate **191**. This was coupled to glycine and deprotected. No extensive purification of this intermediate was performed, as this analogue had poor UV absorbance properties and the impurities present were peptide coupling side products, which were going to be

present in the subsequent coupling to DMT. As such, DMT coupling was performed on this impure mixture and subsequent deprotection yielded the N-methyl amide **199**. For the glycine intermediate **187**, Boc deprotection was performed before reduction, as the secondary carbamate was unstable under these reduction conditions. This was then coupled to an additional glycine residue, yielding intermediate **192** with better UV absorbance properties than its sarcosine counterpart. After Boc deprotection, the intermediate was then coupled to DMT, yielding **200** after another deprotection.

SAR: The binding affinities of these analogues were screened and are shown in **Table 19**. For comparison, the superagonist **168** from the previous chapter was included. With regard to MOR-binding, each analogue in this series possessed single-digit or sub-nanomolar affinity. At DOR, elimination of the core aromatic ring produced well over a ten-fold drop in affinity. The exceptions here are the rigid piperazine **197** and the two amide analogues **199** and **200**. KOR-binding does not change significantly from the original lead **168**, the only exception here being the sarcosine analogue **199**, which has low KOR-affinity. Finally, this series generated analogues that deviate from our original MOR/DOR bifunctional profile and instead appear to promote a MOR/KOR profile. The exception here exists again with the piperazine and amide analogues, due to their ability to maintain high DOR affinity and/or to reduce KOR affinity.

The potency and efficacy of these analogues were also screened in each of these receptors and are shown in **Table 20**. Each of the amine pendant analogues possessed high MOR-efficacy, though were not superagonists like analogue **168**. The amide analogue **195**, while showing significantly reduced MOR-efficacy compared to its amine counterpart **194**, retained upwards of 48 % stimulation. The MOR-potency of these did not vary much compared to **168**, though there were few exceptions. Here the exceptions consist with the rigid piperidine analogue **197**, and the

sarcosine analogue **199**, both of which expressed at least a log unit loss in potency. It should be noted also that conversion to the amide **195** did not affect potency.

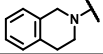
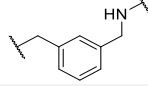
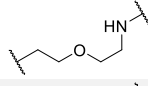
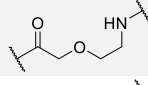
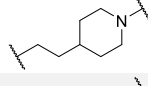
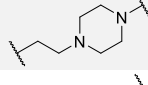
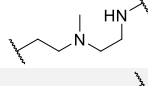
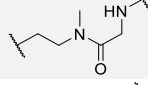
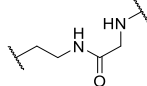
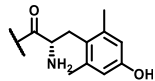
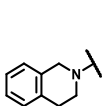
Name	Structure	Binding Affinity, K_i (nM)			Selectivity
		MOR	DOR	KOR	
168		0.23±0.02	4.8±1.0	36.9±3.1*	1:21:160
193		1.5±0.3	142±16	44.2±5.6	1:93:29
194		0.36**	105**	45±12	1:290:125
195		7.8±6.3*	261**	20.6**	1:1373:108
196		0.98**	42.2**	30.5**	1:43:31
197		3.67**	9.55**	124±69*	1:2.6:34
198		0.39**	211**	9.51**	1:540:24
199		6.07**	25.8**	1800±1300*	1:4.3:289
200		1.32±0.38	7.3±1.5	107±35	1:5.5:81

Table 19: Binding affinity of simple core compounds at MOR, DOR, and KOR. Binding affinities (K_i) were obtained by competitive displacement of radiolabeled [3 H] diprenorphine in membrane preparations. Included is **168** for comparison. Selectivity was calculated by dividing the K_i of each receptor by the K_i at MOR for a given compound. All data were from three separate experiments, performed in duplicate unless otherwise noted. These data are reported as the average \pm standard error of the mean. ** N=1, * N=2

DOR-agonism was found to be low in this series. Analogues that did stimulate DOR were weak partial agonists with low potency and efficacy. The greatest efficacy at DOR occurred with the ether analogue **194** and the glycine analogue **200**. This DOR-efficacy was eliminated with the piperazine **197**, the alkyl chain analogue **193**, and the amide analogue **195**. At KOR, these



Potency, EC₅₀ (nM)

Efficacy (% Stimulation)

Name	Structure	MOR	DOR	KOR	MOR	DOR	KOR
168		8.9±2.9	370±190	DNS	148±13	47±12	DNS
193		15.4±1.3	DNS	DNS	80.8±4.5	DNS	DNS
194		10.3±3.7	316±65	921±162*	95.0±7.4	32±16	20.9±4.0*
195		26±20*	DNS*	DNS*	47.9±3.6*	DNS*	DNS*
196		300±220	DNS	DNS*	70±15	DNS	DNS*
197		26.9**	DNS*	>3000**	91.3**	DNS*	>50**
198		24±10	1240±720*	427*	80.0±9.5	27.6±0.5*	34.5*
199		173**	567**	DNS**	88.3**	23.3**	DNS**
200		6.0±1.0	113.5±9.4*	DNS*	86.6±3.3	40.2±1.4	DNS*

Table 20: Potency and efficacy of simple core compounds at MOR, DOR, and KOR. Potency and efficacy data were obtained using agonist induced stimulation of [³⁵S] GTPγS binding. Potency is represented as EC₅₀ (nM) and efficacy as percent maximal stimulation relative to standard agonist DAMGO (MOR), DPDPE (DOR), or U69,593 (KOR) at 10 μM. Included is **168** for comparison. All data were from three separate experiments, performed in duplicate unless otherwise noted. These data are reported as the average ± standard error of the mean. ** N=1, * N=2. DNS=Does Not Stimulate.

analogues either could not stimulate this receptor or were weak partial agonists with very low potency.

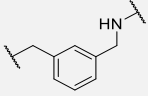
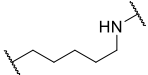
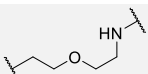
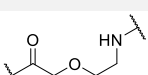
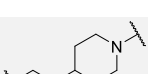
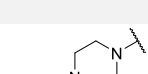



<i>Name</i>	<i>Structure</i>	$T_{1/2}$ (min)	Verapamil $T_{1/2}$ (min)	Stability Ratio	<i>cLogP</i>
168		34.9±4.7	25.7±1.7	1.4±0.2	4.12
193		38.9±2.8	27.6±4.9	1.4±0.3	3.29
194		15.7±1.2	28.1±7.4	0.56±0.15	2.92
195		61.3±4.2	28.1±7.4	2.18±0.59	1.80
196		>120	28.1±7.4	>4.27	3.56
197		79±25	28.1±7.4	2.8±1.2	3.38
198		34.7±1.4	28.1±7.4	1.23±0.33	3.40
199		44±11	28.1±7.4	1.57±0.57	2.80
200		16.6±1.5	27.6±4.9	0.60±0.12	2.26

Table 21: Metabolic stability of simple core compounds in MLM. Included are the compound half-life ($T_{1/2}$), the half-life of the positive control verapamil, and the stability ratio between the compound and the positive control. The stability ratio was calculated by dividing the half-life of the analogue of interest by the half-life of the positive control in that assay. Included is compound **168** for comparison. Individual compounds were tested once, with errors representing the SE in the decay curve regressed onto the data collected in 15-minute intervals. Finally, the *cLogP* of these analogues are included and were calculated using PerkinElmer's ChemDraw® Professional Software.

Metabolic Stability: The metabolic stability of these simplified analogues was also evaluated (**Table 21**). Simple elimination of the core to produce **193** yielded no improvements in stability when compared to **168**. Curiously, incorporation of an ether into this simple alkyl chain (**194**) managed to reduce stability by nearly a factor of 3. The amide of **194** (**195**) subsequently improved the stability of **194** by a factor of 4. The most interesting data came from the piperidine (**196**) and piperazine (**197**) core analogues. Here, the $T_{1/2}$ was greater than 2 hours for **196** and 79 minutes for **197**. Breaking the piperazine ring to produce **198** eliminated these improvements, cutting their stability in half. Finally, the two peptide analogues were also analyzed, with the N-methyl analogue **199** being 2.5 times more stable than desmethyl analogue **200** which was worse than the positive control.

Molecular Modeling: Since we produce of MOR/KOR analogue with a simple alkyl core, analogue **193** was then subject to molecular docking studies (**Figure 19**). This ligand was docked to MOR in the active state, and to DOR and KOR in the inactive state. The interactions that may be present at MOR are largely the same as those for analogue **168** described in Chapter 5. The amine interacts with Asn127 and the aromatic ring interacts with Trp133. The same is true at DOR, with the aromatic ring possessing interactions with Lys108 and a possible interaction with Trp114. The amine, likewise, interacts with the phenol of Tyr109. At KOR, a new interaction appears to emerge. In addition to those provided by Trp124 and Gln115 described previously, the amine also interacts with the phenol of Tyr312. Tyr312 simultaneously interacts with the amide of the DMT residue.

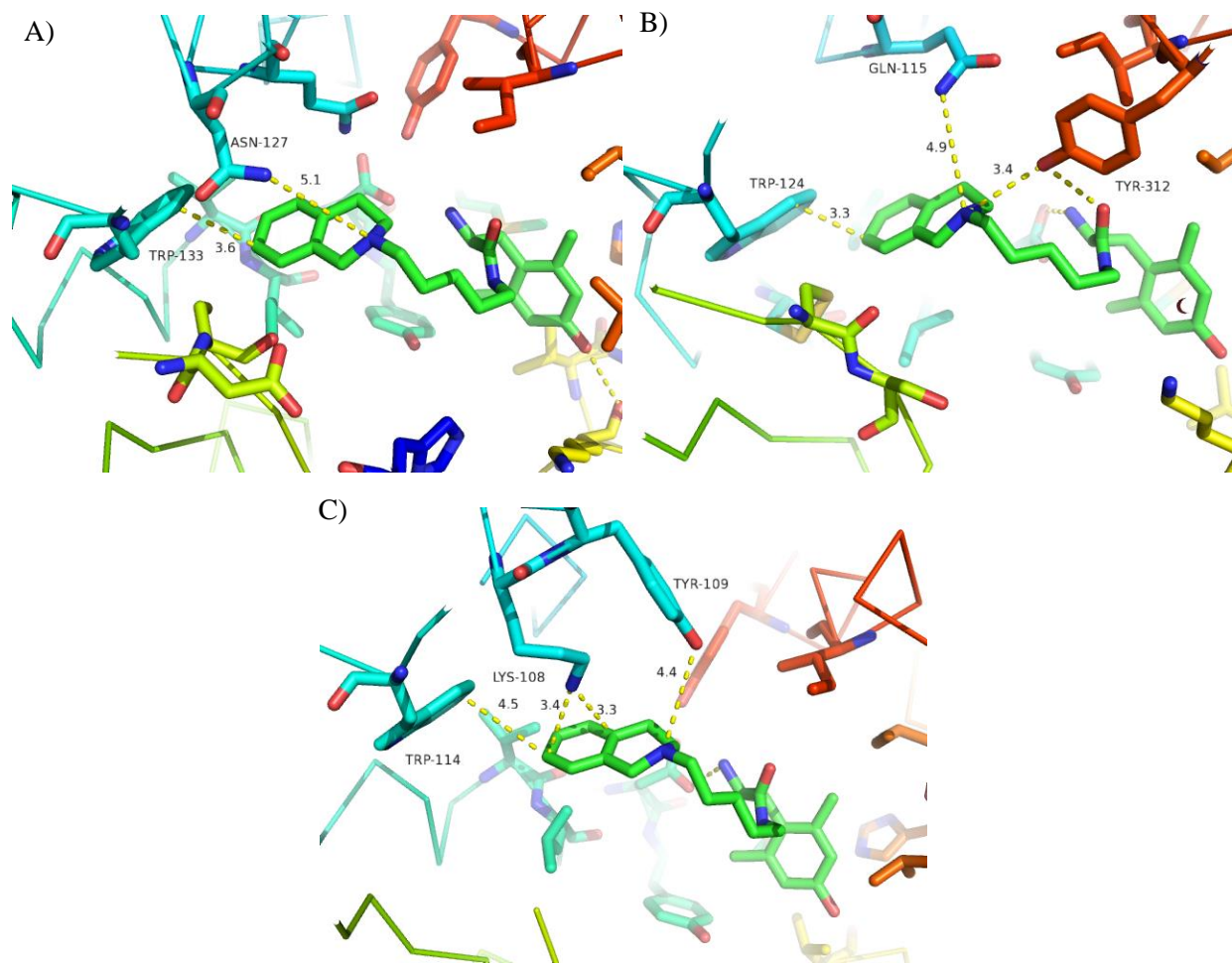


Figure 19: Molecular docking of analogue **193** at the three opioid receptors. Shown are interactions of the tetrahydroisoquinoline pendant with A) MOR in the active state, B) DOR in the inactive state, and C) KOR in the inactive state.

Antinociceptive Activity: In conjunction with the previous chapters, the *in vivo* activity of these analogues was elucidated in the AASA (**Figure 20**). The superagonist **168** is included for comparison and morphine was again used as the positive control. Unlike the superagonist, several of the analogues here were producing antinociception at a dose of 10 mg/kg, including **197-200**, and **193** was expressing antinociception at a dose of 1 mg/kg.

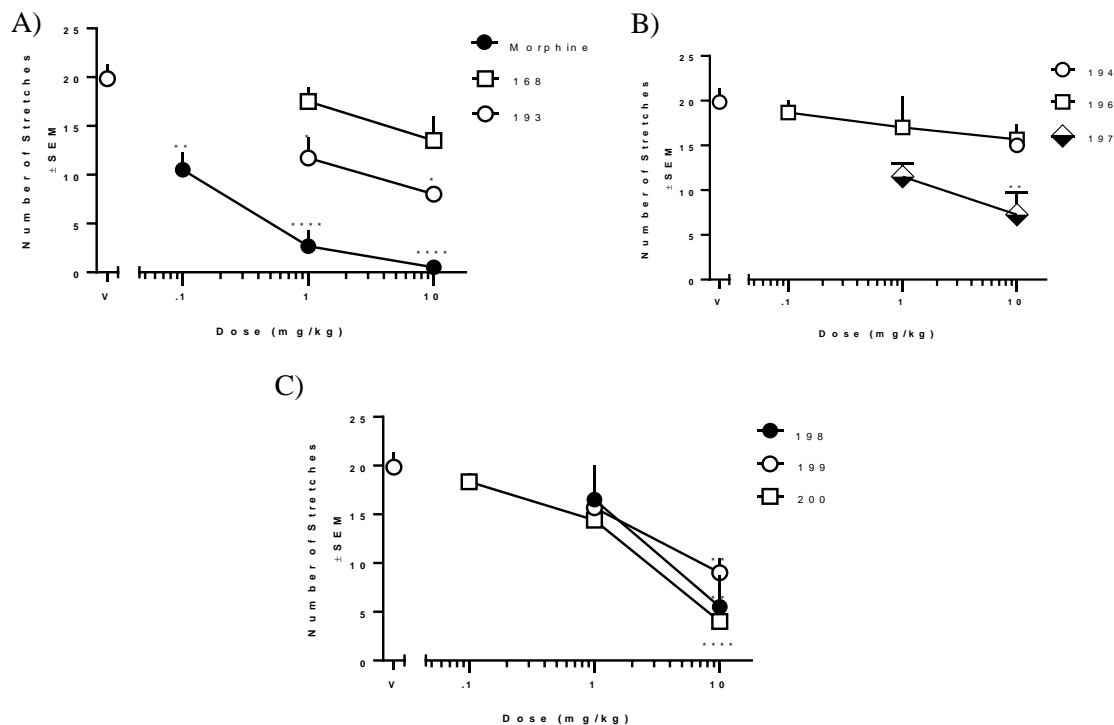


Figure 20: Antinociceptive activity of the **168** and analogues **193-194**, and **197-200** using the AASA. Included is morphine as positive control. Panels A-C represent dose-response curves with the ligands: A) **168** and the alkyl analogue **193**, B) the ether analogue **134** and cyclic analogues **196-197** C) amine and amide analogues **198-200**. * $P < 0.05$ compared to vehicle. ** $P < 0.01$ compared to vehicle. **** $P < 0.0001$ compared to vehicle. N's are between 1 and 6 for each data point.

6.3 Discussion and Conclusions

SAR: The data acquired here further demonstrate the *in vitro* capability of our aromatic-amine pharmacophore to produce MOR-agonists. While no MOR-superagonists were synthesized, all the analogues that possessed the desired amine yielded consistently high levels of MOR-efficacy, and this efficacy was reduced by 45 % when the amine is converted to an amide. This reinforces the importance of the amine for producing MOR-efficacy. When coupled with the MOR-efficacy data of the amide analogues from Chapter 4, these data suggest that the reduced conformational flexibility of the amides conjugated to the aromatic core are contributing in part to their reduced efficacy in that series.

Potency was in general not affected, except for potency losses with the piperidine analogue **196** and the sarcosine analogue **199**. Several factors can be ruled out that could explain this trend: the carbonyl of the amide is tolerated as shown with analogue **200**, the N-methyl is tolerated as shown with analogue **198**, and formation of the ring is tolerated as shown with analogue **197**. The piperidine analogue **196** is more rigid than the piperazine analogue **197**, as the lone pair of the tertiary amine of the latter is capable of inverting across the heteroatom, whereas the piperidine possesses a hydride that cannot invert without rotation of the whole piperidine. This may contribute to the difference in potency in this case. The sarcosine analogue **199** possessed the lowest potency of those that express the aromatic-amine pharmacophore. While the glycine analogue **200** and the N-methyl amine analogue **198** both expressed improved potency, it is conceivable that a combination of both modifications may produce this impaired MOR-potency.

DOR and KOR-agonism were low in this series, though a few trends were observed. The greatest DOR-efficacy and potency came with the glycine analogue **200**. This activity can be attributed to the presence of the hydrogen bond donor on the amide, as removal of this donor in the sarcosine analogue **199** yields losses in potency and efficacy at DOR. Residual KOR-agonism was observed in analogues **194**, **197**, and **198**, each of which can be explained by a hydrogen bond acceptor within the simplified core. It should be noted that the amide analogue **195** did not stimulate KOR, even though it possessed a hydrogen bond acceptor within the core. This though, is consistent with the data shown in Chapters 4 and 5, where residual DOR and KOR agonism appear in analogues that possess the amine where none existed before.

Metabolic Stability: An analysis of the metabolic stability of this series has produced some interesting trends. To begin, the conversion from an aromatic core (**168**) to a simple aliphatic chain (**193**) yielded no improvements in stability. This is despite the fact the aromatic ring is no longer

present to stabilize free radical formation and despite a drop in the cLogP by a single unit. Instead, this is likely a product of increased conformational flexibility in the ligand. These factors can also explain the reduced stability of the ether analogue **194**, whereby there is great flexibility in the ligand and the ether can stabilize the formation of adjacent free radicals. Adding the amide (**195**) to this ether provides a 4-fold stability improvement, likely through a combination of reduced cLogP, reduced flexibility through conjugation, and the carbonyl blocking a possible metabolic site.

Curiously, the piperidine analogue **196** managed to significantly improve the metabolic stability over both the aromatic core analogue **168** and the alkyl chain analogue **193**. This is most likely the product of cyclization, as rigidity in the ligand can deter binding to the CYP enzyme, and the piperidine is less capable of stabilizing metabolism in adjacent positions compared to an aromatic ring. This rigidity contributing to stability is supported with the piperazine analogue **197**, whereby the stability here is 79 minutes. When the piperazine analogue **197** is compared to the N-methyl analogue **198**, in which the only difference between these two analogues is the removal of a single methylene group that destroys the ring system, the stability of **198** drops to less than half of that of **197**. It should be noted that the stability of **197** is less than that of **196**, likely for the same reasons that the ether analogue **194** is less stable than the alkyl analogue **193**.

Finally, the two peptide analogues **199** and **200** were compared. Curiously, the desmethyl analogue **200** was among the least stable in our series, and N-methylation to **199** improved the stability by a factor of 2.5. This is consistent with peptidase activity, as N-methylation can inhibit the degradation of peptide bonds.¹²⁷ A survey of enzymes found in the mouse liver microsomes determined that among many others, aminopeptidase N was present.¹²⁸ This enzyme is currently being considered as a target for indirect opioid analgesics because of its capacity for degrading

opioid peptides.¹²⁹ In particular, it recognizes enkephalins as substrates and produces Tyr-Gly fragments. It is conceivable then, that this peptidase may also recognize the DMT-Gly fragment of our peptidomimetic, the activity of which is consistent with attenuation by N-methylation.

Molecular Modeling: The data revealed by docking analogue **193** to each of the opioid receptors reveals some interesting new trends. At MOR, no new interactions with the receptor appear to manifest, though the distance between the tertiary amine and Asn127 appears to increase as compared to **168**. This may be sufficient to explain the drop in efficacy, though this interaction is still likely present, as **193** is still a potent MOR-agonist.

With regard to DOR, the cation- π interaction is still present. However, the phenol of Tyr109 is further away from the amine by a few Angstroms. Notably, the core aromatic ring of superagonist **168** is not close to any particular residue in DOR, and no interactions with the ring itself is lost upon the removal of this structure to produce analogue **193**. If the argument described in Chapter 5 holds weight, then it is possible that rigidity provided by the aromatic core of **168** helps position the tertiary amine into a favorable interaction between the Tyr109 and the tertiary amine. If this structural rigidity is lost, then this amine cannot adequately engage Tyr109, causing the loss of an important interaction that facilitates DOR-binding.

At KOR, the interactions between the tetrahydroisoquinoline pendant and the residues Gln115 and Trp124 are largely unaltered. However, a new interaction is produced, with the phenol of Tyr312 interacting with both the tertiary amine of the pendant and the amide of the DMT pharmacophore. This additional interaction may help explain the unaltered binding affinity that comes with the loss of the core aromatic ring. As stated in Chapter 5, some of the interactions at each of these receptors are at an increasingly long distance and additional *in silico* studies will be needed to verify any observed trends.

Antinociceptive Activity: Of particular importance to these simplified structures is the fact that most of them retain some antinociceptive activity *in vivo*. In fact, only the ether **194** and the piperidine **195** did not express any activity in this series. Thus far, only **193** expresses statistically significant antinociception at 1 mg/kg, though there are insufficient N's acquired in this series. The piperazine **197** only has 2 out of the desired 6 N's, and statistically significant antinociception may appear with this compound at 1 mg/kg. Ultimately, these data further establish the ability of this pharmacophore to produce MOR-agonists that are active *in vivo*.

Conclusions: The analogues shown in this chapter demonstrate that the aromatic-amine pharmacophore can apply to greatly simplified core structures. Here, MOR-agonism was consistently high, though variable effects at DOR and KOR were observed. Conversion of the amine in **194** to the amide in **195** significantly reduced their efficacy at MOR. This reinforces the observation that the amine is a MOR-efficacy pharmacophore element. These data further suggest that either selective MOR-agonists, bifunctional MOR/DOR, or bifunctional MOR/KOR ligands may be possible depending on how the core is structurally manipulated. MOR/DOR structures appear to be favored with more rigid cores or cores containing an amide, whereas the MOR/KOR ligands favor more flexible cores. With the piperidine and piperazine analogues **196** and **197**, metabolic stability can be greatly improved with increased rigidity of the ligand, all while maintaining moderate to potent MOR-agonism. The implications of this chapter expand beyond these peptidomimetic series and suggest that the aromatic-amine pharmacophore can be used in a wide variety of structures, particularly the previously studied opioid peptides to produce MOR-agonism where none existed previously.

6.4 Experimental

Chemistry

General Methods: All reagents and solvents were obtained commercially and were used without further purification. Intermediates were purified by flash chromatography using a Biotage Isolera One instrument. Most purification methods utilized a hexanes/ethyl acetate solvent system in a Biotage SNAP KP-Sil column, with a linear gradient between 0 and 100% ethyl acetate. Reverse phase column chromatography using a linear gradient of 0% to 100% solvent B (0.1% TFA in acetonitrile) in solvent A (0.1% TFA in water) using a Biotage SNAP Ultra C18 column was utilized for some intermediate amine salts. Purification of final compounds was performed using a Waters semipreparative HPLC with a Vydac protein and peptide C18 reverse phase column, using a linear gradient of 0% to 100% solvent B in solvent A at a rate 1% per minute, monitoring UV absorbance at 230 nm. The purity of final compounds was assessed using a Waters Alliance 2690 analytical HPLC instrument with a Vydac protein and peptide C18 reverse phase column. A linear gradient (gradient A) of 0% to 70% solvent B in solvent A in 70 min, measuring UV absorbance at 230 nm was used to determine purity. All final compounds used for testing were $\geq 95\%$ pure, as determined by analytical HPLC. ^1H NMR and ^{13}C NMR data were obtained on a 500 or 400 MHz Varian spectrometer using CDCl_3 , CD_3OD , $\text{DMSO-}d_6$, or D_2O as solvents. The identities of final compounds were verified by mass spectrometry using an Agilent 6130 LC-MS mass spectrometer in positive ion mode, or an Agilent 6230 TOF HPLC-MS in the positive ion mode.

General Procedure for Coupling of Tetrahydroquinoline Analogues to N-Boc Protected Carboxylic Acids (Procedure A): To a flask containing 1 equivalent of N-Boc protected carboxylic acid was added 1 equivalent of PyBOP and 1 equivalent of tetrahydroisoquinoline or the

tetrahydroquinoline analog. The flask was flushed with argon, DMF was added as solvent, and 10 equivalents of N-methylmorpholine was added. The reaction was stirred overnight, at which point it was concentrated in vacuo. The residue was then partitioned between EtOAc and sat. Na₂CO₃, extracted with EtOAc, the organic layers were combined, dried with MgSO₄, filtered, and concentrated in vacuo. Purification by column chromatography (0-5% MeOH in DCM, or 0-66% EtOAc in Hexanes) yielded the coupled product.

General Procedure for the Deprotection of Boc-Groups using Concentrated HCl (Procedure Ba): To the Boc protected compound was added 2-6 mL of Dioxane and 0.2-0.6 mL concentrated HCl. The solution was stirred at room temperature for 1-5 minutes and concentrated in vacuo. The ensuing salt was suspended in solvent A and was either concentrated in vacuo and triturated with hexanes or purified by reverse phase chromatography (0-100% B in A), yielding the product as a TFA salt.

General Procedure for the Deprotection of Boc-Groups using TFA (Procedure Bb): To the Boc protected compound was added 2 mL of TFA and 2 mL of DCM. The solution was stirred at room temperature for 1-5 minute and concentrated in vacuo. The ensuing salt was either continued without further purification or suspended in solvent A and was purified via reverse phase chromatography (0-100% B in A), yielding the product as a TFA salt.

General Procedure for the Reduction of Amides (Procedure C): To a dried flask containing 1 equivalent of the desired amide under argon was added THF and 7 equivalents of 2 M BH₃*Me₂S complex in THF. The reaction was heated at 75 °C for 3 hours, at which point the reaction was quenched with MeOH and heated for an additional 15 minutes. The reaction was then cooled, concentrated in vacuo, and was used in Procedure G without further purification.

General Procedure for the Coupling of 2',6'-Dimethyltyrosine to Functionalized Amine Salts (Procedure D): To a dried flask containing the amine under argon was added 3 mL of DMF and 10 equivalents of Hunig's base. 1 equivalent of PyBOP and 1 equivalent of 6-Cl-HOBt was added, followed by a 1 equivalent of Boc protected 2',6'-Dimethyltyrosine in 1.5 mL DMF. The solution was stirred overnight at room temperature, concentrated in vacuo, and purified via semipreparative reverse phase HPLC (0.1% TFA in water: 0.1% TFA in acetonitrile). 2 mL of TFA and 2 mL of DCM were then added, and the solution was stirred for an additional hour. The reaction mixture was concentrated in vacuo and purified via an additional semipreparative reverse phase HPLC (0.1% TFA in water: 0.1% TFA in acetonitrile). The product was concentrated in vacuo and lyophilized overnight to yield the final peptidomimetic.

5-(3,4-dihydroisoquinolin-2(1H)-yl)-5-oxopentan-1-aminium trifluoroacetate (181):

See Procedure A: 85 mg (0.39 mmol) of **5-((tert-butoxycarbonyl)amino)pentanoic acid**, 204 mg (0.39 mmol, 1.0 eq.) of PyBOP, 50 μ L (53 mg, 0.39 mmol, 1.0 eq.) of 1,2,3,4-tetrahydroisoquinoline, 430 μ L (396 mg, 3.9 mmol, 10 eq.) of NMM, and 4 mL of DMF. The intermediate was purified by column chromatography (0-50 % EtOAc in Hexanes). Procedure Ba: 5 mL of dioxane and 0.5 mL conc. HCl were added and the solution was concentrated in vacuo after 5 min. Compound **181** (99 mg, Yield=73 %) was isolated as a colorless oil. ^1H NMR (500 MHz, Methanol- d_4) δ 7.23 – 7.09 (m, 4H), 4.69 (s, 1H), 4.68 (s, 1H), 3.78 (t, J = 6.0 Hz, 1H), 3.74 (t, J = 6.0 Hz, 1H), 2.93 (p, J = 6.4 Hz, 3H), 2.84 (t, J = 6.0 Hz, 1H), 2.55 (q, J = 6.6 Hz, 2H), 1.76 – 1.67 (m, 4H). ^{13}C NMR (126 MHz, Methanol- d_4) δ 172.33, 172.29, 160.32, 160.02, 134.68, 134.26, 132.96, 132.60, 128.24, 127.98, 126.60, 126.38, 126.18, 126.08, 126.02, 125.81, 117.21, 114.90, 43.94, 43.15, 39.96, 38.96, 32.12, 31.87, 28.82, 27.93, 26.74, 26.70, 21.30.

2-(2-(3,4-dihydroisoquinolin-2(1H)-yl)-2-oxoethoxy)ethan-1-aminium

trifluoroacetate (182): See Procedure A: 94 mg (0.43 mmol) of **2-(2-((tert-butoxycarbonyl)amino)ethoxy)acetic acid**, 223 mg (0.43 mmol, 1.0 eq.) of PyBOP, 60 μ L (63 mg, 0.47 mmol, 1.1 eq.) of 1,2,3,4-tetrahydroisoquinoline, 470 μ L (432 mg, 4.3 mmol, 10 eq.) of NMM, and 4 mL of DMF. The intermediate was purified by column chromatography (0-5 % MeOH in DCM). Procedure Ba: 5 mL of dioxane and 0.5 mL conc. HCl were added and the solution was concentrated in vacuo after 5 min. Compound **182** (121 mg, Yield=81 %) was isolated as a colorless oil. ^1H NMR (400 MHz, Methanol- d_4) δ 7.21 – 7.12 (m, 4H), 4.69 (s, 1H), 4.55 (s, 1H), 4.43 (s, 1H), 4.42 (s, 1H), 3.82 – 3.74 (m, 3H), 3.59 (t, $J = 6.0$ Hz, 1H), 3.15 (q, $J = 4.5$ Hz, 2H), 2.91 (t, $J = 6.0$ Hz, 1H), 2.85 (t, $J = 6.0$ Hz, 1H). ^{13}C NMR (101 MHz, Methanol- d_4) δ 169.39, 169.35, 161.16, 160.80, 160.44, 160.08, 134.54, 134.14, 132.52, 131.97, 128.26, 127.98, 126.70, 126.50, 126.26, 126.15, 126.03, 125.87, 120.64, 117.75, 114.86, 68.20, 45.19, 43.79, 41.68, 39.89, 39.22, 28.46, 27.74.

4-(2-(3,4-dihydroisoquinolin-2(1H)-yl)-2-oxoethyl)piperidin-1-ium hydrochloride

(183): See Procedure A: 75 mg (0.31 mmol) of **2-(1-(tert-butoxycarbonyl)piperidin-4-yl)acetic acid**, 161 mg (0.31 mmol, 1.0 eq.) of PyBOP, 40 μ L (42 mg, 0.32 mmol, 1.0 eq.) of 1,2,3,4-tetrahydroisoquinoline, 340 μ L (313 mg, 3.1 mmol, 10 eq.) of NMM, and 4 mL of DMF. The intermediate was purified by column chromatography (0-5 % MeOH in DCM). Procedure Ba: 5 mL of dioxane and 0.5 mL conc. HCl were added and the solution was concentrated in vacuo after 1 min. Compound **183** (86 mg, Yield=95 %) was isolated as an off white amorphous solid. ^1H NMR (500 MHz, Methanol- d_4) δ 7.22 – 7.11 (m, 4H), 4.70 (s, 1H), 4.68 (s, 1H), 3.78 (t, $J = 6.0$ Hz, 1H), 3.75 (t, $J = 5.9$ Hz, 1H), 3.37 (ddd, $J = 12.8, 6.3, 3.1$ Hz, 2H), 3.05 – 2.94 (m, 2H), 2.92 (t, $J = 5.9$ Hz, 1H), 2.84 (t, $J = 6.0$ Hz, 1H), 2.49 (t, $J = 7.3$ Hz, 2H), 2.14 (ddtt, $J = 14.4, 10.7, 6.9,$

3.8 Hz, 1H), 2.05 – 1.95 (m, 2H), 1.55 – 1.41 (m, 2H). ¹³C NMR (126 MHz, Methanol-*d*₄) δ 170.84, 170.78, 160.78, 160.49, 134.67, 134.24, 132.94, 132.62, 128.26, 127.99, 126.62, 126.38, 126.19, 126.08, 126.03, 125.80, 117.46, 115.14, 43.92, 43.73, 43.71, 43.26, 39.96, 38.72, 38.52, 30.66, 30.63, 28.87, 28.46, 28.42, 27.92.

1-(2-(3,4-dihydroisoquinolin-2(1H)-yl)-2-oxoethyl)piperazine-1,4-dium

trifluoroacetate (184): See Procedure A: 78 mg (0.32 mmol) of **2-(4-(tert-butoxycarbonyl)piperazin-1-yl)acetic acid**, 172 mg (0.33 mmol, 1.0 eq.) of PyBOP, 50 μL (53 mg, 0.39 mmol, 1.2 eq.) of 1,2,3,4-tetrahydroisoquinoline, 350 μL (322 mg, 3.2 mmol, 10 eq.) of NMM, and 4 mL of DMF. The intermediate was purified by column chromatography (0-5 % MeOH in DCM). Procedure Ba: 5 mL of dioxane and 0.5 mL conc. HCl were added and the solution was concentrated in vacuo after 5 min. Compound **184** (156 mg, Quantitative Yield) was isolated as a white waxy solid. ¹H NMR (500 MHz, Methanol-*d*₄) δ 7.25 – 7.09 (m, 4H), 4.70 (s, 1H), 4.63 (s, 1H), 4.40 (s, 2H), 3.79 (t, *J* = 6.1 Hz, 1H), 3.69 – 3.57 (m, 9H), 2.96 (t, *J* = 6.0 Hz, 1H), 2.87 (t, *J* = 6.1 Hz, 1H). ¹³C NMR (126 MHz, Methanol-*d*₄) δ 163.34, 163.26, 161.82, 161.54, 161.25, 134.44, 134.05, 132.07, 131.59, 128.26, 128.05, 126.90, 126.70, 126.39, 126.31, 126.07, 125.99, 117.61, 115.29, 57.02, 56.93, 49.41, 49.38, 45.84, 44.05, 42.45, 40.69, 40.31, 28.35, 27.64.

2-(3,4-dihydroisoquinolin-2(1H)-yl)-N-methyl-2-oxoethan-1-aminium

trifluoroacetate (185): See Procedure A: 104 mg (0.55 mmol) of **N-(tert-butoxycarbonyl)-N-methylglycine**, 288 mg (0.55 mmol, 1.0 eq.) of PyBOP, 70 μL (74 mg, 0.55 mmol, 1.0 eq.) of 1,2,3,4-tetrahydroisoquinoline, 600 μL (552 mg, 5.5 mmol, 10 eq.) of NMM, and 4 mL of DMF. The intermediate was purified by column chromatography (0-5 % MeOH in DCM). Procedure Ba: 6 mL of dioxane and 0.6 mL conc. HCl were added and the solution was concentrated in vacuo

after 5 min. Compound **185** (132 mg, Yield=75 %) was isolated as a colorless oil that turned purple overtime. ^1H NMR (500 MHz, Methanol- d_4) δ 7.23 – 7.10 (m, 4H), 4.69 (s, 1H), 4.60 (s, 1H), 4.16 (s, 1H), 4.15 (s, 1H), 3.79 (t, J = 6.1 Hz, 1H), 3.63 (t, J = 6.0 Hz, 1H), 2.94 (t, J = 6.0 Hz, 1H), 2.85 (t, J = 6.0 Hz, 1H), 2.78 (s, 3H). ^{13}C NMR (126 MHz, Methanol- d_4) δ 164.05, 164.01, 161.03, 160.74, 160.46, 160.16, 134.42, 134.00, 132.18, 131.60, 128.27, 128.05, 126.81, 126.61, 126.33, 126.24, 126.02, 125.92, 119.71, 117.40, 115.09, 112.77, 49.10, 49.00, 45.56, 43.93, 42.14, 40.08, 32.25, 28.34, 27.67.

tert-butyl (2-(3,4-dihydroisoquinolin-2(1H)-yl)-2-oxoethyl)(methyl)carbamate (186):

See Procedure A: 99 mg (0.52 mmol) of **N-(tert-butoxycarbonyl)-N-methylglycine**, 271 mg (0.52 mmol, 1.0 eq.) of PyBOP, 70 μL (74 mg, 0.55 mmol, 1.1 eq.) of 1,2,3,4-tetrahydroisoquinoline, 580 μL (534 mg, 5.3 mmol, 10 eq.) of NMM, and 4 mL of DMF. The product was purified by column chromatography (0-50 % EtOAc in Hexanes), yielding Compound **186** (152 mg, Yield= 95 %) as a colorless oil. ^1H NMR (500 MHz, Chloroform- d) δ 7.22 – 7.02 (m, 4H), 4.71 (d, J = 9.6 Hz, 1H), 4.57 (s, 1H), 4.13 (d, J = 6.2 Hz, 1H), 4.05 (s, 1H), 3.84 – 3.77 (m, 1H), 3.67 – 3.59 (m, 1H), 2.92 (d, J = 5.4 Hz, 3H), 2.85 (dt, J = 15.7, 5.5 Hz, 2H), 1.46 (s, 6H), 1.39 (s, 3H). ^{13}C NMR (126 MHz, Chloroform- d) δ 167.55, 167.46, 156.22, 134.87, 133.97, 133.23, 132.16, 129.01, 128.85, 128.28, 126.94, 126.62, 126.57, 126.36, 126.07, 125.96, 79.95, 51.02, 50.56, 50.44, 46.29, 44.36, 42.43, 39.93, 35.46, 29.30, 28.36, 28.29.

tert-butyl (2-(3,4-dihydroisoquinolin-2(1H)-yl)-2-oxoethyl)carbamate (187): See Procedure A: 91 mg (0.52 mmol) of **(tert-butoxycarbonyl)glycine**, 270 mg (0.52 mmol, 1.0 eq.) of PyBOP, 70 μL (74 mg, 0.55 mmol, 1.1 eq.) of 1,2,3,4-tetrahydroisoquinoline, 570 μL (524 mg, 5.2 mmol, 10 eq.) of NMM, and 4 mL of DMF. The product was purified by column

chromatography (0-66 % EtOAc in Hexanes), yielding Compound **187** (136 mg, Yield= 90 %) as a yellow oil. ^1H NMR (500 MHz, Chloroform-*d*) δ 7.22 – 7.03 (m, 4H), 5.59 (s, 1H), 4.71 (s, 1H), 4.52 (s, 1H), 4.02 (dd, J = 8.5, 4.4 Hz, 2H), 3.81 (t, J = 6.0 Hz, 1H), 3.58 (t, J = 5.9 Hz, 1H), 2.86 (dt, J = 22.9, 6.0 Hz, 2H), 1.43 (s, 9H). ^{13}C NMR (126 MHz, Chloroform-*d*) δ 167.29, 155.83, 134.70, 133.80, 132.83, 131.68, 128.84, 128.30, 127.12, 126.75, 126.70, 126.55, 126.53, 126.11, 79.61, 45.93, 44.38, 42.64, 42.48, 42.03, 40.06, 29.09, 28.34, 28.29.

tert-butyl (2-(3,4-dihydroisoquinolin-2(1H)-yl)ethyl)(methyl)carbamate (188): See Procedure C: 48 mg (0.16 mmol) of **186**, 550 μL (1.1 mmol, 7.0 eq.) of 2M $\text{BH}_3 \cdot \text{Me}_2\text{S}$ in THF, and 4 mL THF. The concentrated product was purified by column chromatography (0-33 % EtOAc in Hexanes), yielding Compound **188** (30 mg, Yield= 66 %) as a colorless oil. ^1H NMR (500 MHz, Chloroform-*d*) δ 7.26 – 7.13 (m, 3H), 7.02 (d, J = 7.1 Hz, 1H), 4.23 (d, J = 15.6 Hz, 1H), 3.96 – 3.58 (m, 3H), 3.35 – 2.78 (m, 9H), 1.40 (s, 4H), 1.34 (s, 5H). ^{13}C NMR (126 MHz, Chloroform-*d*) δ 129.75, 128.59, 127.60, 127.36, 127.00, 126.78, 80.00, 79.82, 62.10, 61.03, 54.96, 54.79, 54.10, 53.87, 44.29, 43.94, 35.01, 34.70, 28.32, 24.04.

2-(3,4-dihydroisoquinolin-2(1H)-yl)-2-oxoethan-1-aminium trifluoroacetate (189)
Procedure Ba: 54 mg (0.19 mmol) of **187**, 5 mL of dioxane and 0.5 mL conc. HCl were added and the solution was concentrated in vacuo after 5 min. Compound **189** (32 mg, Yield=57 %) was isolated as a pinkish white solid. ^1H NMR (500 MHz, Methanol-*d*₄) δ 7.24 – 7.10 (m, 4H), 4.69 (s, 1H), 4.60 (s, 1H), 4.04 (s, 1H), 4.03 (s, 1H), 3.78 (t, J = 6.1 Hz, 1H), 3.64 (t, J = 6.0 Hz, 1H), 2.94 (t, J = 6.0 Hz, 1H), 2.86 (t, J = 6.1 Hz, 1H). ^{13}C NMR (126 MHz, Methanol-*d*₄) δ 164.95, 164.90, 161.74, 161.46, 161.18, 160.89, 134.48, 134.04, 132.13, 131.57, 128.28, 128.07, 126.91, 126.69,

126.40, 126.32, 126.08, 125.98, 119.96, 117.64, 115.32, 113.00, 45.64, 44.15, 42.23, 40.39, 28.33, 27.66.

2-((2-(3,4-dihydroisoquinolin-2(1H)-yl)-2-oxoethyl)(methyl)amino)-2-oxoethan-1-aminium trifluoroacetate (190): See Procedure A: 47 mg (0.15 mmol) of **185**, 80 mg (0.15 mmol, 1.0 eq.) of PyBOP, 29 mg (0.17 mmol, 1.1 eq.) of N-(tert-butoxycarbonyl)glycine, 170 μ L (156 mg, 1.5 mmol, 10 eq.) of NMM, and 4 mL of DMF. The intermediate was purified by column chromatography (0-5 % MeOH in DCM). Procedure Ba: 5 mL of dioxane and 0.5 mL conc. HCl were added and the solution was concentrated in vacuo after 5 min. Compound **190** (24 mg, Yield=43 %) was isolated as a colorless oil. ^1H NMR (500 MHz, Methanol- d_4) δ 7.23 – 7.12 (m, 4H), 4.71 – 4.66 (m, 2H), 4.45 – 4.40 (m, 2H), 4.00 (s, 2H), 3.79 (q, J = 6.0, 5.6 Hz, 1H), 3.71 (td, J = 6.0, 1.8 Hz, 1H), 3.11 – 3.02 (m, 3H), 2.98 – 2.96 (m, 1H), 2.90 – 2.81 (m, 1H). ^{13}C NMR (126 MHz, Methanol- d_4) δ 167.14, 166.71, 160.08, 159.78, 134.59, 134.22, 133.52, 132.63, 128.81, 128.23, 127.97, 127.93, 127.26, 126.68, 126.58, 126.50, 126.30, 126.24, 126.15, 126.00, 125.89, 117.07, 114.76, 55.11, 49.47, 49.32, 45.76, 44.24, 44.08, 42.29, 42.23, 41.87, 40.16, 39.64, 39.47, 34.68, 34.63, 34.27, 28.49, 27.82, 27.25.

2-(3,4-dihydroisoquinolin-2(1H)-yl)-N-methylethan-1-aminium trifluoroacetate (191): See Procedure Ba: 30 mg (0.16 mmol) of **188**, 5 mL of dioxane and 0.5 mL conc. HCl were added and the solution was concentrated in vacuo after 5 min. The residue was then partitioned between EtOAc and sat. Na_2CO_3 , and extracted with EtOAc. The organic layers were then combined, dried with MgSO_4 , filtered, and concentrated in vacuo. The residue was suspended in solvent A, concentrated in vacuo, and triturated with hexanes. Compound **191** (28 mg, Yield= 89 %) was isolated as a colorless oil. ^1H NMR (500 MHz, Methanol- d_4) δ 7.33 – 7.25 (m, 3H), 7.22 – 7.18

(m, 1H), 4.53 (s, 2H), 3.71 – 3.63 (m, 4H), 3.63 – 3.53 (m, 2H), 3.24 (t, $J = 6.4$ Hz, 2H), 2.82 (s, 3H). ^{13}C NMR (126 MHz, Methanol- d_4) δ 130.47, 128.46, 128.18, 128.15, 127.09, 126.93, 126.88, 126.43, 126.38, 53.31, 53.24, 52.14, 50.94, 50.47, 50.22, 49.57, 42.85, 42.24, 32.58, 27.17, 24.88.

2-((2-(3,4-dihydroisoquinolin-2(1H)-yl)ethyl)amino)-2-oxoethan-1-aminium

trifluoroacetate (192): See Procedure C: 24 mg (0.079 mmol) of **189**, 280 μL (0.56 mmol, 7.1 eq.) of 2M $\text{BH}_3\cdot\text{Me}_2\text{S}$ in THF, and 4 mL THF. Procedure A: 43 mg (0.083 mmol, 1.0 eq.) of PyBOP, 14 mg (0.080 mmol, 1.0 eq.) of N-(tert-butoxycarbonyl)glycine, 90 μL (83 mg, 0.82 mmol, 10 eq.) of NMM, and 4 mL of DMF. Procedure Bb: 2 mL of TFA and 2 mL DCM were added, and the solution was concentrated in vacuo after 1 min. The residue was then purified by reverse phase chromatography. Compound **192** (16 mg, Yield=58 %) was isolated as a colorless oil. ^1H NMR (500 MHz, Methanol- d_4) δ 7.35 – 7.23 (m, 3H), 7.20 (d, $J = 7.2$ Hz, 1H), 4.55 (br s, 2H), 3.99 – 3.68 (m, 5H), 3.65 – 3.40 (m, 3H), 3.22 (s, 2H). ^{13}C NMR (126 MHz, Methanol- d_4) δ 167.41, 160.53, 160.24, 159.94, 130.59, 128.43, 128.09, 127.21, 126.85, 126.41, 117.24, 114.93, 55.08, 53.22, 49.88, 40.13, 33.96, 24.78.

(S)-1-((5-(3,4-dihydroisoquinolin-2(1H)-yl)pentyl)amino)-3-(4-hydroxy-2,6-

dimethylphenyl)-1-oxopropan-2-aminium trifluoroacetate (193): See Procedure C: 30 mg (0.087 mmol) of **181**, 300 μL (0.60 mmol, 6.9 eq.) of 2 M $\text{BH}_3\cdot\text{Me}_2\text{S}$ in THF, and 4 mL of THF. Step 1 of Procedure D: 150 μL (111 mg, 0.86 mmol, 10 eq.) of N,N-diisopropylethylamine, 45 mg (0.086 mmol, 1.0 eq.) of PyBOP, 16 mg (0.094 mmol, 1.1 eq.) of 6-Cl-HOBt, 38 mg (0.093 mmol, 1.1 eq.) of Boc-O-Boc-L-2',6'-dimethyltyrosine, 3+1.5 mL of DMF. Step 2 of Procedure D: 2 mL TFA and 2 mL DCM. Compound **193** (13.1 mg, Yield=29 %) was isolated as a white solid. ^1H NMR (500 MHz, Methanol- d_4) δ 7.80 (t, $J = 5.7$ Hz, 1H), 7.36 – 7.24 (m, 3H), 7.22 (d, $J = 7.4$ Hz,

1H), 6.51 (s, 2H), 4.60 (dd, $J = 14.5, 7.7$ Hz, 1H), 4.32 (t, $J = 14.4$ Hz, 1H), 3.90 – 3.75 (m, 2H), 3.40 (dd, $J = 25.6, 15.6$ Hz, 1H), 3.31 – 3.10 (m, 9H), 3.00 (dd, $J = 13.8, 4.8$ Hz, 1H), 2.97 – 2.87 (m, 1H), 2.27 (s, 6H), 1.81 – 1.65 (m, 2H), 1.35 (dp, $J = 9.1, 6.5$ Hz, 2H), 1.05 (dtt, $J = 21.2, 13.2, 6.7$ Hz, 2H). (MS)EI: 410.3 (M+H), Retention Time: 19.34 min.

(S)-1-((2-(2-(3,4-dihydroisoquinolin-2(1H)-yl)ethoxy)ethyl)amino)-3-(4-hydroxy-2,6-dimethylphenyl)-1-oxopropan-2-aminium trifluoroacetate (194): See Procedure C: 41 mg (0.12 mmol) of **182**, 420 μ L (0.84 mmol, 7.1 eq.) of 2 M $\text{BH}_3 \cdot \text{Me}_2\text{S}$ in THF, and 4 mL of THF. Step 1 of Procedure D: 210 μ L (156 mg, 1.2 mmol, 10 eq.) of N,N-diisopropylethylamine, 63 mg (0.12 mmol, 1.0 eq.) of PyBOP, 21 mg (0.12 mmol, 1.0 eq.) of 6-Cl-HOBt, 50 mg (0.12 mmol, 1.0 eq.) of Boc-O-Boc-L-2',6'-dimethyltyrosine, 3+1.5 mL of DMF. Step 2 of Procedure D: 2 mL TFA and 2 mL DCM. Compound **194** (11.1 mg, Yield=18 %) was isolated as a white solid. ^1H NMR (500 MHz, Methanol- d_4) δ 7.34 – 7.25 (m, 3H), 7.21 (d, $J = 7.5$ Hz, 1H), 6.50 (s, 2H), 4.56 (s, 1H), 4.37 (s, 1H), 3.89 (dd, $J = 11.4, 4.9$ Hz, 1H), 3.83 – 3.72 (m, 2H), 3.69 (ddd, $J = 11.7, 7.7, 4.2$ Hz, 1H), 3.50 – 3.34 (m, 5H), 3.29 – 3.16 (m, 4H), 3.01 (dd, $J = 13.8, 4.9$ Hz, 1H), 2.26 (s, 6H). (MS)EI: 413.3 (M+H), Retention Time: 17.78 min.

(S)-1-((2-(2-(3,4-dihydroisoquinolin-2(1H)-yl)-2-oxoethoxy)ethyl)amino)-3-(4-hydroxy-2,6-dimethylphenyl)-1-oxopropan-2-aminium trifluoroacetate (195): See Procedure D: Step 1: 36 mg (0.10 mmol) of **182**, 180 μ L (134 mg, 1.0 mmol, 10 eq.) of N,N-diisopropylethylamine, 56 mg (0.11 mmol, 1.0 eq.) of PyBOP, 19 mg (0.11 mmol, 1.1 eq.) of 6-Cl-HOBt, 44 mg (0.11 mmol, 1.0 eq.) of Boc-O-Boc-L-2',6'-dimethyltyrosine, 3+1.5 mL of DMF. Step 2: 2 mL TFA and 2 mL DCM. Compound **195** (15.1 mg, Yield=27 %) was isolated as a white solid. ^1H NMR (500 MHz, Methanol- d_4) δ 8.14 (dt, $J = 22.7, 5.2$ Hz, 1H), 7.23 – 7.11 (m, 4H),

6.46 (s, 1H), 6.43 (s, 1H), 4.67 (s, 1H), 4.55 (d, $J = 2.7$ Hz, 1H), 4.16 (qd, $J = 15.0, 6.9$ Hz, 2H), 3.85 (dd, $J = 11.5, 4.9$ Hz, 1H), 3.83 – 3.70 (m, 1H), 3.63 – 3.54 (m, 1H), 3.54 – 3.48 (m, 1H), 3.37 – 3.31 (m, 1H), 3.28 – 3.15 (m, 3H), 3.04 – 2.83 (m, 3H), 2.25 (s, 2H), 2.24 (s, 4H). (MS)EI: 427.3 (M+H), Retention Time: 26.81 min.

(S)-1-(4-(2-(3,4-dihydroisoquinolin-2(1H)-yl)ethyl)piperidin-1-yl)-3-(4-hydroxy-2,6-dimethylphenyl)-1-oxopropan-2-aminium trifluoroacetate (196): See Procedure C: 25 mg (0.067 mmol) of **183**, 250 μ L (0.50 mmol, 7.4 eq.) of 2 M $\text{BH}_3 \cdot \text{Me}_2\text{S}$ in THF, and 4 mL of THF. Step 1 of Procedure D: 120 μ L (89 mg, 0.69 mmol, 10 eq.) of N,N-diisopropylethylamine, 35 mg (0.067 mmol, 1.0 eq.) of PyBOP, 13 mg (0.077 mmol, 1.1 eq.) of 6-Cl-HOBt, 29 mg (0.071 mmol, 1.1 eq.) of Boc-O-Boc-L-2',6'-dimethyltyrosine, 3+1.5 mL of DMF. Step 2 of Procedure D: 2 mL TFA and 2 mL DCM. Compound **196** (2.8 mg, Yield=8 %) was isolated as a white solid. ^1H NMR (500 MHz, Methanol- d_4) δ 7.37 – 7.15 (m, 4H), 6.56 (s, 1H), 6.49 (s, 1H), 4.66 – 4.44 (m, 3H), 4.38 – 4.20 (m, 1H), 3.79 (s, 1H), 3.28 – 3.10 (m, 5H), 3.10 – 3.00 (m, 1H), 2.87 (td, $J = 12.9, 2.6$ Hz, 1H), 2.50 (dtd, $J = 44.8, 13.0, 2.4$ Hz, 1H), 2.29 (s, 4H), 2.23 (s, 2H), 1.73 (dd, $J = 33.7, 13.1$ Hz, 2H), 1.67 – 1.38 (m, 3H), 1.21 (d, $J = 13.2$ Hz, 1H), 1.17 – 1.00 (m, 1H), 0.84 (qd, $J = 13.0, 4.7$ Hz, 1H), -0.30 – -0.63 (m, 1H). (MS)EI: 436.3 (M+H), Retention Time: 20.44 min.

(S)-1-(4-(2-(3,4-dihydroisoquinolin-2(1H)-yl)ethyl)piperazin-1-yl)-3-(4-hydroxy-2,6-dimethylphenyl)-1-oxopropan-2-aminium trifluoroacetate (197): See Procedure C: 70 mg (0.14 mmol) of **184**, 720 μ L (1.4 mmol, 10 eq.) of 2 M $\text{BH}_3 \cdot \text{Me}_2\text{S}$ in THF, and 5 mL of THF. Step 1 of Procedure D: 250 μ L (186 mg, 1.4 mmol, 10 eq.) of N,N-diisopropylethylamine, 76 mg (0.15 mmol, 1.0 eq.) of PyBOP, 25 mg (0.15 mmol, 1.0 eq.) of 6-Cl-HOBt, 59 mg (0.14 mmol, 1.0 eq.) of Boc-O-Boc-L-2',6'-dimethyltyrosine, 3+2.5 mL of DMF. Step 2 of Procedure D: 2 mL TFA

and 2 mL DCM. Compound **197** (2.9 mg, Yield=3.7 %) was isolated as a white solid. ¹H NMR (500 MHz, Methanol-*d*₄) δ 7.35 – 7.23 (m, 3H), 7.22 – 7.12 (m, 1H), 6.52 (s, 2H), 4.53 (dd, *J* = 12.1, 4.4 Hz, 1H), 4.46 (s, 2H), 3.66 (d, *J* = 13.4 Hz, 1H), 3.60 (t, *J* = 6.4 Hz, 2H), 3.54 (t, *J* = 10.5 Hz, 1H), 3.39 (t, *J* = 6.1 Hz, 2H), 3.24 – 3.17 (m, 3H), 3.16 – 3.10 (m, 1H), 3.07 (dd, *J* = 13.8, 4.4 Hz, 1H), 2.80 (q, *J* = 6.4 Hz, 2H), 2.69 – 2.57 (m, 2H), 2.43 – 2.33 (m, 2H), 2.26 (s, 6H), 1.64 – 1.52 (m, 1H). (MS)EI: 437.3 (M+H), Retention Time: 17.60 min.

(S)-1-((2-((2-(3,4-dihydroisoquinolin-2(1H)-yl)ethyl)(methyl)amino)ethyl)amino)-3-(4-hydroxy-2,6-dimethylphenyl)-1-oxopropan-2-aminium trifluoroacetate (198): See Procedure C: 24 mg (0.064 mmol) of **190**, 300 μL (0.60 mmol, 9.4 eq.) of 2 M BH₃*Me₂S in THF, and 4 mL of THF. Step 1 of Procedure D: 110 μL (82 mg, 0.63 mmol, 9.9 eq.) of N,N-diisopropylethylamine, 35 mg (0.67 mmol, 1.1 eq.) of PyBOP, 13 mg (0.077 mmol, 1.2 eq.) of 6-Cl-HOBt, 28 mg (0.068 mmol, 1.1 eq.) of Boc-O-Boc-L-2',6'-dimethyltyrosine, 3+1.5 mL of DMF. Step 2 of Procedure D: 2 mL TFA and 2 mL DCM. Compound **198** (4.9 mg, Yield=14 %) was isolated as a white solid. ¹H NMR (500 MHz, Methanol-*d*₄) δ 7.34 – 7.25 (m, 3H), 7.20 (d, *J* = 7.4 Hz, 1H), 6.51 (s, 2H), 4.49 (s, 2H), 3.84 (dd, *J* = 11.3, 5.1 Hz, 1H), 3.73 – 3.58 (m, 6H), 3.57 – 3.47 (m, 1H), 3.29 – 3.18 (m, 4H), 3.14 (dt, *J* = 11.9, 5.7 Hz, 1H), 3.01 (ddd, *J* = 20.8, 13.6, 6.0 Hz, 2H), 2.83 (s, 3H), 2.25 (s, 6H). (MS)EI: 425.3 (M+H), Retention Time: 16.72 min.

(S)-1-((2-((2-(3,4-dihydroisoquinolin-2(1H)-yl)ethyl)(methyl)amino)-2-oxoethyl)amino)-3-(4-hydroxy-2,6-dimethylphenyl)-1-oxopropan-2-aminium trifluoroacetate (199): See Procedure A: 28 mg (0.092 mmol) of **191**, 47 mg (0.090 mmol, 0.98 eq.) of PyBOP, 18 mg (0.10 mmol, 1.1 eq.) of N-(tert-butoxycarbonyl)glycine, 100 μL (92 mg, 0.91 mmol, 9.9 eq.) of NMM, and 4 mL of DMF. The intermediate was purified by column

chromatography (0-5 % MeOH in DCM), and 25 mg of intermediate was isolated as a crude mixture with tri(pyrrolidin-1-yl)phosphine oxide (approximately 2.5:1 phosphine oxide:intermediate by NMR). No repurification was performed due to poor UV absorbance. Procedure Bb: 25 mg (approximately 0.029 mmol) of crude, 2 mL of TFA and 2 mL DCM were added, and the solution was concentrated in vacuo after 5 min. No purification by reverse phase chromatography was performed. See Procedure D: Step 1: 50 μ L (37 mg, 0.29 mmol, 1.0 eq.) of N,N-diisopropylethylamine, 16 mg (0.031 mmol, 1.1 eq.) of PyBOP, 7 mg (0.041 mmol, 1.4 eq.) of 6-Cl-HOBt, 13 mg (0.32 mmol, 1.1 eq.) of Boc-O-Boc-L-2',6'-dimethyltyrosine, 3+1.5 mL of DMF. Step 2: 2 mL TFA and 2 mL DCM. Compound **199** (10.1 mg, Yield=20 % over 4 steps) was isolated as a white solid. ^1H NMR (500 MHz, Methanol- d_4) δ 7.35 – 7.22 (m, 3H), 7.19 (d, J = 7.4 Hz, 1H), 6.48 (s, 2H), 4.67 (s, 1H), 4.42 (s, 1H), 4.16 – 3.74 (m, 6H), 3.60 – 3.41 (m, 3H), 3.25 – 3.14 (m, 3H), 3.05 (s, 3H), 3.01 (dd, J = 14.1, 5.3 Hz, 1H), 2.24 (s, 6H). (MS)EI: 439.3 (M+H), Retention Time: 16.60 min.

(S)-1-(((2-((2-(3,4-dihydroisoquinolin-2(1H)-yl)ethyl)amino)-2-oxoethyl)amino)-3-(4-hydroxy-2,6-dimethylphenyl)-1-oxopropan-2-aminium trifluoroacetate (200): See Procedure D: Step 1: 15 mg (0.043 mmol) of **192**, 80 μ L (59 mg, 0.46 mmol, 11 eq.) of N,N-diisopropylethylamine, 23 mg (0.044 mmol, 1.0 eq.) of PyBOP, 7 mg (0.041 mmol, 0.96 eq.) of 6-Cl-HOBt, 19 mg (0.046 mmol, 1.1 eq.) of Boc-O-Boc-L-2',6'-dimethyltyrosine, 3+1.5 mL of DMF. Step 2: 2 mL TFA and 2 mL DCM. Compound **200** (7.3 mg, Yield=31 %) was isolated as a white solid. ^1H NMR (400 MHz, Methanol- d_4) δ 7.38 – 7.24 (m, 3H), 7.21 (d, J = 6.6 Hz, 1H), 6.49 (s, 2H), 4.62 (s, 1H), 4.41 (s, 1H), 4.03 – 3.83 (m, 3H), 3.69 (s, 2H), 3.56 (d, J = 16.8 Hz, 1H), 3.41 (t, J = 5.8 Hz, 3H), 3.27 – 3.14 (m, 3H), 3.02 (dd, J = 14.0, 5.2 Hz, 1H), 2.24 (s, 6H). (MS)EI: 425.3 (M+H), Retention Time: 16.30 min.

***In Vitro* Pharmacology**

Cell Lines and Membrane Preparations.

All *in vitro* opioid assays were performed by Ashley Brinkel, Jack Twarozynski, and Jessica Anand. Tissue culture reagents were purchased from Gibco Life Sciences (Grand Island, NY, U.S.) unless otherwise noted. C6-rat glioma cells stably expressing human MOR (C6-MOR) or human DOR (C6-DOR) and Chinese hamster ovary (CHO) cells stably expressing human KOR (CHO-KOR) were used for all *in vitro* assays. Cells were grown to confluence at 37 °C in 5% CO₂ in Dulbecco's modified Eagle medium (DMEM) containing 10% fetal bovine serum and 5% penicillin/streptomycin. Membranes were prepared by washing confluent cells three times with ice cold phosphate buffered saline (0.9% NaCl, 0.61 mM Na₂HPO₄, 0.38 mM KH₂PO₄, pH 7.4). Cells were detached from the plates by incubation in warm harvesting buffer (20 mM HEPES, 150 mM NaCl, 0.68 mM EDTA, pH 7.4) and pelleted by centrifugation at 1600 rpm for 3 min. The cell pellet was suspended in ice-cold 50 mM Tris- HCl buffer, pH 7.4, and homogenized with a Tissue Tearor (Biospec Products, Inc., Bartlesville, OK, U.S.) for 20 s. The homogenate was centrifuged at 15,000 rpm for 20 min at 4°C. The pellet was rehomogenized in 50 mM Tris-HCl with a Tissue Tearor for 10 s, followed by recentrifugation. The final pellet was resuspended in 50 mM Tris-HCl and frozen in aliquots at -80°C. Protein concentration was determined via a BCA protein assay (Thermo Scientific Pierce, Waltham, MA, U.S.) using bovine serum albumin as the standard.

Radioligand Competition Binding Assays.

Radiolabeled compounds were purchased from Perkin-Elmer (Waltham, MA, U.S.). Opioid ligand binding assays were performed by competitive displacement of 0.2 nM [³H]-diprenorphine (250 µCi, 1.85 TBq/mmol) by the peptidomimetic from membrane preparations containing opioid receptors as described above. The assay mixture, containing membranes (20 µg

protein/tube) in 50 mM Tris-HCl buffer (pH 7.4), 0.2 nM [³H]-diprenorphine, and various concentrations of test peptidomimetic, was incubated at room temperature on a shaker for 1 h to allow binding to reach equilibrium. The samples were rapidly filtered through Whatman GF/C filters using a Brandel harvester (Brandel, Gaithersburg, MD, U.S.) and washed three times with 50 mM Tris-HCl buffer, pH 7.4. Bound radioactivity on dried filters was determined by liquid scintillation counting, after saturation with EcoLume liquid scintillation cocktail, in a Wallac 1450 MicroBeta (Perkin-Elmer, Waltham, MA, U.S.). Nonspecific binding was determined using 10 μM naloxone. The results presented are the mean ± standard error (S.E.M.) from at least three separate assays performed in duplicate. K_i (nM) values were calculated using nonlinear regression analysis to fit a logistic equation to the competition data using GraphPad Prism, version 6.0c, (GraphPad Software Inc., La Jolla, CA).

[³⁵S]-GTPγS Binding Assays.

Agonist stimulation of [³⁵S]guanosine 5'-O-[γ-thio]triphosphate ([³⁵S]-GTPγS, 1250 Ci, 46.2 TBq/mmol) binding to G protein was measured as described previously.⁸² Briefly, membranes (10 μg of protein/well) were incubated for 1 h at 25°C in GTPγS buffer (50 mM Tris-HCl, 100 mM NaCl, 5 mM MgCl₂, 1 mM EDTA, pH 7.4) containing 0.1 nM [³⁵S]-GTPγS, 30 μM guanosine diphosphate (GDP), and varying concentrations of test peptidomimetic. G protein activation following receptor activation by peptidomimetic was compared with 10 μM of the standard compounds [D-Ala²,N-MePhe⁴,Gly-ol]enkephalin (DAMGO) at MOR, D-Pen^{2,5}-enkephalin (DPDPE) at DOR, or U69,593 at KOR. The reaction was terminated by vacuum filtration through GF/C filters that were washed 5 times with GTPγS buffer. Bound radioactivity was measured as described above. The results are presented as the mean ± standard error (S.E.M.) from at least three

separate assays performed in duplicate; potency (EC_{50} (nM)) and percent stimulation were determined using nonlinear regression analysis with GraphPad Prism, as above.

Mouse Liver Microsome Stability Assays

All liver microsome assays were performed by Quintara Biosciences. Metabolic stability of testing compounds was evaluated using mouse liver microsomes to predict intrinsic clearance. Mouse liver microsome tissue fractions were obtained from Corning or BioreclamationIVT. The assay was carried out in 96-well microtiter plates at 37°C. Reaction mixtures (25 μ L) contained a final concentration of 1 μ M test compound, 0.1 mg/mL liver microsome protein, and 1 mM NADPH in 100 mM potassium phosphate, pH 7.4 buffer with 3 mM $MgCl_2$. At each of the time points (0, 15, 30, and 60 minutes), 150 μ L of quench solution (acetonitrile with 0.1% formic acid) with internal standard (bucetin) was transferred to each well. Verapamil was included as a positive control to verify assay performance. Plates were sealed, vortexed, and centrifuged at 4°C for 15 minutes at 4000 rpm. The supernatant was transferred to fresh plates for LC/MS/MS analysis. All samples were analyzed on LC/MS/MS using an AB Sciex API 4000 instrument, coupled to a Shimadzu LC-20AD LC Pump system. Analytical samples were separated using a Waters Atlantis T3 dC18 reverse phase HPLC column (20 mm x 2.1 mm) at a flow rate of 0.5 mL/min. The mobile phase consists of 0.1% formic acid in water (solvent A) and 0.1% formic acid in acetonitrile (solvent B). The extent of metabolism was calculated as the disappearance of the test compound, compared to the 0-min time incubation. Initial rates were calculated for the compound concentration and used to determine $T_{1/2}$ values.

Molecular Modeling

All *in silico* experiments were performed by Irina Pogozheva. Modeling of three-dimensional (3D) structures of receptor-ligand complexes was based on available X-ray structures

of the mouse MOR (PDB ID: 5c1m)⁸³ in the active state, human KOR (PDB IDs: 4djh)¹²⁵ in the inactive conformation, and human DOR in the inactive conformation (PDB IDs: 4rwa)¹²⁶. Structures of peptidomimetic ligands were generated using the 3D-Builder Application of QUANTA (Accelrys, Inc) followed by Conformational Search included in the program package. Low-energy ligand conformations (within 2 kcal/mol) that demonstrated the best superposition of aromatic substituents of the ligand core with the pharmacophore elements (DMT and tetrahydroquinoline pendant) of receptor-bound conformations of peptidomimetics were selected for docking into the receptor binding pocket. Ligands were positioned inside the receptor binding cavity to reproduce the binding modes of peptidomimetics and co-crystallized ligands in MOR, DOR, and KOR X-ray structures. The docking pose of each ligand was subsequently refined using the solid docking module of QUANTA.

Animals and *In Vivo* Solutions

All *in vivo* assays were performed by Bryan Sears. Animal care and experimental procedures complied with the US National Research Council's Guide for the Care and Use of Laboratory Animals.⁹¹ Animal studies are reported in compliance with the ARRIVE guidelines.^{92,93} Mice were group-housed with a maximum of five animals per cage in clear polypropylene cages with corn cob bedding and nestlets as enrichment. Mice had free access to food and water at all times. Animals were housed in pathogen-free rooms maintained between 68 and 79 °F and humidity between 30 and 70 % humidity with a 12 h light/dark cycle with lights on at 07:00 h. Experiments were conducted in the housing room during the light cycle. All studies utilize male C57BL/6 mice from Envigo laboratories. Wild type mice weighing between 20-30 g at 7-15 weeks old, were used for behavioral experiments. All drug solutions were injected at a

volume of 10 ml/kg. All drugs were dissolved in 9:1 DMSO/saline solution except for morphine sulphate and 0.6 % acetic acid which were dissolved in saline and water, respectively. All drugs were given sc. except for 0.6 % acetic acid which was given ip.

Acetic Acid Stretch Assay (AASA)

Antinociceptive effects were evaluated in the mouse acetic acid stretch assay in which a noxious stimulus is administered ip. that induces a stretching behavior characterized by constriction of the abdomen followed by extension of the hind limbs. Mice received an injection of 0.6 % acetic acid, placed individually in clear plastic observation cages (10 x 6 x 8 in) with bedding, and the number of stretches were recorded for 20 min. Antinociceptive effects were determined with a 30 min pretreatment dose of compound sc. followed by 0.6 % acetic acid ip. A 5 min latency period after acetic acid injection was establish and total number of stretches were recorded for the following 20 min.

Chapter 7: Aliphatic Heterocycles as Novel Core Elements

7.1 Introduction

Before the full characterization of the aromatic-amine pendants described previously, we were interested in expanding the structural variability of our peptidomimetics. In short, this was a fallback plan if stability, *in vivo*, or *in vitro* improvements did not occur with any further modifications to our original monocyclic aromatic core. The direction we took was to perform a scaffold hop from an aromatic core to a cyclic aliphatic core (**Figure 21**). For these purposes, analogue **70** was used as the lead for this series. This scaffold hop would change the orbital hybridization of three important atoms (**Figure 21**, X, Y, Z) from sp² to sp³. This conversion from aromatic to aliphatic carbons is also correlated to improved drug solubility, success during clinical development,^{130,131} and reduced likelihood of CYP3A4 inhibition.¹³²

These three atoms located at the “joints” of the aromatic core ligand are used to hold the ether, benzyl, and dimethyltyrosine pharmacophores together. In the proposed aliphatic core, if these joints are carbon atoms, then new stereocenters would be introduced into this system, adding additional synthetic and SAR complexity to the ligands. If nitrogen is used instead, the stereocenter problem would not exist, though atoms X and Y cannot both be nitrogen, as this would make the peptidomimetic unstable in aqueous acid. Therefore, a combination of carbon and nitrogen atoms was utilized, of which a piperazine structure was selected to fulfil this role (**Figure 21**). The two nitrogens of the piperazine are spaced far enough apart to prevent acid instability, whereas the number of carbons at these joints are minimized to one, producing only one new stereocenter. One

nitrogen will be used to attach the benzyl pendant and the other will be used to attach an n-propyl group, which is designed to mimic the ethyl ether in the aromatic series. The carbon, thus, will be used to attach the DMT pharmacophore. By converting to this piperazine core, we also managed to improve some of the physiochemical properties of these ligands for BBB penetration, namely cLogP and tPSA,¹³³ without significantly changing their mass. Herein, the SAR of this novel core structure will be discussed. It should be noted that derivatives of this series are not limited to a piperazine structure, merely that the piperazine core will be used as a starting point.

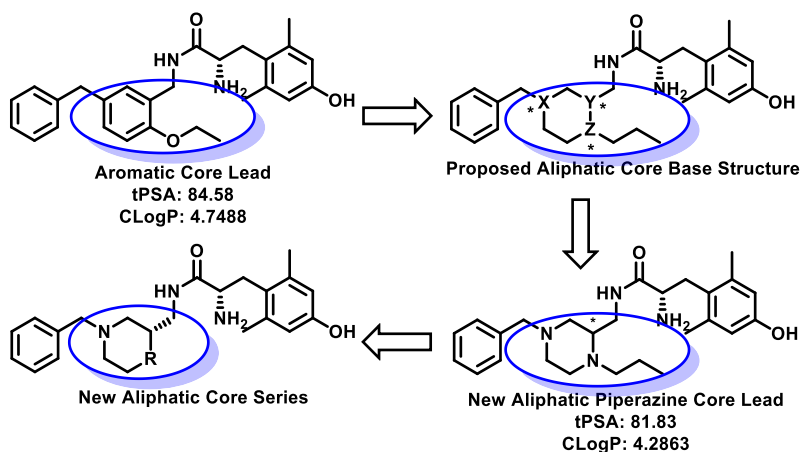


Figure 21: Conversion of the aromatic core peptidomimetic to cyclic aliphatic core peptidomimetics. This conversion would improve PK properties such as cLogP and tPSA without significantly increasing molecular weight.

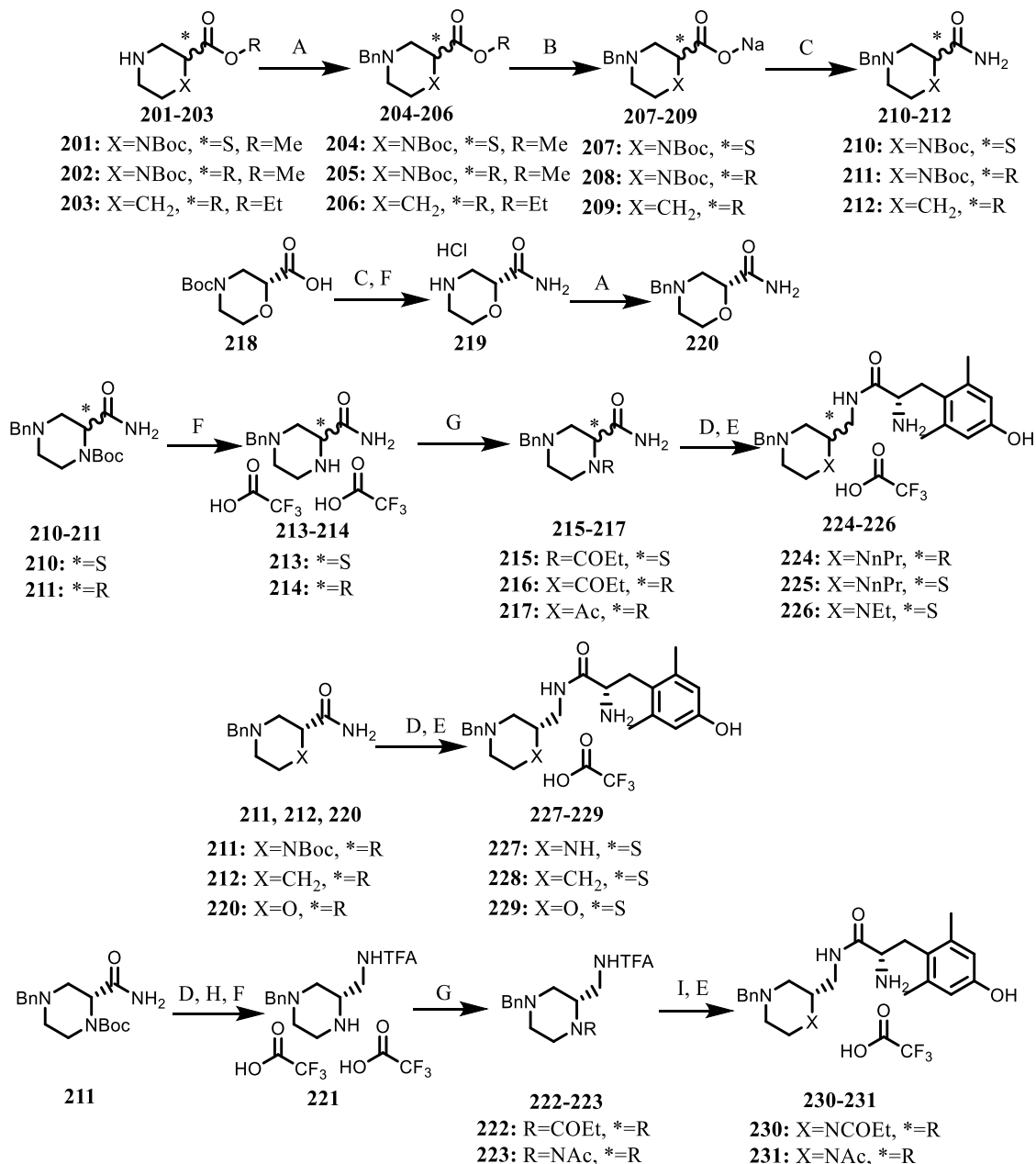
7.2 Results

General Chemistry: To synthesize these new aliphatic core peptidomimetics, commercially available nitrogen containing heterocycles were utilized that possessed a methyl ester. (**Scheme 11**). The appropriate commercially available enantiomer was used as starting material, and the stereochemistry of these heterocycles was maintained throughout the synthesis. This synthesis began with the introduction of the benzyl group through one equivalent of benzyl bromide. Saponification then followed using LiOH, with subsequent workup using sat. NaHCO₃ yields the

product as a sodium carboxylate. This carboxylate was converted into a primary amide using ammonium chloride and PyBOP, at which point the synthesis diverged depending on the analogues desired.

Should alkyl chains coming off the piperazine be desired, the Boc group here would first be removed with TFA and DCM and the subsequent amine would be acylated using neat acyl anhydride. The synthesis would resume with reduction by $\text{BH}_3 \cdot \text{Me}_2\text{S}$ at 65 °C followed by coupling to DMT. Final compounds that contained the piperidine, morpholine, or the unsubstituted piperazine core (**227-229**) were instead immediately subject to reduction by $\text{BH}_3 \cdot \text{Me}_2\text{S}$ at 65 °C followed by PyBOP mediated coupling to Boc protected DMT. In the case of the unsubstituted piperazine, the reduction occurred with the Boc group still present, as this group was not reduced and protected the secondary amine from coupling to DMT. Finally, if amides are desired off the piperazine, then reduction by $\text{BH}_3 \cdot \text{Me}_2\text{S}$ at 65 °C would be performed on the Boc protected piperazine. Here, the reduced primary amine would be protected using trifluoroacetic anhydride and pyridine. This orthogonal protection strategy allowed for selective deprotection of the Boc group and subsequent acylation of the newly liberated secondary amine. This was followed by removal of the TFA group by NaOH and coupling to DMT.

Scheme 11: Synthesis of Analogues 224-231.



A) BnBr, K₂CO₃, DMF. B) LiOH, THF, EtOH, H₂O. C) NH₄Cl, PyBOP, NMM, DMF. D) 2M BH₃*Me₂S, THF. E) 1. DibocDMT, DIEA, PyBOP, HOBT-Cl, DMF. 2. TFA, DCM F) TFA, DCM or conc. HCl, Dioxane G) Acyl₂O, neat. H) TFAA, pyridine. I) NaOH, H₂O, MeOH

SAR: The conversion of aromatic core analogue **70** to the aliphatic core introduced a new stereocenter into our aliphatic core series. As such, we first opted to determine which stereocenter, if any, will be the best for our ligands. Based upon the binding affinity of the R- and S-isomers (**224** and **225** respectively) of the newly introduced stereocenter (**Table 22**) it appears that the S-

Name	Chemical Structure	Binding Affinity, K_i (nM)			Selectivity
		MOR	DOR	KOR	
70		3.6±0.5	4.8±0.9	1200±120	1:1.3:330
224		27±14	390±150	320**	1:14:12
225		1.6±0.3	108±15	62.5**	1:69:40
226		1.08**	44.7**	48.2±3.8*	1:41:45
227		21.6**	0.01**	2000**	1:0.00046:93
228		3.24**	147±70	335**	1:45:103
229		1.54**	112**	483**	1:73:314
230		24.6**	30.1**	585**	1:1.2:24
231		44.3**	60.0**	>3000**	1:1.4:>68

Table 22: Binding affinity of cyclic aliphatic core compounds at human MOR, DOR, and KOR.

Binding affinities (K_i) were obtained by competitive displacement of radiolabeled [^3H] diprenorphine in membrane preparations. Included is **70** for comparison. Selectivity was calculated by dividing the K_i of each receptor by the K_i at MOR for a given compound. All data were from three separate experiments, performed in duplicate unless otherwise noted. These data are reported as the average \pm standard error of the mean. ** N=1, * N=2.

isomer yields a log improvement in affinity at MOR, and a 4-fold improvement in affinity at DOR. When the potencies of these two analogues are compared (**Table 23**), the S-isomer again triumphs over the R-isomer with a 2-log improvement in potency at MOR. Therefore, the S-isomer appears to be the superior diastereomer. Further derivatives were then made with this stereocenter.

Of the additional analogues synthesized in this series, most possessed similar MOR-affinity as piperazine **225**. The only exceptions here are the unmodified piperazine **227**, and the two amide analogues **230** and **231**, which yielded a log unit loss in affinity. DOR-affinity varied little in this series, and most analogues had around 100 nM affinity at this receptor, akin to piperazine **225**. The only exception here is the free piperazine **227** which possessed a 4-log improvement in binding affinity at DOR over the other analogues.

KOR-affinity was found to be 20-fold higher than **70** upon conversion to the new scaffold with the favorable diastereomer **225**. This enhanced affinity is maintained with the other N-alkyl analogue **226**. However, conversion to the morpholine **229**, free piperazine **227**, or N-acyl piperazines **230-231** reduced binding affinity by at least a log unit.

Notable within these analogues is a significant drop in binding affinity balance between MOR and DOR upon conversion to the new core. Four of these analogues possessed 40-fold improved MOR-binding over DOR-binding. The amide analogues **230** and **231** managed to maintain a roughly 1:1 binding affinity balance, whereas the free piperazine **227** massively favored binding to DOR over MOR based on an N of 1. Selectivity over KOR was generally diminished for all analogues, the only exception being the morpholine core compound **229**.

The compounds synthesized herein yielded interesting trends in potency and efficacy at MOR, DOR, and KOR, and are shown in **Table 23**. MOR-potency was generally not significantly

different from the aromatic core analogue **70**, though potency was diminished with the free piperazine and the piperidine analogues **227** and **228** respectively. Interestingly, the two amide analogues **230** and **231** produced no MOR-stimulation whatsoever. Of those that did stimulate MOR, there was little significant variation in efficacy. With regards to DOR, only analogue **230** was capable of stimulating DOR. Even then, the potency and efficacy of this analogue was low.

Name	Structure	Potency, EC_{50} (nM)			Efficacy (% Stimulation)		
		MOR	DOR	KOR	MOR	DOR	KOR
70		72±14	DNS	DNS	75.5±5.8	DNS	DNS
224		>2480	DNS	DNS**	>34.6	DNS	DNS**
225		110±24	DNS*	>1200**	76.0±8.5	DNS*	>40**
226		139**	DNS**	DNS**	62.9**	DNS**	DNS**
227		851**	DNS**	DNS**	76.5**	DNS**	DNS**
228		420**	DNS**	>3000**	81.3**	DNS**	>45**
229		100**	DNS**	>1500**	84.0**	DNS**	>15**
230		DNS**	607**	DNS**	DNS**	21.0**	DNS**
231		DNS**	DNS**	DNS**	DNS**	DNS**	DNS**

Table 23: Potency and efficacy of cyclic aliphatic core compounds at human MOR, DOR, and KOR. Potency and efficacy data were obtained using agonist induced stimulation of [³⁵S] GTPγS binding. Potency is represented as EC_{50} (nM) and efficacy as percent maximal stimulation relative to standard agonist DAMGO (MOR), DPDPE (DOR), or U69,593 (KOR) at 10 μM. Included is **70** for comparison. All data were from three separate experiments, performed in duplicate unless otherwise noted. These data are reported as the average ± standard error of the mean. ** N=1, * N=2. DNS=Does Not Stimulate.

Only three analogues could stimulate KOR, namely the original S-piperazine analogue **225**, the piperidine analogue **228**, and the morpholine analogue **229**. However, the potency of these analogues was poor, with values greater than 1.2 μM .

Metabolic Stability: A few of these analogues were also screened for their metabolic stability. These are shown in **Table 24** and the aromatic precursor **70** was included for comparison. Here only the two piperazine diastereomers **224** and **225** were tested. This conversion yielded no significant changes in metabolic stability compared to the aromatic core analogue **70** and there was no difference in stability between the two diastereomers.

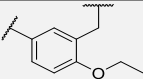
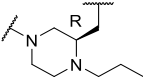
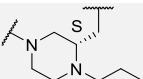
Name	R ¹	T _{1/2} (min)	Verapamil T _{1/2} (min)	Stability Ratio	cLogP
70		23.7±5.9	14.6±1.0	1.6±0.4	4.75
224		38.7±2.0	27.6±4.9	1.4±0.3	4.29
225		37.0±1.2	27.6±4.9	1.3±0.2	4.29

Table 24: Metabolic stability of cyclic aliphatic core compounds in MLM. Included are the compound half-life (T_{1/2}), the half-life of the positive control verapamil, and the stability ratio between the compound and the positive control. The stability ratio was calculated by dividing the half-life of the analogue of interest by the half-life of the positive control in that assay. Included is compound **70** for comparison. Individual compounds were tested once, with errors representing the SE in the decay curve regressed onto the data collected in 15-minute intervals.

Finally, the cLogP of these analogues are included and were calculated using PerkinElmer's ChemDraw® Professional Software.

7.3 Discussion and Conclusions

SAR: The analogues presented in this chapter grant deeper insight into factors necessary to produce bifunctional MOR/DOR ligands. The distinction between the two piperazine diastereomers **224** and **225** points to the importance of the S-isomer, needed to orient the pharmacophore elements properly to interact with the opioid receptors. This stereochemistry is consistent with that of the original bicyclic peptidomimetic series, suggesting similar modes of receptor binding. In general,

conversion to this new scaffold did not reduce MOR-affinity. The exceptions here are the free piperazine **227**, and the two amide analogues **230** and **231** which each yielded a log unit loss in binding affinity. These data point to two different trends. MOR-affinity is reduced by the presence of a hydrogen bond donor in the free piperazine, or by the presence of the amide in the piperazine. For the amide, this loss can be attributed either to a loss of conformational flexibility, or more likely, due to negative interactions between the carbonyl of the ligand and MOR. DOR-affinity was lost upon conversion to this new core and was consistent across most analogues. This suggests that the conversion to the aliphatic core itself is responsible for the loss in affinity rather than any particular functional group. The only exception here is the free piperazine analogue **227**, which possessed subnanomolar binding affinity at DOR. This again points to the hydrogen bond donor in this analogue and may be a useful pharmacophore for DOR selective ligands.

KOR-affinity was increased upon conversion to this aliphatic core, though in this case it was sensitive to changes in functional groups on the core. In general, elimination of the N-alkyl chains or conversion of the N-alkyl groups to N-acyl groups reduced the binding affinity of these analogues at KOR. This suggests that the alkyl group is picking up a specific interaction in KOR, an interaction that can be disrupted with removal of the alkyl chain, or by the incorporation of a carbonyl.

Conversion to the new core also yielded a greater number of MOR-agonists compared to their aromatic core counterparts. Whereas the aromatic core analogues reached an efficacy optimum in compound **70** as illustrated in Chapter 2, here most analogues possessed consistently high MOR-efficacy. This was true regardless of the size or presence of the N-alkyl chain, suggesting the amine connecting the benzyl group may be responsible for MOR activation. This is consistent with the amine portion of the aromatic-amine pharmacophore described in the

previous chapters, the difference here being the distance of that amine from the DMT residue. Interestingly, this efficacy was lost with the two amide analogues **230** and **231**. This can be attributed to interactions of the newly introduced carbonyl negatively interacting with MOR and preventing receptor activation. This factor may also be what is affecting MOR-binding with these two ligands. MOR-potency appears to be retained when a hydrogen bond acceptor exists within the core, as the N-alkyl analogues **225** and **226**, and the morpholine analogue **229** each possessed the highest potency at MOR. Removal of this hydrogen bond acceptor as in the piperidine **228** or the presence of a hydrogen bond donor at this position as in **227** results in losses in MOR-potency.

Consistent with their aromatic core counterparts from Chapter 2, these analogues consistently did not stimulate DOR and KOR with few exceptions. Only the N-propionyl analogue **230** possessed any capability to stimulate DOR, a property that may be a product of its possession of both a carbonyl and a sufficiently long alkyl chain. The N-ethyl piperazine, piperidine and morpholine analogues **226**, **228**, and **229** were very weak KOR-partial agonists. Two of these analogues were the smallest in this series and did not possess a hydrogen bond donor in the ring. As such, it is possible that a hydrogen bond donor here may prevent KOR-stimulation, or that this can be attenuated by short alkyl chains.

Metabolic Stability: While these new analogues managed to reduce the cLogP by half a unit, no significant differences in stability were observed compared to aromatic analogue **70** where tested. Unlike the diastereomers discussed in Chapter 3, inversion of the core stereocenter between **224** and **225** did not yield any differences in stability. This suggests that the CYP enzyme is unable to target this stereocenter. Furthermore, the failure to improve stability may be a product of the piperazine nitrogens stabilizing free radical formation on adjacent positions. Thus far, only the

more lipophilic cyclic aliphatic core analogues were tested for stability. Additional screening of the smaller, less lipophilic analogues may yet yield stability improvements.

Conclusions: The analogues synthesized herein reinforce the utility of our aromatic-amine pharmacophore. Here, the difference lies in the distance the pharmacophore is from the DMT pendant. While these analogues possess reduced potency compared to those of the previous chapters, they suggest that the aromatic-amine pharmacophore can tolerate differences in positioning and alternative forms of rigidification in the core of the ligand. In this case, shifting of the pharmacophore position makes the pharmacophore more dependent on core modifications to retain MOR-potency, and efficacy can only be eliminated with distal amides in this series. Notably, while losses in DOR affinity were observed, only one analogue could weakly stimulate DOR. Likewise, only a few could weakly stimulate KOR. If bifunctional MOR/DOR ligands are desired from this series, additional derivatization is necessary to recover the lost DOR-affinity.

7.4 Experimental

Chemistry

General Methods: All reagents and solvents were obtained commercially and were used without further purification. Intermediates were purified by flash chromatography using a Biotage Isolera One instrument. Most purification methods utilized a hexanes/ethyl acetate solvent system in a Biotage SNAP KP-Sil column, with a linear gradient between 0 and 100% ethyl acetate. Reverse phase column chromatography using a linear gradient of 0% to 100% solvent B (0.1% TFA in acetonitrile) in solvent A (0.1% TFA in water) using a Biotage SNAP Ultra C18 column was utilized for some intermediate amine salts. Purification of final compounds was performed using a Waters semipreparative HPLC with a Vydac protein and peptide C18 reverse phase column,

using a linear gradient of 0% to 100% solvent B in solvent A at a rate 1% per minute, monitoring UV absorbance at 230 nm. The purity of final compounds was assessed using a Waters Alliance 2690 analytical HPLC instrument with a Vydac protein and peptide C18 reverse phase column. A linear gradient (gradient A) of 0% to 70% solvent B in solvent A in 70 min, measuring UV absorbance at 230 nm was used to determine purity. All final compounds used for testing were $\geq 95\%$ pure, as determined by analytical HPLC. ^1H NMR and ^{13}C NMR data were obtained on a 500 or 400 MHz Varian spectrometer using CDCl_3 , CD_3OD , $\text{DMSO-}d_6$, or D_2O as solvents. The identities of final compounds were verified by mass spectrometry using an Agilent 6130 LC-MS mass spectrometer in positive ion mode, or an Agilent 6230 TOF HPLC-MS in the positive ion mode.

General Procedure for N-Benzyl Attachment (Procedure A): To a flame dried flask containing cyclic secondary amine was added 2 equivalents of potassium carbonate and the flask was flushed with argon. 4 mL of DMF was added and 1.2 equivalents of benzyl bromide was added dropwise. The flask was stirred overnight at room temperature and concentrated in vacuo. The residue was partitioned between EtOAc and sat. Na_2CO_3 and extracted with EtOAc. The organic layers were combined, dried with MgSO_4 , and filtered. The filtrate was concentrated in vacuo and the residue was purified via column chromatography (0 to 20 % EtOAc in Hexanes) yielding the N-benzylated product.

General Procedure for the Saponification of Esters (Procedure B): To a flask containing 1 equivalent of the desired ester was added 7 equivalents of LiOH, 2 mL of THF, 2 mL of EtOH, and 2 mL of H_2O . The reaction was stirred for 4-6 hours under ambient atmosphere and temperature. Upon completion, the solvent was quenched with sat. NaHCO_3 concentrated in vacuo,

suspended in acetone, and filtered. The precipitate was washed with additional acetone, and the filtrate was concentrated in vacuo, yielding the saponified product as a sodium carboxylate.

General Procedure for Primary Amide Formation (Procedure C): To a flask containing 1 equivalent of the sodium carboxylate was added 1 equivalent of PyBOP and 1 equivalent of ammonium chloride. The flask was flushed with argon, DMF was added as solvent, and 10 equivalents of N-methylmorpholine were added. The reaction was stirred overnight, at which point it was partitioned between DCM and 2M NaOH. The product was then extracted with DCM and the organic layer was filtered and concentrated in vacuo. The residue was then purified via column chromatography (0-10 % methanol in DCM or EtOAc).

General Procedure for the Reduction of Amides (Procedure D): To a dried flask containing 1 equivalent of the desired amide under argon was added THF and 7 equivalents of 2 M $\text{BH}_3 \cdot \text{Me}_2\text{S}$ complex in THF. The reaction was heated at 65 °C for 3 hours, at which point the reaction was quenched with MeOH and heated for an additional 15 minutes. The reaction was then cooled, concentrated in vacuo, and was used without further purification.

General Procedure for the Coupling of 2',6'-Dimethyltyrosine to Functionalized Amine Salt (Procedure E): To a dried flask containing the amine under argon was added 3 mL of DMF and 10 equivalents of Hunig's base. 1 equivalent of PyBOP and 1 equivalent of 6-Cl-HOBt was added, followed by a 1 equivalent of doubly Boc protected 2',6'-Dimethyltyrosine in 1.5 mL DMF. The solution was stirred overnight at room temperature, concentrated in vacuo, and purified via semipreparative reverse phase HPLC (0.1% TFA in water: 0.1% TFA in acetonitrile). 2 mL of TFA and 2 mL of DCM were then added, and the solution was stirred for an additional hour. The reaction mixture was concentrated in vacuo and purified via an additional semipreparative reverse

phase HPLC (0.1% TFA in water: 0.1% TFA in acetonitrile). The product was concentrated in vacuo and lyophilized overnight to yield the final peptidomimetic.

General procedure for the deprotection of Boc groups on intermediates using TFA and DCM (Procedure Fa): To a flask containing the Boc protected intermediate was added 2 mL of TFA and 2 mL of DCM. The solution was stirred for 1 hour under ambient atmosphere and temperature. The solution was then concentrated in vacuo, yielding the deprotected product as a TFA salt.

General procedure for the deprotection of Boc groups on intermediates using conc. HCl and Dioxane (Procedure Fb): To a flask containing the Boc protected intermediate was added 2 mL of dioxane and 0.2 mL of conc. HCl. The solution was stirred for 1 minute under ambient atmosphere and temperature. The solution was then concentrated in vacuo and triturated with DCM, yielding the deprotected product as an HCl salt.

General procedure for the acylation of the piperazine core analogues (Procedure Ga): To a dried flask containing the Boc deprotected piperazine under argon was added neat acyl anhydride. The reaction was stirred for 1 hour and concentrated in vacuo. The product was then partitioned between 2M NaOH and DCM. The compound was extracted with DCM, filtered, and concentrated in vacuo yielding the desired acylated compound.

General procedure for the acylation of the piperazine core analogues (Procedure Gb): To a dried flask containing the Boc deprotected piperazine under argon was added neat acyl anhydride. The reaction was stirred for 1 hour and concentrated in vacuo. The product was then partitioned between sat. NaHCO₃ and DCM. The compound was extracted with DCM, filtered, concentrated

in vacuo and purified via column chromatography (10% MeOH in DCM) yielding the desired acylated compound.

General procedure for the trifluoroacetyl protection of reduced primary amides (Procedure H):

To a dried flask containing a stir bar and the just reduced crude primary amine under argon was added 7 equivalents of trifluoroacetic anhydride and 4 mL of pyridine. The solution was stirred at room temperature overnight. The reaction was then concentrated in vacuo and partitioned between DCM and an aqueous solution of saturated NaHCO₃. The product was then extracted with DCM, and the combined extracts were filtered and concentrated in vacuo. Purification by column chromatography (0 to 60 % EtOAc in Hexanes) yielded the protected amine.

General procedure for the deprotection of trifluoroacetamides (Procedure I): To a flask equipped with the trifluoroacetyl protected amide and a stir bar was added 2 mL of MeOH and 2 mL of 2M NaOH in water. The solution was stirred for 2 hours, at which point the solution was either directly concentrated in vacuo, or first quenched with an aqueous solution of saturated NaHCO₃ before being concentrated in vacuo. The residue was suspended in acetonitrile and filtered, leaving the deprotected amine that was used without further purification.

1-(tert-butyl) 2-methyl (S)-4-benzylpiperazine-1,2-dicarboxylate (204): See Procedure A: 120 mg (0.49 mmol) of **1-(tert-butyl) 2-methyl (S)-piperazine-1,2-dicarboxylate (201)**, 135 mg (0.98 mmol, 2.0 eq.) of potassium carbonate, 50 μ L (72 mg, 0.42 mmol, 0.86 eq.) of benzyl bromide, and 4 mL of DMF. Compound **204** (143 mg, Yield=87 %) was isolated as a colorless oil. ¹H NMR (400 MHz, Chloroform-*d*) δ 7.35 – 7.18 (m, 5H), 4.71 (s, 0.5H), 4.54 (s, 0.5H), 3.81 (dd, *J* = 38.4, 12.0 Hz, 1H), 3.73 (s, 1.5H), 3.70 (s, 1.5H), 3.57 (t, *J* = 13.1 Hz, 1H), 3.43 (t, *J* = 14.2 Hz, 1H), 3.35 – 3.24 (m, 1.5H), 3.18 (td, *J* = 12.6, 3.6 Hz, 0.5H), 2.77 (dd, *J* = 21.2, 11.5 Hz, 1H),

2.18 (td, $J = 11.2, 4.0$ Hz, 1H), 2.09 (t, $J = 11.7$ Hz, 1H), 1.47 (s, 5H), 1.42 (s, 4H). ^{13}C NMR (101 MHz, Chloroform-*d*) δ 171.36, 171.09, 155.86, 155.36, 137.67, 128.74, 128.15, 127.18, 80.27, 62.31, 55.53, 54.37, 53.49, 52.47, 52.32, 51.99, 41.99, 41.03, 28.33, 28.27.

1-(tert-butyl) 2-methyl (R)-4-benzylpiperazine-1,2-dicarboxylate (205): See Procedure A: 189 mg (0.77 mmol) of **1-(tert-butyl) 2-methyl (R)-piperazine-1,2-dicarboxylate (202)**, 218 mg (1.6 mmol, 2.0 eq.) of potassium carbonate, 110 μL (158 mg, 0.92 mmol, 1.2 eq.) of benzyl bromide, and 5 mL of DMF. Compound **205** (229 mg, Yield=89 %) was isolated as a colorless oil. ^1H NMR (500 MHz, Chloroform-*d*) δ 7.33 – 7.21 (m, 5H), 4.71 (s, 0.5H), 4.54 (s, 0.5H), 3.81 (dd, $J = 48.8, 13.1$ Hz, 1H), 3.73 (s, 1.5H), 3.70 (s, 1.5H), 3.56 (t, $J = 14.4$ Hz, 1H), 3.43 (dd, $J = 18.2, 13.3$ Hz, 1H), 3.35 – 3.24 (m, 1.5H), 3.18 (td, $J = 12.7, 3.7$ Hz, 0.5H), 2.77 (dd, $J = 26.9, 11.2$ Hz, 1H), 2.18 (td, $J = 12.5, 11.7, 4.0$ Hz, 1H), 2.10 (td, $J = 11.5, 3.5$ Hz, 1H), 1.47 (s, 5H), 1.43 (s, 4H). ^{13}C NMR (126 MHz, Chloroform-*d*) δ 171.32, 171.06, 155.85, 155.34, 137.68, 128.73, 128.14, 127.17, 80.23, 62.33, 62.30, 55.55, 54.38, 53.50, 52.47, 52.33, 51.97, 51.93, 42.01, 41.04, 28.33, 28.27.

Ethyl (R)-1-benzylpiperidine-3-carboxylate (206): See Procedure A: 133 mg (0.85 mmol) of **ethyl (R)-piperidine-3-carboxylate (203)**, 236 mg (1.7 mmol, 2.0 eq.) of potassium carbonate, 120 μL (173 mg, 1.0 mmol, 1.2 eq.) of benzyl bromide, and 4 mL of DMF. Compound **206** (129 mg, Yield=62 %) was isolated as a colorless oil. ^1H NMR (400 MHz, Chloroform-*d*) δ 7.38 – 7.20 (m, 5H), 4.11 (q, $J = 7.2$ Hz, 2H), 3.52 (q, $J = 13.4$ Hz, 2H), 2.95 (d, $J = 11.2$ Hz, 1H), 2.72 (d, $J = 11.4$ Hz, 1H), 2.58 (ddd, $J = 14.1, 6.9, 3.8$ Hz, 1H), 2.23 (t, $J = 10.5$ Hz, 1H), 2.10 – 1.98 (m, 1H), 1.92 (dt, $J = 12.8, 4.1$ Hz, 1H), 1.72 (dt, $J = 13.0, 3.8$ Hz, 1H), 1.66 – 1.42 (m, 2H), 1.23 (t, $J = 7.1$ Hz, 3H). ^{13}C NMR (101 MHz, Chloroform-*d*) δ 174.23, 138.24, 129.04, 128.16, 126.97, 63.28, 60.22, 55.39, 53.59, 41.88, 26.96, 24.52, 14.21.

Sodium (S)-4-benzyl-1-(tert-butoxycarbonyl)piperazine-2-carboxylate (207): See Procedure B: 118 mg (0.35 mmol) of **204**, 42.5 mg (1.77 mmol, 5.0 eq.) of LiOH, 2 mL of EtOH, 2 mL of THF, 2 mL of H₂O. Compound **207** (108 mg, Yield= 89 %) was isolated as the sodium salt and as a colorless oil. ¹H NMR (400 MHz, Methanol-*d*₄) δ 7.32 (d, *J* = 6.7 Hz, 2H), 7.26 (t, *J* = 7.3 Hz, 2H), 7.24 – 7.14 (m, 1H), 4.36 (br s, 1H), 3.74 (d, *J* = 13.0 Hz, 1H), 3.57 – 3.33 (m, 4H), 2.71 (br s, 1H), 2.15 (dd, *J* = 11.2, 4.6 Hz, 1H), 1.94 (td, *J* = 11.9, 3.5 Hz, 1H), 1.43 (s, 9H). ¹³C NMR (101 MHz, Methanol-*d*₄) δ 176.18, 137.59, 128.76, 127.75, 126.63, 79.43, 62.31, 54.80, 52.18, 27.32.

Sodium (R)-4-benzyl-1-(tert-butoxycarbonyl)piperazine-2-carboxylate (208): See Procedure B: 118 mg (0.35 mmol) of **205**, 42.5 mg (1.77 mmol, 5.0 eq.) of LiOH, 2 mL of EtOH, 2 mL of THF, 2 mL of H₂O. Compound **208** (121 mg, Quantitative Yield) was isolated as the sodium salt and as a colorless oil. ¹H NMR (400 MHz, Methanol-*d*₄) δ 7.32 (d, *J* = 6.7 Hz, 2H), 7.26 (t, *J* = 7.4 Hz, 3H), 7.24 – 7.14 (m, 1H), 4.37 (s, 1H), 3.74 (d, *J* = 13.0 Hz, 1H), 3.57 – 3.34 (m, 6H), 2.71 (s, 1H), 2.15 (dd, *J* = 11.2, 4.6 Hz, 1H), 1.94 (td, *J* = 11.8, 3.5 Hz, 1H), 1.43 (s, 9H). ¹³C NMR (101 MHz, Methanol-*d*₄) δ 176.21, 137.56, 128.78, 127.76, 126.64, 79.45, 62.33, 54.83, 52.18, 27.34.

Sodium (R)-1-benzylpiperidine-3-carboxylate (209): See Procedure B: 120 mg (0.49 mmol) of **206**, 61 mg (2.5 mmol, 5.3 eq.) of LiOH, 3 mL of EtOH, 3 mL of THF, 3 mL of H₂O. Compound **209** (121 mg, Quantitative Yield) was isolated as the sodium salt and as a white waxy solid. ¹H NMR (400 MHz, Methanol-*d*₄) δ 7.36 – 7.19 (m, 5H), 3.53 (d, *J* = 12.8 Hz, 2H), 3.49 (d, *J* = 12.8 Hz, 2H), 3.08 (ddt, *J* = 11.3, 3.7, 1.6 Hz, 1H), 2.84 (d, *J* = 11.6 Hz, 1H), 2.39 (tt, *J* = 11.9, 3.8 Hz, 1H), 2.04 (t, *J* = 11.3 Hz, 1H), 2.00 – 1.89 (m, 2H), 1.73 – 1.64 (m, 1H), 1.58 (qt, *J* = 12.9,

3.9 Hz, 1H), 1.34 (qd, $J = 12.6, 4.4$ Hz, 1H). ^{13}C NMR (101 MHz, Methanol- d_4) δ 181.51, 137.00, 129.50, 127.82, 126.92, 63.20, 56.71, 53.45, 45.02, 28.05, 24.56.

Tert-butyl (S)-4-benzyl-2-carbamoylpiperazine-1-carboxylate (210): See Procedure C: 126 mg (0.37 mmol) of **207**, 193 mg (0.37 mmol, 1.0 eq.) of PyBOP, 21 mg (0.39 mmol, 1.1 eq.) of ammonium chloride, 410 μL (377 mg, 3.7 mol, 10 eq.) of NMM, and 4 mL of DMF. Compound **210** (78 mg, Yield= 66 %) was isolated using standard phase chromatography (EtOAc) as a colorless oil. ^1H NMR (500 MHz, Chloroform- d) δ 7.33 – 7.20 (m, 5H), 6.38 (br s, 1H), 6.12 (br s, 1H), 4.59 (br s, 1H), 3.96 (br s, 1H), 3.58 – 3.46 (m, 2H), 3.35 (dt, $J = 11.7, 2.0$ Hz, 1H), 3.12 (br s, 1H), 2.75 (d, $J = 11.2$ Hz, 1H), 2.17 (dd, $J = 11.7, 4.3$ Hz, 1H), 2.04 (td, $J = 11.7, 3.5$ Hz, 1H), 1.45 (s, 9H). ^{13}C NMR (126 MHz, Chloroform- d) δ 172.77, 137.06, 129.04, 128.31, 127.33, 80.89, 62.62, 52.90, 52.13, 28.30.

Tert-butyl (R)-4-benzyl-2-carbamoylpiperazine-1-carboxylate (211): See Procedure C: 231 mg (0.68 mmol) of **208**, 352 mg (0.68 mmol, 1.0 eq.) of PyBOP, 39 mg (0.73 mmol, 1.1 eq.) of ammonium chloride, 740 μL (681 mg, 6.7 mol, 10.0 eq.) of NMM, and 5 mL of DMF. Compound **211** (217 mg, Quantitative Yield) was isolated using standard phase chromatography (10% MeOH in DCM) as a yellow oil. ^1H NMR (500 MHz, Chloroform- d) δ 7.32 – 7.18 (m, 5H), 6.34 (br s, 1H), 6.03 (br s, 1H), 4.59 (br s, 1H), 3.96 (br s, 1H), 3.54 (d, $J = 13.2$ Hz, 1H), 3.49 (d, $J = 13.3$ Hz, 1H), 3.35 (dt, $J = 11.6, 2.0$ Hz, 1H), 3.12 (br s, 1H), 2.75 (d, $J = 11.3$ Hz, 1H), 2.17 (dd, $J = 11.7, 4.3$ Hz, 1H), 2.03 (td, $J = 11.8, 3.5$ Hz, 1H), 1.46 (s, 9H). ^{13}C NMR (126 MHz, Chloroform- d) δ 172.68, 137.19, 129.00, 128.29, 127.29, 80.84, 62.64, 52.93, 52.13, 28.30.

(S)-1-benzylpiperidine-3-carboxamide (212): See Procedure C: 26 mg (0.11 mmol) of **209**, 58 mg (0.11 mmol, 1.0 eq.) of PyBOP, 6 mg (0.11 mmol, 1.0 eq.) of ammonium chloride, 120 μL (110 mg, 1.1 mol, 10 eq.) of NMM, and 4 mL of DMF. Compound **212** (24 mg,

Quantitative Yield) was isolated using standard phase chromatography (10% MeOH in DCM) as a white solid. ^1H NMR (500 MHz, Chloroform-*d*) δ 7.75 (br s, 1H), 7.43 – 6.70 (m, 5H), 5.68 (br s, 1H), 3.50 (d, $J = 12.9$ Hz, 1H), 3.47 (d, $J = 12.9$ Hz, 1H), 2.84 (br s, 1H), 2.72 (br s, 1H), 2.50 (p, $J = 4.4$ Hz, 1H), 2.37 (br s, 1H), 2.19 (br s, 1H), 1.89 (br s, 1H), 1.79 – 1.68 (m, 1H), 1.67 – 1.50 (m, 2H). ^{13}C NMR (126 MHz, Chloroform-*d*) δ 177.75, 137.43, 129.16, 128.43, 127.41, 63.44, 54.91, 53.77, 41.72, 26.90.

(R)-2-carbamoylmorpholin-4-ium chloride (219): See Procedure C and Fb: 82 mg (0.36 mmol) of **(R)-4-(tert-butoxycarbonyl)morpholine-2-carboxylic acid (218)**, 187 mg (0.36 mmol, 1.0 eq.) of PyBOP, 20 mg (0.37 mmol, 1.1 eq.) of ammonium chloride, 390 μL (359 mg, 3.5 mmol, 10.0 eq.) of NMM, and 4 mL of DMF. No column chromatography was performed. 2 mL of Dioxane and 0.2 mL of conc. HCl. Compound **219** (30 mg, Yield=51 %) was isolated as a colorless oil. ^1H NMR (400 MHz, Methanol-*d*₄) δ 4.33 (dd, $J = 10.9, 2.9$ Hz, 1H), 4.19 (ddd, $J = 13.0, 3.9, 1.9$ Hz, 1H), 3.93 (td, $J = 13.1, 12.3, 2.7$ Hz, 1H), 3.59 (dd, $J = 12.7, 1.7$ Hz, 1H), 3.24 – 3.14 (m, 2H), 3.09 (dd, $J = 12.9, 11.0$ Hz, 1H). ^{13}C NMR (101 MHz, Methanol-*d*₄) δ 170.74, 72.20, 63.12, 44.11, 42.37.

(S)-4-benzylmorpholine-2-carboxamide (220): See Procedure A: 30 mg (0.18 mmol) of **219**, 25 μL (36 mg, 0.21 mmol, 1.2 eq.) of BnBr, 52 mg (0.38 mmol, 2.1 eq.) of K_2CO_3 , and 4 mL DMF. Compound **220** (24 mg, Yield= 61 %) was isolated as a white solid. ^1H NMR (400 MHz, Chloroform-*d*) δ 7.34 – 7.22 (m, 5H), 6.51 (br s, 1H), 5.75 (br s, 1H), 4.06 (dd, $J = 10.5, 2.8$ Hz, 1H), 3.90 (ddd, $J = 11.3, 3.4, 1.7$ Hz, 1H), 3.70 (td, $J = 11.3, 2.5$ Hz, 1H), 3.56 (d, $J = 13.0$ Hz, 1H), 3.51 (d, $J = 13.1$ Hz, 1H), 3.20 (ddd, $J = 11.6, 2.9, 1.9$ Hz, 1H), 2.67 (dq, $J = 11.7, 2.0$ Hz, 1H), 2.16 (td, $J = 11.5, 3.4$ Hz, 1H), 2.05 (dd, $J = 11.5, 10.5$ Hz, 1H). ^{13}C NMR (101 MHz, Chloroform-*d*) δ 172.83, 137.12, 129.17, 128.33, 127.31, 75.50, 66.64, 63.03, 55.12, 52.35.

(3S)-1-benzyl-3-carbamoylpiperazine-1,4-dium-2-ylum trifluoroacetate (213): See Procedure Fa: 78 mg (0.24 mmol) of **211**, 2 mL TFA, and 2 mL of DCM. Compound **213** (103 mg, 94 % yield) was isolated as a yellow oil. ¹H NMR (500 MHz, Methanol-*d*₄) δ 7.48 – 7.31 (m, 5H), 4.23 (dd, *J* = 11.1, 3.6 Hz, 1H), 4.05 (s, 2H), 3.59 (dd, *J* = 12.8, 2.0 Hz, 1H), 3.54 (dt, *J* = 14.1, 3.2 Hz, 1H), 3.40 – 3.32 (m, 2H), 3.00 – 2.86 (m, 2H). ¹³C NMR (126 MHz, Methanol-*d*₄) δ 167.20, 132.25, 129.98, 128.75, 128.62, 61.06, 55.32, 51.23, 41.01.

(3R)-1-benzyl-3-carbamoylpiperazine-1,4-dium-2-ylum trifluoroacetate (214): See Procedure Fa: 79 mg (0.25 mmol) of **211**, 2 mL TFA, and 2 mL of DCM. Compound **214** (98 mg, 89 % yield) was isolated as a yellow oil. ¹H NMR (500 MHz, Methanol-*d*₄) δ 7.49 – 7.40 (m, 5H), 4.24 (dd, *J* = 11.2, 3.5 Hz, 1H), 4.13 (s, 2H), 3.65 (dd, *J* = 12.6, 2.9 Hz, 1H), 3.60 – 3.55 (m, 1H), 3.43 – 3.32 (m, 2H), 3.04 – 2.94 (m, 2H). ¹³C NMR (126 MHz, Methanol-*d*₄) δ 166.87, 131.35, 130.21, 129.07, 128.75, 61.02, 55.06, 50.97, 40.73.

(S)-4-benzyl-1-propionylpiperazine-2-carboxamide (215): See Procedure Ga: 33 mg (0.074 mmol) of **213** and 1.5 mL of propionic anhydride. Compound **215** (14 mg, Yield=69 %) was isolated as a colorless oil. ¹H NMR (500 MHz, Methanol-*d*₄) δ 7.40 – 7.17 (m, 5H), 5.03 (dt, *J* = 3.8, 1.6 Hz, 1H), 4.53 – 4.33 (m, 1H), 3.79 (d, *J* = 13.2 Hz, 1H), 3.61 – 3.46 (m, 3H), 3.39 (tt, *J* = 13.5, 2.1 Hz, 1H), δ 3.03 (td, *J* = 13.0, 3.7 Hz, 0.3H), 2.88 – 2.78 (m, 1H), 2.57 – 2.39 (m, 2H), 2.35 – 2.22 (m, 0.7H), 2.15 (dd, *J* = 11.9, 4.4 Hz, 1H), 2.09 (td, *J* = 11.8, 3.5 Hz, 0.7H), 2.02 (td, *J* = 12.0, 3.6 Hz, 0.3H), 1.11 (t, *J* = 7.4 Hz, 3H). ¹³C NMR (126 MHz, Methanol-*d*₄) δ 174.97, 173.45, 137.30, 128.73, 128.67, 127.94, 127.89, 126.89, 61.97, 56.61, 53.61, 53.50, 52.85, 52.32, 52.03, 43.15, 39.24, 25.95, 25.66, 8.30, 8.20.

(R)-4-benzyl-1-propionylpiperazine-2-carboxamide (216): See Procedure Ga: 26 mg (0.058 mmol) of **214** and 1.5 mL of propionic anhydride. Compound **216** (13 mg, Yield=81 %)

was isolated as a colorless oil. ^1H NMR (500 MHz, Chloroform-*d*) δ 7.45 – 7.22 (m, 5H), 6.21 (br s, 0.5H), 5.84 (br s, 0.5H), 5.73 (br s, 0.5H), 5.18 (br s, 0.5H), 4.59 – 4.45 (m, 0.5H), 4.35 (s, 0.5H), 3.70 (d, $J = 13.5$ Hz, 0.5H), 3.56 (d, $J = 8.0$ Hz, 1.5H), 3.54 – 3.42 (m, 1H), 3.38 (d, $J = 11.9$ Hz, 0.5H), 3.25 (d, $J = 11.9$ Hz, 0.5H), 3.00 – 2.82 (m, 1.5H), 2.60 (dq, $J = 15.0, 7.3$ Hz, 0.5H), 2.51 – 2.32 (m, 2H), 2.25 (dd, $J = 11.9, 4.0$ Hz, 0.5H), 2.17 (d, $J = 10.8$ Hz, 0.5H), 2.13 – 2.04 (m, 1H), 1.20 – 1.10 (m, 3H). ^{13}C NMR (126 MHz, Chloroform-*d*) δ 173.77, 172.11, 171.72, 129.11, 129.07, 128.58, 128.38, 127.74, 127.47, 62.70, 62.48, 56.47, 53.27, 52.53, 52.40, 46.26, 43.17, 38.68, 26.64, 26.44, 26.37, 26.27, 9.26.

(R)-1-acetyl-4-benzylpiperazine-2-carboxamide (217): See Procedure Ga: 21 mg (0.047 mmol) of **214** and 2 mL of Ac_2O . Compound **217** (14 mg, Quantitative Yield) was isolated as a colorless oil. ^1H NMR (500 MHz, Chloroform-*d*) δ 7.44 (br s, 0.5H), 7.38 – 7.24 (m, 5H), 6.20 (s, 0.5H), 5.73 (s, 0.5H), 5.61 (s, 0.5H), 5.17 (dt, $J = 3.7, 1.7$ Hz, 0.5H), 4.50 (d, $J = 12.9$ Hz, 0.5H), 4.29 (s, 0.5H), 3.66 (d, $J = 13.2$ Hz, 0.5H), 3.61 – 3.46 (m, 2.5H), 3.36 (dt, $J = 11.9, 1.9$ Hz, 0.5H), 3.24 (dt, $J = 12.1, 1.9$ Hz, 0.5H), 2.99 – 2.87 (m, 1H), 2.84 (d, $J = 12.1$ Hz, 0.5H), 2.28 (dd, $J = 12.0, 4.0$ Hz, 0.5H), 2.23 (s, 1.5H), 2.17 – 2.06 (m, 3H). ^{13}C NMR (126 MHz, Chloroform-*d*) δ 171.47, 170.62, 136.50, 129.11, 129.03, 128.60, 128.37, 127.77, 127.45, 62.70, 62.48, 57.41, 53.22, 52.46, 52.32, 38.55, 21.53.

(3S)-1-benzyl-3-((2,2,2-trifluoroacetamido)methyl)piperazine-1,4-dium trifluoroacetate (221): See Procedure D, H, and Fa: 44 mg (0.14 mmol) of **211**, 480 μL (0.96 mmol, 7.0 eq.) of 2M $\text{BH}_3^*\text{Me}_2\text{S}$ in THF, and 4 mL of THF. 40 μL (60 mg, 0.29 mmol, 2.1 eq.) of trifluoroacetic anhydride and 4 mL of pyridine. 2 mL of TFA and 2 mL of DCM. Compound **221** (25 mg, Yield= 34 %) was isolated using reverse phase chromatography (0 to 60 % B in A) as a colorless oil. ^1H NMR (500 MHz, Methanol-*d*₄) δ 7.64 – 7.25 (m, 5H), 4.20 (d, $J = 2.4$ Hz,

2H), 3.74 (dtd, $J = 11.4, 5.6, 3.1$ Hz, 1H), 3.66 – 3.55 (m, 3H), 3.48 (t, $J = 15.6$ Hz, 2H), 3.36 (td, $J = 13.8, 13.2, 3.3$ Hz, 1H), 3.10 (td, $J = 12.8, 3.4$ Hz, 1H), 3.00 (dd, $J = 13.1, 11.4$ Hz, 1H). ^{13}C NMR (126 MHz, Methanol- d_4) δ 160.57, 160.26, 159.10, 158.80, 131.44, 130.18, 129.01, 128.70, 116.93, 114.65, 60.96, 53.73, 50.91, 41.95, 39.00.

(S)-N-((4-benzyl-1-propionylpiperazin-2-yl)methyl)-2,2,2-trifluoroacetamide (222):

See Procedure Gb: 25 mg (0.047 mmol) of **221** and 2 mL propionic anhydride. Compound **222** (12 mg, Yield=71 %) was isolated as a yellow oil. ^1H NMR (500 MHz, Chloroform- d) δ 7.61 (s, 1H), 7.40 – 7.25 (m, 6H), 4.83 (dt, $J = 9.5, 4.0$ Hz, 1H), 4.20 (ddd, $J = 14.1, 10.4, 6.9$ Hz, 1H), 3.62 (d, $J = 13.1$ Hz, 1H), 3.57 (d, $J = 13.0$ Hz, 1H), 3.53 – 3.39 (m, 2H), 3.23 (dt, $J = 14.1, 3.9$ Hz, 1H), 2.89 (d, $J = 10.9$ Hz, 1H), 2.82 (d, $J = 12.0$ Hz, 1H), 2.39 – 2.24 (m, 2H), 2.20 (dd, $J = 12.0, 4.2$ Hz, 1H), 2.10 (td, $J = 11.8, 3.8$ Hz, 1H), 1.11 (t, $J = 7.4$ Hz, 3H). ^{13}C NMR (126 MHz, Chloroform- d) δ 174.68, 128.89, 128.50, 127.56, 62.63, 53.96, 52.83, 47.40, 41.58, 26.71, 9.19.

(S)-N-((1-acetyl-4-benzylpiperazin-2-yl)methyl)-2,2,2-trifluoroacetamide (223): See

Procedure Gb: 24 mg (0.045 mmol) of **221** and 2 mL acetic anhydride. Compound **223** (12 mg, Yield=77 %) was isolated as a colorless oil. ^1H NMR (500 MHz, Chloroform- d) δ 7.64 (s, 1H), 7.40 – 7.26 (m, 5H), 4.80 (dd, $J = 9.9, 4.7$ Hz, 1H), 4.26 – 4.08 (m, 1H), 3.63 – 3.46 (m, 3H), 3.42 (d, $J = 13.0$ Hz, 1H), 3.27 (dt, $J = 14.1, 4.0$ Hz, 1H), 2.88 (dp, $J = 11.5, 2.1$ Hz, 1H), 2.80 (dt, $J = 11.9, 1.9$ Hz, 1H), 2.19 (dd, $J = 12.0, 4.3$ Hz, 1H), 2.12 (dd, $J = 11.6, 4.1$ Hz, 1H), 2.08 (s, 3H). ^{13}C NMR (126 MHz, Chloroform- d) δ 171.29, 137.20, 128.85, 128.49, 127.51, 62.65, 53.99, 52.86, 47.41, 42.63, 41.70, 21.45.

(S)-1-(((R)-4-benzyl-1-propylpiperazin-2-yl)methyl)amino)-3-(4-hydroxy-2,6-

dimethylphenyl)-1-oxopropan-2-aminium trifluoroacetate (224): See Procedure D and E: 17 mg (0.044 mmol) of **215**, 160 μL (0.32 mmol, 7.3 eq.) of 2 M $\text{BH}_3^*\text{Me}_2\text{S}$ in THF, and 4 mL of

THF. Step 1 of E: 80 μ L (59 mg, 0.46 mmol, 10.4 eq.) of N,N-diisopropylethylamine, 24 mg (0.046 mmol, 1.1 eq.) of PyBOP, 8 mg (0.047 mmol, 1.1 eq.) of 6-Cl-HOBt, 21 mg (0.051 mmol, 1.2 eq.) of Boc-O-Boc-L-2',6'-dimethyltyrosine, 3+1.5 mL of DMF. Step 2 of E: 2 mL TFA and 2 mL DCM. Compound **224** (3.6 mg, Yield=15 %) was isolated as a white solid. ^1H NMR (499 MHz, Deuterium Oxide) δ 7.38 – 7.28 (m, 3H), 7.28 – 7.23 (m, 2H), 6.50 (s, 2H), 3.89 (dd, J = 11.1, 6.0 Hz, 1H), 3.77 (d, J = 13.0 Hz, 1H), 3.64 (d, J = 13.1 Hz, 1H), 3.49 (dd, J = 14.1, 2.5 Hz, 1H), 3.22 – 3.12 (m, 2H), 3.07 – 2.61 (m, 9H), 2.53 (br s, 1H), 2.09 (s, 6H), 1.55 (ddt, J = 17.8, 11.3, 5.8 Hz, 1H), 1.44 (tt, J = 12.7, 6.4 Hz, 1H), 0.80 (t, J = 7.3 Hz, 3H). (MS)EI: 439.3 (M+H), Retention Time: 20.51 min.

(S)-1-(((S)-4-benzyl-1-propylpiperazin-2-yl)methyl)amino)-3-(4-hydroxy-2,6-dimethylphenyl)-1-oxopropan-2-aminium trifluoroacetate (225): See Procedure D and E: 11 mg (0.028 mmol) of **216**, 100 μ L (0.20 mmol, 7.1 eq.) of 2 M $\text{BH}_3\cdot\text{Me}_2\text{S}$ in THF, and 4 mL of THF. Step 1 of E: 50 μ L (37 mg, 0.29 mmol, 10.1 eq.) of N,N-diisopropylethylamine, 17 mg (0.033 mmol, 1.2 eq.) of PyBOP, 8 mg (0.047 mmol, 1.7 eq.) of 6-Cl-HOBt, 12 mg (0.029 mmol, 1.0 eq.) of Boc-O-Boc-L-2',6'-dimethyltyrosine, 3+1.5 mL of DMF. Step 2 of E: 2 mL TFA and 2 mL DCM. Compound **225** (1.4 mg, Yield=9 %) was isolated as a white solid. ^1H NMR (500 MHz, Deuterium Oxide) δ 7.41 – 7.32 (m, 5H), 6.50 (s, 2H), 4.27 (s, 2H), 3.90 (dd, J = 10.7, 6.0 Hz, 1H), 3.72 (d, J = 14.1 Hz, 1H), 3.62 – 3.42 (m, 3H), 3.34 – 3.18 (m, 3H), 3.16 – 2.93 (m, 5H), 2.56 (td, J = 11.8, 4.9 Hz, 1H), 2.09 (s, 6H), 1.57 (ddt, J = 19.2, 14.2, 6.7 Hz, 1H), 1.45 (dq, J = 17.3, 5.7 Hz, 1H), 0.78 (t, J = 7.3 Hz, 3H). (MS)EI: 439.3 (M+H), Retention Time: 20.53 min.

(S)-1-(((S)-4-benzyl-1-ethylpiperazin-2-yl)methyl)amino)-3-(4-hydroxy-2,6-dimethylphenyl)-1-oxopropan-2-aminium trifluoroacetate (226): See Procedure D and E: 14 mg (0.054 mmol) of **217**, 190 μ L (0.38 mmol, 7.0 eq.) of 2 M $\text{BH}_3\cdot\text{Me}_2\text{S}$ in THF, and 4 mL of

THF. Step 1 of E: 100 μ L (74 mg, 0.57 mmol, 10.7 eq.) of N,N-diisopropylethylamine, 29 mg (0.056 mmol, 1.0 eq.) of PyBOP, 10 mg (0.059 mmol, 1.1 eq.) of 6-Cl-HOBt, 23 mg (0.056 mmol, 1.0 eq.) of Boc-O-Boc-L-2',6'-dimethyltyrosine, 3+1.5 mL of DMF. Step 2 of E: 2 mL TFA and 2 mL DCM. Compound **226** (4.4 mg, Yield=15 %) was isolated as a white solid. ^1H NMR (500 MHz, Deuterium Oxide) δ 7.39 – 7.33 (m, 5H), 6.50 (s, 2H), 4.25 (s, 2H), 3.90 (dd, J = 10.6, 6.1 Hz, 1H), 3.69 (d, J = 14.1 Hz, 1H), 3.57 (d, J = 13.7 Hz, 1H), 3.50 (dd, J = 15.2, 4.3 Hz, 2H), 3.33 (dt, J = 14.1, 4.4 Hz, 1H), 3.29 – 3.15 (m, 3H), 3.15 – 2.93 (m, 4H), 2.68 (dq, J = 13.8, 6.9 Hz, 1H), 2.08 (s, 6H), 1.10 (t, J = 7.2 Hz, 3H). (MS)EI: 425.3 (M+H), Retention Time: 19.22 min.

(S)-1-(((S)-4-benzylpiperazin-2-yl)methyl)amino)-3-(4-hydroxy-2,6-dimethylphenyl)-1-oxopropan-2-aminium trifluoroacetate (227): See Procedure D and E: 21 mg (0.066 mmol) of **211**, 230 μ L (0.46 mmol, 7.0 eq.) of 2 M $\text{BH}_3\cdot\text{Me}_2\text{S}$ in THF, and 4 mL of THF. Step 1 of E: 120 μ L (89 mg, 0.69 mmol, 10.5 eq.) of N,N-diisopropylethylamine, 36 mg (0.069 mmol, 1.1 eq.) of PyBOP, 11 mg (0.065 mmol, 1.0 eq.) of 6-Cl-HOBt, 27 mg (0.066 mmol, 1.0 eq.) of Boc-O-Boc-L-2',6'-dimethyltyrosine, 3+1.5 mL of DMF. Step 2 of E: 2 mL TFA and 2 mL DCM. Compound **227** (8.9 mg, Yield=27 %) was isolated as a white solid. ^1H NMR (500 MHz, Deuterium Oxide) δ 7.41 – 7.36 (m, 3H), 7.36 – 7.29 (m, 2H), 6.51 (s, 2H), 4.16 (s, 2H), 3.88 (dd, J = 10.4, 6.2 Hz, 1H), 3.46 (d, J = 12.6 Hz, 2H), 3.40 (dd, J = 14.6, 6.8 Hz, 1H), 3.28 (d, J = 12.4 Hz, 2H), 3.14 – 2.93 (m, 5H), 2.79 (dd, J = 13.7, 12.1 Hz, 1H), 2.08 (s, 6H). (MS)EI: 397.3 (M+H), Retention Time: 17.13 min.

(S)-1-(((S)-1-benzylpiperidin-3-yl)methyl)amino)-3-(4-hydroxy-2,6-dimethylphenyl)-1-oxopropan-2-aminium trifluoroacetate (228): See Procedure D and E: 46 mg (0.14 mmol) of **212**, 485 μ L (0.97 mmol, 7.0 eq.) of 2 M $\text{BH}_3\cdot\text{Me}_2\text{S}$ in THF, and 4 mL of THF. Step 1 of E: 240 μ L (178 mg, 1.4 mmol, 10.0 eq.) of N,N-diisopropylethylamine, 74 mg

(0.14 mmol, 1.0 eq.) of PyBOP, 24 mg (0.14 mmol, 1.0 eq.) of 6-Cl-HOBt, 58 mg (0.14 mmol, 1.0 eq.) of Boc-O-Boc-L-2',6'-dimethyltyrosine, 3+1.5 mL of DMF. Step 2 of E: 2 mL TFA and 2 mL DCM. Compound **228** (13.2 mg, Yield=19 %) was isolated as a white solid. ¹H NMR (400 MHz, Methanol-*d*₄) δ 8.09 (t, *J* = 6.0 Hz, 1H), 7.48 (s, 5H), 6.50 (s, 2H), 4.26 (d, *J* = 13.0 Hz, 1H), 4.20 (d, *J* = 13.0 Hz, 1H), 3.87 (dd, *J* = 11.6, 5.0 Hz, 1H), 3.37 (d, *J* = 12.5 Hz, 1H), 3.28 – 3.16 (m, 3H), 2.99 (dd, *J* = 13.7, 5.0 Hz, 1H), 2.80 – 2.65 (m, 2H), 2.41 (t, *J* = 12.3 Hz, 1H), 2.26 (s, 6H), 1.91 – 1.72 (m, 2H), 1.62 (qt, *J* = 15.0, 3.8 Hz, 1H), 1.29 (d, *J* = 13.3 Hz, 1H), 0.86 (qd, *J* = 12.9, 3.8 Hz, 1H). (MS)EI: 396.3 (M+H), Retention Time: 16.86 min.

(S)-1-(((S)-4-benzylmorpholin-2-yl)methyl)amino)-3-(4-hydroxy-2,6-dimethylphenyl)-1-oxopropan-2-aminium trifluoroacetate (229): See Procedure D and E: 23 mg (0.10 mmol) of **220**, 365 μL (0.73 mmol, 7.0 eq.) of 2 M BH₃*Me₂S in THF, and 4 mL of THF. Step 1 of E: 180 μL (134 mg, 1.0 mmol, 9.9 eq.) of N,N-diisopropylethylamine, 55 mg (0.11 mmol, 1.0 eq.) of PyBOP, 19 mg (0.11 mmol, 1.1 eq.) of 6-Cl-HOBt, 44 mg (0.11 mmol, 1.0 eq.) of Boc-O-Boc-L-2',6'-dimethyltyrosine, 3+1.5 mL of DMF. Step 2 of E: 2 mL TFA and 2 mL DCM. Compound **229** (5.5 mg, Yield=10 %) was isolated as a white solid. ¹H NMR (400 MHz, Deuterium Oxide) δ 7.43 – 7.24 (m, 5H), 6.50 (s, 2H), 4.18 (d, *J* = 13.0 Hz, 1H), 4.09 (d, *J* = 13.0 Hz, 1H), 3.93 – 3.71 (m, 2H), 3.48 (t, *J* = 12.7 Hz, 1H), 3.42 – 3.29 (m, 2H), 3.24 (d, *J* = 12.7 Hz, 1H), 3.05 (dd, *J* = 13.8, 11.9 Hz, 2H), 2.95 (dd, *J* = 14.1, 5.4 Hz, 1H), 2.86 (dd, *J* = 13.3, 4.8 Hz, 1H), 2.74 (dd, *J* = 14.5, 7.0 Hz, 1H), 2.38 (t, *J* = 11.7 Hz, 1H), 2.07 (s, 6H). (MS)EI: 398.2 (M+H), Retention Time: 15.79 min.

(S)-1-(((S)-4-benzyl-1-propionylpiperazin-2-yl)methyl)amino)-3-(4-hydroxy-2,6-dimethylphenyl)-1-oxopropan-2-aminium trifluoroacetate (230): See Procedure I and E: 12 mg (0.034 mmol) of **222**, 2 mL of 2M NaOH, and 2 mL of MeOH. The solution was quenched

with saturated NaHCO₃ in water before being concentrated in vacuo. Step 1 of E: 80 μ L (59 mg, 0.46 mmol, 13.7 eq.) of N,N-diisopropylethylamine, 25 mg (0.048 mmol, 1.4 eq.) of PyBOP, 6 mg (0.035 mmol, 1.1 eq.) of 6-Cl-HOBt, 23 mg (0.049 mmol, 1.5 eq.) of Boc-O-Boc-L-2',6'-dimethyltyrosine, 3+1.5 mL of DMF. Step 2 of E: 2 mL TFA and 2 mL DCM. Compound **230** (6.7 mg, Yield=35 %) was isolated as a white solid. ¹H NMR (500 MHz, Methanol-*d*₄) δ 7.51 (s, 5H), 6.65 (s, 2H), 4.81 – 4.70 (m, 1H), 4.53 (dd, *J* = 12.1, 4.6 Hz, 1H), 4.28 (d, *J* = 12.9 Hz, 1H), 3.77 (d, *J* = 12.9 Hz, 1H), 3.64 (dd, *J* = 14.1, 10.2 Hz, 1H), 3.47 – 3.37 (m, 2H), 3.27 – 3.15 (m, 2H), 3.13 (dd, *J* = 13.8, 4.6 Hz, 1H), 3.06 (dd, *J* = 14.1, 6.6 Hz, 1H), 2.77 (d, *J* = 12.7 Hz, 1H), 2.54 (dd, *J* = 13.4, 4.4 Hz, 1H), 2.27 (s, 6H), 2.23 (q, *J* = 7.6 Hz, 2H), 1.12 (t, *J* = 7.6 Hz, 3H), 0.92 (td, *J* = 12.5, 3.9 Hz, 1H). (MS)EI: 453.3 (M+H), Retention Time: 17.14 min.

(S)-1-(((S)-1-acetyl-4-benzylpiperazin-2-yl)methyl)amino)-3-(4-hydroxy-2,6-dimethylphenyl)-1-oxopropan-2-aminium trifluoroacetate (231): See Procedure I and E: 10 mg (0.029 mmol) of **223**, 2 mL of 2M NaOH, and 2 mL of MeOH. The solution was concentrated in vacuo directly. Step 1 of E: 50 μ L (37 mg, 0.29 mmol, 9.9 eq.) of N,N-diisopropylethylamine, 15 mg (0.029 mmol, 1.0 eq.) of PyBOP, 7 mg (0.041 mmol, 1.4 eq.) of 6-Cl-HOBt, 12 mg (0.029 mmol, 1.0 eq.) of Boc-O-Boc-L-2',6'-dimethyltyrosine, 3+1.5 mL of DMF. Step 2 of E: 2 mL TFA and 2 mL DCM. Compound **231** (3.9 mg, Yield=24 %) was isolated as a white solid. ¹H NMR (500 MHz, Deuterium Oxide) δ 7.44 – 7.37 (m, 3H), 7.30 – 7.25 (m, 2H), 6.57 (s, 2H), 4.50 (dd, *J* = 11.5, 5.4 Hz, 1H), 4.12 (d, *J* = 13.0 Hz, 1H), 3.77 (d, *J* = 13.0 Hz, 1H), 3.49 – 3.35 (m, 2H), 3.29 (td, *J* = 14.2, 13.1, 2.6 Hz, 1H), 3.08 (dd, *J* = 11.6, 5.6 Hz, 4H), 2.82 (d, *J* = 12.6 Hz, 1H), 2.49 (dd, *J* = 13.5, 4.6 Hz, 1H), 2.09 (s, 6H), 1.79 (s, 3H), 0.67 (td, *J* = 12.3, 3.3 Hz, 1H). (MS)EI: 439.3 (M+H), Retention Time: 17.09 min.

***In Vitro* Pharmacology**

Cell Lines and Membrane Preparations.

All *in vitro* opioid assays were performed by Ashley Brinkel, Jack Twarozynski, and Jessica Anand. Tissue culture reagents were purchased from Gibco Life Sciences (Grand Island, NY, U.S.) unless otherwise noted. C6-rat glioma cells stably expressing human MOR (C6-MOR) or human DOR (C6-DOR) and Chinese hamster ovary (CHO) cells stably expressing human KOR (CHO-KOR) were used for all *in vitro* assays. Cells were grown to confluence at 37 °C in 5% CO₂ in Dulbecco's modified Eagle medium (DMEM) containing 10% fetal bovine serum and 5% penicillin/streptomycin. Membranes were prepared by washing confluent cells three times with ice cold phosphate buffered saline (0.9% NaCl, 0.61 mM Na₂HPO₄, 0.38 mM KH₂PO₄, pH 7.4). Cells were detached from the plates by incubation in warm harvesting buffer (20 mM HEPES, 150 mM NaCl, 0.68 mM EDTA, pH 7.4) and pelleted by centrifugation at 1600 rpm for 3 min. The cell pellet was suspended in ice-cold 50 mM Tris- HCl buffer, pH 7.4, and homogenized with a Tissue Tearor (Biospec Products, Inc., Bartlesville, OK, U.S.) for 20 s. The homogenate was centrifuged at 15,000 rpm for 20 min at 4°C. The pellet was rehomogenized in 50 mM Tris-HCl with a Tissue Tearor for 10 s, followed by recentrifugation. The final pellet was resuspended in 50 mM Tris-HCl and frozen in aliquots at -80°C. Protein concentration was determined via a BCA protein assay (Thermo Scientific Pierce, Waltham, MA, U.S.) using bovine serum albumin as the standard.

Radioligand Competition Binding Assays.

Radiolabeled compounds were purchased from Perkin-Elmer (Waltham, MA, U.S.). Opioid ligand binding assays were performed by competitive displacement of 0.2 nM [³H]-diprenorphine (250 μCi, 1.85 TBq/mmol) by the peptidomimetic from membrane preparations containing opioid receptors as described above. The assay mixture, containing membranes (20 μg

protein/tube) in 50 mM Tris-HCl buffer (pH 7.4), 0.2 nM [³H]-diprenorphine, and various concentrations of test peptidomimetic, was incubated at room temperature on a shaker for 1 h to allow binding to reach equilibrium. The samples were rapidly filtered through Whatman GF/C filters using a Brandel harvester (Brandel, Gaithersburg, MD, U.S.) and washed three times with 50 mM Tris-HCl buffer, pH 7.4. Bound radioactivity on dried filters was determined by liquid scintillation counting, after saturation with EcoLume liquid scintillation cocktail, in a Wallac 1450 MicroBeta (Perkin-Elmer, Waltham, MA, U.S.). Nonspecific binding was determined using 10 μM naloxone. The results presented are the mean ± standard error (S.E.M.) from at least three separate assays performed in duplicate. K_i (nM) values were calculated using nonlinear regression analysis to fit a logistic equation to the competition data using GraphPad Prism, version 6.0c, (GraphPad Software Inc., La Jolla, CA).

[³⁵S]-GTPγS Binding Assays.

Agonist stimulation of [³⁵S]guanosine 5'-O-[γ-thio]triphosphate ([³⁵S]-GTPγS, 1250 Ci, 46.2 TBq/mmol) binding to G protein was measured as described previously.⁸² Briefly, membranes (10 μg of protein/well) were incubated for 1 h at 25°C in GTPγS buffer (50 mM Tris-HCl, 100 mM NaCl, 5 mM MgCl₂, 1 mM EDTA, pH 7.4) containing 0.1 nM [³⁵S]-GTPγS, 30 μM guanosine diphosphate (GDP), and varying concentrations of test peptidomimetic. G protein activation following receptor activation by peptidomimetic was compared with 10 μM of the standard compounds [D-Ala²,N-MePhe⁴,Gly-ol]enkephalin (DAMGO) at MOR, D-Pen^{2,5}-enkephalin (DPDPE) at DOR, or U69,593 at KOR. The reaction was terminated by vacuum filtration through GF/C filters that were washed 5 times with GTPγS buffer. Bound radioactivity was measured as described above. The results are presented as the mean ± standard error (S.E.M.) from at least three

separate assays performed in duplicate; potency (EC_{50} (nM)) and percent stimulation were determined using nonlinear regression analysis with GraphPad Prism, as above.

Mouse Liver Microsome Stability Assays

All liver microsome assays were performed by Quintara Biosciences. Metabolic stability of testing compounds was evaluated using mouse liver microsomes to predict intrinsic clearance. Mouse liver microsome tissue fractions were obtained from Corning or BioreclamationIVT. The assay was carried out in 96-well microtiter plates at 37°C. Reaction mixtures (25 μ L) contained a final concentration of 1 μ M test compound, 0.1 mg/mL liver microsome protein, and 1 mM NADPH in 100 mM potassium phosphate, pH 7.4 buffer with 3 mM $MgCl_2$. At each of the time points (0, 15, 30, and 60 minutes), 150 μ L of quench solution (acetonitrile with 0.1% formic acid) with internal standard (bucetin) was transferred to each well. Verapamil was included as a positive control to verify assay performance. Plates were sealed, vortexed, and centrifuged at 4°C for 15 minutes at 4000 rpm. The supernatant was transferred to fresh plates for LC/MS/MS analysis. All samples were analyzed on LC/MS/MS using an AB Sciex API 4000 instrument, coupled to a Shimadzu LC-20AD LC Pump system. Analytical samples were separated using a Waters Atlantis T3 dC18 reverse phase HPLC column (20 mm x 2.1 mm) at a flow rate of 0.5 mL/min. The mobile phase consists of 0.1% formic acid in water (solvent A) and 0.1% formic acid in acetonitrile (solvent B). The extent of metabolism was calculated as the disappearance of the test compound, compared to the 0-min time incubation. Initial rates were calculated for the compound concentration and used to determine $T_{1/2}$ values.

Molecular Modeling

All *in silico* experiments were performed by Irina Pogozheva. Modeling of three-dimensional (3D) structures of receptor-ligand complexes was based on available X-ray structures

of the mouse MOR (PDB IDs: 4dkl and 5c1m)^{1, 2} and the human KOR (PDB IDs: 4djh and 6b73)^{3, 4} in the inactive and active conformations, respectively, and the human DOR in the inactive conformation (PDB IDs: 4n6h, 4rwa)^{5, 6}. Structures of peptidomimetic ligands were generated using the 3D-Builder Application of QUANTA (Accelrys, Inc) followed by Conformational Search included in the program package. Low-energy ligand conformations (within 2 kcal/mol) that demonstrated the best superposition of aromatic substituents of the ligand core with the pharmacophore elements (Tyr1 and Phe3) of receptor-bound conformations of cyclic tetrapeptides **7** were selected for docking into the receptor binding pocket. Ligands were positioned inside the receptor binding cavity to reproduce the binding modes of cyclic tetrapeptides and co-crystallized ligands in MOR, DOR, and KOR X-ray structures. The docking pose of each ligand was subsequently refined using the solid docking module of QUANTA.

Chapter 8: Conclusions and Future Directions

8.1 Conclusions

Core Modifications and Stability: The impetus for this project was to address problems in the metabolic stability of the original bicyclic core series. This instability was endemic to the core itself, and no superficial modification to either the bicyclic core or the benzyl pendant could eliminate this instability. Chapters 2 and 3 demonstrated that conversion of this bicyclic core into a monocyclic aromatic core could yield stability improvements while retaining our desired bifunctional MOR/DOR profile and these data are summarized in **Figure 22**. The main source of instability was found to be the benzylic position connecting the aromatic core to the DMT pendant (**Figure 22**, red circle) and was sensitive to the stereochemistry of alkyl groups on this position.

The conversion to the monocyclic core was initially met with losses in MOR-agonism, a necessary component of our desired bifunctional opioid profile. This was significantly ameliorated by the incorporation of short chain ethers onto the aromatic core (**Figure 22**, blue circle), of which the ethyl ether was the best. Additional modifications were pursued on the aromatic ring (**Figure 22**, purple circle). These structural elements improved MOR-potency in some cases, but generally reduced what stability gains were made upon conversion to this new core. Overall, the conversion to this monocyclic core was promising in terms of both their MOR/DOR bifunctional profile and their stability. However, the MOR-potency and the metabolic stability of these ligands still left room for improvement.

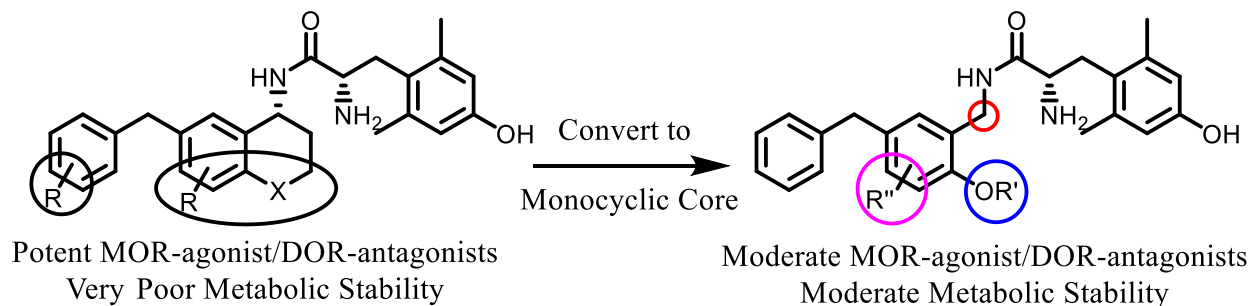


Figure 22: Summary of results from Chapters 2 and 3. Bicyclic core analogues are typically potent MOR-agonist/DOR-antagonists but express very poor metabolic stability in MLM. This instability is not affected by superficial modifications (black circles) to the ligand. Conversion to a monocyclic core improved stability and identified a major metabolic hotspot (red circle). Moderate MOR-agonism was achieved with short chain ethers (blue circle), and additional core modifications yielded no overall improvements (purple circle).

Discovery of Aromatic-Amine Pharmacophore: While the improvements in the ligands thus far were promising, we were interested in further optimizing these peptidomimetics. A survey of analogues synthesized previously in our lab indicated that amine pendants were tolerated in the bicyclic series, and therefore might be of utility in our monocyclic series. As such, these amine pendants were incorporated into our monocyclic core peptidomimetic series (**Figure 23**). Initially, a series of amine pendant analogues containing an ethyl ether on the core were synthesized. This series suggested that simple monocyclic amine pendants improved metabolic stability while consistently maintaining high levels of MOR-efficacy. However, this was at the cost of MOR-potency in some cases.

This lost potency can not only be restored, but improved upon by the addition of an aromatic ring onto the cyclic amine pendant. This retains the MOR-efficacy of these analogues, albeit at the cost of some of the improvements in stability. Conformational flexibility of the pendant as illustrated by the benzyl amines does not drastically affect the MOR-agonist characteristics of these analogues, though this comes at a cost to metabolic stability and selectivity over KOR. Finally, members of this series were shown to possess *in vivo* activity as illustrated by

the acetic acid stretch assay (AASA). This activity was inhibited by the opioid antagonist naloxone and show that these analogues are inducing their antinociception via the opioid receptors. These analogues were not active in the warm water tail withdrawal (WWTW) suggesting that these ligands operate on peripheral opioid receptors and not central opioid receptors.

The *in vitro* and stability performance of these new amine pharmacophores warranted further investigation into their scope as MOR-agonists. To this end, a series of matrices were constructed that examined the effects of both the amine pendant and aromatic core modification on both the opioid profile and metabolic stability. These matrices revealed that the amine alone can generate high MOR-efficacy, and that the aromatic ring on the pendant can generate high MOR-potency, all independent of the identity of the core modification. Two MOR-superagonists

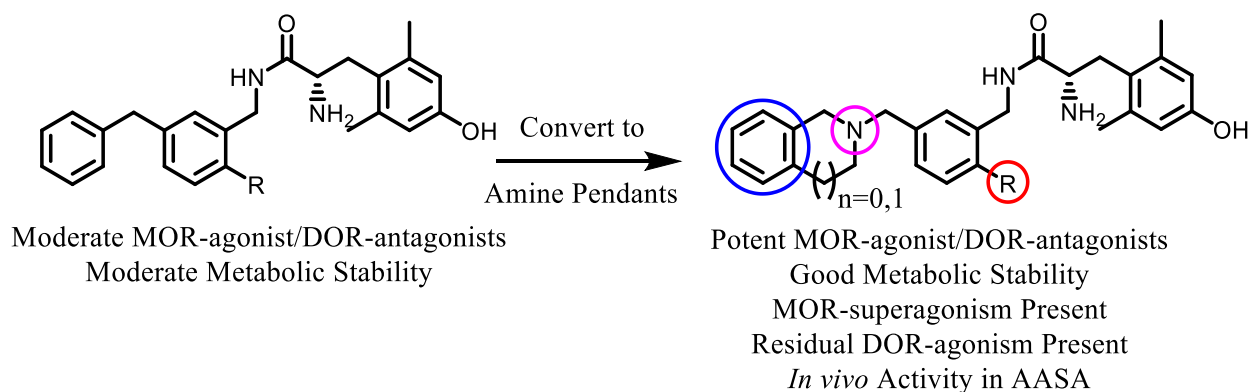


Figure 23: Summary of results from Chapters 4 and 5, which discuss the discovery of the aromatic-amine pharmacophore. The initial monocyclic core analogues used a benzyl pendant and relied upon R-groups on the aromatic core for activity. Conversion to pendants that contain an amine (purple circle) managed to drastically improve stability and MOR-efficacy. If this was coupled with an aromatic ring (blue circle) then improvements in MOR-potency were also observed, though at the cost of some stability improvements. The potency and efficacy at MOR of the aromatic-amine pharmacophore was largely independent of the identity of the R group on the aromatic core (red circle) and in some cases produced MOR-superagonists. Members of this series were active in the acetic acid stretch assay (AASA), of which that activity was opioid receptor mediated. Finally, it should be noted that residual DOR-agonism was present in some of these analogues.

were synthesized in this series, both containing an aromatic-amine pharmacophore. Finally, metabolic stability was consistently high for the monocyclic amine pendants, whereas the stability

of the aromatic-amine pendant analogues was dependent on the identity of the aromatic core modification.

The Aromatic-Amine Pharmacophore with New Cores: As illustrated above, the aromatic-amine pharmacophore shows great promise in producing MOR-agonists. Since this agonism was insensitive to the identity of the aromatic core modifications, we sought to determine if this activity was retained when the aromatic core was removed. This design strategy (**Figure 24**) yielded analogues that possessed simplified structures, albeit with increased conformational flexibility. As such, some conformationally restricted analogues were included to supplement this series. The aromatic-amine pharmacophore was found to produce potent and efficacious MOR-agonists in these simplified structures. Only the conformationally rigid analogues exhibited reduced MOR-potency, though MOR-efficacy was still high, indicating that positioning of the aromatic part of the pharmacophore in these ligands may need optimization.

DOR and KOR effects tended to vary within this series. The cyclic analogues possessed high DOR-affinity with no appreciable efficacy, whereas the amides possessed high DOR-affinity and were partial agonists at this receptor. Conversely, the more conformationally flexible analogues in this series exhibited reduced DOR-affinity. The effects at KOR were largely the inverse of that at DOR. The amides and the piperazine analogues possess reduced KOR-affinity, whereas the more flexible ligands had greater binding affinity at KOR than DOR. Finally, there were no initial improvements in metabolic stability with these flexible analogues, indicating that improvements garnered from eliminating the aromatic ring were countered by the increases in flexibility. Restricting this flexibility without using an aromatic ring was found to produce significant stability improvements.

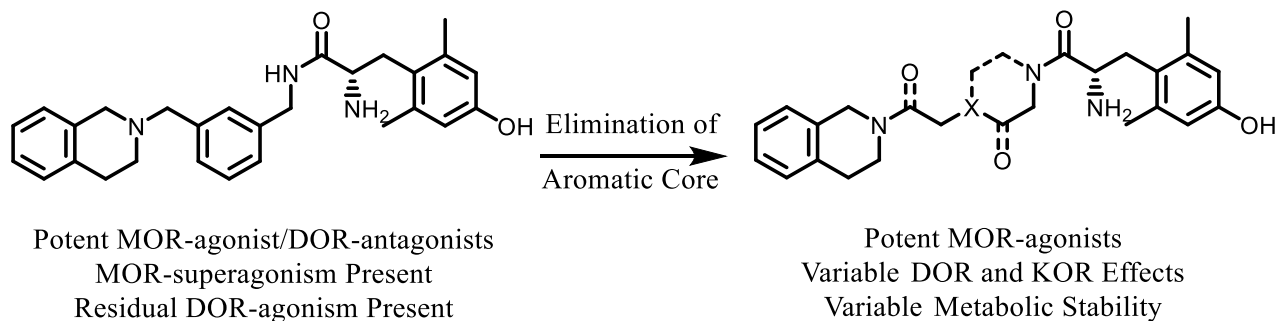


Figure 24: Summary of results from Chapter 6. The tetrahydroisoquinoline pendant (which stands-in as the aromatic-amine pharmacophore) enabled consistently high MOR-efficacy and potency in these simplified analogues. DOR-affinity, efficacy and potency tended to be variable, as well as their metabolic stability.

In addition to the analogues described above, a miscellaneous set of analogues were synthesized that converted the aromatic core into a cyclic aliphatic core (**Figure 25**) using the ethyl ether analogue as a lead. This introduced a new stereocenter, of which the S-isomer was found to optimum (**Figure 25**, purple circle), and required an amine to attach the benzyl pendant (**Figure 25**, blue circle). While these analogues were initially made as a contingency to replace the aromatic core, they had the effect of introducing the aromatic-amine pharmacophore in an altered structure. Here, the amine fulfilled its role in producing consistently high MOR-efficacy, though the MOR-potency of these compounds was diminished. This may be attributed to the shortened distance between the aromatic-amine pharmacophore and the DMT pendant within the ligand. This potency was also dependent on the identity of the substituent that replaced the ethyl ether (**Figure 25**, red circle). Moderate potency was retained when there is only a hydrogen bond acceptor at this position, and all MOR-agonism was lost when this substituent was an amide. While not in an optimal configuration, these analogues show that the aromatic-amine pharmacophore can still yield MOR-agonists.

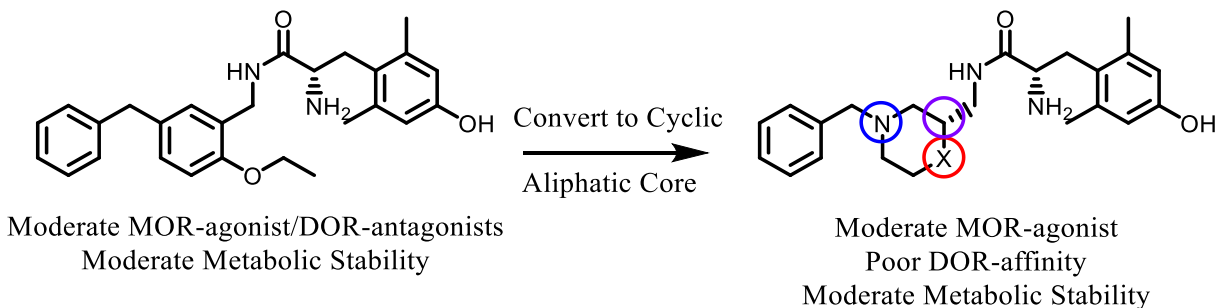


Figure 25: Summary of Results from Chapter 7. This series generated analogues that used an amine to connect the benzyl pendant (blue circle) and introduced a new stereocenter (purple circle). This amine managed to also induce high MOR-efficacy, though the potency and efficacy here was dependent on the identity of X (red circle).

8.2 Future Directions

General Considerations: The SAR campaigns described herein show the development of the aromatic-amine pharmacophore. While the aromatic part mimics phenylalanine in the endogenous opioids, the amine is a novel element for MOR stimulation. They show how variations within the core structure, be it through removal of core elements or conversion of core elements into new forms can maintain MOR efficacy and potency with variability in their effects at DOR and KOR. Though promising in terms of their novelty, size, and stability, the *in vivo* properties of these analogues need to be further elucidated and the variations in the opioid profile that have developed near the end of these campaigns need to be further characterized. Fortunately, these ligands can be diversified in a wide number of directions to achieve these goals. The scope of these analogues is shown in **Figure 26**.

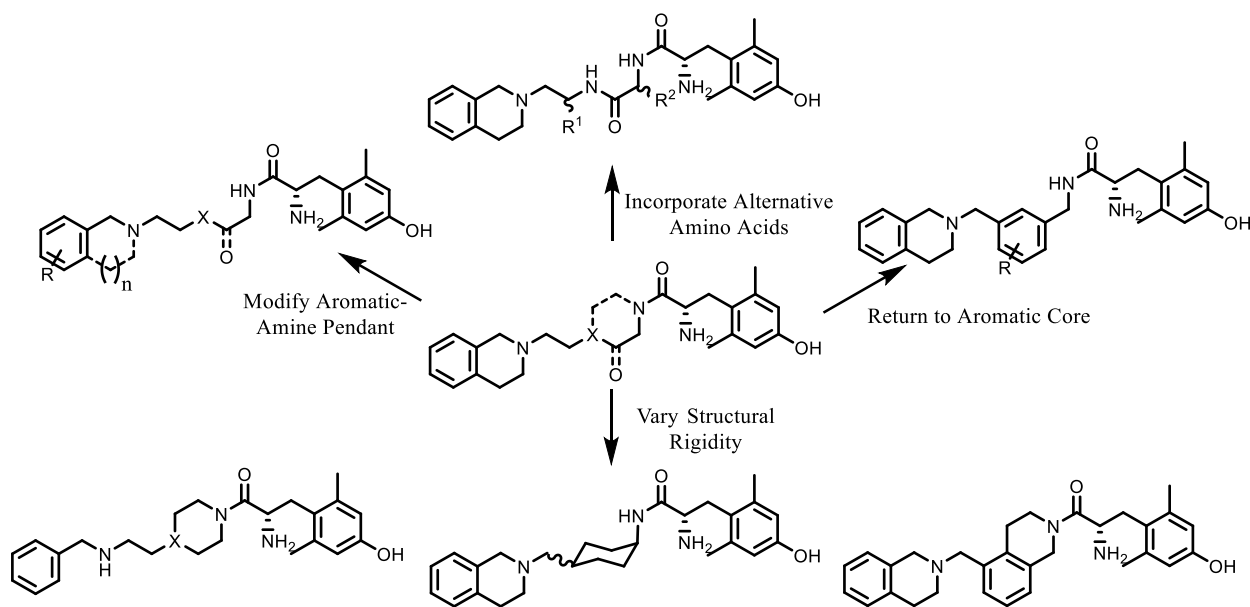


Figure 26: General design scope upon which future analogues may be developed. Further derivatives can follow several different pathways. These can include modifications of the aromatic-amine pendant, the incorporation of alternative amino acids into the peptide core, a return to the aromatic core with further derivatization on the core, or the exploration of alternative rigid structures to hold the two pharmacophores together.

Modify Aromatic Amine Pendant: One of the simplest means of diversifying our SAR is through the direct alteration of our aromatic-amine pharmacophore. This can open the door to a wide variety of new structures that can modulate our opioid profile, improve stability, and reduce potential toxicity. Some of the first modifications here can focus on improving several of these factors simultaneously and are shown in **Figure 27**. Here, the aromatic ring can be modified through the introduction of fluoro groups or by converting the benzene ring to a pyridine ring. In addition to expanding our knowledge on the effects of these substituents in our *in vitro* opioid profile, these changes can also improve the PK properties of these ligands. Both moieties are electron poor and can therefore prevent CYP metabolism by altering the electronics of the core, and in the case of fluoro groups, through steric effects as well. Care must be taken with the pyridine analogues, as improper positioning of the pyridine ring can produce a CYP inhibitor and facilitate drug-drug interactions.¹³⁴ Finally, these moieties can reduce the basicity of the adjacent amine,

which reduces the likelihood of hERG (human ether-à-go-go-related gene) inhibition, a common source of drug toxicity that can result in lethal heart arrhythmias.¹³⁵

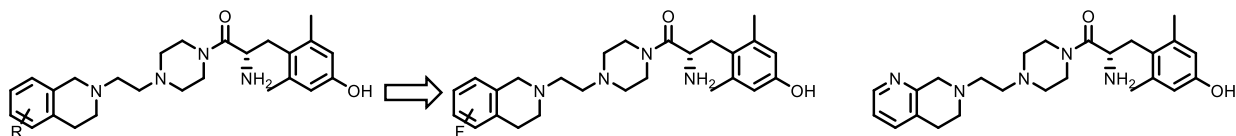


Figure 27: Proposed analogues to be synthesized that modify the aromatic-amine pharmacophore. These analogues are aimed at preventing CYP metabolism and reducing the basicity of the amine.

Incorporate Alternative Amino Acids into Chain: The peptide core analogues **199** and **200** have potential to produce MOR/DOR bifunctional ligands. Considering that the endogenous opioids are peptides, the introduction of various side chains off the peptide backbone can yield some interesting properties. The Tyr-D-Ala motif occurs in the deltorphins and dermorphins, as well as the synthetic opioid peptides [D-Ala², D-Leu⁵]-enkephalin (DADLE) and biphalin. Replacement of Tyr with DMT in deltorphin B yielded a bifunctional MOR/DOR ligand,¹³⁶ and show that D-Ala may be useful in our series.

DMT-Tic-OH is a dipeptide that was found to be a potent and selective DOR-antagonist.¹³⁷ This motif has found its way into a large number of other opioid peptides, many of which are described in the introduction to Chapter 6. Therefore, the incorporation of our aromatic-amine pharmacophore into these peptides can greatly modulate the opioid activity of these ligands, and further our understanding of the opioid peptides (**Figure 28**).

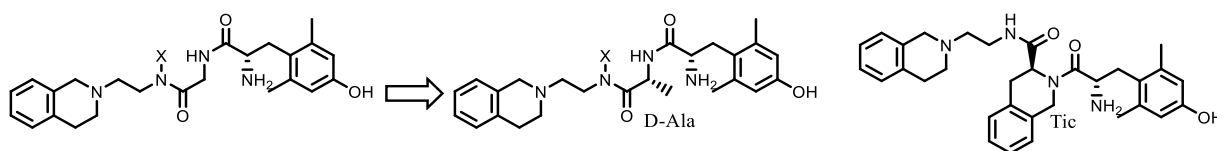


Figure 28: Proposed peptide derivatives of analogues **199** and **200**. These derivatives incorporate D-Ala and Tic into the peptide chain, residues of which are found repeatedly in the literature.

Return to the Aromatic Core: While the simplified core analogues described in Chapter 6 opened many possibilities for further derivatization and demonstrated the potential of the aromatic-amine pharmacophore to activate MOR, this by no means rules out further modifications to analogues described in previous chapters. The aromatic core preserved our mixed MOR/DOR efficacy profile, many of which were MOR-agonist/DOR-antagonists. Furthermore, the MOR-superagonists synthesized herein all possessed an aromatic core. Here, the aromatic core can be altered by incorporating functional groups akin to those described above with the aromatic-amine pendant (**Figure 29**).

These may have additional beneficial effects, namely that these compounds may reduce KOR affinity, and therefore improve selectivity. The peptide analogues **199** and **200** displayed reduced binding affinity at KOR compared to both their aromatic and simple alkyl core analogues. This is unlikely to be an effect of core rigidity from the amide bond, as the aromatic analogues **132**, **168**, and **172** had greater rigidity than **199** and **200**. Instead, it is more likely an effect of the carbonyl acting as a hydrogen bond acceptor, a trend further suggested by the morpholino analogue **229**. As such, incorporation of hydrogen bond acceptors within the ring, in the form of a pyridine core for example, may mimic this interaction and reduce KOR binding without affecting MOR and DOR.

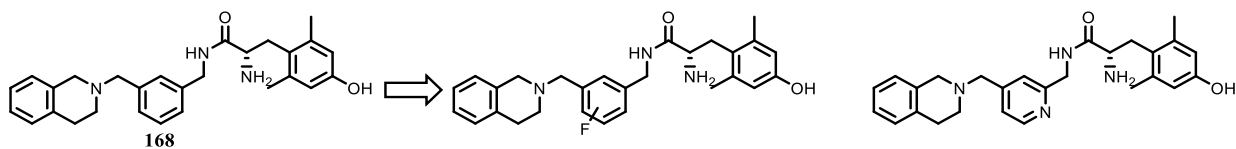


Figure 29: Proposed analogues that modify the aromatic core. These analogues are aimed at preventing CYP metabolism, reducing the basicity of the amine, and may be able to reduce KOR binding affinity.

Vary Structural Rigidity: Part of the guiding philosophy for the synthesis of the piperidine and piperazine analogues **196** and **197** was to reintroduce structural rigidity into our analogues after

the elimination of the aromatic core. The complete elimination of the original metabolically labile bicyclic core yielded benefits in terms of stability, simplicity in structure, and shortened synthesis. This came at the cost of high conformational flexibility in the ligand. **196** and **197** eliminated some of this flexibility and improved metabolic stability. It is possible that the structural orientation that was introduced by these ring systems may not be optimal. Therefore, the introduction of alternative conformationally rigid core systems may be of great benefit to our opioid and PK profile (**Figure 30**). One is the cyclohexane core structure, which can yield cis and trans isomers that orientate the pharmacophore elements in different directions. Furthermore, tying down the aromatic core into a tetrahydroisoquinoline core can yield even greater levels of structural rigidity if desired. Similar analogues that possess this tetrahydroisoquinoline core have been synthesized in this lab and show promising opioid profiles.¹³⁸

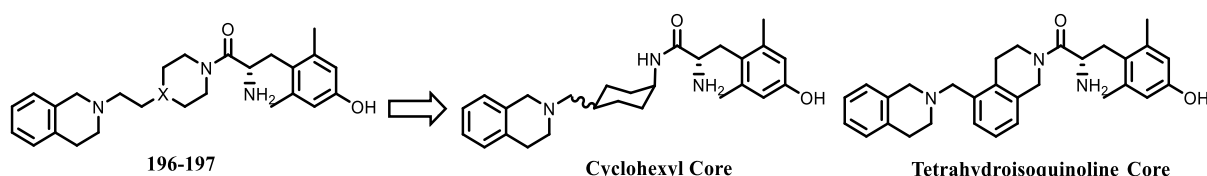


Figure 30: Rigid cyclic core derivatives akin to analogues **196-197**. These analogues are aimed at reducing the conformational flexibility of our ligands and may further improve our opioid and PK profiles.

Cyclic Aliphatic Core Derivatives: In addition to those analogues described above, the cyclic aliphatic core analogues described in Chapter 7 may still be of some value. These compounds have been shown to have good MOR binding affinity and efficacy, though their MOR potency and DOR binding affinity leave room for improvement. Here, the morpholine core analogue **229** will be used, due to its opioid properties and ease of synthesis (**Figure 31**). Previously reported (see Chapter 1) and unpublished data suggest that a 2-naphthyl pendant instead of a benzyl pendant was

of value in the bicyclic series. This may translate into this series as well and may improve the MOR-potency of these ligands.

Furthermore, the incorporation of something akin to our aromatic-amine pharmacophore described in Chapters 4-6 may yield some interesting properties. In this case, the amine portion of this pharmacophore will have to be moved, as using it as a joint to connect it to the rest of the peptidomimetic will introduce instability to aqueous acid on this scaffold. Since a carbon atom will be at this position, a new stereocenter will be introduced and can easily be synthesized using commercially available tetrahydroisoquinoline carboxylate (Tic) amino acids and our established reduction chemistry.

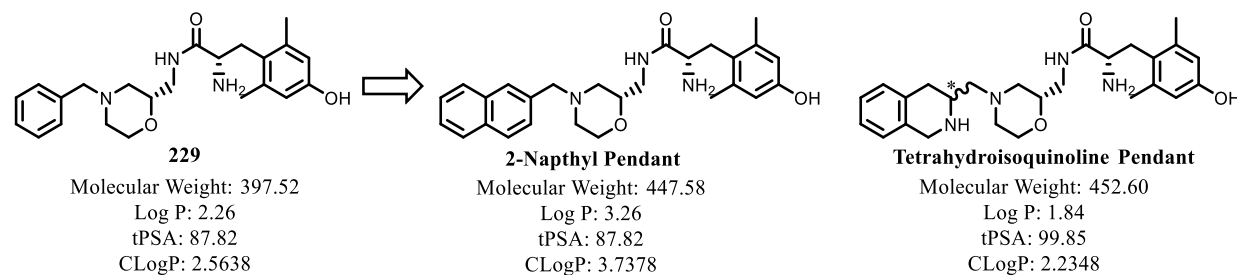


Figure 31: Proposed derivatives of the cyclic aliphatic analogue **229**. These analogues are aimed at improving MOR potency and DOR binding affinity, or by incorporating an aromatic-amine pharmacophore.

Final Conclusions: The data collected in this dissertation may have wide implications in the development of future opioid ligands and in their pharmacology. While the initial aims of this project were to improve the metabolic stability of our peptidomimetic series, the direction this series took allowed us to discover the aromatic-amine pharmacophore. Classically, opioid peptides required relatively large peptide chains that needed cyclization in order to activate their respective opioid receptors. This required multiple steps from starting material to synthesize and was limited by the availability of chiral amino acids. Our aromatic-amine pharmacophore allowed us to greatly simplify structure of our original peptidomimetic, to the point where no ring systems were needed

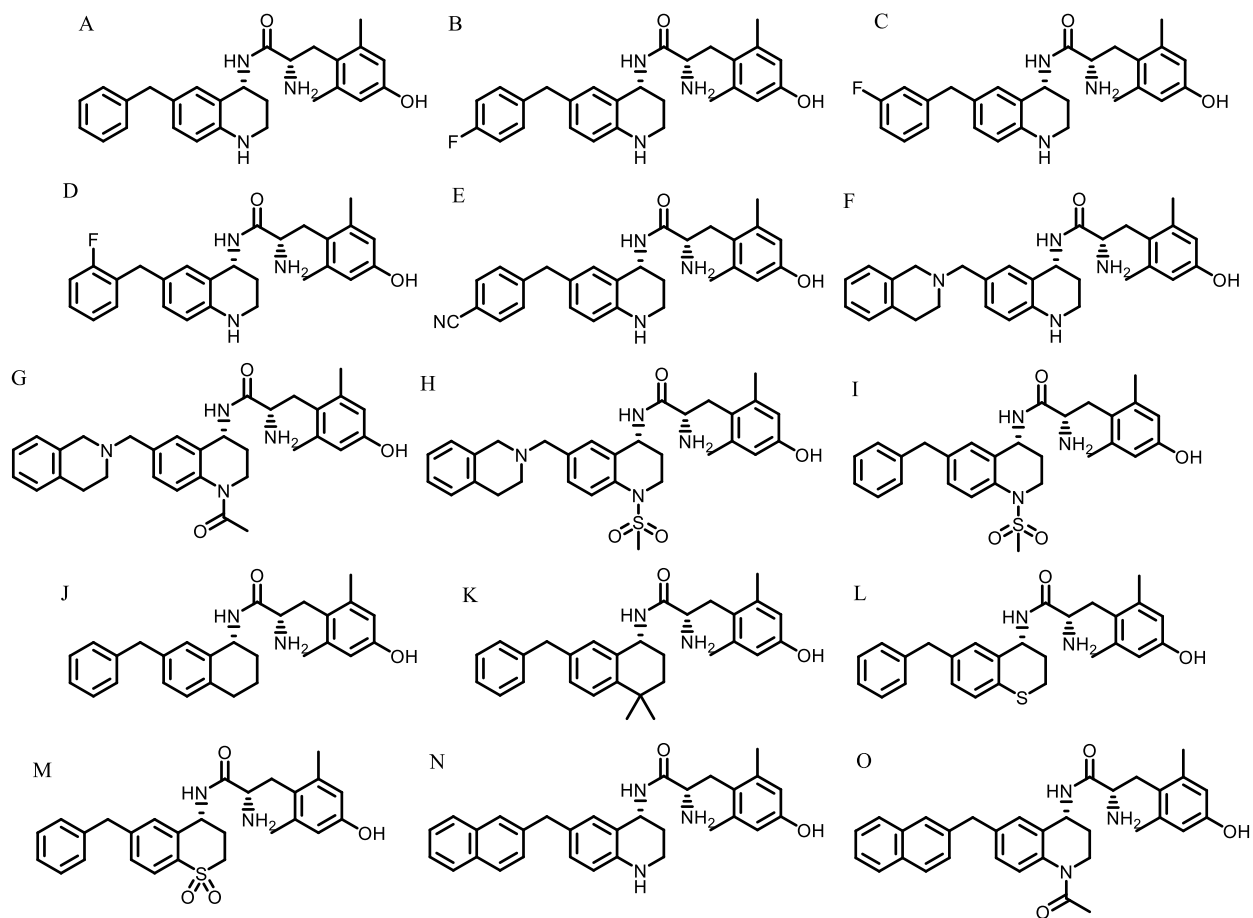
to yield potent and efficacious MOR-agonists. These analogues required relatively few steps to synthesize, and the variability of their effects at DOR at KOR suggest that these analogues may be developed into either selective MOR-agonists, or bifunctional MOR/DOR or MOR/KOR ligands.

Of particular value within these analogues was the possibility of developing MOR-superagonists. DAMGO is frequently used as the standard MOR-agonist for studying MOR-potency and efficacy. A ligand then that has an efficacy 48 % higher than the standard agonist may have pharmacological effects *in vivo* beyond that of the known MOR-agonists. Future research will therefore be needed to understand the pharmacological scope of these ligands.

In the end, our original goal of improving the metabolic stability of our peptidomimetic series while retaining our opioid profile was met. This included simplified synthetic schemes and opened the door for a whole host of new derivatives that are more readily accessible. Furthermore, these analogues were active in the AASA, and their activity was shown to be mediated by action on the opioid receptors. The work provided here not only pushes the development of our ligands to become opioid analgesics with reduced side-effects, but also expands our understanding of how to activate the μ -opioid receptor.

Appendix

Structures of Analogues Found in **Figure 5**



References

- (1) Zee, A. Van. The Promotion and Marketing of OxyContin: Commercial Triumph, Public Health Tragedy. *Am. J. Public Health* **2009**, 99 (2), 221–227. <https://doi.org/10.2105/AJPH.2007.131714>.
- (2) Office, U. S. G. A. *PRESCRIPTION DRUGS OxyContin Abuse and Diversion and Efforts to Address the Problem*; 2003.
- (3) Cicero, T. J.; Inciardi, J. A.; Munoz, A. Trends in Abuse of OxyContin® and Other Opioid Analgesics in the United States: 2002–2004. *J. Pain* **2005**, 6 (10), 662–672. <https://doi.org/10.1016/j.jpain.2005.05.004>.
- (4) Gilson, A. M.; Ryan, K. M.; Joranson, D. E.; Dahl, J. L. A Reassessment of Trends in the Medical Use and Abuse of Opioid Analgesics and Implications for Diversion Control: 1997–2002. *J. Pain Symptom Manage.* **2004**, 28 (2), 176–188. <https://doi.org/10.1016/j.jpainsymman.2004.01.003>.
- (5) Wonder, C. <https://www.drugabuse.gov/related-topics/trends-statistics/overdose-death-rates>.
- (6) Seth, P.; Rudd, R. A.; Noonan, R. K.; Haegerich, T. M. Quantifying the Epidemic of Prescription Opioid Overdose Deaths. *Am. J. Public Health* **2018**, 108 (4), 500–502. <https://doi.org/10.2105/AJPH.2017.304265>.
- (7) Lipari, R. N.; Park-lee, E.; Tice, P. *Key Substance Use and Mental Health Indicators in the United States: Results from the 2018 National Survey on Drug Use and Health*; 2018.
- (8) Dahlhamer, J.; Lucas, J.; Zelaya, C.; Nahin, R.; Mackey, S.; DeBar, L.; Kerns, R.; Von Korff, M.; Porter, L.; Helmick, C. Prevalence of Chronic Pain and High-Impact Chronic Pain Among Adults — United States, 2016. *MMWR. Morb. Mortal. Wkly. Rep.* **2018**, 67 (36), 1001–1006.
- (9) Health, N. I. of. *National Pain Strategy, A Comprehensive Population Health-Level Strategy for Pain*; 2015.
- (10) Blondell, R. D.; Azadfar, M.; Wisniewski, A. M. Pharmacologic Therapy for Acute Pain. *Am. Fam. Physician* **2013**, 87 (11), 766–772.
- (11) Vargas-schaffer, G. Is the WHO Analgesic Ladder Still Valid? *Can. Fam. Physician* **2010**, 56, 514–517.
- (12) Lutz, P.-E.; Kieffer, B. L. Opioid Receptors: Distinct Roles in Mood Disorders. *Trends Neurosci.* **2013**, 36 (3), 195–206. <https://doi.org/10.1016/j.tins.2012.11.002>. Opioid.
- (13) Fine, P. G. Chapter 2: The Endogenous Opioid System. In *A Clinical Guide to Opioid Analgesia*; 2004; pp 9–15.
- (14) Loyd, D. R.; Murphy, A. Z. The Role of the Periaqueductal Gray in the Modulation of

- Pain in Males and Females: Are the Anatomy and Physiology Really That Different? *Neural Plast.* **2009**, *2009*, 1–12. <https://doi.org/10.1155/2009/462879>.
- (15) Kosten, T. R.; George, T. P. The Neurobiology of Opioid Dependence: Implications for Treatment. *Sci. Pract. Perspect.* **2002**, *1* (1), 13–20.
- (16) Manglik, A.; Lin, H.; Aryal, D. K.; McCorvy, J. D.; Dengler, D.; Corder, G.; Levit, A.; Kling, R. C.; Bernat, V.; Hübner, H.; et al. Structure-Based Discovery of Opioid Analgesics with Reduced Side Effects. *Nature* **2016**, *537*, 185–190. <https://doi.org/10.1038/nature19112>.
- (17) DeWire, S. M.; Yamashita, D. S.; Rominger, D. H.; Liu, G.; Cowan, C. L.; Graczyk, T. M.; Chen, X.-T.; Pitis, P. M.; Gotchev, D.; Yuan, C.; et al. A G Protein-Biased Ligand at the μ -Opioid Receptor Is Potently Analgesic with Reduced Gastrointestinal and Respiratory Dysfunction Compared with Morphine. *J. Pharmacol. Exp. Ther.* **2013**, *344*, 708–717. <https://doi.org/10.1124/jpet.112.201616>.
- (18) Kruegel, A. C.; Gassaway, M. M.; Kapoor, A.; Váradi, A.; Majumdar, S.; Filizola, M.; Javitch, J. A.; Sames, D. Synthetic and Receptor Signaling Explorations of the Mitragyna Alkaloids: Mitragynine as an Atypical Molecular Framework for Opioid Receptor Modulators. *J. Am. Chem. Soc.* **2016**, *138*, 6754–6764. <https://doi.org/10.1021/jacs.6b00360>.
- (19) Madariaga-Mazón, A.; Marmolejo-Valencia, A. F.; Li, Y.; Toll, L.; Houghten, R. A.; Martinez-Mayorga, K. Mu-Opioid Receptor Biased Ligands: A Safer and Painless Discovery of Analgesics? *Drug Discov. Today* **2017**, *22* (11), 1719–1729. <https://doi.org/10.1016/j.drudis.2017.07.002>.
- (20) Hill, R.; Disney, A.; Conibear, A.; Sutcliffe, K.; Dewey, W.; Husbands, S.; Bailey, C.; Kelly, E.; Henderson, G. The Novel μ -Opioid Receptor Agonist PZM21 Depresses Respiration and Induces Tolerance to Antinociception. *Br. J. Pharmacol.* **2018**, *175*, 2653–2661. <https://doi.org/10.1111/bph.14224>.
- (21) Zamarripa, C. A.; Edwards, S. R.; Qureshi, H. N.; Yi, J. N.; Blough, B. E.; Freeman, K. B. The G-Protein Biased Mu-Opioid Agonist, TRV130, Produces Reinforcing and Antinociceptive Effects That Are Comparable to Oxycodone in Rats. *Drug Alcohol Depend.* **2018**, *192*, 158–162. <https://doi.org/10.1016/j.drugalcdep.2018.08.002>.
- (22) Altarifi, A. A.; David, B.; Muchhala, K. H.; Blough, B. E.; Akbarali, H.; Negus, S. S. Effects of Acute and Repeated Treatment with the Biased Mu Opioid Receptor Agonist TRV130 (Oliceridine) on Measures of Antinociception, Gastrointestinal Function & Abuse Liability in Rodents. *J. Psychopharmacol.* **2017**, *31* (6), 730–739. <https://doi.org/10.1177/0269881116689257>.Effects.
- (23) Kliewer, A.; Schmiedel, F.; Sianati, S.; Bailey, A.; Bateman, J. T.; Levitt, E. S.; Williams, J. T.; Christie, M. J.; Schulz, S. Phosphorylation-Deficient G-Protein-Biased μ -Opioid Receptors Improve Analgesia and Diminish Tolerance but Worsen Opioid Side Effects. *Nat. Commun.* **2019**, *10* (367), 1–11. <https://doi.org/10.1038/s41467-018-08162-1>.
- (24) Fundytus, M. E.; Schiller, P. W.; Shapiro, M.; Weltrowska, G.; Coderre, T. J. Attenuation of Morphine Tolerance and Dependence with the Highly Selective δ -Opioid Receptor Antagonist TIPP[Ψ]. *Eur. J. Pharmacol.* **1995**, *286*, 105–108. [https://doi.org/10.1016/0014-2999\(95\)00554-X](https://doi.org/10.1016/0014-2999(95)00554-X).

- (25) Abdelhamid, E. E.; Sultana, M.; Portoghese, P. S.; Takemori, A. E. Selective Blockage of Delta Opioid Receptors Prevents the Development of Morphine Tolerance and Dependence in Mice. *J. Pharmacol. Exp. Ther.* **1991**, *258* (1), 299–303.
- (26) Hepburn, M. J.; Little, P. J.; Gingras, J.; Kuhn, C. M. Differential Effects of Naltrindole on Morphine-Induced Tolerance and Physical Dependence in Rats. *J. Pharmacol. Exp. Ther.* **1997**, *281* (3), 1350–1356.
- (27) Zhu, Y.; King, M. A.; Schuller, A. G. P.; Nitsche, J. F.; Reidl, M.; Elde, R. P.; Unterwald, E.; Pasternak, G. W.; Pintar, J. E. Retention of Supraspinal Delta-like Analgesia and Loss of Morphine Tolerance in δ Opioid Receptor Knockout Mice. *Neuron* **1999**, *24* (1), 243–252. [https://doi.org/10.1016/S0896-6273\(00\)80836-3](https://doi.org/10.1016/S0896-6273(00)80836-3).
- (28) Kest, B.; Lee, C. E.; McLemore, G. L.; Inturrisi, C. E. An Antisense Oligodeoxynucleotide to the Delta Opioid Receptor (DOR-1) Inhibits Morphine Tolerance and Acute Dependence in Mice. *Brain Res. Bull.* **1996**, *39* (3), 185–188. [https://doi.org/10.1016/0361-9230\(95\)02092-6](https://doi.org/10.1016/0361-9230(95)02092-6).
- (29) Lee, P. H. K.; McNutt, R. W.; Chang, K.-J. A Nonpeptidic Delta Opioid Receptor Agonist, BW373U86, Attenuates the Development and Expression of Morphine Abstinence Precipitated by Naloxone in Rat. *J. Pharmacol. Exp. Ther.* **1993**, *267* (2), 883–887.
- (30) Su, Y.; McNutt, R. W.; Chang, K. Delta-Opioid Ligands Reverse Alfentanil-Induced Respiratory Depression but Not Antinociception. *J. Pharmacol. Exp. Ther.* **1998**, *287* (3), 815–823.
- (31) O'Neill, S. J.; Collins, M. A.; Pettit, H. O.; McNutt, R. W.; Chang, K. Antagonistic Modulation Between the Delta Opioid Agonist BW373U86 and the Mu Opioid Agonist Fentanyl in Mice. *J. Pharmacol. Exp. Ther.* **1997**, *282* (1), 271–277.
- (32) Yamazaki, M.; Suzuki, T.; Narita, M.; Lipkowski, A. W. The Opioid Peptide Analogue Biphalin Induces Less Physical Dependence than Morphine. *Life Sciences*. 2001, pp 1023–1028. [https://doi.org/10.1016/S0024-3205\(01\)01194-8](https://doi.org/10.1016/S0024-3205(01)01194-8).
- (33) Yadlapalli, J. S. K.; Ford, B. M.; Ketkar, A.; Wan, A.; Penthala, N. R.; Eoff, R. L.; Prather, P. L.; Dobretsov, M.; Crooks, P. A. Antinociceptive Effects of the 6-O-Sulfate Ester of Morphine in Normal and Diabetic Rats: Comparative Role of Mu- and Delta-Opioid Receptors. *Pharmacol. Res.* **2016**, *113*, 335–347. <https://doi.org/10.1016/j.phrs.2016.09.012>.Antinociceptive.
- (34) Pasquinucci, L.; Parenti, C.; Turnaturi, R.; Aricò, G.; Marrazzo, A.; Prezzavento, O.; Ronsisvalle, S.; Georgoussi, Z.; Fourla, D.; Scoto, G. M.; et al. The Benzomorphan-Based LP1 Ligand Is a Suitable MOR/DOR Agonist for Chronic Pain Treatment. *Life Sci.* **2012**, *90* (1), 66–70. <https://doi.org/10.1016/j.lfs.2011.10.024>.
- (35) Yadlapalli, J. S. K.; Dogra, N.; Walbaum, A. W.; Wessinger, W. D.; Prather, P. L.; Crooks, P. A.; Dobretsov, M. Evaluation of Analgesia, Tolerance and the Mechanism of Action of Morphine-6-O-Sulfate across Multiple Pain Modalities in Sprague-Dawley Rats. *Anesth. Analg.* **2017**, *125* (3), 1021–1031. <https://doi.org/10.1213/ANE.0000000000002006>.
- (36) Turnaturi, R.; Aricò, G.; Ronsisvalle, G.; Parenti, C.; Pasquinucci, L. Multitarget Opioid

- Ligands in Pain Relief: New Players in an Old Game. *Eur. J. Med. Chem.* **2016**, *108*, 211–228. <https://doi.org/10.1016/j.ejmech.2015.11.028>.
- (37) Ananthan, S. Opioid Ligands with Mixed μ/δ Opioid Receptor Interactions: An Emerging Approach to Novel Analgesics. *AAPS J.* **2006**, *8* (1), E118–E125. <https://doi.org/10.1208/aapsj080114>.
- (38) Wells, J. L.; Bartlett, J. L.; Ananthan, S.; Bilsky, E. J. In Vivo Pharmacological Characterization of SoRI 9409, a Nonpeptidic Opioid Mu-Agonist/Delta-Antagonist That Produces Limited Antinociceptive Tolerance and Attenuates Morphine Physical Dependence. *J. Pharmacol. Exp. Ther.* **2001**, *297* (2), 597–605.
- (39) Healy, J. R.; Bezawada, P.; Shim, J.; Jones, J. W.; Kane, M. A.; MacKerell, A. D.; Coop, A.; Matsumoto, R. R. Synthesis, Modeling, and Pharmacological Evaluation of UMB 425, a Mixed μ Agonist/ δ Antagonist Opioid Analgesic with Reduced Tolerance Liabilities. *ACS Chem. Neurosci.* **2013**, *4*, 1256–1266. <https://doi.org/10.1021/cn4000428>.
- (40) Ananthan, S.; Saini, S. K.; Dersch, C. M.; Xu, H.; McGlinchey, N.; Giuvelis, D.; Bilsky, E. J.; Rothman, R. B. 14-Alkoxy- and 14-Acyloxypyridomorphinans: μ Agonist/ δ Antagonist Opioid Analgesics with Diminished Tolerance and Dependence Side Effects. *J. Med. Chem.* **2012**, *55*, 8350–8363. <https://doi.org/10.1021/jm300686p>.
- (41) Váradi, A.; Marrone, G. F.; Palmer, T. C.; Narayan, A.; Szabó, M. R.; Le Rouzic, V.; Grinnell, S. G.; Subrath, J. J.; Warner, E.; Kalra, S.; et al. Mitragynine/Corynantheidine Pseudoindoxyls As Opioid Analgesics with Mu Agonism and Delta Antagonism, Which Do Not Recruit β -Arrestin-2. *J. Med. Chem.* **2016**, *59*, 8381–8397. <https://doi.org/10.1021/acs.jmedchem.6b00748>.
- (42) Schiller, P. W.; Fundytus, M. E.; Merovitz, L.; Weltrowska, G.; Nguyen, T. M.; Lemieux, C.; Chung, N. N.; Coderre, T. J. The Opioid μ Agonist/ δ Antagonist DIPP-NH₂[Ψ] Produces a Potent Analgesic Effect, No Physical Dependence, and Less Tolerance than Morphine in Rats. *J. Med. Chem.* **1999**, *42*, 3520–3526. <https://doi.org/10.1021/jm980724+>.
- (43) Anand, J. P.; Kochan, K. E.; Nastase, A. F.; Montgomery, D.; Griggs, N. W.; Traynor, J. R.; Mosberg, H. I.; Jutkiewicz, E. M. In Vivo Effects of μ Opioid Receptor Agonist/ δ Opioid Receptor Antagonist Peptidomimetics Following Acute and Repeated Administration. *Br. J. Pharmacol.* **2018**, *175*, 2013–2027. <https://doi.org/10.1111/bph.14148>.
- (44) Hughes, J.; Smith, T. W.; Kosterlitz, H. W.; Fothergill, L. A.; Morgan, B. A.; Morris, H. R. Identification of Two Related Pentapeptides from the Brain with Potent Opiate Agonist Activity. *Nature* **1975**, *258*, 577–579.
- (45) Goldstein, A.; Lowery, P. J. Effect of the Opiate Antagonist Naloxone on Body Temperature in Rats. *Life Sci.* **1975**, *17*, 927–931.
- (46) Naqvi, T.; Haq, W.; Mathur, K. B. Structure–Activity Relationship Studies of Dynorphin A and Related Peptides. *Peptides* **1998**, *19* (7), 1277–1292.
- (47) Przewłocki, R.; Przewłocka, B. Opioids in Chronic Pain. *Eur. J. Pharmacol.* **2001**, *429*, 79–91.
- (48) Montecucchi, P. C.; Castiglione, R. de; Piani, S.; Gozzini, L.; Erspamer, V. Amino Acid

- Composition and Sequence of Dermorphin, a Novel Opiate-like Peptide from the Skin of *Phyllomedusa Sauvagei*. *Int. J. Pept. Protein Res.* **1981**, *17*, 275–283.
- (49) Kreil, G.; Barra, D.; Simmaco, M.; Erspamer, V.; Erspamer, G. F.; Negri, L.; Severini, C.; Corsi, R.; Melchiorri, P. Deltorphin, a Novel Amphibian Skin Peptide with High Selectivity and Affinity for δ Opioid Receptors. *Eur. J. Pharmacol.* **1989**, *162*, 123–128.
- (50) Janecka, A.; Fichna, J.; Janecki, T. Opioid Receptors and Their Ligands. *Curr. Top. Med. Chem.* **2004**, *4*, 1–17. <https://doi.org/10.1016/B978-0-12-013318-5.50008-4>.
- (51) Hanka, B. K.; Lane, A. C.; Lord, J. A. H.; Morgan, B. A.; Rance, M. J.; Smith, C. F. C. Analogues of β -LPH61–64 Possessing Selective Agonist Activity at μ -Opiate Receptors. *Eur. J. Pharmacol.* **1981**, *70*, 531–540.
- (52) Mosberg, H. I.; Hurst, R.; Hruby, V. J.; Gee, K.; Yamamura, H. I.; Galligan, J. J.; Burks, T. F. Bis-Penicillamine Enkephalins Possess Highly Improved Specificity toward δ Opioid Receptors. *Proc. Natl. Acad. Sci. U. S. A.* **1983**, *80*, 5871–5874. <https://doi.org/10.1073/pnas.80.19.5871>.
- (53) Bryant, S. D.; Jinsmaa, Y.; Salvadori, S.; Okada, Y.; Lazarus, L. H. Dmt and Opioid Peptides: A Potent Alliance. *Biopolym. - Pept. Sci. Sect.* **2003**, *71*, 86–102. <https://doi.org/10.1002/bip.10399>.
- (54) Mosberg, H. I.; Omnaas, J. R.; Medzihradsky, F.; Smith, C. B. Cyclic, Disulfide- and Dithioether-Containing Opioid Tetrapeptides: Development of a Ligand with High Delta Opioid Receptor Selectivity and Affinity. *Life Sci.* **1988**, *43* (12), 1013–1020. [https://doi.org/10.1016/0024-3205\(88\)90547-4](https://doi.org/10.1016/0024-3205(88)90547-4).
- (55) Lomize, A. L.; Flippen-Anderson, J. L.; George, C.; Mosberg, H. I. Conformational Analysis of the δ Receptor-Selective, Cyclic Opioid Peptide, Tyr-Cyclo[D-Cys-Phe-D-Pen]OH (JOM-13). Comparison of X-Ray Crystallographic Structures, Molecular Mechanics Simulations, and 1H NMR Data. *J. Am. Chem. Soc.* **1994**, *116* (2), 429–436. <https://doi.org/10.1021/ja00081a001>.
- (56) Mosberg, H.; Dua, R. K.; Pogozheva, I. D.; Lomize, A. L. Development of a Model for the δ -Opioid Receptor Pharmacophore. 4. Residue 3 Dehydrophenylalanine Analogues of Tyr-c[D-Cys-Phe-D-Pen]OH (JOM-13) Confirm Required Gauche Orientation of Aromatic Side Chain. *Biopolymers* **1996**, *39*, 287–296.
- (57) Lomize, A. L.; Pogozheva, I. D.; Mosberg, H. Development of a Model for the δ -Opioid Receptor Pharmacophore: 3. Comparison of the Cyclic Tetrapeptide Tyr-c[D-Cys-Phe-D-Pen]OH with Other Conformationally Constrained & Receptor Selective Ligands. *Biopolymers* **1996**, *38*, 221–234.
- (58) Mosberg, H. I.; Lomize, A. L.; Wang, C.; Kroona, H.; Heyl, D. L.; Sobczyk-Kojiro, K.; Ma, W.; Mousigian, C.; Porreca, F. Development of a Model for the δ Opioid Receptor Pharmacophore. 1. Conformationally Restricted Tyr1 Replacements in the Cyclic δ Receptor Selective Tetrapeptide Tyr-c[D-Cys-Phe-D-Pen]OH (JOM-13). *J. Med. Chem.* **1994**, *37*, 4371–4383. <https://doi.org/10.1021/jm00051a015>.
- (59) Mosberg, H. I.; Omnaas, J. R.; Lomize, A.; Heyl, D. L.; Nordan, I.; Mousigian, C.; Davis, P.; Porreca, F. Development of Model for the δ Opioid Receptor Pharmacophore. 2. Conformationally Restricted Phe3 Replacements in the Cyclic δ Receptor Selective

- Tetrapeptide Tyr-c[D-Cys-Phe-D-Pen]OH (JOM-13). *J. Med. Chem.* **1994**, *37*, 4384–4391. <https://doi.org/10.1021/jm00051a016>.
- (60) Wang, C.; McFadyen, I. J.; Traynor, J. R.; Mosberg, H. I. Design of a High Affinity Peptidomimetic Opioid Agonist from Peptide Pharmacophore Models. *Bioorganic Med. Chem. Lett.* **1998**, *8*, 2685–2688. [https://doi.org/10.1016/S0960-894X\(98\)00472-7](https://doi.org/10.1016/S0960-894X(98)00472-7).
- (61) Mosberg, H. I.; Yeomans, L.; Harland, A. A.; Bender, A. M.; Sobczyk-Kojiro, K.; Anand, J. P.; Clark, M. J.; Jutkiewicz, E. M.; Traynor, J. R. Opioid Peptidomimetics: Leads for the Design of Bioavailable Mixed Efficacy μ Opioid Receptor (MOR) Agonist/ δ Opioid Receptor (DOR) Antagonist Ligands. *J. Med. Chem.* **2013**, *56*, 2139–2149. <https://doi.org/10.1021/jm400050y>.
- (62) Harland, A. A.; Pogozheva, I. D.; Griggs, N. W.; Trask, T. J.; Traynor, J. R.; Mosberg, H. I. Placement of Hydroxy Moiety on Pendant of Peptidomimetic Scaffold Modulates Mu and Kappa Opioid Receptor Efficacy. *ACS Chem. Neurosci.* **2017**, *8*, 2549–2557. <https://doi.org/10.1021/acscchemneuro.7b00284>.
- (63) Harland, A. A.; Yeomans, L.; Griggs, N. W.; Anand, J. P.; Pogozheva, I. D.; Jutkiewicz, E. M.; Traynor, J. R.; Mosberg, H. I. Further Optimization and Evaluation of Bioavailable, Mixed-Efficacy μ -Opioid Receptor (MOR) Agonists/ δ -Opioid Receptor (DOR) Antagonists: Balancing MOR and DOR Affinities. *J. Med. Chem.* **2015**, *58*, 8952–8969. <https://doi.org/10.1021/acs.jmedchem.5b01270>.
- (64) Bender, A. M.; Griggs, N. W.; Anand, J. P.; Traynor, J. R.; Jutkiewicz, E. M.; Mosberg, H. I. Asymmetric Synthesis and in Vitro and in Vivo Activity of Tetrahydroquinolines Featuring a Diverse Set of Polar Substitutions at the 6 Position as Mixed-Efficacy μ Opioid Receptor/ δ Opioid Receptor Ligands. *ACS Chem. Neurosci.* **2015**, *6*, 1428–1435. <https://doi.org/10.1021/acscchemneuro.5b00100>.
- (65) Harland, A. A.; Bender, A. M.; Griggs, N. W.; Gao, C.; Anand, J. P.; Pogozheva, I. D.; Traynor, J. R.; Jutkiewicz, E. M.; Mosberg, H. I. Effects of N-Substitutions on the Tetrahydroquinoline (THQ) Core of Mixed-Efficacy μ -Opioid Receptor (MOR)/ δ -Opioid Receptor (DOR) Ligands. *J. Med. Chem.* **2016**, *59*, 4985–4998. <https://doi.org/10.1021/acs.jmedchem.6b00308>.
- (66) Nastase, A. F.; Griggs, N. W.; Anand, J. P.; Fernandez, T. J.; Harland, A. A.; Trask, T. J.; Jutkiewicz, E. M.; Traynor, J. R.; Mosberg, H. I. Synthesis and Pharmacological Evaluation of Novel C-8 Substituted Tetrahydroquinolines as Balanced-Affinity Mu/Delta Opioid Ligands for the Treatment of Pain. *ACS Chem. Neurosci.* **2018**, *9*, 1840–1848. <https://doi.org/10.1021/acscchemneuro.8b00139>.
- (67) Nastase, A. F.; Anand, J. P.; Bender, A. M.; Montgomery, D.; Griggs, N. W.; Fernandez, T. J.; Jutkiewicz, E. M.; Traynor, J. R.; Mosberg, H. I. Dual Pharmacophores Explored via Structure–Activity Relationship (SAR) Matrix: Insights into Potent, Bifunctional Opioid Ligand Design. *J. Med. Chem.* **2019**, *62*, 4193–4203. <https://doi.org/10.1021/acs.jmedchem.9b00378>.
- (68) Bender, A. M.; Griggs, N. W.; Gao, C.; Trask, T. J.; Traynor, J. R.; Mosberg, H. I. Rapid Synthesis of Boc-2',6'-Dimethyl-L-Tyrosine and Derivatives and Incorporation into Opioid Peptidomimetics. *ACS Med. Chem. Lett.* **2015**, *6*, 1199–1203. <https://doi.org/10.1021/acsmchemlett.5b00344>.

- (69) Gu, C.; Collins, R.; Holsworth, D. D.; Walker, G. S.; Voorman, R. L. Metabolic Aromatization of N-Alkyl-1,2,3,4-Tetrahydroquinoline Substructures to Quinolinium by Human Liver Microsomes and Horseradish Peroxidase. *Drug Metab. Dispos.* **2006**, *34* (12), 2044–2055. <https://doi.org/10.1124/dmd.106.012286.quinoline>.
- (70) Bender, A. M.; Clark, M. J.; Agius, M. P.; Traynor, J. R.; Mosberg, H. I. Synthesis and Evaluation of 4-Substituted Piperidines and Piperazines as Balanced Affinity μ Opioid Receptor (MOR) Agonist/ δ Opioid Receptor (DOR) Antagonist Ligands. *Bioorganic Med. Chem. Lett.* **2014**, *24*, 548–551. <https://doi.org/10.1016/j.bmcl.2013.12.021>.
- (71) Shiotani, K.; Li, T.; Miyazaki, A.; Tsuda, Y.; Yokoi, T.; Ambo, A.; Sasaki, Y.; Bryant, S. D.; Lazarus, L. H.; Okada, Y. Design and Synthesis of Opioidmimetics Containing 2',6'-Dimethyl-L-Tyrosine and a Pyrazinone-Ring Platform. *Bioorganic Med. Chem. Lett.* **2007**, *17*, 5768–5771. <https://doi.org/10.1016/j.bmcl.2007.08.058>.
- (72) Shiotani, K.; Li, T.; Miyazaki, A.; Tsuda, Y.; Bryant, S. D.; Ambo, A.; Sasaki, Y.; Lazarus, L. H.; Okada, Y. Synthesis of 3,6-Bis[H-Tyr/H-Dmt-NH(CH₂)_{m,n}]-2(1H)Pyrazinone Derivatives: Function of Alkyl Chain Length on Opioid Activity. *Bioorganic Med. Chem. Lett.* **2006**, *16*, 5793–5796. <https://doi.org/10.1016/j.bmcl.2006.08.079>.
- (73) Jinsmaa, Y.; Okada, Y.; Tsuda, Y.; Shiotani, K.; Sasaki, Y.; Ambo, A.; Bryant, S. D.; Lazarus, L. H. Novel 2',6' -Dimethyl-L-Tyrosine-Containing Pyrazinone Opioid Mimetic μ -Agonists with Potent Antinociceptive Activity in Mice. *J. Pharmacol. Exp. Ther.* **2004**, *309* (1), 432–438. <https://doi.org/10.1124/jpet.103.060061.logical>.
- (74) Jinsmaa, Y.; Miyazaki, A.; Fujita, Y.; Li, T.; Fujisawa, Y.; Shiotani, K.; Tsuda, Y.; Yokoi, T.; Ambo, A.; Sasaki, Y.; et al. Oral Bioavailability of a New Class of μ -Opioid Receptor Agonists Containing 3,6-Bis[Dmt-NH(CH₂)_n]-2(1H)-Pyrazinone with Central-Mediated Analgesia. *J. Med. Chem.* **2004**, *47* (10), 2599–2610. <https://doi.org/10.1021/jm0304616>.
- (75) Li, T.; Shiotani, K.; Miyazaki, A.; Fujita, Y.; Tsuda, Y.; Ambo, A.; Sasaki, Y.; Jinsmaa, Y.; Marczak, E.; Bryant, S. D.; et al. New Series of Potent δ -Opioid Antagonists Containing the H-Dmt-Tic-NH-Hexyl-NH-R Motif. *Bioorganic Med. Chem. Lett.* **2005**, *15*, 5517–5520. <https://doi.org/10.1016/j.bmcl.2005.08.073>.
- (76) Okada, Y.; Tsuda, Y.; Fujita, Y.; Yokoi, T.; Sasaki, Y.; Ambo, A.; Konishi, R.; Nagata, M.; Salvadori, S.; Jinsmaa, Y.; et al. Unique High-Affinity Synthetic μ -Opioid Receptor Agonists with Central- and Systemic-Mediated Analgesia. *J. Med. Chem.* **2003**, *46* (15), 3201–3209. <https://doi.org/10.1021/jm020459z>.
- (77) Chandrakumar, N. S.; Yonan, P. K.; Stapelfeld, A.; Savage, M.; Rorbacher, E.; Contreras, P. C.; Hammond, D. Preparation and Opioid Activity of Analogues of the Analgesic Dipeptide 2,6-Dimethyl-L-Tyrosyl-N-(3-Phenylpropyl)-D-Alaninamide. *J. Med. Chem.* **1992**, *35* (2), 223–233. <https://doi.org/10.1021/jm00080a005>.
- (78) Neilan, C. L.; Husbands, S. M.; Breeden, S.; Ko, M. C.; Aceto, M. D.; Lewis, J. W.; Woods, J. H.; Traynor, J. R. Characterization of the Complex Morphinan Derivative BU72 as a High Efficacy, Long-Lasting μ -Opioid Receptor Agonist. *Eur. J. Pharmacol.* **2004**, *499*, 107–116. <https://doi.org/10.1016/j.ejphar.2004.07.097>.
- (79) Purington, L. C.; Sobczyk-Kojiro, K.; Pogozheva, I. D.; Traynor, J. R.; Mosberg, H. I. Development and in Vitro Characterization of a Novel Bifunctional μ -Agonist/ δ -

- Antagonist Opioid Tetrapeptide. *ACS Chem. Biol.* **2011**, *6*, 1375–1381.
<https://doi.org/10.1021/cb200263q>.
- (80) Stepan, A. F.; Mascitti, V.; Beaumont, K.; Kalgutkar, A. S. Metabolism-Guided Drug Design. *Medchemcomm* **2013**, *4*, 631–652. <https://doi.org/10.1039/c2md20317k>.
- (81) Henry, S. P.; Fernandez, T. J.; Anand, J. P.; Griggs, N. W.; Traynor, J. R.; Mosberg, H. I. Structural Simplification of a Tetrahydroquinoline-Core Peptidomimetic μ -Opioid Receptor (MOR) Agonist/ δ -Opioid Receptor (DOR) Antagonist Produces Improved Metabolic Stability. *J. Med. Chem.* **2019**, *62*, 4142–4157.
<https://doi.org/10.1021/acs.jmedchem.9b00219>.
- (82) Traynor, J. R.; Nahorski, S. R. Modulation by μ -Opioid Agonists of Guanosine-5'-O-(3-[35S]Thio)Triphosphate Binding to Membranes from Human Neuroblastoma SH-SY5Y Cells. *Mol. Pharmacol.* **1995**, *47*, 848–854.
- (83) Huang, W.; Manglik, A.; Venkatakrishnan, A. J.; Laeremans, T.; Feinberg, E. N.; Sanborn, A. L.; Kato, H. E.; Livingston, K. E.; Thorsen, T. S.; Kling, R. C.; et al. Structural Insights into M-Opioid Receptor Activation. *Nature* **2015**, *524*, 315–321.
<https://doi.org/10.1038/nature14886>.
- (84) Xu, J.; Liu, Z.; Yang, X.; Wang, L.; Chen, G.; Liu, J. One-Pot Asymmetric Synthesis of α -Trifluoromethylated Amines from α -Trifluoromethyl Ketones. *Tetrahedron* **2010**, *66*, 8933–8937. <https://doi.org/10.1016/j.tet.2010.09.047>.
- (85) Colyer, J. T.; Andersen, N. G.; Tedrow, J. S.; Soukup, T. S.; Faul, M. M. Reversal of Diastereofacial Selectivity in Hydride Reductions of N-Tert-Butanesulfinyl Imines. *J. Org. Chem.* **2006**, *71*, 6859–6862. <https://doi.org/10.1021/jo0609834>.
- (86) Böhm, H.-J.; Banner, D.; Bendels, S.; Kansy, M.; Kuhn, B.; Müller, K.; Obst-Sander, U.; Stahl, M. Fluorine in Medicinal Chemistry. *ChemBioChem* **2004**, *5*, 637–643.
<https://doi.org/10.1002/cbic.200301023>.
- (87) Junien, J. L.; Wettstein, J. G. Role of Opioids in Peripheral Analgesia. *Life Sci.* **1992**, *51* (26), 2009–2018.
- (88) Stein, C. Peripheral Analgesic Actions of Opioids. *J. Pain Symptom Manage.* **1991**, *6* (3), 119–124.
- (89) Stein, C. New Concepts in Opioid Analgesia New Concepts in Opioid Analgesia, Expert Opinion on Investigational Drugs. *Expert Opin. Investig. Drugs* **2018**, *27* (10), 765–775.
<https://doi.org/10.1080/13543784.2018.1516204>.
- (90) Spahn, V.; Del Vecchio, G.; Labuz, D.; Rodriguez-Gaztelumendi, A.; Massaly, N.; Temp, J.; Durmaz, V.; Sabri, P.; Reidelbach, M.; Machelkska, H.; et al. A Nontoxic Pain Killer Designed by Modeling of Pathological Receptor Conformations. *Science (80-.)*. **2017**, *355*, 966–969. <https://doi.org/10.1126/science.aai8636>.
- (91) Council, N. R. *Guide for the Care and Use of Laboratory Animals*; 2011.
- (92) Mcgrath, J. C.; Lilley, E. Implementing Guidelines on Reporting Research Using Animals (ARRIVE Etc.): New Requirements for Publication in BJP. *Br. J. Pharmacol.* **2015**, *172*, 3189–3193. <https://doi.org/10.1111/bph.12955>.
- (93) Kilkenny, C.; Browne, W.; Cuthill, I. C.; Emerson, M.; Altman, D. G. Animal Research:

- Reporting in Vivo Experiments: The ARRIVE Guidelines. *Br. J. Pharmacol.* **2010**, *160*, 1577–1579. <https://doi.org/10.1111/j.1476-5381.2010.00872.x>.
- (94) Balboni, G.; Salvadori, S.; Guerrini, R.; Negri, L.; Giannini, E.; Bryant, S. D.; Lazarus, L. H. Synthesis and Opioid Activity of N,N-Dimethyl-Dmt-Tic-NH-CH(R)-R' Analogues: Acquisition of Potent δ Antagonism. *Bioorg. Med. Chem.* **2003**, *11*, 5435–5441. <https://doi.org/10.1016/j.bmc.2003.09.039>.
- (95) Dietis, N.; McDonald, J.; Molinari, S.; Calo, G.; Guerrini, R.; Rowbotham, D. J.; Lambert, D. G. Pharmacological Characterization of the Bifunctional Opioid Ligand H-Dmt-Tic-Gly-NH-Bzl (UFP-505). *Br. J. Anaesth.* **2012**, *108* (2), 262–270. <https://doi.org/10.1093/bja/aer377>.
- (96) Dietis, N.; Niwa, H.; Tose, R.; McDonald, J.; Ruggieri, V.; Filafferro, M.; Vitale, G.; Micheli, L.; Ghelardini, C.; Salvadori, S.; et al. In Vitro and In Vivo Characterization of the Bifunctional μ and δ Opioid Receptor Ligand UFP-505. *Br. J. Pharmacol.* **2018**, *175*, 2881–2896. <https://doi.org/10.1111/bph.14199>.
- (97) Balboni, G.; Onnis, V.; Congiu, C.; Zotti, M.; Sasaki, Y.; Ambo, A.; Bryant, S. D.; Jinsmaa, Y.; Lazarus, L. H.; Lazzari, I.; et al. Further Studies on the Effect of Lysine at the C-Terminus of the Dmt-Tic Opioid Pharmacophore. *Bioorganic Med. Chem.* **2007**, *15* (9), 3143–3151. <https://doi.org/10.1016/j.bmc.2007.02.039>.
- (98) Balboni, G.; Fiorini, S.; Baldisserotto, A.; Trapella, C.; Sasaki, Y.; Ambo, A.; Marczak, E. D.; Lazarus, L. H.; Salvadori, S. Further Studies on Lead Compounds Containing the Opioid Pharmacophore Dmt-Tic. *J. Med. Chem.* **2008**, *51* (16), 5109–5117. <https://doi.org/10.1021/jm800587e.Further>.
- (99) Balboni, G.; Salvadori, S.; Trapella, C.; Knapp, B. I.; Bidlack, J. M.; Lazarus, L. H.; Peng, X.; Neumeyer, J. L. Evolution of the Bifunctional Lead μ Agonist/ δ Antagonist Containing the 2',6'-Dimethyl-1-Tyrosine-1,2,3,4-Tetrahydroisoquinoline-3-Carboxylic Acid (Dmt-Tic) Opioid Pharmacophore. *ACS Chem. Neurosci.* **2010**, *1* (2), 155–164. <https://doi.org/10.1021/cn900025j>.
- (100) Balboni, G.; Guerrini, R.; Salvadori, S.; Bianchi, C.; Rizzi, D.; Bryant, S. D.; Lazarus, L. H. Evaluation of the Dmt-Tic Pharmacophore: Conversion of a Potent δ -Opioid Receptor Antagonist into a Potent δ Agonist and Ligands with Mixed Properties. *J. Med. Chem.* **2002**, *45* (3), 713–720. <https://doi.org/10.1021/jm010449i>.
- (101) Balboni, G.; Onnis, V.; Congiu, C.; Zotti, M.; Sasaki, Y.; Ambo, A.; Bryant, S. D.; Jinsmaa, Y.; Lazarus, L. H.; Trapella, C.; et al. Effect of Lysine at C-Terminus of the Dmt-Tic Opioid Pharmacophore. *J. Med. Chem.* **2006**, *49* (18), 5610–5617. <https://doi.org/10.1021/jm060741w>.
- (102) Ballet, S.; Feytens, D.; Wachter, R. De; Vlaeminck, M. De; Marczak, E. D.; Salvadori, S.; Graaf, C. de; Rognan, D.; Negri, L.; Lattanzi, R.; et al. Conformationally Constrained Opioid Ligands: The Dmt-Aba and Dmt-Aia versus Dmt-Tic Scaffold. *Bioorganic Med. Chem. Lett.* **2009**, *19*, 433–437. <https://doi.org/10.1016/j.bmcl.2008.11.051>.
- (103) Ballet, S.; Salvadori, S.; Trapella, C.; Bryant, S. D.; Jinsmaa, Y.; Lazarus, L. H.; Negri, L.; Giannini, E.; Lattanzi, R.; Tourwe, D.; et al. New 2',6'-Dimethyl-L-Tyrosine (Dmt) Opioid Peptidomimetics Based on the Aba-Gly Scaffold. Development of Unique μ -Opioid Receptor Ligands. *J. Med. Chem.* **2006**, *49* (13), 3990–3993.

<https://doi.org/10.1021/jm0603264>.

- (104) Ballet, S.; Feytens, D.; Buysse, K.; Chung, N. N.; Lemieux, C.; Tumati, S.; Keresztes, A.; Van Duppen, J.; Lai, J.; Varga, E.; et al. Design of Novel Neurokinin 1 Receptor Antagonists Based Onconformationally Constrained Aromatic Amino Acids and Discovery of a Potent Chimeric Opioid Agonist-Neurokinin 1 Receptor Antagonist. *J. Med. Chem.* **2011**, *54* (7), 2467–2476. <https://doi.org/10.1021/jm1016285.Design>.
- (105) Betti, C.; Starnowska, J.; Mika, J.; Dyniewicz, J.; Frankiewicz, L.; Novoa, A.; Bochynska, M.; Keresztes, A.; Kosson, P.; Makuch, W.; et al. Dual Alleviation of Acute and Neuropathic Pain by Fused Opioid Agonist-Neurokinin 1 Antagonist Peptidomimetics. *ACS Med. Chem. Lett.* **2015**, *6*, 1209–1214. <https://doi.org/10.1021/acsmedchemlett.5b00359>.
- (106) Guillemyn, K.; Starnowska, J.; Lagard, C.; Dyniewicz, J.; Rojewska, E.; Mika, J.; Chung, N. N.; Utard, V.; Kosson, P.; Lipkowski, A. W.; et al. Bifunctional Peptide-Based Opioid Agonist – Nociceptin Antagonist Ligands for Dual Treatment of Acute and Neuropathic Pain. *J. Med. Chem.* **2016**, *59*, 3777–3792. <https://doi.org/10.1021/acs.jmedchem.5b01976>.
- (107) Guillemyn, K.; Kleczkowska, P.; Lesniak, A.; Dyniewicz, J.; Van Der Poorten, O.; Van Den Eynde, I.; Keresztes, A.; Varga, E.; Lai, J.; Porreca, F.; et al. Synthesis and Biological Evaluation of Compact, Conformationally Constrained Bifunctional Opioid Agonist - Neurokinin-1 Antagonist Peptidomimetics. *Eur. J. Med. Chem.* **2015**, *92*, 64–77. <https://doi.org/10.1016/j.ejmech.2014.12.033>.
- (108) Novoa, A.; Dorpe, S. Van; Wynendaele, E.; Spetea, M.; Bracke, N.; Stalmans, S.; Betti, C.; Chung, N. N.; Lemieux, C.; Zuegg, J.; et al. Variation of the Net Charge, Lipophilicity and Side Chain Flexibility in Dmt1 -DALDA: Effect on Opioid Activity and Biodistribution. *J. Med. Chem.* **2012**, *55* (22), 9549–9561. <https://doi.org/10.1021/jm3008079.Variation>.
- (109) Starnowska, J.; Costante, R.; Guillemyn, K.; Popiolek-barczyk, K.; Chung, N. N.; Lemieux, C.; Keresztes, A.; Duppen, J. Van; Mollica, A.; Streicher, J.; et al. Analgesic Properties of Opioid/NK1 Multitarget Ligands with Distinct in Vitro Profiles in Naive and Chronic Constriction Injury Mice. *ACS Chem. Neurosci.* **2017**, *8*, 2315–2324. <https://doi.org/10.1021/acschemneuro.7b00226>.
- (110) Vandormael, B.; Fourla, D.; Gramowski-Voß, A.; Kosson, P.; Weiss, D. G.; Schroder, O. H. U.; Lipkowski, A.; Georgoussi, Z.; Tourwe, D. Superpotent [Dmt1]Dermorphin Tetrapeptides Containing the 4-Aminotetrahydro-2-Benzazepin-3-One Scaffold with Mixed μ/δ Opioid Receptor Agonistic Properties. *J. Med. Chem.* **2011**, *54*, 7848–7859. <https://doi.org/10.1021/jm200894e>.
- (111) Li, Y.; Cazares, M.; Wu, J.; Houghten, R. A.; Toll, L.; Dooley, C. Potent M-Opioid Receptor Agonists from Cyclic Peptides Tyr-c[D-Lys- Xxx-Tyr-Gly]: Synthesis, Biological, and Structural Evaluation. *J. Med. Chem.* **2016**, *59*, 1239–1245. <https://doi.org/10.1021/acs.jmedchem.5b01899>.
- (112) Li, Y.; Dooley, C. T.; Mislser, J. A.; Debevec, G.; Giulianotti, M. A.; Cazares, M. E.; Maida, L.; Houghten, R. A. Fluorescent Mu Selective Opioid Ligands from a Mixture Based Cyclic Peptide Library. *ACS Comb. Sci.* **2012**, *14* (12), 673–679.

<https://doi.org/10.1021/co300110t>.Fluorescent.

- (113) Lee, Y. S.; Qu, H.; Davis, P.; Ma, S. W.; Vardanyan, R.; Lai, J.; Porreca, F.; Hrubby, V. J. Chiral Effect of a Phe Residue in Position 3 of the Dmt1-L (or D)-Tic2 Analogues on Opioid Functional Activities. *ACS Med. Chem. Lett.* **2013**, *4*, 656–659. <https://doi.org/10.1021/ml400115n>.
- (114) Wang, Y.; Yang, J.; Liu, X.; Zhao, L.; Yang, D.; Zhou, J.; Wang, D.; Mou, L.; Wang, R. Endomorphin-1 Analogs Containing α -Methyl- β -Amino Acids Exhibit Potent Analgesic Activity after Peripheral Administration. *Org. Biomol. Chem.* **2017**, *15*, 4951–4955. <https://doi.org/10.1039/c7ob01115f>.
- (115) Nair, P.; Yamamoto, T.; Cowell, S.; Kulkarni, V.; Moye, S.; Navratilova, E.; Davis, P.; Ma, S.-W.; Vanderah, T. W.; Lai, J.; et al. Discovery of Tripeptide-Derived Multifunctional Ligands Possessing Delta/Mu Opioid Receptor Agonist and Neurokinin 1 Receptor Antagonist Activities. *Bioorg. Med. Chem. Lett.* **2015**, *25* (17), 3716–3720. <https://doi.org/10.1016/j.bmcl.2015.06.030>.Discovery.
- (116) Liu, X.; Zhao, L.; Wang, Y.; Zhou, J.; Wang, D.; Zhang, Y.; Zhang, X.; Wang, Z.; Yang, D.; Mou, L.; et al. MEL-N16: A Series of Novel Endomorphin Analogs with Good Analgesic Activity and a Favorable Side Effect Profile. *ACS Chem. Neurosci.* **2017**, *8*, 2180–2193. <https://doi.org/10.1021/acschemneuro.7b00097>.
- (117) Liu, X.; Wang, Y.; Xing, Y.; Yu, J.; Ji, H.; Kai, M.; Wang, Z.; Wang, D.; Zhang, Y.; Zhao, D.; et al. Design, Synthesis, and Pharmacological Characterization of Novel Endomorphin-1 Analogues as Extremely Potent M-Opioid Agonists. *J. Med. Chem.* **2013**, *56*, 3102–3114. <https://doi.org/10.1021/jm400195y>.
- (118) Fujita, Y.; Tsuda, Y.; Li, T.; Motoyama, T.; Takahashi, M.; Shimizu, Y.; Yokoi, T.; Sasaki, Y.; Ambo, A.; Kita, A.; et al. Development of Potent Bifunctional Endomorphin-2 Analogues with Mixed μ -/ δ -Opioid Agonist and δ -Opioid Antagonist Properties. *J. Med. Chem.* **2004**, *47*, 3591–3599. <https://doi.org/10.1021/jm030649p>.
- (119) Biondi, B.; Giannini, E.; Negri, L.; Melchiorri, P.; Lattanzi, R.; Rosso, F.; Ciocca, L.; Rocchi, R. Opioid Peptides: Synthesis and Biological Activity of New Endomorphin Analogues. *Int. J. Pept. Res. Ther.* **2006**, *12* (2), 145–151. <https://doi.org/10.1007/s10989-006-9015-6>.
- (120) Gao, Y.; Liu, X.; Liu, W.; Qi, Y.; Liu, X.; Zhou, Y.; Wang, R. Opioid Receptor Binding and Antinociceptive Activity of the Analogues of Endomorphin-2 and Morphiceptin with Phenylalanine Mimics in the Position 3 or 4. *Bioorganic Med. Chem. Lett.* **2006**, *16*, 3688–3692. <https://doi.org/10.1016/j.bmcl.2006.04.063>.
- (121) Schiller, P. W.; Weltrowska, G.; Berezowska, I.; Nguyen, T. M.-D.; Wilkes, B. C.; Lemieux, C.; Chung, N. N. The TIPP Opioid Peptide Family: Development of δ Antagonists, δ Agonists, and Mixed μ Agonist/ δ Antagonists. *Biopolym. - Pept. Sci. Sect.* **1999**, *51*, 411–425.
- (122) Page, D.; Naismith, A.; Schmidt, R.; Coupal, M.; Labarre, M.; Gosselin, M.; Bellemare, D.; Payza, K.; Brown, W. Novel C-Terminus Modifications of the Dmt-Tic Motif: A New Class of Dipeptide Analogues Showing Altered Pharmacological Profiles Toward the Opioid Receptors. *J. Med. Chem.* **2001**, *44*, 2387–2390. <https://doi.org/10.1021/jm015532k>.

- (123) Gach-Janczak, K.; Piekielna-Ciesielska, J.; Adamska-Bartłomiejczyk, A.; Perlikowska, R.; Kruszyński, R.; Kluczyk, A.; Krzywik, J.; Sukiennik, J.; Cerlesi, M. C.; Calo, G.; et al. Synthesis and Activity of Opioid Peptidomimetics with B2- and B3-Amino Acids. *Peptides* **2017**, *95*, 116–123. <https://doi.org/10.1016/j.peptides.2017.07.015>.
- (124) Touati-Jallabe, Y.; Bojnik, E.; Legrand, B.; Mauchauffée, E.; Chung, N. N.; Schiller, P. W.; Benyhe, S.; Averlant-Petit, M. C.; Martinez, J.; Hernandez, J. F. Cyclic Enkephalins with a Diversely Substituted Guanidine Bridge or a Thiourea Bridge: Synthesis, Biological and Structural Evaluations. *J. Med. Chem.* **2013**, *56*, 5964–5973. <https://doi.org/10.1021/jm4008592>.
- (125) Wu, H.; Wacker, D.; Mileni, M.; Katritch, V.; Han, G. W.; Vardy, E.; Liu, W.; Thompson, A. A.; Huang, X.; Carroll, F. I.; et al. Structure of the Human κ -Opioid Receptor in Complex with JD1c. *Nature* **2012**, *485*, 327–332. <https://doi.org/10.1038/nature10939>.
- (126) Fenalti, G.; Zatsepin, N. A.; Betti, C.; Giguere, P.; Han, G. W.; Ishchenko, A.; Liu, W.; Guillemyn, K.; Zhang, H.; James, D.; et al. Structural Basis for Bifunctional Peptide Recognition at Human δ -Opioid Receptor. *Nat. Struct. Mol. Biol.* **2015**, *22* (3), 265–268. <https://doi.org/10.1038/nsmb.2965>.
- (127) Chatterjee, J.; Rechenmacher, F.; Kessler, H. N-Methylation of Peptides and Proteins: An Important Element for Modulating Biological Functions. *Angew. Rev.* **2013**, *52*, 254–269. <https://doi.org/10.1002/anie.201205674>.
- (128) Peng, F.; Zhan, X.; Li, M.; Fang, F.; Li, G.; Li, C.; Zhang, P.; Chen, Z. Proteomic and Bioinformatics Analyses of Mouse Liver Microsomes. *Int. J. Proteomics* **2012**, *2012*, 1–24. <https://doi.org/10.1155/2012/832569>.
- (129) Raffa, R. B.; Pergolizzi Jr, J. V.; Taylor Jr, R.; Ossipov, M. H. Indirect-Acting Strategy of Opioid Action Instead of Direct Receptor Activation: Dual-Acting Enkephalinase Inhibitors (DENKIs). *J. Clin. Pharm. Ther.* **2018**, *43*, 443–449. <https://doi.org/10.1111/jcpt.12687>.
- (130) Lovering, F.; Bikker, J.; Humblet, C. Escape from Flatland: Increasing Saturation as an Approach to Improving Clinical Success. *J. Med. Chem.* **2009**, *52* (21), 6752–6756. <https://doi.org/10.1021/jm901241e>.
- (131) Ritchie, T. J.; Macdonald, S. J. F.; Young, R. J.; Pickett, S. D. The Impact of Aromatic Ring Count on Compound Developability: Further Insights by Examining Carbo- and Hetero-Aromatic and -Aliphatic Ring Types. *Drug Discov. Today* **2011**, *16* (3–4), 164–171. <https://doi.org/10.1016/j.drudis.2010.11.014>.
- (132) Ritchie, T. J.; Macdonald, S. J. F. The Impact of Aromatic Ring Count on Compound Developability – Are Too Many Aromatic Rings a Liability in Drug Design? *Drug Discov. Today* **2009**, *14* (21/22), 1011–1020. <https://doi.org/10.1016/j.drudis.2009.07.014>.
- (133) Waterbeemd, H. Van De; Camenisch, G.; Folkers, G.; Chretien, J. R.; Raevsky, O. A. Estimation of Blood-Brain Barrier Crossing of Drugs Using Molecular Size and Shape, and H-Bonding Descriptors. *J. Drug Target.* **1998**, *6* (2), 151–165. <https://doi.org/10.3109/10611869808997889>.
- (134) Kumar, S.; Sharma, R.; Roychowdhury, A. Modulation of Cytochrome-P450 Inhibition (CYP) in Drug Discovery: A Medicinal Chemistry Perspective. *Curr. Med. Chem.* **2012**,

19 (21), 3605–3621.

- (135) Johnson, S. R.; Yue, H.; Conder, L.; Shi, H.; Doweiko, A. M.; Levesque, P. Estimation of HERG Inhibition of Drug Candidates Using Multivariate Property and Pharmacophore SAR. *Bioorg. Med. Chem.* **2007**, *15*, 6182–6192. <https://doi.org/10.1016/j.bmc.2007.06.028>.
- (136) Guerrini, R.; Capasso, A.; Sorrentino, L.; Anacardio, R.; Bryant, S. D.; Lazarus, L. H.; Attila, M.; Salvadori, S. Opioid Receptor Selectivity Alteration by Single Residue Replacement: Synthesis and Activity Profile of [Dmt]Deltorphin B. *Eur. J. Pharmacol.* **1996**, *302*, 37–42.
- (137) Salvadori, S.; Attila, M.; Balboni, G.; Bianchi, C.; Bryant, S. D.; Crescenzi, O.; Guerrini, R.; Picone, D.; Tancredi, T.; Temussi, P. A.; et al. δ Opioidmimetic Antagonists: Prototypes for Designing a New Generation of Ultrasensitive Opioid Peptides. *Mol. Med.* **1995**, *1* (6), 678–689.
- (138) Montgomery, D.; Anand, J. P.; Griggs, N. W.; Fernandez, T. J.; Hartman, J. G.; Sanchez-Santiago, A. A.; Pogozeva, I. D.; Traynor, J. R.; Mosberg, H. I. Novel Dimethyltyrosine – Tetrahydroisoquinoline Peptidomimetics with Aromatic Tetrahydroisoquinoline Substitutions Show in Vitro Kappa and Mu Opioid Receptor Agonism. *ACS Chem. Biol.* **2019**, *10* (8), 3682–3689. <https://doi.org/10.1021/acchemneuro.9b00250>.